RESERVOIR CHARACTERIZATION OF CLASTIC CYCLE SEQUENCES IN THE PARADOX FORMATION OF THE HERMOSA GROUP, PARADOX BASIN, UTAH

by Bruce D. Trudgill and W. Curtis Arbuckle

OPEN-FILE REPORT 543
UTAH GEOLOGICAL SURVEY
a division of
UTAH DEPARTMENT OF NATURAL RESOURCES
2009

Utah Geological Survey
60 years
1949 2009
Excellence, Integrity, and Objectivity

RESERVOIR CHARACTERIZATION OF CLASTIC CYCLE SEQUENCES IN THE PARADOX FORMATION OF THE HERMOSA GROUP, PARADOX BASIN, UTAH

by

Bruce D. Trudgill
Department of Geolog and Geological Engineering
Colorado School of Mines
Golden, Colorado 80401
303-273-3883
btrudgil@mines.edu

W. Curtis Arbuckle
Department of Geolog and Geological Engineering
Colorado School of Mines
Golden, Colorado 80401
303-273-3800
warbuckl@mines.edu

OPEN-FILE REPORT 543
UTAH GEOLOGICAL SURVEY
a division of
UTAH DEPARTMENT OF NATURAL RESOURCES
2009

STATE OF UTAH
Jon Huntsman, Jr., Governor

DEPARTMENT OF NATURAL RESOURCES
Michael Styler, Executive Director

UTAH GEOLOGICAL SURVEY
Richard G. Allis, Director

PUBLICATIONS
contact
Natural Resources Map & Bookstore
1594 W. North Temple
telephone: 801-537-3320
toll-free: 1-888-UTAH MAP
Web site: http://mapstore.utah.gov
email: geostore@utah.gov

UTAH GEOLOGICAL SURVEY
contact
1594 W. North Temple, Suite 3110
Salt Lake City, UT 84114
telephone: 801-537-3300
Web site: http://geology.utah.gov

This open-file report was prepared by the authors under contract to the Utah Department of Natural Resources, Utah Geological Survey. The report has not undergone the full UGS review process, and may not necessarily conform to UGS technical, editorial, or policy standards. Therefore, it may be premature for an individual or group to take action based on its content.

The Utah Department of Natural Resources, Utah Geological Survey, makes no warranty, expressed or implied, regarding the suitability of this product for a particular use. The Utah Department of Natural Resources, Utah Geological Survey, shall not be liable under any circumstances for any direct, indirect, special, incidental, or consequential damages with respect to claims by users of this product.

TABLE OF CONTENTS

EXECUTIVE SUMMARY 1

INTRODUCTION 2
Purpose of Study and Research Objectives 2
Acknowledgements 2

REGIONAL GEOLOGICAL SETTING 3
Structural Framework 4
The Ancestral Rocky Mountains and the Uncompahgre Uplift 4
Basin Formation 5
Salt Structures and Geometries 9
Stratigraphic Framework 10
Pennsylvanian 14
Hermosa Group (Atokan – Virgilian) 14
Paradox Formation (Desmoinesian) 14

EVAPORITE DEPOSITIONAL CYCLES AND ENVIRONMENTS, REGIONAL CORRELATIONS, CLASTIC INTERBEDS AND SALT (HALITE) LITHOLOGIES 15
Evaporite Cycles and Regional Correlations 15
Clastic Zone Interbeds 22
Anhydrite (Transgressive) 22
Silty Dolomite (Transgressive) 25
Black Shale (Transgressive and Regressive) 26
Silty Dolomite (Regressive) 28
Anhydrite (Regressive) 29
Sandstone and Turbidities 29
Halite Beds 30

CLIMATE CONTROLS ON EVAPORITE CYCLICITY 30
Evaporites and Climate 30
Global Climate During the Pennsylvanian 31
Pennsylvanian Cyclicity and Climate Controlled Sedimentation 32

WELL AND OUTCROP DATA ANALYSIS 34
General Well Information 34
Well Logs 35
Core 36
Outcrop 36
Mud Logs 37
QEMSCAN Samples 37
QEMSCAN Analysis 40
Transgressive and Regressive Comparisons 40
Basin Correlation 40
Grain Size, Grain Density and Porosity Estimates 49

EVAPORITE CYCLE ISOPACH MAPS AND ANALYSIS 50
Isopach Map Suite 50
Map Analysis and Observations 50
Mapping Problems and Potential Sources of Error 76

DISCUSSION 78
Pennsylvanian Cyclicity of the Northern Paradox Basin – Paradox Formation 78
Sequence Stratigraphy and Palynomorphs: Relating to Milankovitch Periodicity .. 79
Comparing Sequence Stratigraphy and Palynomorph Cycle Boundaries 79
Paradox Formation – Depositional Age and Timing 80
Sedimentation Rates 81
Total Age of the Paradox Formation 81
Age Per Depositional Cycle 82
Subsidence 84
The Formation and Timing of the Uncompahgre Uplift and Paradox Basin 84
The Uncompahgre Uplift and its Impact on the Northern Paradox Basin 85
Uncompahgre Uplift – Unanswered Questions 86
Early Clastic Sediment Supply 88
Paradox and Uncompahgre Uplift Formation Model Comparison 88
The Paradox Basin: A Pull-apart Basin 88
The Paradox Basin: A Flexural Model 89
The Paradox Basin and Eagle Valley Evaporites – A New Perspective 90
Late Paleozoic Glacial Evidence on the Uncompahgre Plateau 91
Hydrocarbon Exploration – Economic Potential 92
Carbonate Reservoirs 29
Fine Grained Sands – Turbidites 92

CONCLUSIONS AND RECOMMENDATIONS 92
Periodicity and Mechanisms Involving Pennsylvanian Cyclicity – Paradox Formation 92
Basin Formation and the Evolution of the Uncompahgre Uplift 93
Recommendations for Future Work 94
REFERENCES 96

LIST OF TABLES

Table 1: Location data for the five samples used for QEMSCAN analysis 40
Table 2: Mineral assemblage % for the five QEMSCAN samples 46
Table 3: Depositional rates for each lithology within an ideal evaporite cycle 81
Table 4: Age estimates for the Paradox Formation for 10 wells based on calculations using lithology thicknesses and sedimentation rates 82
Table 5: Estimated sedimentation rates and age duration of deposition for evaporite cycle 2 of the Coors Energy, Coors USA 1-10LC well 83

LIST OF FIGURES

Figure 1: Map illustrating the structural features and highlands in and around the Paradox Basin 3
Figure 2: Map of western North America illustrating several Paleozoic and Mesozoic tectonic features 4
Figure 3:Index map of the northern Paradox Basin showing important well locations and cross-section A-A' 6
Figure 4: Seismic line A-A' showing the position of the Uncompahgre fault zone over what are interpreted as Paleozoic rocks 7
Figure 5: Generalized cross section of the northern Paradox Basin including the fault system of the Uncompahgre Front 8
Figure 6: Map showing the location of the Eagle Basin and the Eagle Valley evaporates 9
Figure 7: Barbeau's flexural model of the Paradox Basin 10
Figure 8: Structural features of the northern Paradox Basin 11
Figure 9: Generalized column illustrating the stratigraphic units in the northern Paradox Basin 12
Figure 10: Correlation chart for Precambrian through Tertiary rocks of the Paradox Basin 15
Figure 11: Isopach map totaling all of the Pennsylvanian and Permian strata within the Paradox Basin 16
Figure 12: Structure contour map of the top of the Pennsylvanian Paradox salt 17
Figure 13: Map showing the location of Paradox sedimentation and the three major water entryways into the basin 18
Figure 14: Isopach map of the Paradox Salt 19
Figure 15: Isopach map totaling all of the Pennsylvanian and Permian strata within the Paradox Basin 20
Figure 16: Mississippian through Permian correlation chart of the Paradox Basin 21
Figure 17: Facies stratigraphy of evaporite cycle 2 from the Cane Creek No. 1 core 22
Figure 18: A type log from the Coors Energy Coors USA 1-10LC well highlighting the clastic interval of evaporite cycle 3 23
Figure 19: Regional correlation of facies from an idealized evaporite cycle found in the northern half of the basin, to a carbonate cycle typically found further south in the basin 23
Figure 20: Index map showing the locations of several prominent oil/gas fields, uplifts, monoclines, anticlines and three well locations in the southern Paradox Basin 24
Figure 21: A diagrammatic section from north to south across the Paradox Basin 25
Figure 22: Diagram showing the relationship between greenhouse (periods of little to no polar ice) and icehouse (periods where polar ice exists) conditions, global CO_2 and eustasy 33
Figure 23 First and second order cycles of relative sea-level change during the Phanerozoic 34
Figure 24: Chart showing the stratigraphic orders and cycle sequences and associated nomenclature, duration and area of effect 35
Figure 25: Map showing the location of the caprock outcrop used for field study and sample collection along Onion Creek in the middle of the Onion Creek salt wall 37
Figure 26: A clastic interbed overlain by caprock located along the Onion Creek salt

wall 38
Figure 27: An example of a black shale overlain by a silty dolomite 38
Figure 28: A fine-grained, fractured, laminated sandstone about 10 feet (3.05 m) thick near the edge of the caprock exposure, Onion Creek salt wall, Utah 39
Figure 29: Mineral compilation for transgressive sample 2184.0 (ft) (cycle 2) using a 25 µm measurement spacing 41
Figure 30: Mineral compilation for transgressive sample 2446.1 (ft) (cycle 3) using a 25 µm measurement spacing 42
Figure 31: Mineral compilation for regressive sample 2134.8 (ft) (cycle 2) using a 25 µm measurement spacing 43
Figure 32: Mineral compilation for regressive sample 2377.1 (ft) (cycle 3) using a 25 µm measurement spacing 44
Figure 33: Figure graphically showing the mineral assemblage for the five QEMSCAN analyzed samples 45
Figure 34: Mineral compilation for the Onion Creek outcrop sample using a 25 µm measurement spacing 47
Figure 35: Mineral assemblage for all five samples using a 10 µm measurement spacing .. 48
Figure 36: Graph and table displaying the average grain size distribution for all five QEMSCAN analyzed samples 49
Figure 37: Graph and table displaying the grain density distribution for all five QEMSCAN analyzed samples 50
Figure 38: Comparison pyrite content, zircon content and grain density for the five QEMSCAN analyzed samples 51
Figure 39: Graph and table displaying the estimated porosity for all five QEMSCAN analyzed samples 52
Figure 40: Isopach map of evaporite cycle 29 within the Paradox Formation 53
Figure 41: Isopach map of evaporite cycle 28 within the Paradox Formation 54
Figure 42: Isopach map of evaporite cycle 27 within the Paradox Formation 55
Figure 43: Isopach map of evaporite cycle 26 within the Paradox Formation 56
Figure 44: Isopach map of evaporite cycle 25 within the Paradox Formation 57
Figure 45: Isopach map of evaporite cycle 24 within the Paradox Formation 58
Figure 46: Isopach map of evaporite cycle 23 within the Paradox Formation 59
Figure 47: Isopach map of evaporite cycle 20 within the Paradox Formation 60
Figure 48: Isopach map of evaporite cycle 17 within the Paradox Formation 61
Figure 49: Isopach map of evaporite cycle 13 within the Paradox Formation 62
Figure 50: Isopach map of evaporite cycle 12 within the Paradox Formation 63
Figure 51: Isopach map of evaporite cycle 11 within the Paradox Formation 64
Figure 52: Isopach map of evaporite cycle 10 within the Paradox Formation 65
Figure 53: Isopach map of evaporite cycle 9 within the Paradox Formation 66
Figure 54: Isopach map of evaporite cycle 8 within the Paradox Formation 67
Figure 55: Isopach map of evaporite cycle 7 within the Paradox Formation 68
Figure 56: Isopach map of evaporite cycle 6 within the Paradox Formation 69
Figure 57: Isopach map of evaporite cycle 2 within the Paradox Formation 70
Figure 58: Isopach map of evaporite cycle 1 within the Paradox Formation. 71
Figure 59: Map showing the location of cross sections A-A', B-B' and C-C' 72
Figure 60: Well cross section A-A' 73

Figure 61: Well cross section B-B' 74
Figure 62: Well cross section C-C' 75
Figure 63: A paleogeographic and isopach map of the Honaker Trail Formation 77
Figure 64: Diagram showing the comparison between third order cycle boundaries identified by Weber *et al*. (1995) and palynomorph biostratigraphic zones recognized by Rueger (1996) 80
Figure 65: Map showing the total age duration estimate for the depositional units within the Paradox Formation 83
Figure 66: A schematic diagram illustrating the possible progression of the Uncompahgre Uplift throughout Desmoinesian time 86
Figure 67: Map showing the location of the GCRL Energy Ltd. Seismosaur Federal #1 well 87
Figure 68: Figure and map showing the location and strata of Unaweep Canyon 91
Figure 69: Map showing the location of the Paradox Basin #1 well 94
Figure 70: Illustration of the expected lithologies encountered by the Golden State Resources Paradox Basin #1 well 95

LIST OF APPENDICES

Appendix A: Well database A-1
Appendix B: Isopach maps B-1
Appendix C: Evaporite cycle age estimates C-1

EXECUTIVE SUMMARY

Evaporitic cycles are found throughout the Paradox Formation of the Pennsylvanian Hermosa Group and comprise at least 29 defined cycles containing siliciclastic as well as evaporitic facies. Each cycle can consist of black shale, dolomite, anhydrite and halite. Potash is also very commonly associated with the halite facies. There is now significant evidence from both well and field data of sandstone beds within the clastic cycles of significant thickness.

The purpose of this study is to correlate and map the distribution of poorly understood clastic cycles across the northern part of the Paradox Basin. The deliverables include core and field sample descriptions, an integrated well database, and isopach maps.

The results of this study allow us to critically assess the currently accepted depositional models for the Paradox Formation. The cyclicity observed within the Paradox Formation is the result of several related factors including regional and local tectonics, subsidence, sediment availability and supply, climate, and finally glacio-eustatic sea-level fluctuations.

Stratigraphic rock relationships and palynomorph data indicate there are five, third-order sequences comprising the Paradox and lower Honaker Trail formations. Therefore, we interpret that each individual evaporite cycle was deposited as a fourth-order sequence having 100,000 – 500,000 year duration. Indisputable evidence that Milankovitch cyclicity solely controlled the cyclic depositional patterns observed in the Paradox Basin is currently unavailable. However, it is clear that orbitally forced cycles strongly influenced sedimentation within the evaporite sequences.

Age estimates for the entire Paradox Formation are highly subjective to the thickness and lithology types of the clastic zones. Greater thicknesses within the clastic zones (particularly within the black shales and dolomites) indicate longer depositional episodes and thus provide further indication about sediment source and supply.

Isopach maps of individual evaporite cycles clearly illustrate the northern Paradox Basin formed due to several dynamic processes. The maps suggest the basin was somewhat tectonically active even before Pennsylvanian time. They also indicate there could have been salt movement as early as the end of the Desmoinesian farther to the east as a result of early Cutler deposition (and resultant differential sediment loading).

The northern Paradox Basin experienced an 8 million year period (308 – 300 Ma) of relatively rapid subsidence. The Uncompahgre Uplift was slower to develop in the northern Paradox Basin compared to the San Luis Uplift farther to the south. However, even though the Uncompahgre was not significantly elevated until near the end of the Pennsylvanian, it subtlety influenced depositional patterns and was accompanied by significant basin subsidence. Further evidence of early-eroded arkosic material suggests the Uncompahgre went through several stages or pulses of uplift with the largest occurring near the end of Desmoinesian time.

Several models propose different evolutionary scenarios for the Uncompahgre Uplift/Paradox Basin systems. From the results of this study, it seems reasonable to conclude that the Paradox and Eagle basins were connected during the initial cycles of salt deposition. However, the Uncompahgre started to uplift soon thereafter, and the flexural response to this uplift led to increasing accommodation and the development of a foredeep in an evolving foreland basin.

Age estimates of the Paradox Formation support conclusions that the eastern half of the basin is much older, deeper, and started to develop earlier than the rest of the basin (possibly starting in Late Atokan or Early Desmoinesian time).

During Paradox Formation deposition, the two main sources of sediment supply into the basin were the Uncompahgre Uplift to the east, and the San Luis Uplift near the southern margin of the basin. Evidence suggests both sources added substantial material into the depths of the basin. However, once the Uncompahgre became a strongly positive structure it had by far a greater impact on clastic supply, at least in the northern half of the basin.

INTRODUCTION

The Paradox Basin, located in southwestern Colorado and southeastern Utah, is generally defined by the regional extent of Pennsylvanian age evaporites. Diapiric salt walls that trend northwest-southeast parallel the Ancestral Rocky Mountain Uncompahgre Uplift (located on the northeastern margin of the basin) characterize the northern part of the basin.

Evaporites are found in the Paradox Formation of the Pennsylvanian Hermosa Group and comprise at least 29 well-defined cycles containing siliciclastic, as well as evaporite facies. Each cycle typically consists of black shales, silty dolomites, anhydrite and halite and often contains significant amounts of hydrocarbons. The cycles are the result of relative and eustatic sea-level fluctuations combined with local tectonics, climate, sediment supply, and rapid subsidence.

The important relationship between the Paradox Basin and the Uncompahgre Uplift is not fully understood. Without much agreement, many previous authors have suggested different models involving the timing and formation of the uplift relative to the basin subsidence. Therefore, a better understanding of the structural and stratigraphic associations between the Uncompahgre Uplift and the Paradox Basin is important, as it relates directly to the reservoir characterization of the Paradox Formation clastic intervals.

Purpose of Study and Research Objectives

This study is intended to map and correlate the evaporite facies within the Pennsylvanian Paradox Formation throughout the northern Paradox Basin. This includes correlating individual evaporite cycles and their respective clastic zones. The resulting associations are used to better understand the cyclicity of the Paradox Formation and its relationship to the structural development and evolution of the Ancestral Rocky Mountain Uncompahgre Uplift.

The specific research objectives for this study are:

- Create subsurface isopach maps for the individual evaporite cycles of the Paradox Formation,
- Correlate cycles and cycle boundaries across the study area,
- Calculate depositional age estimates used to determine duration, length, and total age of each cycle,
- Describe the petrology of samples from selected clastic intervals,
- Characterize and understand the clastic material within the evaporite cycles and attempt to distinguish the provenance of such materials,
- Compare the Paradox evaporite cycles to other Pennsylvanian cyclothems in an attempt to determine the influence of glacio-eustatic cyclicity on Paradox deposition, and
- Analyze cycle thickness with relationship to the proximity of the Uncompahgre Uplift. Such comparison helps understand the timing and evolution of the Uncompahgre.

Acknowledgments

This study was partly funded by the Utah Geological Survey whom we gratefully thank. We would also like to thank the Advanced Mineralogy Research Center at the Colorado School of Mines for performing the mineralogy analysis. Gary Nydegger and Chuck Kluth are thanked for stimulating discussion on the evolution of the Paradox Basin.

REGIONAL GEOLOGICAL SETTING

The Ancestral Rocky Mountains correspond to a series of uplifted continental basement blocks in the western United States. These uplifts are separated by a series of basins filled mostly by syn-orogenic coarse-grained deposits of Pennsylvanian-Permian age. Located in the center of the Colorado Plateau, the Paradox Basin is one of these depressions; it is a large (265 km x 190 km) asymmetric basin developed along the southwestern flank of the Uncompahgre Uplift (Figure 1). The boundaries of the basin to the west have commonly been defined by the extent of salt deposited during Pennsylvanian time (Figure 1). The Paradox Basin is part of the present day Colorado Plateau and is a roughly oval shaped area located in southwestern Colorado and southeastern Utah.

The basin lies adjacent to the

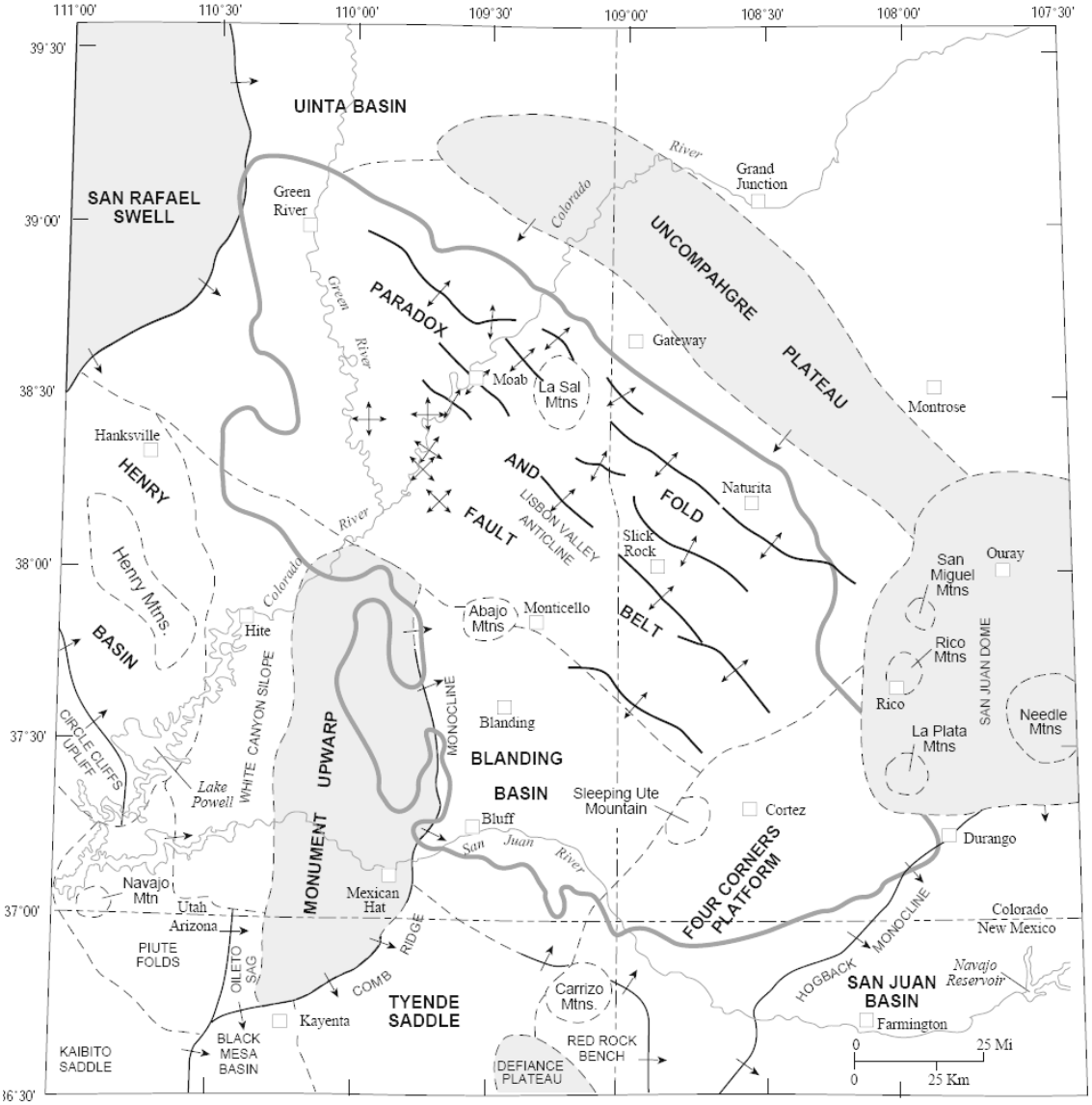

Figure 1: Map illustrating the structural features and highlands in and around the Paradox Basin. The La Sal, Abajo, Sleeping Ute and La Plata mountains are igneous intrusive centers all of Tertiary age. The solid gray outline marks the maximum extent of salt within the Paradox Basin (after Nuccio and Condon, 1996).

southwestern margin of the Uncompahgre Uplift and to the east of the San Juan Dome (Figure 1). The southeastern edge of the basin is bordered by a lineament named the Hogback monocline and thus the San Juan Basin (Stevenson and Baars, 1986). The south and southwestern sides are generally structurally uncontrolled as the basin edge follows the Four Corners Lineament and crosses the Monument Upwarp where it almost reaches the Henry Mountains (Figure 1). The basin then extends northwest to the San Rafael Swell and associated lineament. Finally, the northern boundary of the basin extends just south of the Uinta Basin but is influenced by several structural features including the Uncompahgre Uplift (Figure 1) (Stevenson and Baars, 1986; Condon, 1995).

The tectonic mechanism responsible for the formation of the Paradox Basin is highly controversial. One of the main theories envisions a pure pull-apart basin caused by strike-slip motion and associated extension and rotation along Pennsylvanian basement faults. Another concept models the basin as a flexural depression directly associated with the rise of the Uncompahgre Uplift. Definite conclusions on basin formation are difficult because of the structural complexity near the uplift. Salt tectonic activity has also hampered the ability to reconstruct the basin evolution during the critical Pennsylvanian Period.

Structural Framework

The Paradox Basin is structurally complex. Basin evolution was the result of a combination of the Uncompahgre Uplift evolution, salt evacuation and an underlying complicated basement framework.

The Ancestral Rocky Mountains and the Uncompahgre Uplift

The Ancestral Rocky Mountains (ARM) are a series of Pennsylvanian uplifts and

Figure 2: Map of western North America illustrating several Paleozoic and Mesozoic tectonic features. The deformation in this region during Pennsylvanian time was apparently the result of a continent to continent collision between the southwestern part of North America and South America – Africa (Kluth, 1986; image modified from Blakey, 2007).

associated basins in what is now the south and western United States (Figure 2).

The timing and orientation of the ARM are thought to be a response to an intraplate orogenic event called the Ouachita – Marathon Orogeny (Kluth, 1986). This event is the result of a continent to continent collision suturing the southern margin of North America with South America – Africa. Suturing and uplifting started during the late Mississippian and continued through early Pennsylvanian time but slowed in the Permian (Raup and Hite, 1992; Kluth, 1986). Basins or troughs, genetically related to the uplifts separate many of the ARM ranges. The Paradox Basin is one of these depressions and lies adjacent to the southwestern flank of the ARM Uncompahgre Uplift (Figure 1).

The Uncompahgre Uplift trends northwest-southeast and is along the northwest flank of the Transcontinental Arch (Figure 2) (Maughan and Perry, 1986). It is roughly 30 miles (48 km) wide and 100 miles (160 km) long and extends from near Ridgeway, Colorado to the Cisco Dome, Utah (Figure 1) (Cater, 1970). Uplift of the Uncompahgre began as early as Atokan time, but may have been restricted to the very southeastern extent of the uplift (more involving the San Luis Uplift). However, by the Late Desmoinesian time, massive amounts of coarse arkosic material were being shed from the uplift in the northwestern half of the basin (Baars and Stevenson, 1981). This significant uplift event and erosional pattern continued into the Permian.

The southwestern edge of the uplift is defined by the Ridgeway thrust fault or fault system. Near Gateway, Colorado this fault system displays nearly 26,000 feet (7,900 m) of offset between the deepest part of the Paradox Basin and the Uncompahgre Uplift (Stevenson and Baars, 1986). Several deep wells (encountering Mississippian strata and older) have been drilled in the very northeast part of the basin.

The No. 1 McCormick Federal “C” well, located northwest of Cisco, Utah, drilled to a total depth of 19,302 feet (5,883 m) (Figures 3, 4 and 5). After 3,600 feet (1,097 m) of Mesozoic strata, the well continued to drill through about 14,000 feet (4,267 m) of granitic basement before penetrating the Uncompahgre fault zone followed by 1,702 feet (59 m) of Paleozoic rocks (Frahme and Vaughn, 1983). The moderate angle reverse fault has a dip of around 50° – 55° to the northeast and displays over 14,000 feet (4,267 m) of offset (White and Jacobson, 1983). Figure 4 is an interpreted northeast-southwest trending seismic line roughly through the well. Figure 5 is a generalized cross section across the same line.

Basin Formation

There are numerous theories as to how and why the Paradox Basin formed. In the past, it has been referred to as a tectonic depression but, this failed to consider timing and structural tectonics. Stevenson and Baars (1986) believe the basin formed due to pull-apart tectonics, while Kluth (1986) believes the development of the Paradox Basin and Uncompahgre Uplift are associated with the collision of North America and South America – Africa resulting in the Ouachita – Marathon Orogeny. This suturing event formed a series of intracratonic block uplifts (ARM) and related basins like the Uncompahgre Uplift and Paradox Basin, respectively; the margins between uplift and basin generally display significant vertical movement along faulted structural boundaries.

Further investigation by Kluth and DuChene (2006) postulated that the Paradox and Eagle Valley (central western Colorado, Figure 6) basins were connected before the rise of the Uncompahgre Uplift. They discussed how sediment loading from the Permian Cutler Formation caused the

evaporites of the Pennsylvanian Paradox Formation to evacuate and form diapiric walls. These salt structures grew by down-building of adjacent depocenters. Therefore, the early development of the Paradox Basin itself was not connected to the formation of the Uncompahgre Uplift.

Barbeau (2003) interpreted the Paradox Basin as an intraforeland flexural basin. He suggested the Paradox Basin formed due to flexural subsidence associated with the ARM Uncompahgre Uplift based on the subsidence history, shape, structural relationships and facies architecture of the basin.

This model uses the idea of a foredeep zone that formed adjacent to the uplift as a

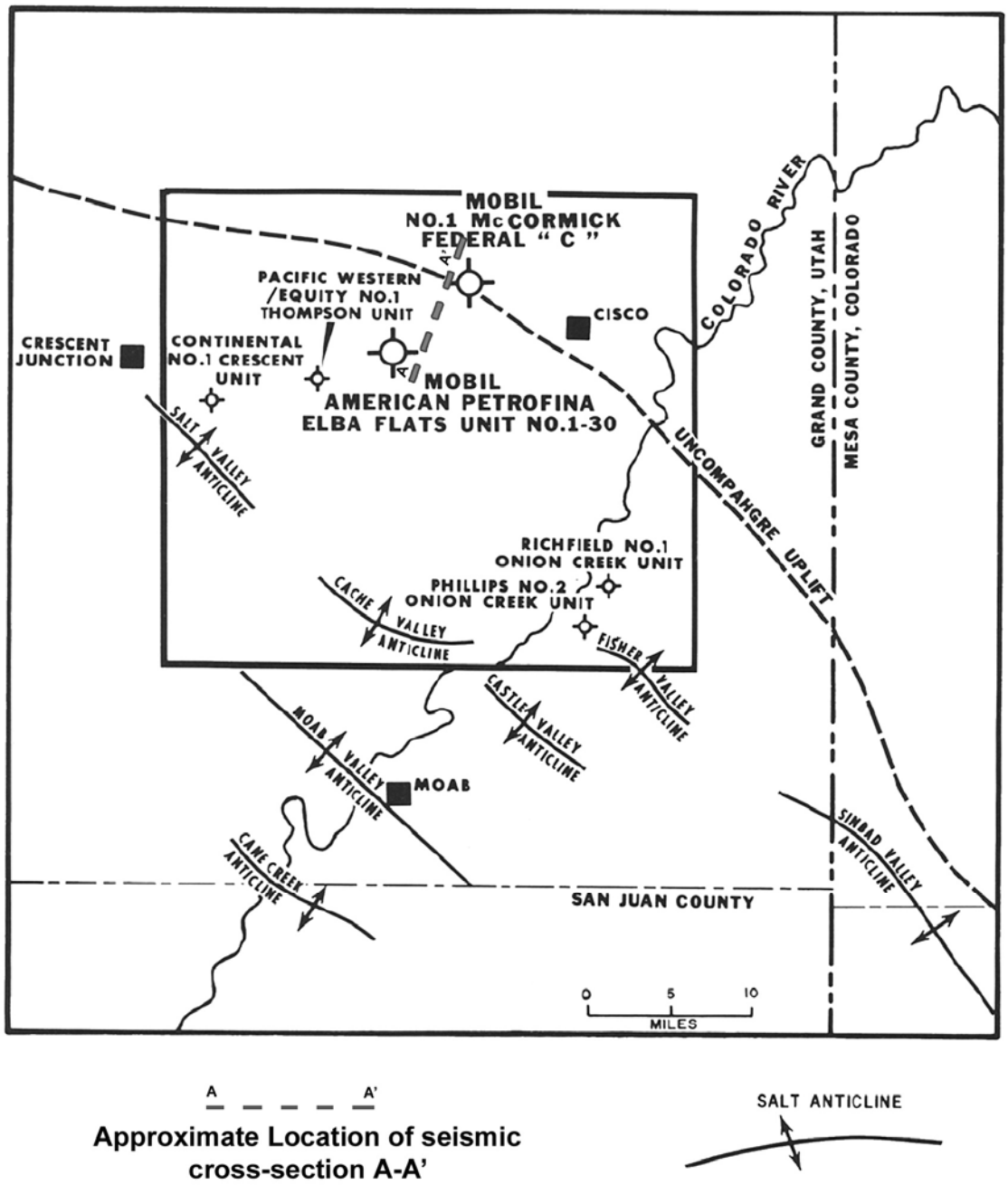

Figure 3: Index map of the northern Paradox Basin showing important well locations and cross section A-A' (modified after Frahme and Vaughn, 1983).

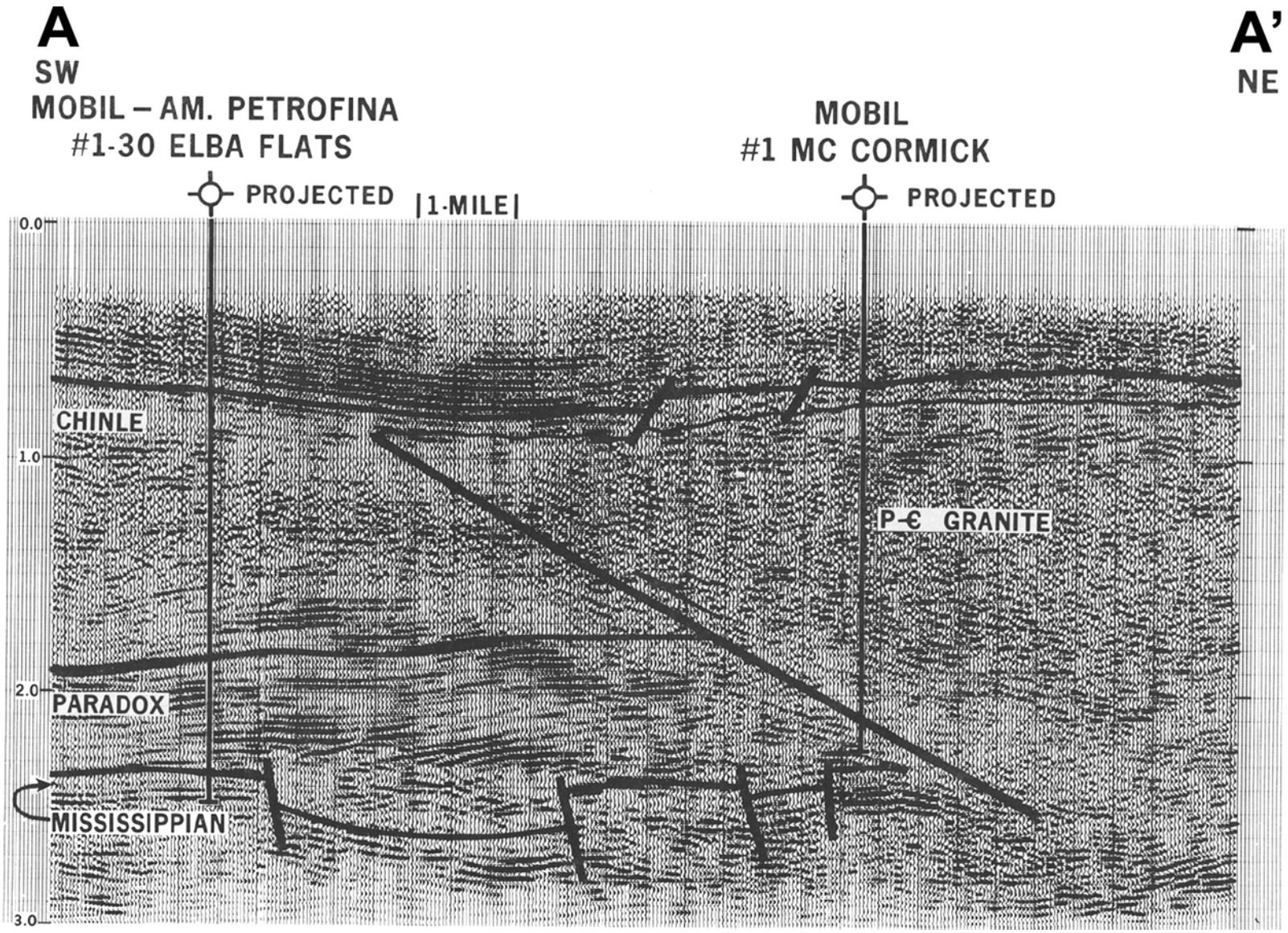

Figure 4: Seismic line A-A' showing the position of the Uncompahgre fault zone over what is interpreted as Paleozoic rocks (modified after Frahme and Vaughn, 1983).

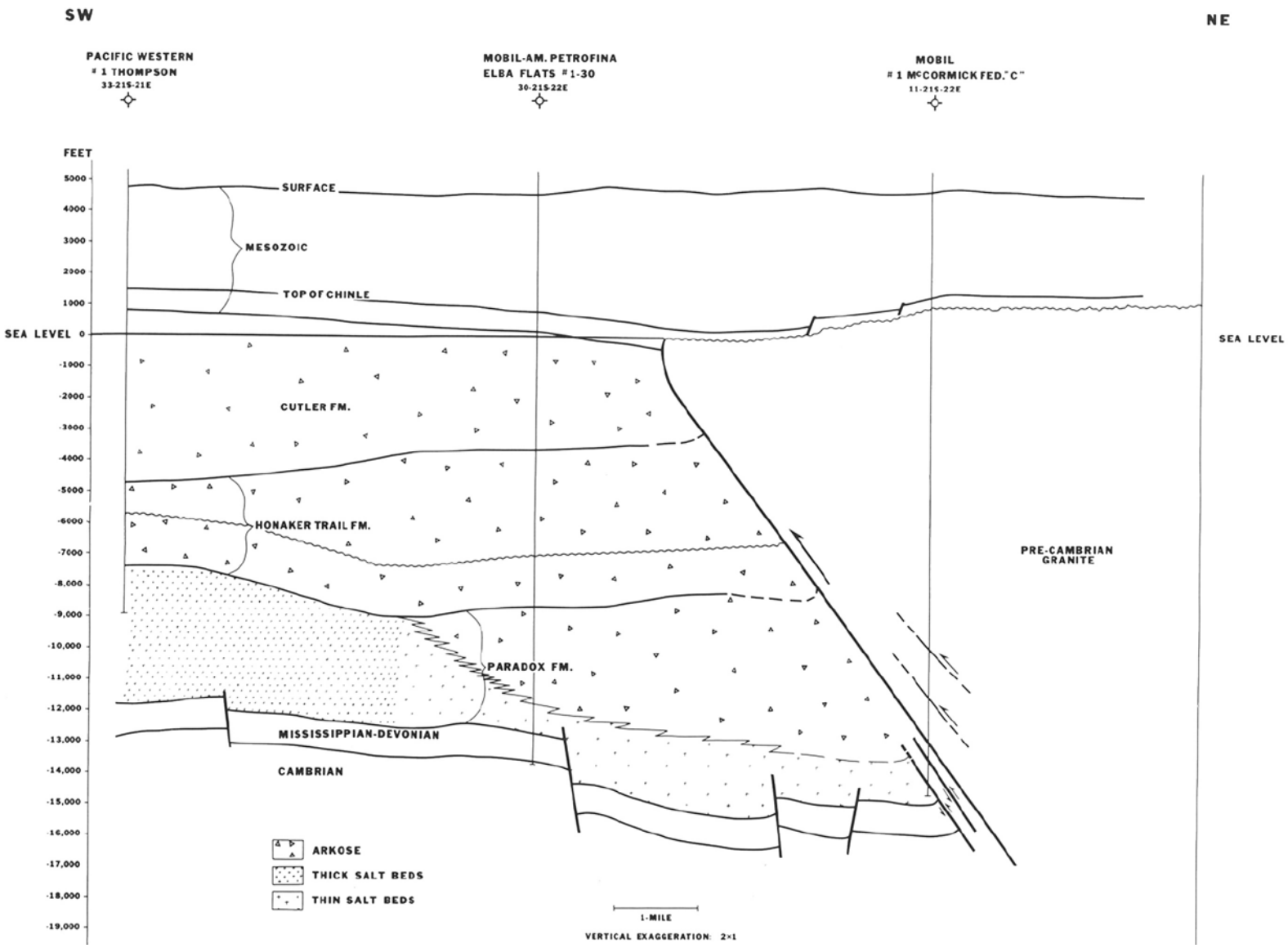

Figure 5: Generalized cross section of the northern Paradox Basin including the fault system of the Uncompahgre Front. The cross section is roughly along the seismic line A-A' seen in Figure 4 (after Frahme and Vaughn, 1983).

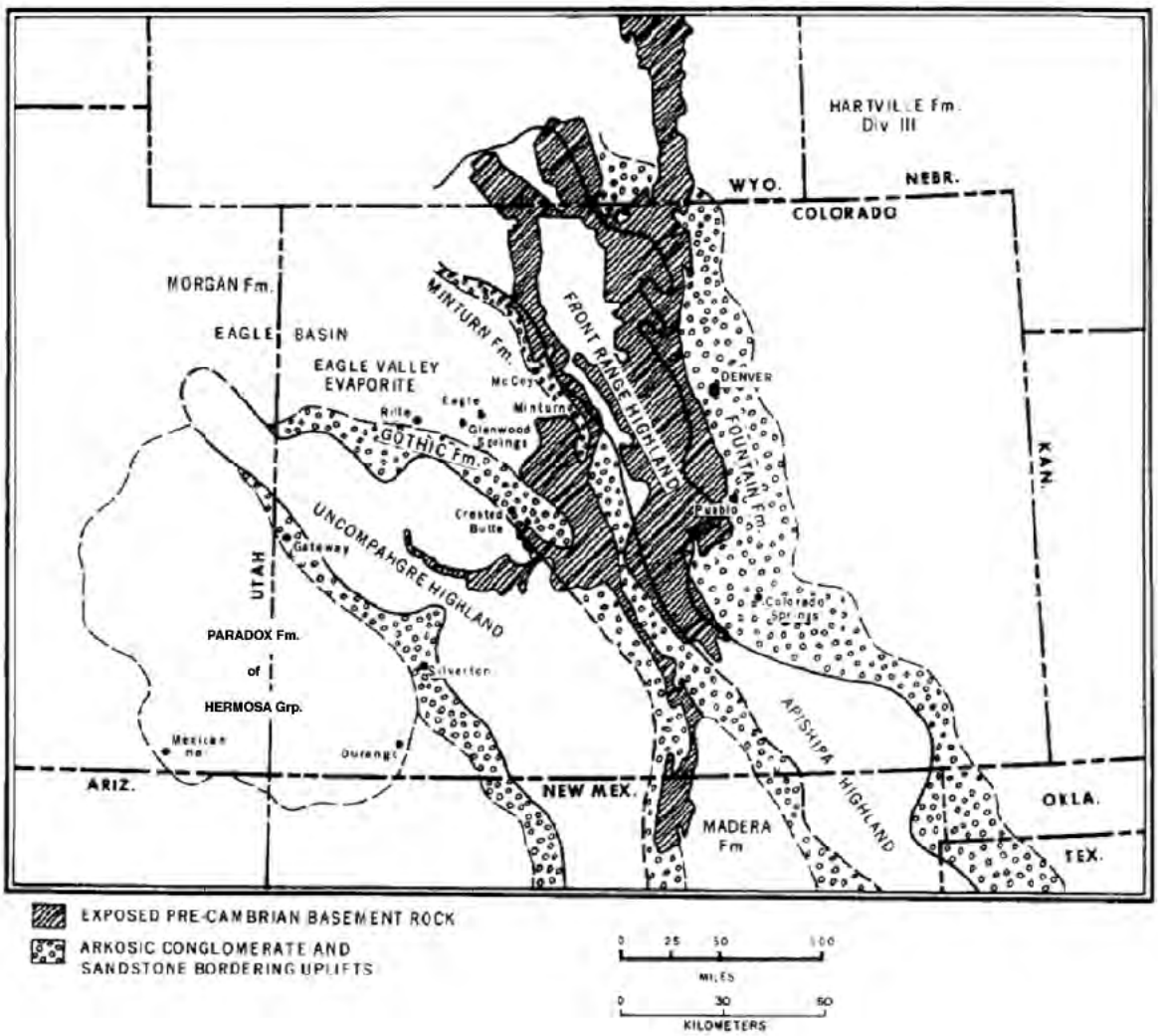

Figure 6: Map showing the location of the Eagle Basin and the Eagle Valley evaporites (after Tillman, 1971).

response to the crustal flexure of the Uncompahgre thrust (Figure 7). Because of this flexure, Barbeau (2003) also suggested a positive crustal rebound structure called a forebulge that is thought to be associated with the carbonate shelf that rims the south and southwestern edges of the basin.

Salt Structures and Geometries

The northern Paradox Basin is home to a variety of salt structures ranging from complex faulted diapirs and exposed salt walls to buried salt pillows (Figure 8). The area is commonly referred to as the "Paradox fold and fault belt" (Kelley, 1955; Kelley, 1958) and overlies the deepest section of the basin. Here depositional salt thicknesses ranged between 5,000 feet (1,500 m) and 8,000 feet (2,400 m) (Baars and Stevenson, 1981).

Salt structure geometries vary across the basin from northeast to southwest. The most striking features are the prominent salt walls or collapsed anticlines commonly referred to as "salt valleys". The Salt Valley Anticline, Onion Creek diapir/Fisher Valley salt structure and the Sinbad Valley Anticline are all located close to the Uncompahgre Uplift. Moving farther to the southwest are the smaller Castle Valley and Moab/Spanish Valley anticlines. It is important to note that

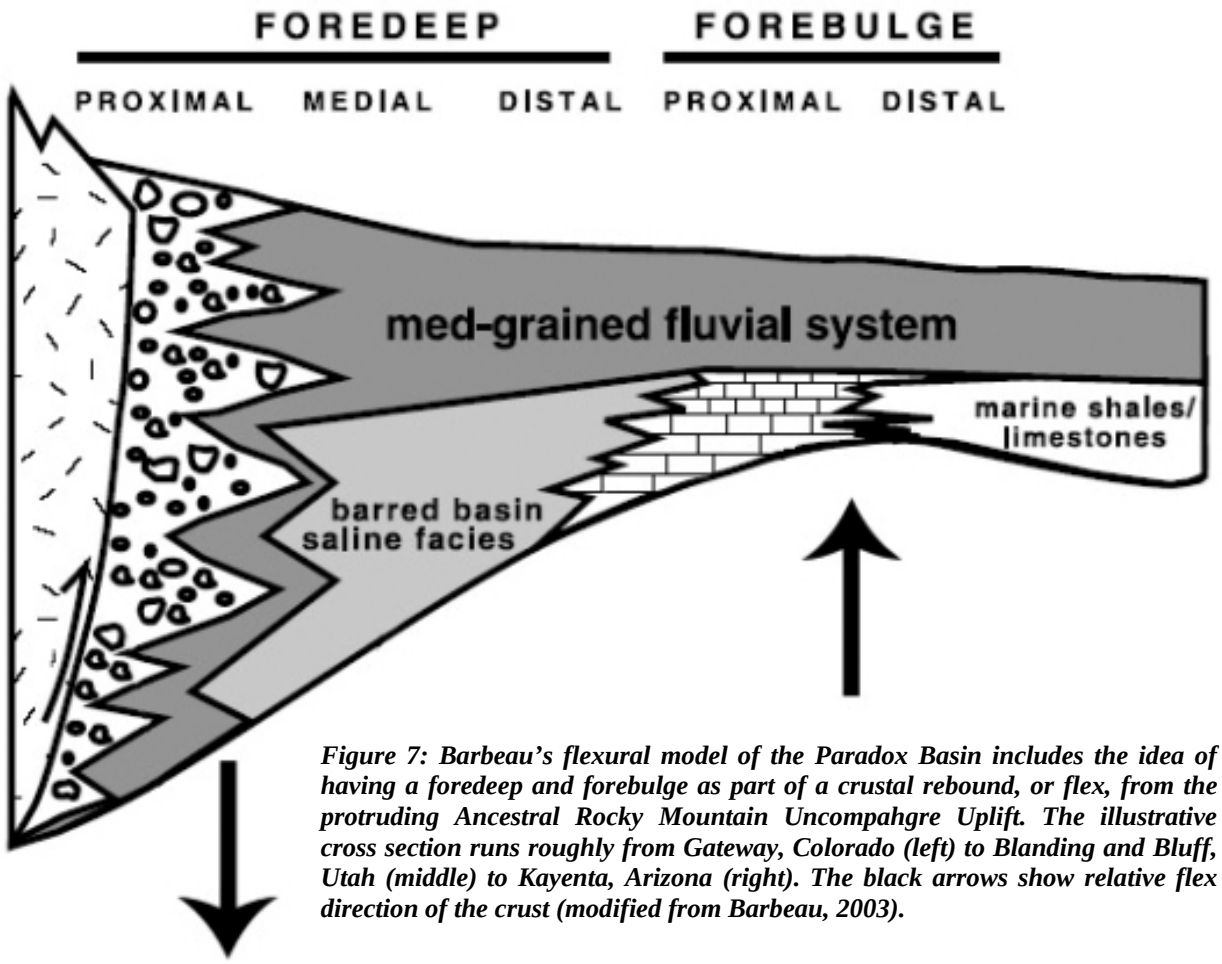

Figure 7: Barbeau's flexural model of the Paradox Basin includes the idea of having a foredeep and forebulge as part of a crustal rebound, or flex, from the protruding Ancestral Rocky Mountain Uncompahgre Uplift. The illustrative cross section runs roughly from Gateway, Colorado (left) to Blanding and Bluff, Utah (middle) to Kayenta, Arizona (right). The black arrows show relative flex direction of the crust (modified from Barbeau, 2003).

all of these structures trend northwest-southeast and strike parallel to the uplift. Southwest of Moab, Utah, and beyond the major salt walls, are several buried salt structures that tend to be broader and less structurally complex. The Cane Creek Anticline is an example of such a feature that is underlain by a salt pillow that gently deformed the overlying strata to create the associated anticline (Trudgill *et. al*, 2004). Many of the larger salt structures are controlled by major northwest-southeast striking basement faults positioned on the southwest boundary of the structures (Shoemaker *et al*., 1958; Cater and Elston, 1963; Joesting *et. al*, 1966). These faults proved to be an important factor in salt tectonics because they provided a lateral barrier and a vertical pathway for salt flowage (Baars, 1966).

As salt accumulated in the deeper parts of the basin, alluvial fans consisting of thick arkosic material (undifferentiated Cutler Formation) were being shed off the Uncompahgre Uplift (Baars and Stevenson, 1982). Differential sediment loading from the Cutler onto the underlying salt caused rapid salt movement away from the load of the deposited arkosic material. Jones (1959) calculated a shear strength, using geologic conditions, of less the 30 kg/cm^2 would cause salt to flow. This would be equivalent to about 1,000 feet (300 m) or less of overlying sediments.

Stratigraphic Framework

The Paradox Basin is comprised of a thick sequence of sedimentary rocks that overlie a complex series of Proterozoic basement rocks.

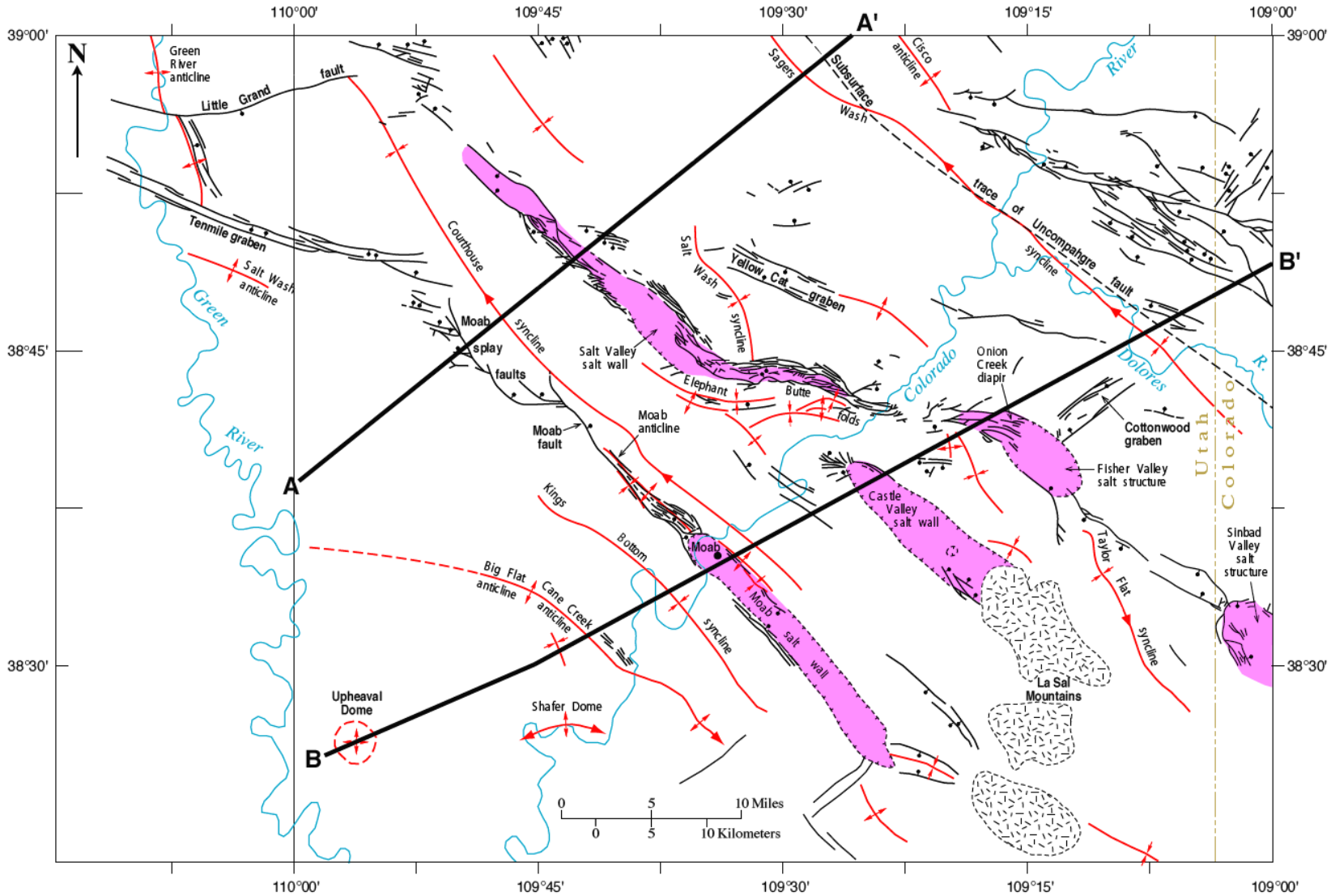

Figure 8: Structural features of the northern Paradox Basin. Near surface salt structures are highlighted in pink (after Doelling, 2001; Trudgill et. al, 2004).

Cambrian through Jurassic strata overlie basement rocks throughout most of the basin (Figures 9a, 9b, 9c, and 10) with the exception of several Tertiary igneous intrusive cores that are scattered throughout the basin.

Detailed descriptions of the stratigraphic units within the Paradox Basin are compiled in a number of publications (e.g., Baars, 1987; Nuccio and Condon, 1996). For the purpose of this study, we will confine our stratigraphic analysis to the Paradox Formation of the Hermosa Group.

	Age	Formation		Members and Other	Thickness feet (meters)	Lithology and Other
318.1 Ma	PENN.	Molas				
	MISS.	Leadville Limestone			200-600 (61-183)	Gray to cream, massive, fossiliferous limestone and brown dolomite; algal laminations, crinoid fragments, cherty intervals and oolites are common; deposited in a series of upward-shoaling cycles ranging from shallow marine tidally dominated shelf through supratidal and lagoonal.
359.2 Ma	DEVONIAN	Ouray			0-200 (0-61)	Light to dark brown, gray limestone with green and purple clay intervals; dolomite, anhydrite, pyrite, crinoid fragments and oolites are common; formed in a shallow shelf marine environment.
		Elbert Group	Upper Elbert		50-600 (15-183)	Gray, brown, dense, platy dolomite interstratified green shale and quartzite; can contain salt clasts, fish remains and stromatolites; formed in a shallow shelf marine environment.
			McCracken Sandstone		0-122 (0-37)	Gray to red, fine to medium grained, poorly sorted, glauconitic, sandstone with intervals of gray-green shale and argillaceous dolomite; some areas are bioturbated.
		Aneth			190 (58)	Brown to black, dense limestone, dolomite and shale; common anyhdrite and fish plates, scales and plant remains; may have been a transgressive deposit during normal marine conditions.
416-488.3 Ma	CAMBRIAN	Lynch Dolomite			100-1,000 (30-305)	Gray to tan to black, massive dolomite along with a thin shale unit near the top; shale partings are common; fossil evidence suggests a marine environment of deposition.
		Maxfield Limestone			570 (174)	Brown, tan, gray, dense, limestone and dolomite; contains interlaminated green micaceous, silty shales; interpreted as a marine deposit based on fossil content.
		Ophir			160-430 (49-131)	Red, gray, brown, micaceous, sand to silty shales, with several significant intervals of brown to greenish sandstone and dark bluish-gray limestone; trilobites are located in the lower member.
		Tintic Quartzite			270-2,800 (82-853)	White, green, pink, fine to medium grained, cross-bedded sandstone; minor amounts of interbedded shale and clay along with very coarse to pebbly conglomerate and abundant amounts of feldspar.
542 Ma	PRECAMBRIAN	Uncompahgre				Interlayered quartzites, phyllites and slates with very minor amounts of siltstone and conglomerate; Early to Middle Proterozoic; unknown thickness.
		Granite / Metamorphics				Many various rock types including biotitic gneisses, felsic and hornblendic gneisses, schists, granites, quartz monzonites, metavolcanics, etc; unknown thickness.

Note: No vertical scale intended. Quaternary and Tertiary rocks are ommitted from this diagram.

Figure 9a: Generalized column illustrating the stratigraphic units in the northern Paradox Basin (compiled from Stokes, 1948; Bradish and Clair, 1956; Wright et al., 1962; Molenaar, 1981, Kamola and Chan, 1988; Currie, 1998; Trudgill et al., 2004; Draut, 2005). Continued on the next two pages.

Age	Formation		Members and Other	Thickness feet (meters)	Lithology and Other
JURASSIC	S.R.G.	Carmel			
	Glen Canyon Group	Navajo Ss.		0-740 (0-226)	Tan to pink, medium grained, massive sandstone with large cross-beds; eolian and interdune; forms hummocky benches and rounded cliffs.
		Kayenta		100-300 (30-91)	Red, purple, brown, orange fine to coarse grained, irregular bedded, silty sandstone and siltstone with some shale, limestone and conglomerate.
		Wingate Ss.		250-450 (76-137)	Orange, red, brown fine to medium grained sandstone; cross-bedded; cliff forming; eolian dunes and interdunes.
199.6 Ma					
TRIASSIC	Chinle			0-1,250 (0-381)	Red, brown, purple, green clayey, silty shales with some sandstone, conglomerate, limestone and siltstone; calcareous; silicified wood and vertebrate bones; alluvial fan deposits and stream channels.
	Moenkopi			0-2,500 (0-762)	Dark brown to brown, red, sandy, silty shales; some medium grained sandstone; generally calcareous; abundant gypsum and conglomerate; deposited in shallow near shore waters (tidal flats, flood plains).
251 Ma					
PERMIAN	Kaibab Limestone			0-60 (0-18)	Shallow marine limestone and dolomite; oolites; top zone is intertidal.
	Cutler Group	De Chelly Ss.		375 (114)	Gray, tan to reddish-brown, fine to medium grained, poorly sorted sandstone.
		White Rim Ss.		0-430 (0-131)	Tan to gray, quartz rich sandstone; generally shows good cross-bedding (dunes).
		Organ Rock Sh.		800 (244)	Red to brown, sandy mudstones and siltstones; some very fine grained sandstones.
		Cedar Mesa Ss.	Undiff. Cutler	500 (152)	White to pink, fine to medium grained massive sandstone; some very large tangential cross-bedding.
		Elephant Canyon /Rico	0-3,000? (0-915)	400 (123)	Red to brown, fine grained limestone, sandstone, and shale.
					Coarse arkosic material shed from the SW flank of the Uncompahgre Uplift.
299 Ma					
PENNSYLVANIAN	Hermosa Group	Honaker Trail	Productive 'pay zones'	0-5,000 (0-1,524)	Arkosic clastics interbedded with marine black shales and gray to tan, fine, dense to porous, sandy, cherty limestones, dolomites and siltstones. Fusulinids, crinoids, gastropods, corals (solitary and colonial), trilobites, brachiopods and bryozoans can be abundant; deposited in a shallow normal marine environment with intertounging carbonate and coastal shoals.
		Paradox	Ismay, D. C., Barker Creek, Alkali Gulch; Caprock (locally exposed)	0-14,000 (0-4,267)	29 salt (halite) cycles with interbeds consisting of anhydrite, silty dolomite and black shale. Formation grades south laterally into limestone and dolomite; deposited in a restricted marine environment controlled by tectonics and sea-level change; thicknesses increase dramatically in relation to the salt walls and associated structures.
		Pinkerton Trail		100-250 (30-76)	Interbedded marine black shale, siltstone, buff to tan dolomite/limestone and anhydrite. Often cherty and fossiliferous.
	Molas			20-80 (6-25)	Red siltstones and shales interbedded with limestones, sandstones and conglomerates; abundant open marine fossils include fusulinids, foraminifera, trilobites, brachiopods, bryozoan, echnoids, ostracods and pelecypods.
318.1 Ma					
MISS.	Leadville Limestone				

Note: No vertical scale intended. Quaternary and Tertiary rocks are ommitted from this diagram.

Figure 9b: Continued.

Age	Formation	Members and Other	Thickness feet (meters)	Lithology and Other
CRETACEOUS	Mancos Shale	Juana Lopez	2,000-3,000 (610-914)	Dark gray, fissile marine shale with a few lenses of yellow sandstone and marl.
	Dakota Sandstone		0-200 (0-61)	Yellow lenticular sandstone with some conglomeratic sandstone; interbedded carbonaceous shale and impure coal.
	Burro Canyon / Cedar Mountain		50-300 (15-91)	Varicolored shales with chert, limestone, conglomerate and sandstones; terrestrial sediments.
145.5 Ma				
JURASSIC	Morrison	Brushy Basin	300-750 (100-229)	Multicolored, bentonitic mudstone with minor amounts of sandstone, conglomerate, and limestone.
		Salt Wash	200-300 (61-91)	White, gray, red sandstone and mudstone; gypsum at the base; fluvial; thin local limestone beds.
		Tidwell	10-46 (3-14)	Interbedded mudstone and sandstone; tidal flat or tidally influenced fluvial channels.
	Summerville		0-200 (0-61)	Red, gray, green siltstone, shale and sandstone; contains chert concretions and gypsum.
	San Rafael Group: Curtis		0-200 (0-61)	Gray, green, shaly sandstone that grades eastward into the Summerville and Entrada formations.
		Moab	40-65 (12-20)	Well sorted, well rounded, fine grained feldspathic sandstone, with some quartzose sandstone.
	Entrada	Slick Rock	200-320 (61-98)	Red to brown, medium to fine grained sandstone; massive; silty in some areas; partly eolian in origin.
		Dewey Bridge	50-150 (15-46)	Red, brown, sandy siltstone and silty sandstone; irregular folding; clayey.
	Carmel		0-150 (0-46)	Red, soft, sandy shales with some sandstones and mudstones; may be locally absent; marine and non-marine.
	G.C. Group: Navajo Sandstone			

Note: No vertical scale intended. Quaternary and Tertiary rocks are ommitted from this diagram.

Figure 9c: Continued.

Pennsylvanian

Hermosa Group (Atokan – Virgilian)

The Hermosa Group is comprised of three formations: the Pinkerton Trail, the Paradox and the Honaker Trail, from oldest to youngest (Figure 9b). This group consists of both marine and evaporitic sediments in the northern and central parts of the basin. To the south and southwest, abundant carbonate mounds represent the edge of the basin and have historically produced hydrocarbons.

Paradox Formation (Desmoinesian)

The Paradox Formation is the middle of three formations comprising the Hermosa Group (Figure 9b and 11). It formed due to the influence of several processes including basin subsidence, eustatic and relative sea-level fluctuations, tectonic influences, and intra-basin depositional cyclicity.

The deepest part of the Paradox Basin lies adjacent to the Uncompahgre Uplift (Figures 11 and 12) and exhibits the thickest section of the Paradox Formation. As the basin slowly subsided, open marine waters were restricted from entering the basin partly because of several uplifts rimming the basin. There were, however, several sags or sills that still allowed for some circulation including 1) a trough in the south connected to what is now the San Juan Basin, 2) from the west through the Freemont Sag, and 3) another from the

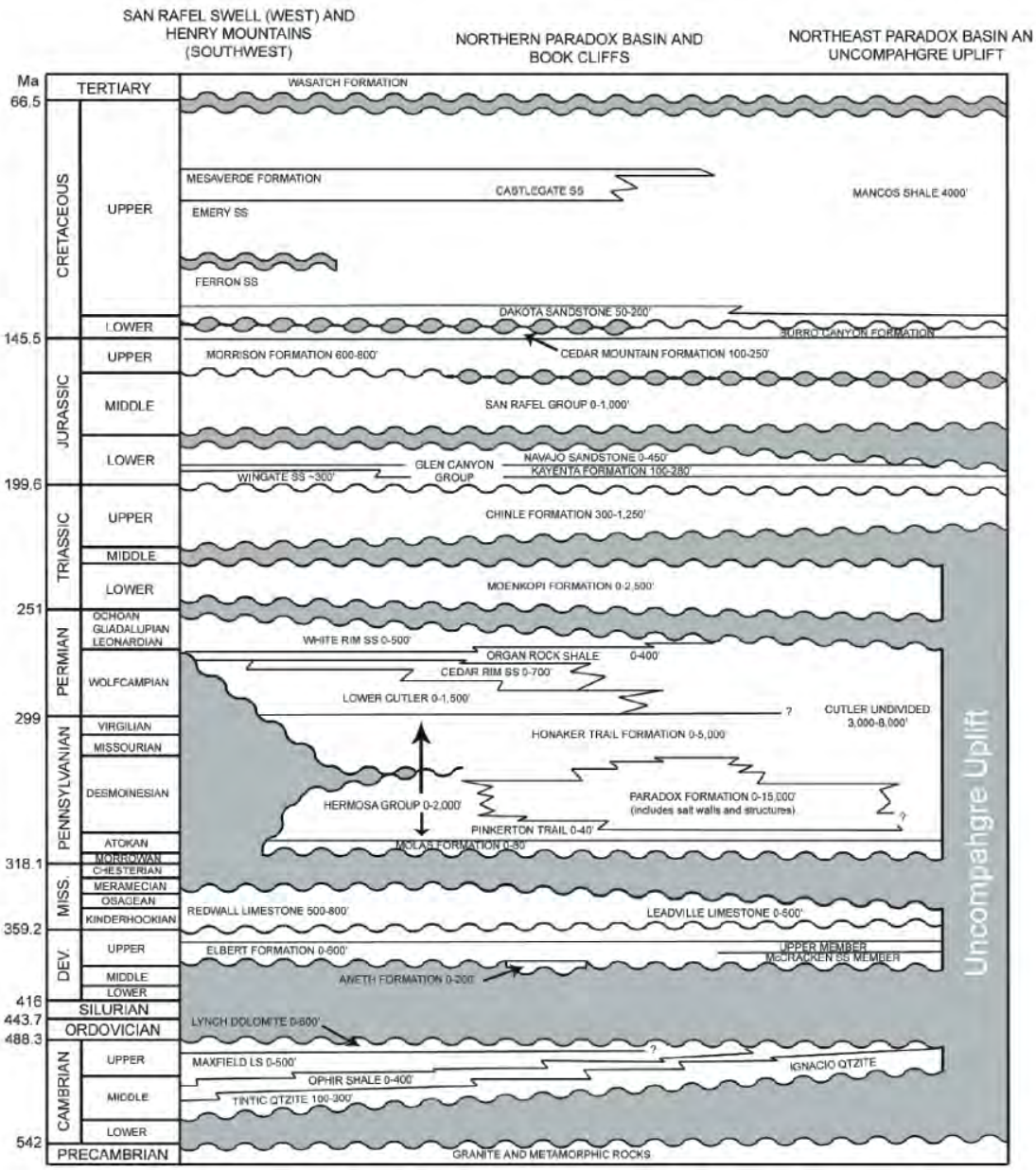

Figure 10: Correlation chart for Precambrian through Tertiary rocks of the Paradox Basin. Note the change from east to west involving the Uncompahgre Uplift and the overlying strata. Evidence from wells drilled adjacent to the Uncompahgre display the termination of Cambrian through Lower Triassic rocks against the uplift. Compiled from Molenaar (1981), Baars (1987) and Nuccio and Condon (1996).

Oquirrh Basin to the northwest (Figure 13) (Wengerd, 1962; Baars and Stevenson, 1982). The San Juan trough, or Cabezon sag, was bounded to the west by the Zuni and Defiance uplifts and to the east by the southern end of the Uncompahgre Uplift and the Nacimiento Uplift. The Oquirrh Sag was bounded to the south by the Emery Uplift, a positive structure beneath what is now the San Rafael Swell, and to the northeast by the northwestern edge of the Uncompahgre Uplift. The Freemont Sag was located between the Circle Cliffs and the Emery Uplift (Wengerd, 1962; Baars and Stevenson, 1982). Baars and Stevenson (1982) also suggest several other smaller troughs into the Paradox Basin including one

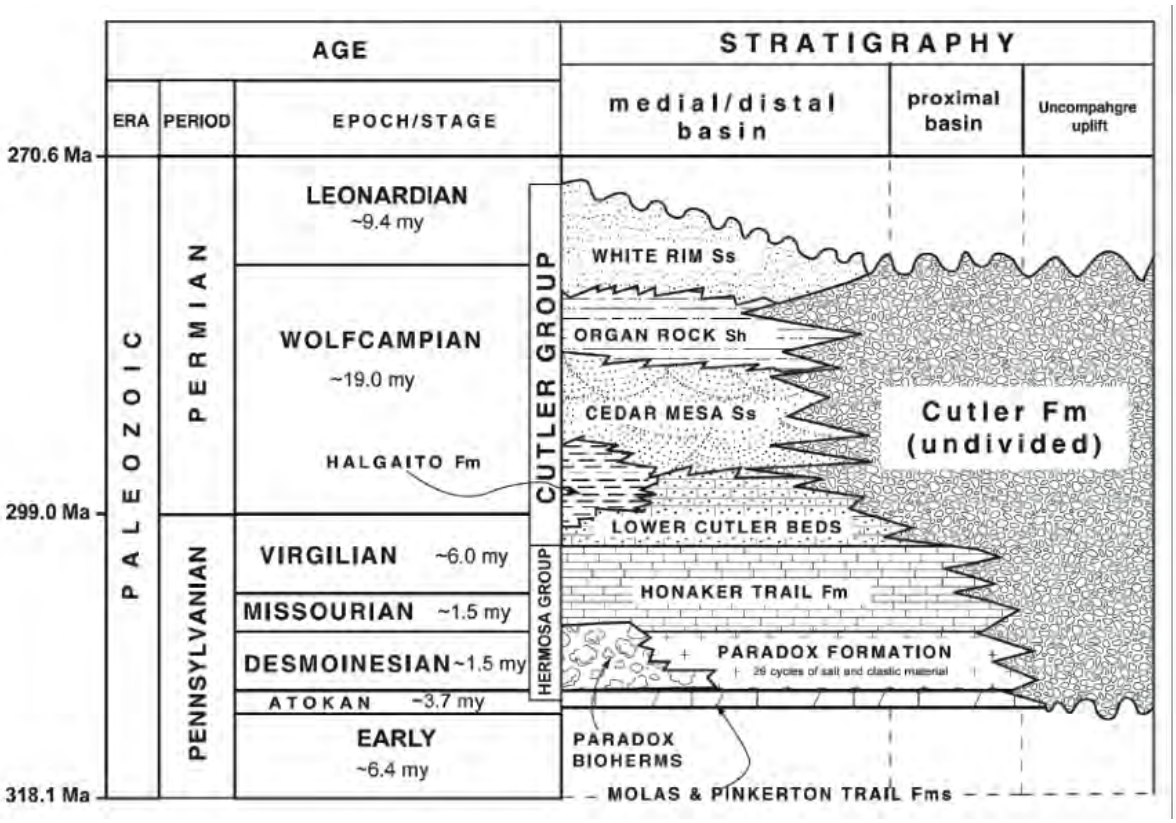

Figure 11: Stratigraphic column of the Pennsylvanian – Permian illustrating basin-fill units within the Paradox Basin (after Barbeau, 2003 and Gradstein et al., 2004).

from the southwest across what is now the Black Mesa Basin.

Due to the restriction of open marine waters along the edge of the basin, poor circulation created a stagnant evaporite depositional environment throughout much of Desmoinesian time (Baars and Stevenson, 1982). Because of these conditions, salt deposition began in the deepest area of the basin first, gradually thickening to as much as 5,000 to 8,000 feet (1,500 – 2,400 m) (Figures 14, 15). Such restricted conditions inhibited most biogenic carbonates from accumulating except in the southern part of the basin where phylloid green algae flourished and created carbonate buildups (Baars and Stevenson, 1982). These mounds presently produce the majority of the oil from within the Paradox Basin.

Hite (1960) identified at least 29 evaporite cycles within the Paradox Formation (see figure 21). However, it is possible deeper parts of the basin could have more cycles, but a lack of good well data and varying amounts of salt tectonics make identification difficult. Several of the upper cycles have been grouped together into zones and named based on the same time equivalent intervals found in the southern end of the basin. These zones include the Ismay, Desert Creek, Akah, and Barker Creek (Figure 16).

The upper contact with the overlying Honaker Trail Formation is considered gradational. It is composed of several hundred feet of anhydrite and carbonates above the last (Hite's [1960] cycle number one) halite and black shale interval/cycle. These carbonates are thought to be equivalent to the Ismay and Desert Creek carbonate zones found in the southern part of the basin. However, in the northern half of the basin, the Ismay and Desert Creek stages are extremely saline

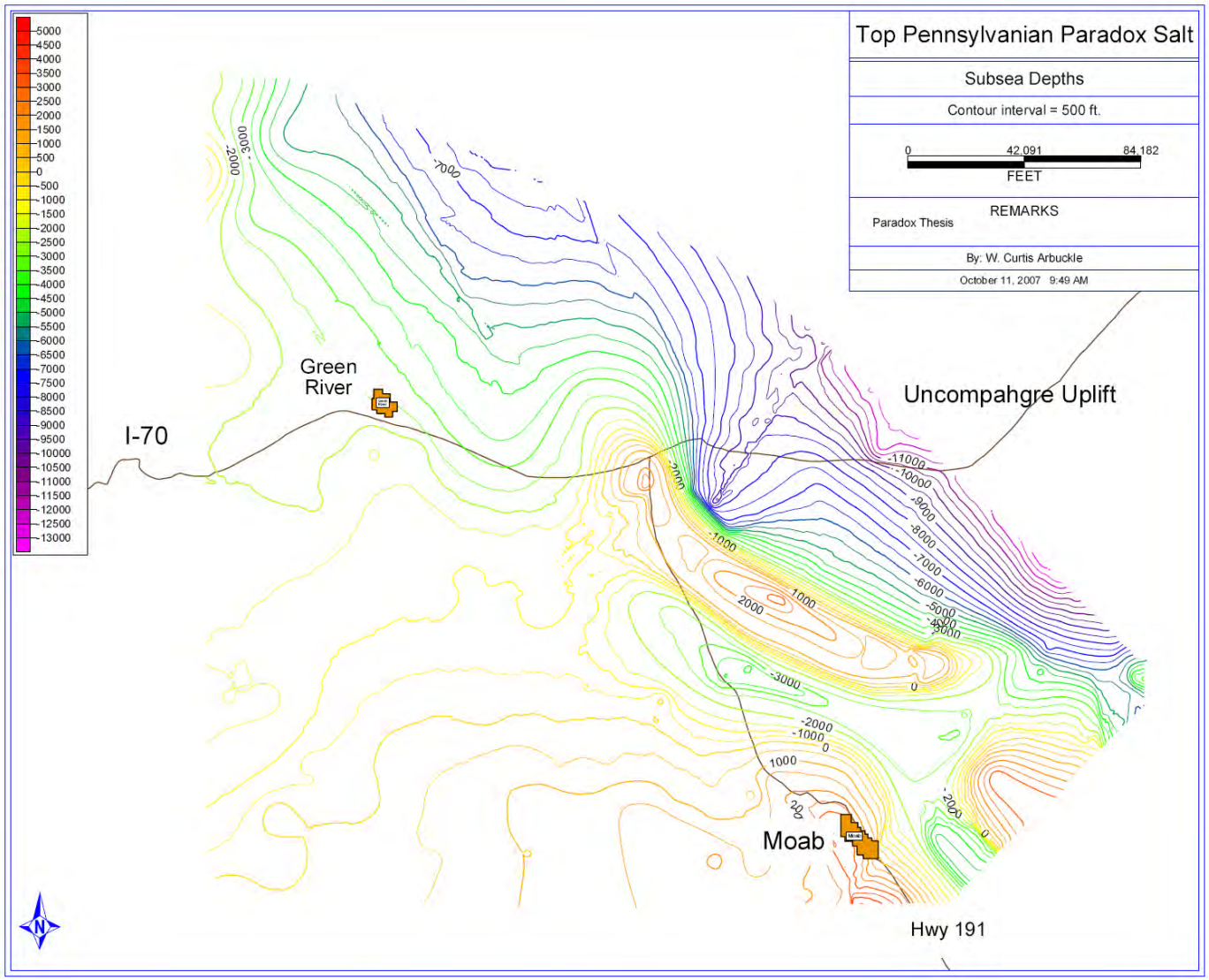

Figure 12: Structure contour map of the top of the Pennsylvanian Paradox salt. Note how the structure dips severely from the top of the Salt Valley Anticline northeast towards the Uncompahgre Uplift. Contour interval = 500 feet (152 m) (relative to sea level; negative numbers are subsea depths).

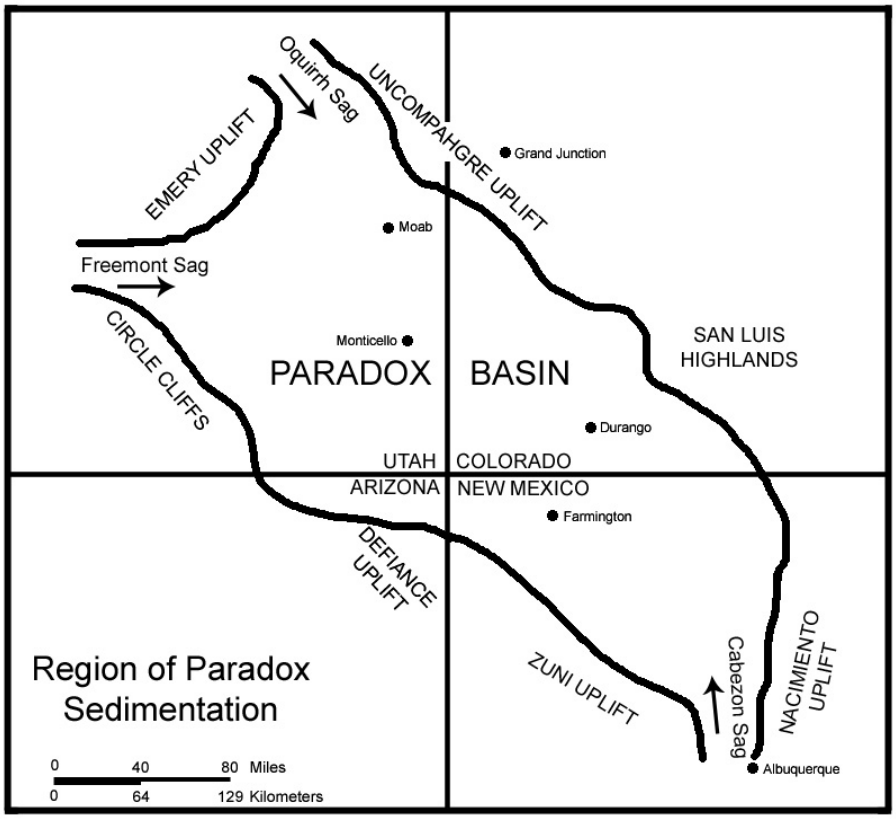

Figure 13: Map showing the location of Paradox sedimentation and the three major water entryways into the basin (modified from Wengerd, 1962).

when compared to the same intervals in the south, Where they are dominated by porous carbonate mounds deposited in normal marine conditions (Brown, 1960).

EVAPORITE DEPOSITIONAL CYCLES AND ENVIRONMENTS, REGIONAL CORRELATIONS, CLASTIC INTERBEDS AND SALT (HALITE) LITHOLOGIES

The Paradox Formation contains at least 29 well defined evaporite cycles composed of halite beds in association with penesaline and siliciclastic rocks or interbeds (Hite, 1960). Each halite bed represents the final stage in a complete or partial evaporite cyclothem that also contains an ordered vertical sequence of shale, dolomite/siltstone and anhydrite. Depending on position within the basin, this same order of facies can also be observed laterally.

Evaporite Cycles and Regional Correlations

An idealized evaporite cycle would consist of (from bottom to top): anhydrite, silty dolomite, black shale, silty dolomite, anhydrite and halite (Figures 17 and 18). The upper and lower contacts of each cycle are disconformities caused by extreme changes in brine concentration. Some of the cycles are incomplete and are missing one of more lithologies within the clastic zones. However, other cycles have additional interbeds that are out of sequence from the idealized model.

Each cycle can be broken into transgressive and regressive phases (Figure 17). The lower anhydrite bed marks the start of the transgressive phase and decreasing salinity due to an influx of seawater into the basin caused by a rapid rise in sea level (probably both eustatic and tectonically controlled). Sea level reached a maximum

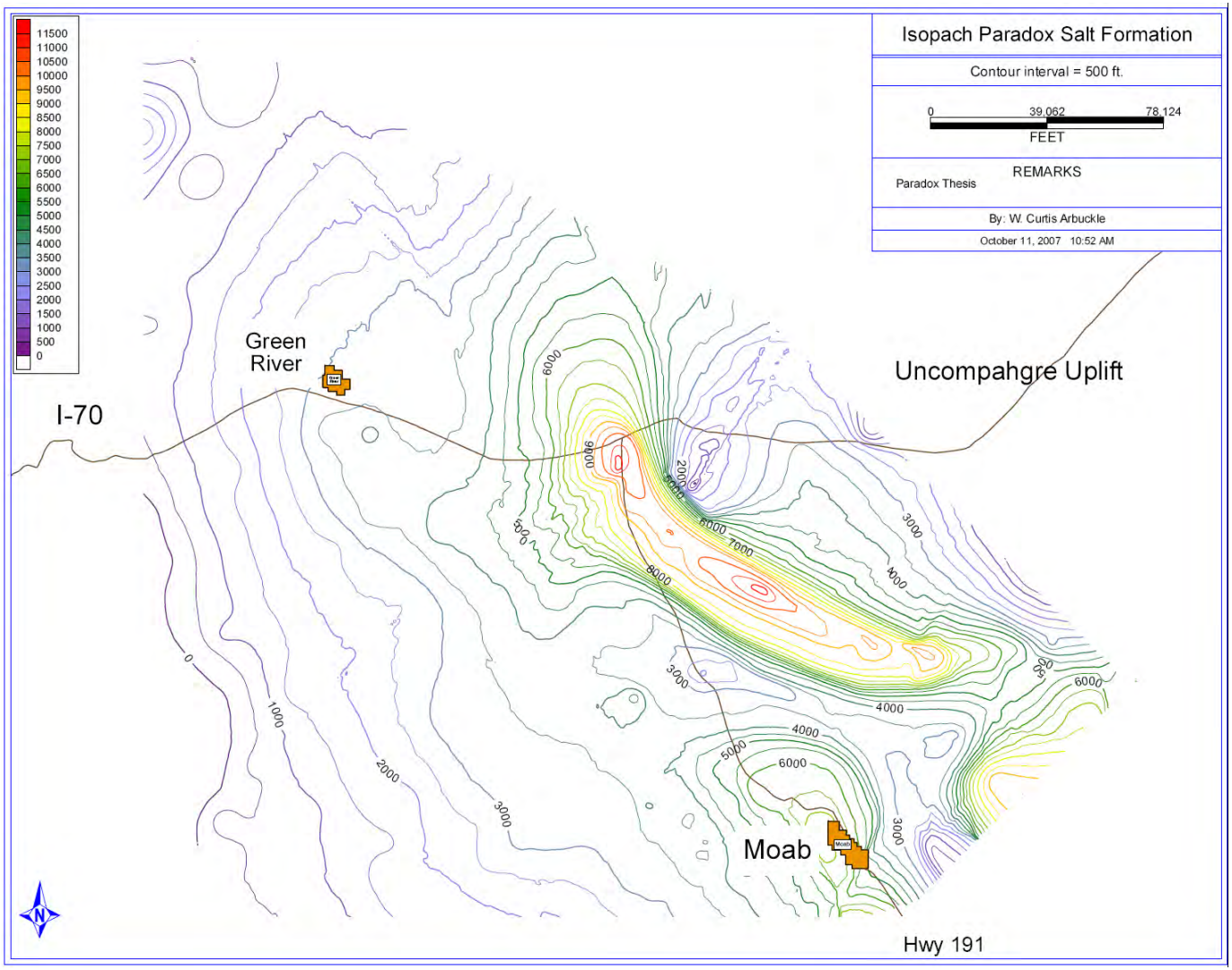

Figure 14: Isopach map of the Paradox Salt. Contour interval = 500 feet (152 m).

during the deposition of the black shale. This marks the end of the transgression and the start of the regressive phase (falling sea level and increasing salinity). The black shale could be considered a condensed section, but it is unclear how much time would be represented by such a highstand. The deposition of the second half of the black shale marks the start of sea-level fall. After this point, the interbed depositional series reverses until the point where salinity concentrations reach halite saturation and halite precipitation completes the cycle.

This same series of salinity and sea-level conditions can be observed in the carbonate cycles in the southern part of the Paradox Basin. The discovery of natural gas in 1945 at Barker Creek initiated a frenzy of hydrocarbon exploration (Malin, 1958). When additional discoveries were made in

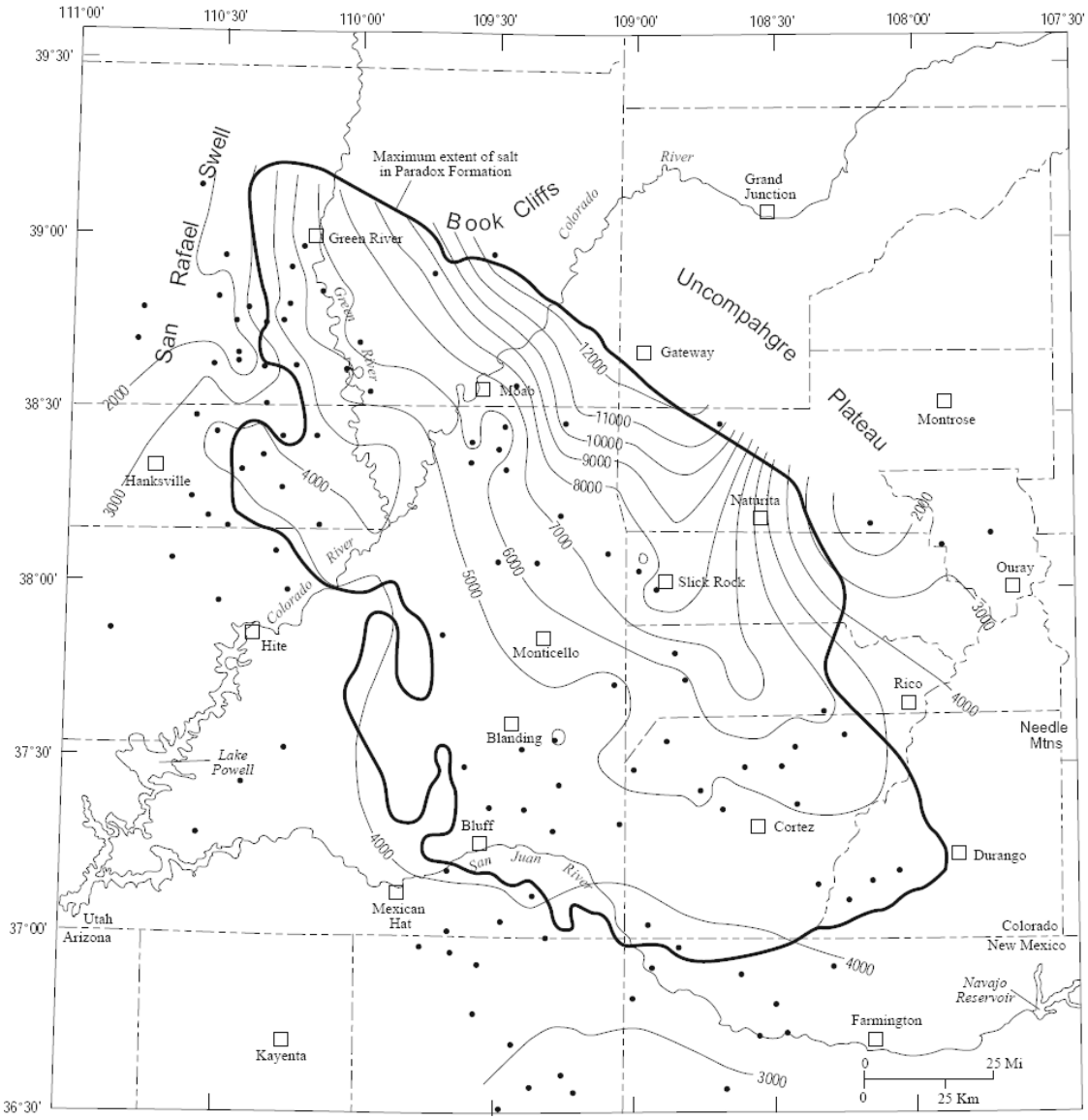

Figure 15: Isopach map totaling all of the Pennsylvanian and Permian strata within the Paradox Basin. Note how thicknesses increase in the northeast part of the basin. This is attributed to the clastic influx of coarse arkosic material shed off the Uncompahgre Highlands. This area is also the deepest part of the basin (after Nuccio and Condon, 1996). Contour interval = 1,000 feet (328 m).

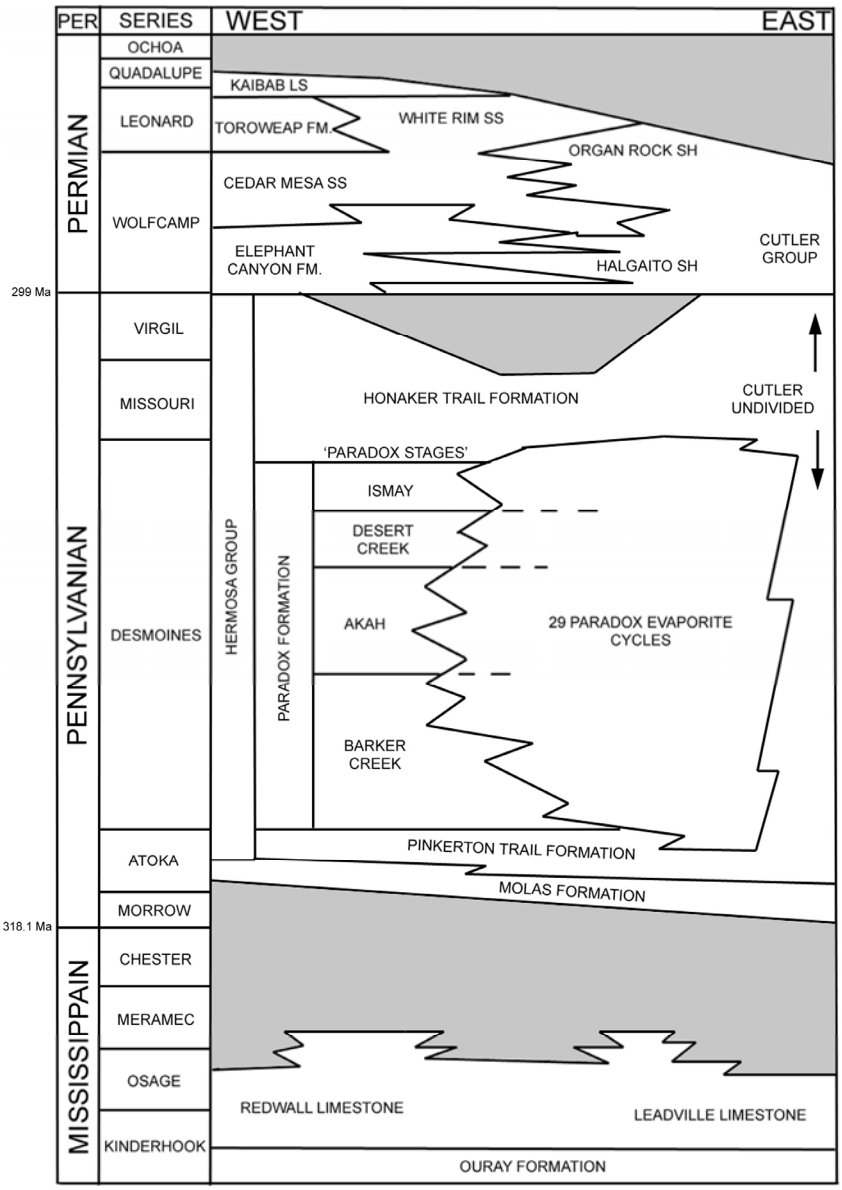

Figure 16: Mississippian through Permian correlation chart of the Paradox Basin. Gray areas represent missing time. Here the four main 'Paradox stages', which are based on productive intervals found in the southern edge of the basin, are represented. These stages are bounded and characterized by time correlative black shale intervals that make correlations possible between the carbonate cycles in the southern half of the basin and the evaporite cycles located further north (modified from Baars and Stevenson, 1982).

southeastern Utah and southwestern Colorado, important producing intervals or 'pay zones' were given informal names after the fields or locations where the first production was recorded. These intervals are all Pennsylvanian in age and include, from oldest to youngest, the Alkali Gulch, Barker Creek, Akah, Desert Creek and Ismay zones (Herman and Barkell, 1957; Malin, 1958; Peterson, 1966; Hite and Buckner, 1981; Reid and Berghorn, 1981). After Hite (1960) studied the evaporite sequences farther north, regional correlations were possible between the evaporite and carbonate depositional environments (Figure 19). The black shales found in both systems make excellent time sensitive rock units that can be correlated across the basin. Hite and Buckner (1981) were able to make this correlation using both outcrop and well data. They correlated shale and carbonate facies of the Cane Creek Anticline southward to exposures on the Raplee Anticline, which is about 25 miles (40 km) west of the Aneth Field (Figure 20).

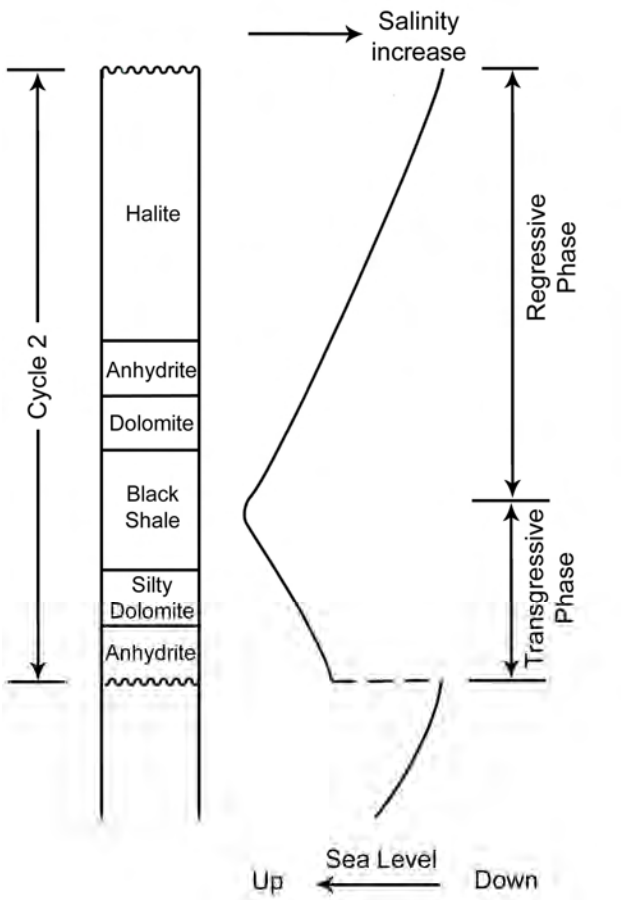

Figure 17: Facies stratigraphy of evaporite cycle 2 from the Cane Creek No. 1 core (T 26S, R 20E, sec. 25). The curve represents relative sea level and salinity during the deposition of each facies. Notice how the change from transgressive to regressive occurs during the deposition of the middle of the black shale. This point also marks the reversal in order of facies (modified from Raup and Hite, 1992).

From these correlations, they could associate the producing carbonate intervals (Barker Creek, Akah, Desert Creek, Ismay, etc.) in the southern part of the basin to time equivalent evaporite cycles located farther north. It is important to note these producing carbonate zones don't represent complete cycles, only intervals of production. Therefore, direct correlations between producing intervals may not encompass complete evaporite cycles and vise versa.

Figure 21 is a diagrammatic section from north to south across the basin. It shows the correlation of the 29 evaporite cycles to the carbonate producing intervals found in the south. The Ismay interval is correlative to cycles 1 – 3, but can also include the lower portion of the Honaker Trail Formation. The Desert Creek matches with cycles 4 and 5, followed by the Akah zone with cycles 6 – 9. The Barker Creek zone is equivalent to cycles 10 – 19. The Alkali Gulch interval is mainly found on the Colorado side of the basin, but can roughly be time correlated to some of the oldest evaporite cycles (20 – 29) (Lockridge, 1958; Baars *et al*., 1967). Note how all 29 cycles can only be found in the older, deeper, northern half of the basin. In fact, many of the older cycles are not found south of the Gibson Dome area (Figure 22).

Clastic Zone Interbeds

Economically and scientifically interesting elements of the Paradox evaporite cycles are the clastic intervals. Most of the clastic interbeds are composed of anhydrite, dolomite and/or siltstone, and organic rich black shale (Figure 18). The contacts between each interbed are thought to be conformable and gradational (Raup and Hite, 1992). Some clastic zones are incomplete and may not incorporate all of the lithologies (generally the black shales) into each cycle. This may be dependent on location, as the lithologies for each cycle can change over short distances.

Anhydrite (Transgressive)

Anhydrite ($CaSO_4$) overlies the halite bed of the previous evaporite cycle. The anhydrite interval is composed mostly of anhydrite, but also contains minor amounts of quartz, dolomite, mica, clay minerals and pyrite (Raup and Hite, 1992). It can also be divided into two textures, laminated and nodular. The laminated zones are purely depositional whereas the nodular zones are probably a result of the recrystallization process from gypsum ($CaSO_4 \cdot 2H_2O$) to anhydrite in a less

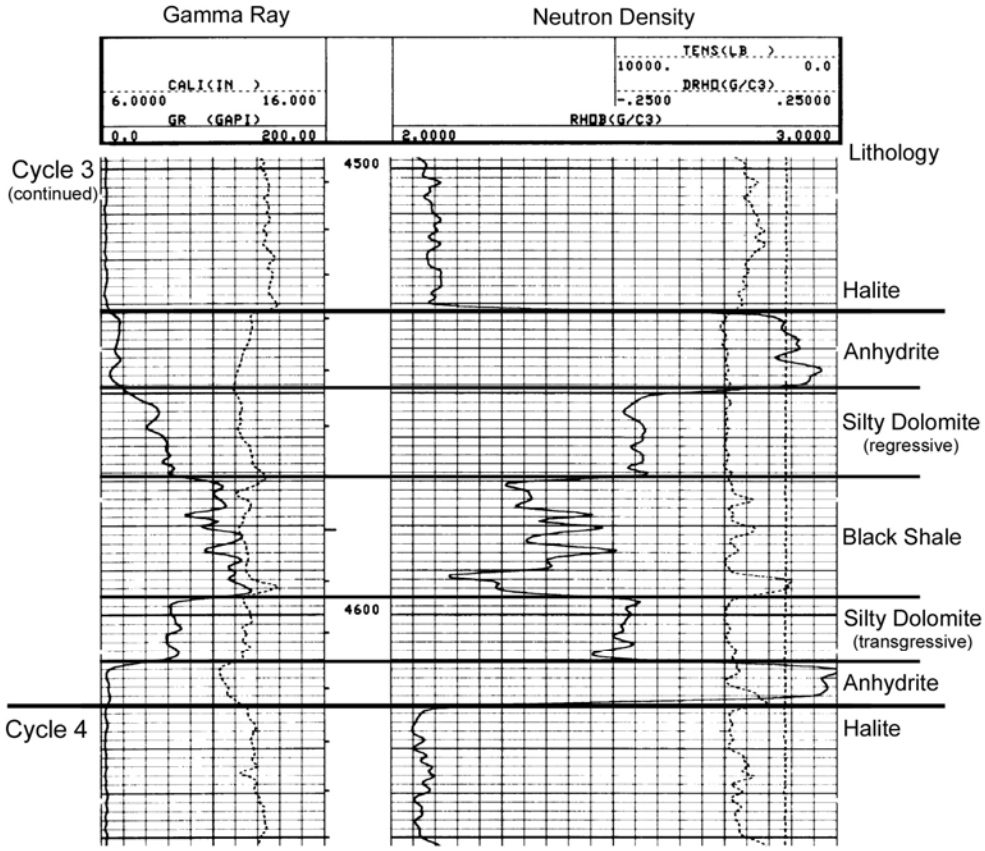

Figure 18: A type log from the Coors Energy Coors USA 1-10LC well (T 26S, R 20E, sec. 10) highlighting the clastic interval of evaporite cycle 3.

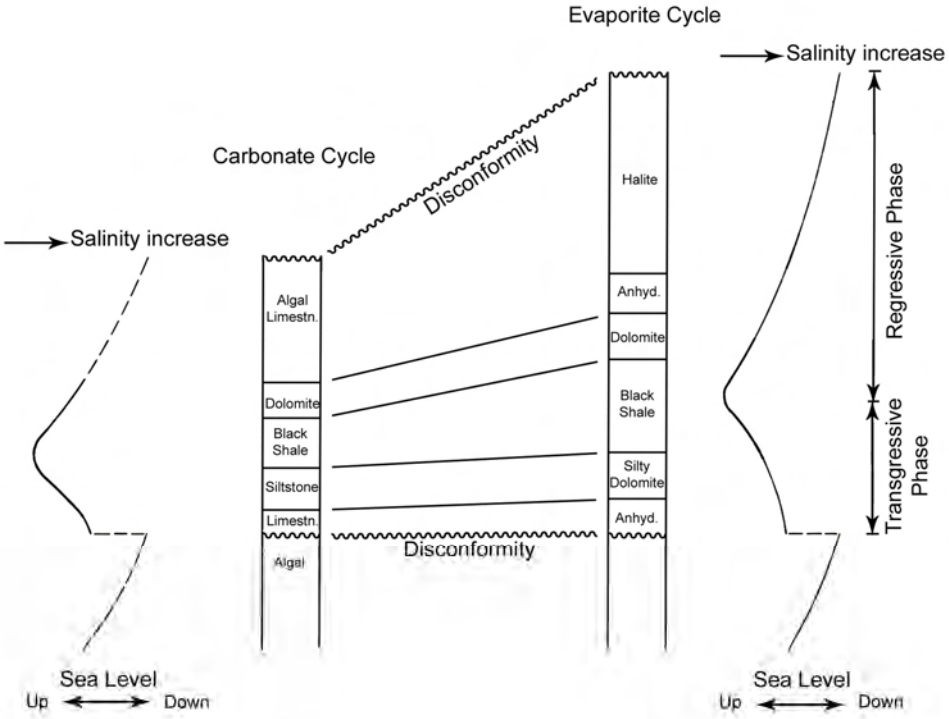

Figure 19: Diagram showing the regional correlation of facies from an idealized evaporite cycle (right) found in the northern half of the basin, to a carbonate cycle (left) typically found further south in the basin. The curves show relative sea level and salinity conditions for each facies during deposition (modified from Hite and Buckner, 1981).

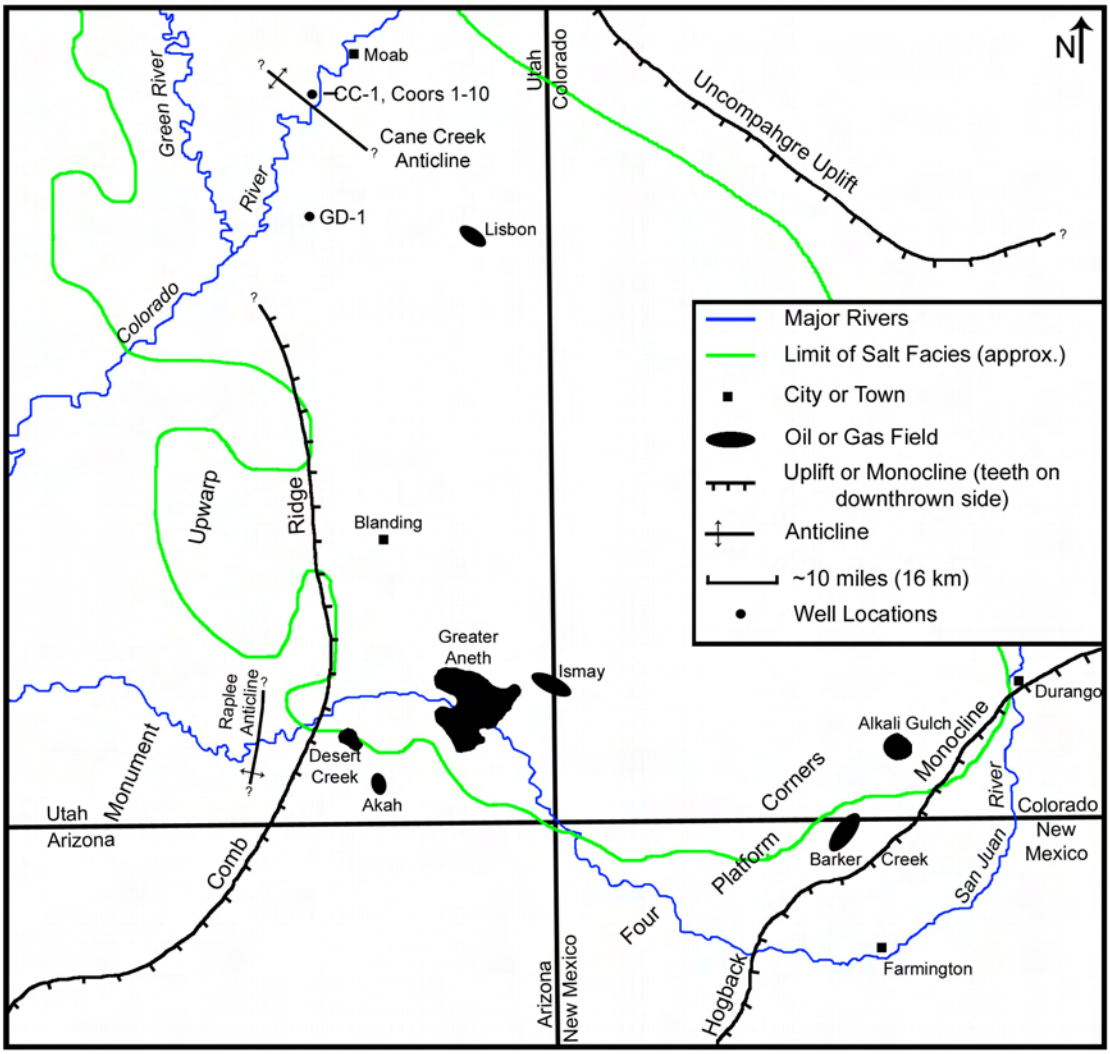

Figure 20: Index map showing the locations of several prominent oil/gas fields, uplifts, monoclines, anticlines and three well locations (CC-1, Cane Creek No. 1 corehole; Coors 1-10, Coors Energy Coors USA 1-10LC well; GD-1, Gibson Dome No. 1 corehole) in the southern Paradox Basin (modified from Peterson, 1966).

saline solution and at temperatures above 50° C (Raup and Hite, 1992; Warren, 1999).

The contact with the underlying halite is very well defined and can be considered a solution disconformity. This boundary is caused by a rise in local sea level that results in an influx of marine water, which lowers the salinity level and erodes the uppermost section of the underlying halite (Hite, 1968). The influx of marine water marks the beginning of the transgressive phase of each evaporite cycle. The marine waters not only dilute the remaining brine, but also re-supply it with calcium and sulfate. As a result, laminated calcium sulfate deposits accumulate (probably in the form of gypsum) as the brine becomes less saline. Over time, the entire zone may be converted from gypsum to anhydrite (Raup and Hite, 1992).

Anhydrite precipitation rates vary depending on depositional environments. On average less than 0.04 inch (1 mm) of anhydrite is formed annually. Hite and Buckner (1981) suggest a rate of about 0.03 inch (0.8 mm) per year based on halite sedimentation rates. However, it is not uncommon to see annual layers around 0.2 inch (5 mm) thick. Precipitation of 0.2 inch (5

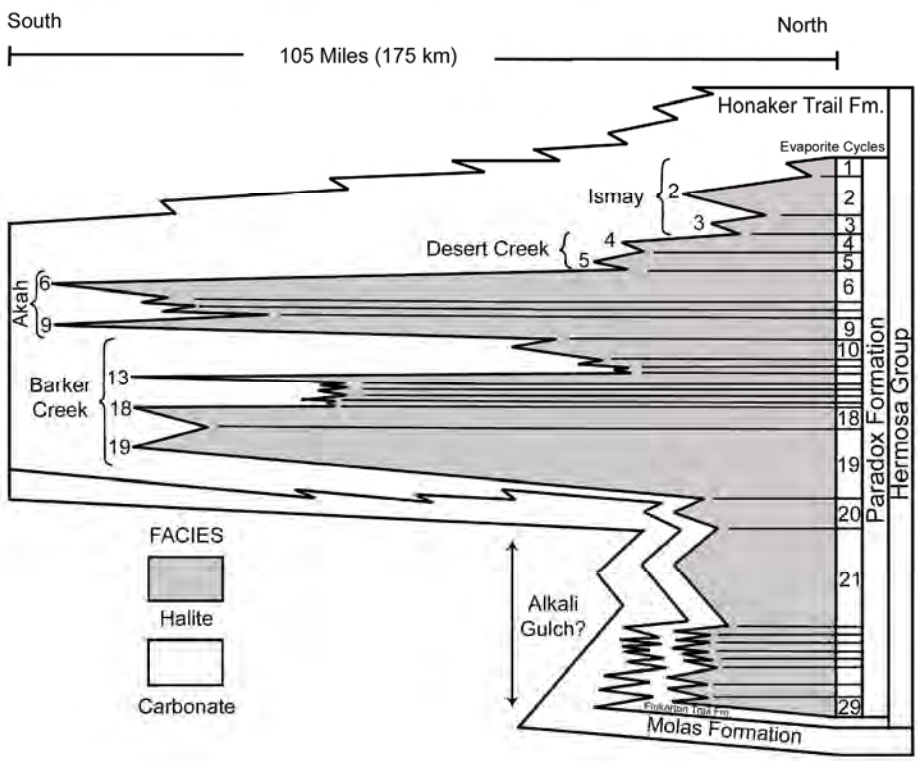

Figure 21: A diagrammatic section from north to south across the Paradox Basin. It shows the correlation of the 29 evaporite cycles in relationship to the carbonate producing intervals found in the south. Note how evaporite cycles 6, 9, 13, 18 and 19 mark the maximum extent of salt deposition into the southern half of the basin. Also, note how cycles 20 – 29 are limited to only the northern, deepest parts of the basin (modified from Hite and Buckner, 1981).

mm) requires the complete evaporation of ~46 feet (14 m) of normal seawater or ~13 feet (4 m) of brine saturated with calcium sulfate (Braitsch, 1971). Overall, an average of only about 3 feet (1 m) of gypsum/anhydrite would be precipitated from 3,280 feet (1,000 m) of seawater (Borchert and Muir, 1964). It is also important to note that some compaction (upwards of 40%) occurs during the dewatering of gypsum to anhydrite (Kupfer, 1989). Transgressive anhydrite thicknesses within the northern Paradox Basin range from zero to >20 feet (>6 m).

Silty Dolomite (Transgressive)

In many of the evaporite cycles within the Paradox Basin, an interval of silty dolomite overlies the transgressive anhydrite beds. These dolomitic sequences are composed of mainly dolomite, but also contain significant amounts of quartz, feldspar (orthoclase and plagioclase) and mica. There are also small zones or stringers of halite, anhydrite and black shale. Considerable amounts of silt and clay are present within the dolomite. Most of the dolomite is fine to very fine grained with a sugary or sucrosic texture (Raup and Hite, 1992). These rocks usually lack distinct bedding structures possibly due to bioturbation (Raup and Hite, 1992).

The transgressive dolomite precipitated as the brine within the basin became increasingly less saline due to an influx of seawater enriched with bicarbonate ions (HCO_3^-). It is unclear whether the dolomite is a result of primary or secondary precipitation. Raup and Hite (1992) proposed it was primary precipitation by referring to the sucrosic texture of the rock and how the reduced dissolved sulfate in the basin brines could contribute to the conditions needed for primary dolomite precipitation. However, changes in the physical properties of chemical sediments, like texture, can change drastically over geologic time and across relatively short distances. Some wells penetrating the same transgressive zone have been reported to contain limestone in association with dolomite. This suggests the dolomite formed

due to secondary dolomitization processes altering the originally deposited silty limestone. It is even plausible to suggest a process like seepage – reflux dolomitization could occur (Tucker and Wright, 1990). Here, porewaters rich in magnesium are released from under- or overlying evaporite rocks (mainly from halite beds and the water lost during the gypsum to anhydrite dewatering reaction) to facilitate the dolomitization process.

Interestingly enough, both precipitation sequences can occur simultaneously in different sections of the basin. First, rapid changes of water level in transgressive basins are certainly possible, especially near the basin margins. This could cause any subaqueously precipitated carbonates to become exposed and subject to syndepositional, subaerial diagenesis (secondary precipitation). Secondly, the Mg/Ca ratio in hypersaline environments fluctuates as the salinity concentration fluctuates (Warren, 1999). Therefore, during the early stages of carbonate precipitation a lower Mg/Ca ratio is dominant. As the brine becomes more saline, the Mg/Ca ratio is heightened due to the loss of calcium already exhausted during the precipitation of early, calcium rich carbonates. Thus, subsequent carbonates are precipitated from brines with increasing amounts of magnesium, substituting for the lack of calcium in the system. The resulting carbonates are typically dolomites, enriched in magnesium that was concentrated as a product of primary precipitation. Within the Paradox Basin, secondary precipitation might occur on the southern shelf and along the margins of the basin, whereas primary precipitation is more likely in the deeper areas of the basin.

The transgressive phase of the Paradox cycles consistently contains larger amounts of silt than the regressive sequence. This is attributed to the incoming transgressive sea churning up sediments along the shores and low-lying areas of the basin (Hite and Buckner, 1981). This matter would then become deposited along with the precipitation of, in this case, the carbonaceous dolomites. Also seen throughout the northern part of the basin is the presence of detrital quartz and feldspar within the dolomite. Some mineralogical estimates of quartz and feldspar reach upwards of 40 percent the total mineralogy and can be observed in core (Raup and Hite, 1992). The origin of such a large quantity of material is debatable. The nearest known sources are the Uncompahgre Uplift bounding the east side of the basin, and the shelf margin in the southwest. Some possible transport methods include saline density currents, small scale turbidites and eolian systems.

If it is assumed that during dolomite precipitation the basin brine was at, or very near, calcium bicarbonate saturation, sedimentation rates can be calculated. Using an aggressive evaporation rate of about 13 feet (4 m) of brine water per/year, and assuming constant replacment by marine water influxes, Hite and Buckner (1981) calculated a deposition rate of 0.007 inch (0.17 mm) per year. Yang (2000) and Kirkland and Evans (1981) also arrived at similar sedimentation rates of 0.004 – 0.008 inch per year (0.1 – 0.2 mm/year), and 0.006 inch per year (0.15 mm/year) respectively. With the addition of quartz, silt, and other clastic material into the transgressive dolomite, the sedimentation rate should be increased to around 0.008 inch per year (0.2 mm/year). Transgressive silty dolomite thicknesses within the northern Paradox Basin range from zero to >30 feet (>9 m) per individual bed.

Black Shale (Transgressive and Regressive)

An organic-rich black shale overlies transgressive silty dolomite. It tends to be very carbonaceous and is composed of

dolomite, calcite, quartz, mica, clay minerals (illite) and minor amounts of sphalerite, feldspar and pyrite (can be abundant). Silt sized quartz grains can account for as much as 40 percent of the total mineralogy, while carbonate grains comprise between 20 – 30 percent (Raup and Hite, 1992). The siliciclastic material found within the black shales probably was deposited by saline density currents, light turbidites or originated from an eolian source (Raup and Hite, 1992). Some small shells (brachiopods) and associated shell fragments, fern pinnules and carbonized plant stems, along with conodonts indicate there was some biological activity during deposition (Herman and Barkell, 1957). It is very common to see vertical fractures within the shale ranging from <0.04 inch (<1 mm) to over 2.8 inches (7 cm) in width. These fractures are generally filled with halite or in some rare cases carnallite (Hite, 1960). Some of the interbedded shales are highly radioactive reaching over 300 API on several of the gamma ray well logs. These hot shales are typically located within cycles 10, 13, and 21. The contact with the underlying dolomite is generally gradational, however in some wells it can be abrupt.

The black shales were deposited when sea level was at its highest and thus the salinity was at its lowest throughout the basin. This allowed the shales to be deposited basin wide making them good time correlation units. The sometimes abundant pyrite within the black shales indicates the shales were deposited in a humid, reducing, euxinic environment, which is opposite of most evaporite settings where an arid, oxygenated environment is more prevalent (Hite, 1968). Interestingly, Herman and Barkell (1957) report that some of the black shale intervals from the basin center thicken and progressively grade into gray-green shales, siltstones, and even redbeds as they near the Uncompahgre Uplift along the eastern margin of the basin. However, most of the shales change very little from north to south, varying only in thickness, with the thicker sections located on the southeastern shelf and in the basin interior (Hite and Buckner, 1981).

Most of the black shales range from 0.5 – 13 weight percent organic matter. The organic matter was probably derived from algae and bacteria from both marine and terrestrial sources (Raup and Hite, 1992). There is also evidence of marine plankton and organic material that was swept into the basin via the Silverton fan delta because of fluvial influxes (Hite *et al.*, 1984). RockEval pyrolysis data from several shale intervals in the upper Paradox Formation suggest a mixture of types II and III kerogen make up the organic matter (Hite *et al.*, 1984). Dense, anoxic, highly saline brines that formed during the regressive phase of each evaporite cycle preserved the organic matter. Three main shale intervals have been the main focus of study about generated hydrocarbons. These include the Gothic Shale of cycle 3, the Chimney Rock shale of cycle 5 and the Cane Creek shale of cycle 23. However, many of the other shale intervals exhibit the same generation potential as the three listed above and need to be studied in further detail. The Gothic shale has a total organic carbon (TOC) of 2 – 3 percent, while the Chimney Rock shale has a TOC of about 1.46 percent (Hite *et al*., 1984). The Cane Creek shale is a combination of anhydrite, shale and silty dolomite and not just shale. Nonetheless, several shale zones within the Cane Creek contain TOC values ranging from 0.42 – 3.96 percent. Vitrinite reflectance values (R_o) for shales within the Paradox Formation range from 0.42 – 0.54 which puts these rocks at the beginning of catagenesis, and thus, the start of the oil window. However, palynomorph data suggest these R_o values are minimum indicators of thermal maturity. An explanation of why the R_o values are suppressed involves the relationship of vitrinite and exinite macerals and bacterial reworking of organic matter in

anoxic environments, which is discussed in further detail by Hite *et al*., (1984).

The black shales within the clastic interbeds represent the point in the evaporite cycle when the system transitioned from transgressive to regressive. It is assumed the first half of the black shale interval is transgressive and the second half is regressive. This transition point is difficult to determine because the mineralogy is consistent throughout the bed. One could also assume the black shale represents a condensed section within the cycle, but again this would be hard to determine on a macro or microscopic level. However, it is clear that sometime during the deposition of the shale sea level began to fall and was accompanied by an overall rise in salinity.

Black shale sedimentation rates are difficult to determine because the shales were deposited as a combination of chemical, clastic, and organic components. One way to calculate the sedimentation rate is to compare organic matter within the shales to organic carbon production rates (Hite and Buckner, 1981). Evaporite settings, like the enormous saline lakes in eastern Africa or even the Great Salt Lake in northern Utah, are modern analogs to what the Paradox Basin might have been like during shale deposition. These highly saline settings don't support normal marine life, but do facilitate an enormous amount of biogenic activity that is greater than any upwelling zones located throughout the world (Kirkland and Evans, 1981). Unfortunately, the organic carbon production rates in these extreme locations are highly variable, so more typical production rates from traditional marine waters were used. Modern oceanic waters produce between 50 g/m^3/year (open ocean) and 300 g/m^3/year (upwelling zones) of organic carbon (Tissot and Welte, 1984). Hite and Buckner (1981) note that the Paradox shales have an average density of 1.8 g/cm^3 and contain an average of 5.42 weight percent TOC (calculated from RockEval data in Hite *et al*., (1984)). Therefore, each cubic meter of shale contains roughly 97,520 grams of organic carbon. This value of 97,520 grams when divided by the organic carbon production rates of 50 g/m^3/ year and 300 g/m^3/year results in deposition rates of 0.02 inch (0.51 mm) and 0.12 inch (3.08 mm) respectively for the black shales within the Paradox Formation.

Clastic zone shale thicknesses in the northern Paradox Basin vary greatly. Depending on its location in the basin, a shale zone may not be represented in a particular cycle, but several miles away it can be measured in feet. With that said, shale thicknesses range from nothing to >20 feet (>6 m). Since the Cane Creek interval is not a clean shale but a mixed zone of shale, anhydrite and carbonates, its total thickness is not represented here.

Silty Dolomite (Regressive)

In a typical cycle, black shale is overlain by regressive dolomite that is very similar to the transgressive dolomite discussed above. Both dolomites have the same sucrosic texture, however the regressive dolomite contains less (but still abundant) detrital material. This is most likely the result of falling sea level and the dwindling availability of additional clastic material entering the basin, unlike the transgressive phase where new material is mobilized with rising water levels.

Although less abundant, quartz and other silt-sized siliciclastic grains are still found within the regressive dolomite. It is important to note that sedimentation rates for dolomites and black shales are rather slow compared to anhydrite or halite zones. Therefore, the abundance of siliciclastic material transported into the basin may not have increased substantially during transgressive times. If the rate of siliciclastic material entering the basin remained relatively unchanged throughout

each cycle, siliciclastic material would accumulate in larger quantities within the sediments that have slower sedimentation rates like the black shales and dolomites.

Much like the transgressive dolomite, the regressive silty dolomite has an estimated precipitation rate ranging from about 0.004 – 0.008 inch (0.1 – 0.2 mm) per year. Because there was likely less siliciclastic material, a rate of .0067 inch (0.17 mm) per year, as suggested by Hite and Bucker (1981), is appropriate. Individual regressive dolomite zone thicknesses within the northern Paradox Basin range from nothing to >30 feet (>9 m).

Anhydrite (Regressive)

Overlying the regressive dolomite is a zone of laminated anhydrite. The boundary between the anhydrite and the underlying regressive dolomite is transitional with thin layers of alternating anhydrite and dolomite. Raup and Hite (1992) noted the presence of small pseudomorphs of anhydrite and gypsum in this transition zone. These pseudomorphs are consistent with rising salinity levels.

The anhydrite was precipitated as the brine concentration became more saline as water levels fell. This zone is very similar to the transgressive anhydrite except for the textural features described next. It is thought the fine and wavy laminations are the result of anhydrite replacement of carbonate algal mats (Raup and Hite, 1992). The upper portion of the zone contains pseudomorphs of anhydrite and is sometimes interlaced with the overlying halite. These pseudomorphs represent some sort of extreme change in salinity and their formation is not fully understood. Halite beds conformably overlie the upper boundary, above the pseudomorphs.

Like the transgressive anhydrite discussed previously, precipitation rates for the regressive anhydrite are considered comparable, at about 0.03 inch (0.8 mm) per year. Individual regressive anhydrite zone thicknesses, within the northern Paradox Basin, range from nothing to >20 feet (>6 m)

Sandstone and Turbidities

Several wells drilled in the northern Paradox Basin have encountered sandstone beds within the clastic intervals of the evaporite cycles. The sandstones are fine- to medium-grained and are characterized by small scale cross-laminations (mainly clay), graded bedding, poor sorting, and sole marks (Hite and Buckner, 1981). Fragments of vascular plants and clasts of gray shale are also found throughout the sandstone. These defining characteristics suggest the sandstone units found within the clastic intervals are turbidites (Bauma, 2000; D. L. Rasmussen, 2007, personal communication).

If these sandstones are indeed turbidites then the grain size distribution does not point to a clastic source from the southern shelf of the basin because Hite and Buckner (1981) noted that the medium-grained, poorly sorted sandstones lie adjacent to fine-grained, silt sized rocks derived from the south. This suggests the turbidites originated from the Uncompahgre Uplift in the east.

The timing and position of the turbidites within the evaporite cycles is important and gives clues on how and why they formed. Some of the sandstone units identified in cores taken from the Salt Valley area are located above underlying halite beds, thus placing the turbidites at the beginning of a transgression into the basin (Hite and Buckner, 1981). During transgressive times, a rising sea level could initiate turbidity currents from fan deltas along the base of the Uncompahgre Uplift. Other sandstones are located randomly throughout the clastic interbed sequence. These turbidites might have been triggered by earthquakes, floods, and storms or from slumping directly off the uplift (Hite and Buckner, 1981).

Halite Beds

Probably the most defining characteristic about the Paradox Basin is the presence of salt. Halite makes up most of these salt or saline facies and is equigranular with anhedral grains ranging from about 0.06 to 0.5 inch (1.5 to 12.5 mm) in diameter. The salt ranges in color between clear, white, orange, gray and amber (Hite, 1960). Color is determined by the amount of impurities within the halite including shale, anhydrite, clay, potash, organic matter, and fluid hydrocarbons. The contact with the underlying regressive anhydrite is usually gradational and the contact with the overlying transgressive anhydrite is unconformable.

The halite beds were deposited during a time of sea-level lowstand where the influx of marine waters into the basin was minimal. This caused the remaining brine to become increasingly saturated with salts initiating the deposition of halite. However, there was still enough marine water entering the basin to recharge the remaining brine. This allowed the halite intervals to reach impressive thicknesses. The halite beds also contain thin laminations of shale, silt, anhydrite or potash that are thought to mark seasonal changes in salinity, clastic sediment supply, and temperature (Raup and Hite, 1992). Spacing between laminations ranges from 0.25 to 18 inches (0.64 to 46 cm), but averages around 2.5 inches (6.35 cm) (Hite, 1960; Raup and Hite, 1992).

As discussed earlier with the black shales, evaporite environments generate large amounts of organic material. Most of the organic matter that is produced or flows into a basin via marine influxes is typically well preserved. Oxygen solubility is extremely low in saline-rich brines and thus inhibits aerobic decay. Anaerobic sulfate reducing bacteria use only minor amounts of organic matter in their metabolism and in doing so expel large volumes of H_2S, limiting the growth of other halophillic bacteria (Hite *et al*., 1984). Therefore, during halite deposition much of this organic matter is captured and preserved within the salt and associated pore fluids. Halite beds can have up to 35 percent porosity (Ver Planck, 1958) trapping organic-rich fluids, which can contain anywhere from 250 ppm organic carbon in halite to upwards of 3,000 ppm organic carbon in potash beds (Hite *et al*., 1984). Over time these salt beds compacted and the organic rich fluids were expelled into the over and underlying clastic zones. These clastic intervals, now charged with significant amounts of organic material, would make favorable source and reservoir rocks.

Halite sedimentation rates can range from 0.4 – 59 inches (1 – 150 cm) per year. Analysis in Saskatchewan, Canada by Wardlaw and Schwerdtner (1966) resulted in a reasonable deposition rate of about 2 inches (5 cm) per year. Similar results were calculated by Hite and Buckner (1981) by counting seasonal laminae composed of anhydrite and shale/silt. They concluded an average precipitation rate of 1.57 inches (4 cm) per year. Halite bed thicknesses within the northern Paradox Basin range between 15 (4.5 m) feet near the edge of the evaporite facies to over 990 feet (300 m) near the salt walls and anticlines (Hite, 1960). The halite bed within cycle 6 is usually the thickest individual interval at around 330 feet (100 m).

CLIMATE CONTROLS ON EVAPORITE CYCLICITY

Evaporites and Climate

Today evaporites typically form where more water leaves a system than enters it. Therefore, evaporites generally precipitate in arid and semiarid regions of the world. Interestingly, these regions usually lie between 15° and 45° north and south latitudes. Here large convection cells of moist

air are warmed near the equator causing them to rise, and then cool (losing moisture in the form of precipitation), where they descend back down to the Earth's surface at around 30° latitude (Warren, 1989). The colder, dryer air absorbs available water particles as it falls creating a landscape that is deficient in moisture, thus resulting in a desert-like environment. These undersaturated air masses are the main driving force in the evaporation process, and are coupled with changes in air temperature, storm frequency, wind speed and direction, brine concentration, and humidity (Sonnenfeld, 1984). The moving air masses that descend back down to the Earth's surface are known as prevailing easterlies, or trade winds, and are deflected westward due to the Coriolis effect (Sonnenfeld, 1984).

During the Desmoinesian (~309.4 – 305.5 Ma [Gradstein *et al*., 2004]), the Paradox Basin was situated near these arid zones. Maps created by Bambach *et al*. (1980) place the Paradox Basin roughly between about 8° and 14° north latitude. Similarly, map published by Blakey (2007) situate the basin at roughly between 7° and 9° north latitude. Weber *et al*. (1995) illustrates the position of the northern Paradox Basin at 15° north latitude during the Pennsylvanian. Although slightly different not in the typical evaporate latitudes, these sources acknowledge that the position of the Paradox Basin, during Paradox Formation deposition, would be favorable for evaporite precipitation. Zharkov (1981) also notes how the position of these arid zones around the Earth's surface can change depending on the location of the continents. The arrangement of the continents also influences the position of seas, oceans, ocean currents and weather patterns, and dictates paleoclimate zonations (Zharkov, 1981). Therefore, the arid zones we observe today (between 15° and 45° north and south latitudes) may not exactly be representative of the same arid zones exhibited during the Desmoinesian.

Global Climate During the Pennsylvanian

Changes in sea level can depend on the existence or absence of polar ice caps. During periods when the polar ice caps are non-existent, high amplitude sea-level fluctuations (controlled by tectonics and climate) are attributed to second and third order cycles that create oscillations in sea level on the scale of tens of feet (Figure 22) (Vail *et al*. 1977; Warren, 1999). Smaller, but higher frequency fourth and fifth order cycles only occur on a scale of a few feet during greenhouse periods (times when little or no polar ice is present) because the change in sea level is dominated by second and third order cycles.

By comparison, almost the opposite can be said during periods when thick polar ice caps are present (icehouse). Here high amplitude sea-level changes are dominated by fourth and fifth order cycles that are a result of ice volume fluctuations likely dictated by Milankovitch cycles (Figure 22) (Warren, 1999). The larger second and third order cycles that control the greenhouse periods are still present, but they experience a much longer period and a lower frequency thus having a smaller immediate effect then the fourth and fifth order cycles (Warren, 1999).

The late Paleozoic was characterized by a lowstand first order cycle (Figure 23) (Fischer, 1984). This is attributed to icehouse conditions following the assembly of the super-continents (Gondwanaland and Euramerica) in the southern hemisphere (Veevers and Powell, 1987). Vail *et al*. (1977) documented a second order regression marking the end of the Mississippian (Figure 30) and highlighting an unconformity of approximately 4.5 million years (Hallam, 1992). The Pennsylvanian is characterized by a slight second order rise or transgression in sea level (Vail *et al*., 1977), which can be further broken down into several smaller third and fourth order cycles. These are observed in the evaporite and carbonate cycles of the

Paradox Formation. This cyclical interval matches one of the glacial episodes proposed by Veevers and Powell (1987) undoubtedly linking glacio-eustatic influenced controls with the deposition of the evaporite cycles of the Paradox Formation.

Pennsylvanian Cyclicity and Climate Controlled Sedimentation

Pennsylvanian cyclicity has long been recognized in the central and western United States. Moore (1936) noticed cyclical repetition in marine limestones and shales in Kansas and how they created, what he deemed as, cyclothems. Hite and Buckner (1981) also recognized similar cyclic activity in the Paradox Basin involving both the evaporite sequences and related carbonate cycles in the southern part of the basin. Heckel (1986) believes these cyclothems represent marine transgressions and regressions.

Since the location of the Paradox Basin, during the Pennsylvanian, was roughly at 10° N latitude, it is likely the cyclic deposition of the Paradox Formation was climatically influenced (Rueger, 1996). Wanless and Shepard (1936) first suggested these Pennsylvanian cyclothems were caused by fluctuations in sea level brought on by volume changes involving Gondwanaland glaciation. Their theory involves the increase and decrease of ice volume creating global, cyclic, climate change resulting in what we recognize today as periods of transgression and regression. As continental ice accumulated, both humidity and sea level would fall, restricting open marine contact with inland seas (Rueger, 1996) and basins like the Paradox Basin. During drops in sea level, the Paradox Formation evaporites would be deposited. A loss in volume of Gondwanaland glacial ice would result in an opposite situation, where inland seas and basins would have a direct connection with marine waters due to a rise in sea level (Rueger, 1996). In the Paradox Basin, during times of higher eustatic sea level, the organic-rich black shales, within the clastic zones, would have been deposited.

Weber *et al*. (1995) were able to break the Desmoinesian for the southern part of the Paradox Basin into five stratigraphic sequences ranging between 800,000 years and two million years. The duration of the sequences indicates they are associated third order composite cycles or sequences (Figure 23). The sequence boundaries were determined by examining outcrop and seismic evidence involving subaerial exposure, onlapping of evaporite wedges, regionally correlated black laminated shales and mudstones, and aggradational growth of carbonates that likely formed during times of sea-level highstand.

The first (1) of these third order sequences encompasses the entire Alkali Gulch evaporite interval which correlates to cycles 20 – 29 (Figure 21) and is defined as a lowstand evaporite wedge (Weber *et al*., 1995). The second (2) third order sequence is characterized by the Barker Creek interval (cycles 10 – 18) (Figure 24) and is described as a lowstand evaporite wedge (Weber *et al*., 1995). The Akah and Desert Creek zones (cycles 4 – 9) (Figure 22) together comprise the third (3), third order sequence. The Akah interval represents a lowstand systems tract but also contains what is thought to be the maximum flooding surface for the Desmoinesian – Lower Missourian second order transgressive/regressive supersequence (Weber *et al*., 1995). The Desert Creek is identified as a highstand/transgressive systems tract that is responsible for the deposition of the Chimney Rock shale (cycle 5) and the carbonate buildups or mounds located on the southwestern shelf of the basin. The fourth (4) third order sequence is defined as a progradational composite sequence and incorporates the Ismay (cycles 1 – 3) (Figure

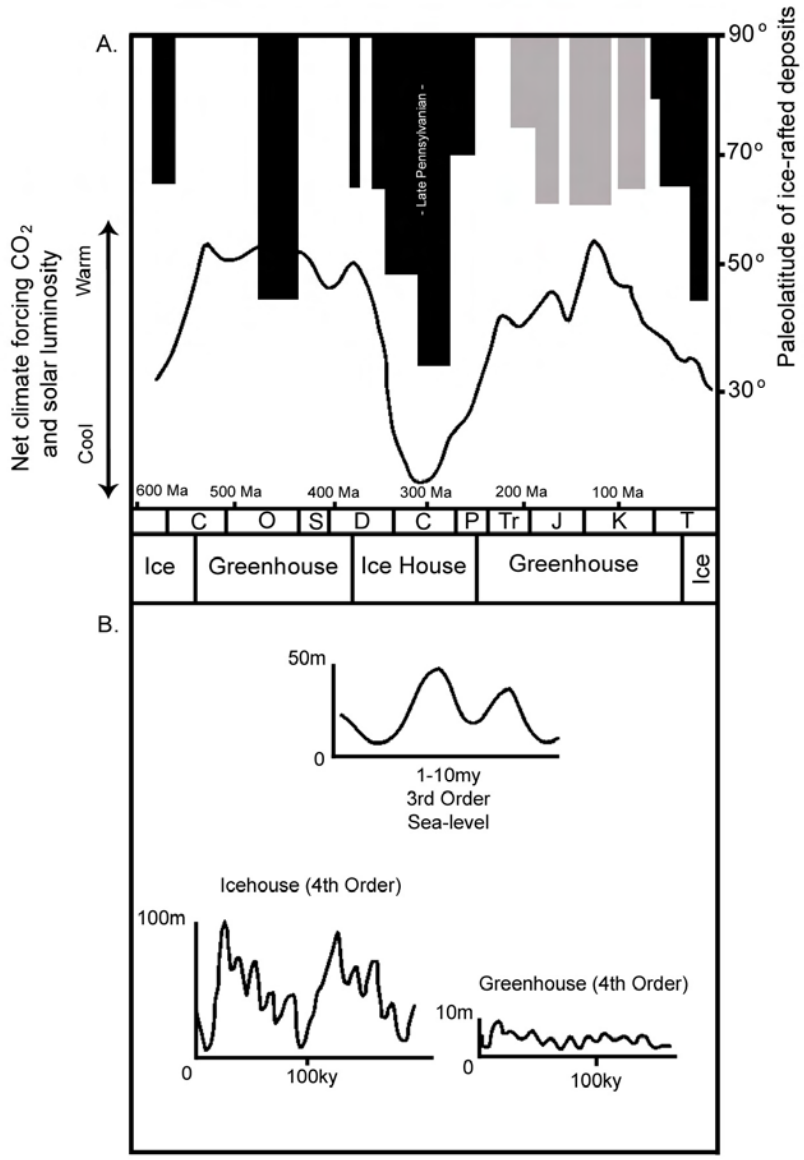

Figure 22: Diagram showing the relationship between greenhouse (periods of little to no polar ice) and icehouse (periods where polar ice exists) conditions, global CO_2 and eustasy. Part A: illustration showing paleolatitudinal extent of marine ice-rafted deposits (gray) and continental ice-rafted deposits (black). The curve plots net forcing of climate due to changes in CO_2 and solar luminosity. Ages, time periods and general greenhouse/icehouse episodes are shown on the horizontal axis. Part B: diagram showing typical third order sea-level curves with a 1 – 10 million year period. There are also two examples of fourth order cycles with superimposed fifth order sea-level curves drawn during times of both icehouse and greenhouse environments (modified from Warren, 1999).

21) and part of the lower Honaker Trail Formation. The final third order sequence (5) identified by Weber *et al*. (1995) is a highstand systems tract and comprised of non-evaporite rocks within the Honaker Trail Formation.

Four of the five third order Desmoinesian sequences (1 – 4) described above involve evaporite cycles of the Paradox Formation. It is important to note how each cycle can be characterized as a fourth order sequence (Figure 24) ranging in duration from 100,000 – 500,000 years with modes of 100,000 years and 450,000 years (Weber *et al*., 1995). These time intervals closely relate to eccentricity cycles defined by the Milankovitch theory.

Weber *et al*. (1995) were also able to correlate all of the third order cycles (1 – 5) identified in the Paradox Basin with other third order sequences characterized in the Mid-continent of North America using fusulinid and foraminifera correlation points. They were also able to tentatively match the third order sequences in the Paradox Basin with major cycle boundaries identified by Heckel (1986) in Kansas using major transgressive/regressive black shales. They concluded that the Chimney Rock shale

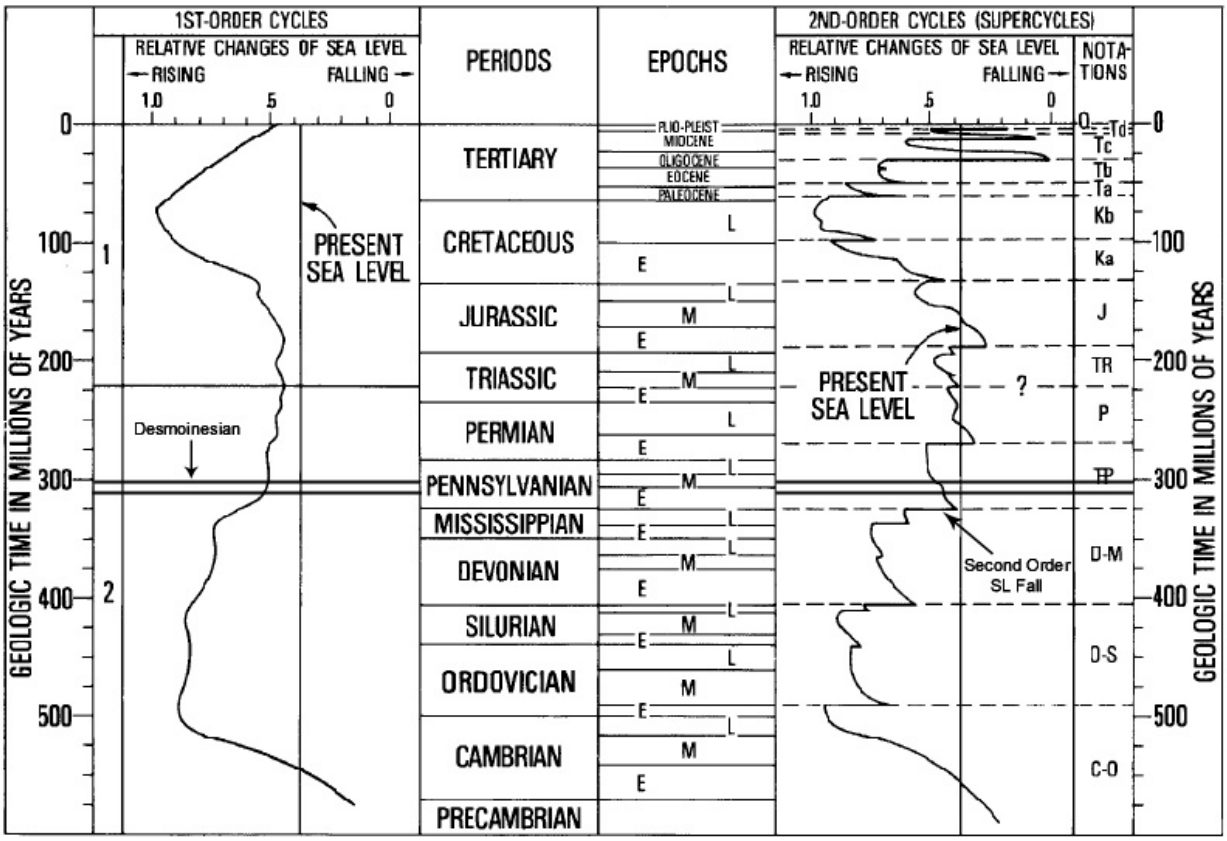

Figure 23 Figure illustrating first and second order cycles of relative sea-level change during the Phanerozoic (modified from Vail et al., 1977).

(evaporite cycle 5) and the Gothic shale (evaporite cycle 3) were correlative to the Verdigris (Oakley shale) and Lower Fort Scott (Excello shale) cycles (Heckel, 1986; Weber *et al*., 1995).

WELL AND OUTCROP DATA ANALYSIS

Well logs, mud logs, outcrop samples, and core were all analyzed in order to better understand the complex structural and stratigraphic Pennsylvanian salt system and its relationship to the Uncompahgre Uplift. This information forms the primary dataset for this study.

General Well Information

Well information for over 500 wells was obtained through the Utah Division of Oil, Gas and Mining (2007) Website and includes wells from Grand, Emery and San Juan counties. These data include well locations (latitude, longitude, township, range, section, etc.), elevations (kelly bushing, ground, derrick floor), API numbers, well names, operators, total depths, completion dates, and well type/status. Any perforation and formation test data were also acquired along with information on cored, producing and pay/show intervals where available.

Formation top data were gathered from a variety of sources. The primary source was the Utah Division of Oil, Gas and Mining (2007) Website. The tops were located from the well files listed under each individual well. Scout tickets reserved at the Denver Earth Resources Library (2007) were also used in the assembly of the formation tops database. The above well information was compiled into a *PETRA* (IHS) database specifically designed only for this project.

Unfortunately, there are two major

Stratigraphic Sequence Hierarchy

Sequence Order	Duration (Ma) Range	Duration (Ma) Mode	Stratigraphic Nomenclature (Greenhouse)	Stratigraphic Nomenclature (Icehouse)	Area of Effect
1st	350-500	450	Megasequence Set		Global
	50-100+	80	Megasequence Set		
2nd	20-50	30	Supersequence Set		Regional
	5-20	10	Supersequence		
3rd	0.5-5	1	Sequence	Composite Sequence	Local
4th	0.1-0.5	0.1; 0.45	Parasequence Set Parasequence	Sequence	
5th/6th	0.01-0.1	0.02; 0.04	Parasequence Bed Sets	Parasequence Set Parasequence	
> 6th (Events)	<0.01		Beds Laminae	Parasequence Bed Sets Laminae	

Figure 24: Chart showing the stratigraphic orders and cycle sequences and associated nomenclature, duration and area of effect (modified from Weber et al., 1995).

problems within the data set involving a lack of well information. First, there are an insufficient number of useful wells located east of the Salt Valley Anticline compared to the amount west of the structure. This creates problems when attempting to correlate from the west side of the study area to the east. Secondly, since Arches National Monument became a national park in 1971, (National Park Service, 2007) no further exploration drilling as been authorized and thus creates a significant void within the study area.

Well Logs

Well logs for over 120 wells were acquired from the Utah Division of Oil, Gas and Mining (2007) Website (Appendix A, Table A-1). Many of the wells within the study area were drilled pre-1990 and poor log quality made some unreadable and uninterpretable. Most of the available logs consisted of sonic, resistivity, gamma ray-neutron, and density-neutron logs with a variety of other atypical logs. These logs were calibrated and added to the *PETRA* database described above.

Available formation tops were then added to the logs and adjusted for errors. Additionally, any formation tops not already available were picked from the well logs. This included identifying the top and bottom of the Paradox salt plus each individual halite and clastic interval. These zones were labeled 1 – 29 (and beyond) following Hite's (1960) informal system of nomenclature where the evaporite cycles are identified numerically.

Well logs in conjunction with geologic

well reports obtained from the Utah Division of Oil, Gas and Mining (2007) Website were also used to identify three main lithological units within the clastic intervals for 10 wells (Appendix A, Table A-2). These specific 10 wells were used because of their geographical location, completeness of stratigraphy through the Paradox Formation, quality of well logs, and the number of evaporite cycles identified. The lithological units included anhydrite, black shale, and silty dolomite (both transgressive and regressive). Individual facies thicknesses for each clastic zone, as well as total lithological thicknesses for the 10 wells, were calculated and tallied. These lithologies, along with their respective sedimentation rates, were used to estimate the time of total deposition for individual evaporite cycles and thus for the entire Paradox Formation.

Core

To augment the well data, the Delhi-Taylor Oil Company Cane Creek No. 1 core (T 26S, R 20E, sec. 25) was studied. The well was drilled approximately along the crest of the Cane Creek Anticline (Figure 20) in Grand County, Utah as a potash exploratory well (Raup and Hite, 1992). The cored interval starts at a depth of 1,825 feet (556 m) in the lower Honaker Trail Formation and proceeds to the bottom of the well at a depth of 2,805 feet (855 m) (evaporite cycle 5 of the Paradox Formation). The core encompasses all of cycles 2, 3, 4 and the halite section of cycle 5. Cycles 2 and 3 are typical, well preserved evaporite sequences. Cycle 4 is much thinner than the previous two cycles and lacks the repetitious clastic zone lithologies also observed in cycles 2 and 3. The halite of cycle 5 is roughly 127 feet (38.7 m) thick and the upper 10 – 12 feet (3 – 3.7 m) is chiefly composed of sylvite (KCl) in association with halite. This potash-bearing zone is currently being mined by Intrepid Mining, LLC (Raup and Hite, 1992; Intrepid Mining, 2006).

For the purposes of this study, describing and logging the core was deemed unnecessary, as this had already been thoroughly completed by several authors including Raup and Hite (1992). Instead, specific questions were addressed while studying the core which included observing thickness variations of interbedded anhydrite and detrital laminae within the halite zones, characterizing the boundary between cycles, identifying textures within the anhydrite intervals, and noting the presence of fractures (cemented or un-cemented) within the organic-rich black shales.

Outcrop

Outcrop samples were gathered from the Onion Creek area south of Utah State Highway 128 (Figure 25). The exposed caprock is mainly composed of gypsum, anhydrite, and the remains of what appear to be clastic intervals. Several tributaries or drainages feed into Onion Creek and have cut narrow canyons into a salt diapir. A side canyon along Onion Creek (N38° 41' 58.2", W109° 16' 48.2") offers good access to the outcrops and cuts down vertically through the caprock revealing a cross-sectional profile. However, since the rocks have undergone chemical and physical changes during the caprock formation process, it is very difficult to identify which clastic zones within the stratigraphical sequence are exposed (Figure 26). Several wells in the area suggest this outcrop is correlative to somewhere within the first 10 evaporite cycles. Samples of black shale, dolomite/siltstone and gypsum were collected from several locations along this canyon (Figure 27).

An exposed bed of fine-grained, fractured, laminated sandstone is located on the northern edge of the caprock (Figure 28). The sandstone might represent a turbidite bed, but

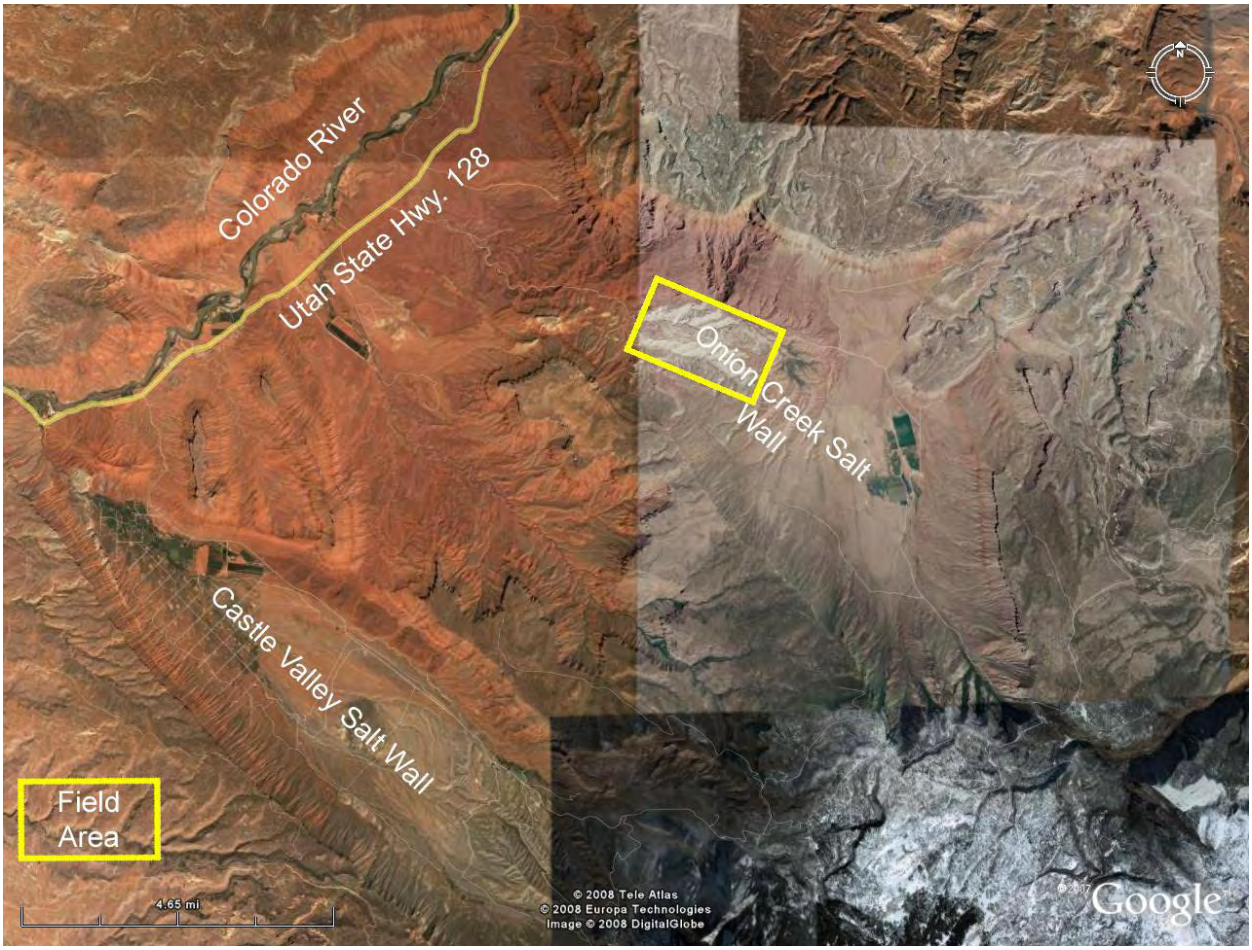

Figure 25: Map showing the location of the caprock outcrop used for field study and sample collection along Onion Creek in the middle of the Onion Creek salt wall. Image modified from Google Earth (2007).

because the area is so structurally distorted and complex, it is difficult to ascertain the placement of the bed within the stratigraphic sequence. The sandstone is located adjacent to red-bed shales considered to be part of the Moenkopi Formation. Therefore, because of the physical position next to the caprock and its relationship adjacent to the Moenkopi Formation, it is thought the sandstone bed represents part of the Cutler Group.

Mud Logs

Gasconade Oil Company and Delta Petroleum Corporation generously provided mud logs from several recently drilled wells for this project. These wells include several drilled by Delta Petroleum in their Greentown (Greentown St. 36-11, T 21S, R 16E, sec. 26; Greentown St. 32-42, T 22S, R 17E, sec. 32; Samson Federal 28-11, T 22S, R 17E, sec. 28) and Salt Valley (Salt Valley St. 25-12, T 22S, R 19E, sec. 25) project areas (Delta Petroleum, 2008). Due to confidentiality restrictions, at the present time the information obtained and used from these wells cannot be recreated for public display within this study. However, the data were analyzed and used in this report.

QEMSCAN Samples

QEMSCAN is an electron-beam analytical instrument that uses four nitrogen-free EDS (Energy Dispersive Spectrometer) x-ray detectors, BSE (and SE analysis), and a

Figure 26: A clastic interbed overlain by caprock located along the Onion Creek salt wall. The distortion of the beds is attributed to salt wall and caprock formation processes. A rock hammer (left side of the image) is used for scale.

Figure 27: An example of a black shale overlain by a silty dolomite. The photograph was taken along the caprock of the Onion Creek salt wall. Rock hammer is used for scale.

Figure 28: A fine-grained, fractured, laminated sandstone about 10 feet (3.05 m) thick near the edge of the caprock exposure, Onion Creek salt wall, Utah.

proprietary software platform to capture a wide spectrum of elemental abundance data on a pixel basis, and image the data so they can be assessed as required. Developed for the mining industry, the instrument achieves rapid image analysis and data acquisition for thousands of grains in a short time, enabling quick assessment of compositional variation, distribution, grain shape, and mineral assemblages. It is applied to the analysis of mineralogy, alteration, ore petrology, well cuttings, stratigraphic correlations, cements, environmental soil and dust, tissue and medical, and forensic geoscience.

Five samples were sent to the Advanced Mineralogy Research Center, Colorado School of Mines, Golden, Colorado for detailed mineralogical, porosity and grain size analysis. Four of the samples were chosen from the Delhi-Taylor Oil Company Cane Creek No. 1 core (T 26S, R 20E, sec. 25) and were generously borrowed courtesy of the USGS Core Research Center located at the Denver Federal Center, Denver, Colorado (Table 1). The fifth sample was taken from a hand specimen collected along the Onion Creek diapir.

The purpose of testing these five dolomitic samples was to understand their mineralogical composition. This involved two objectives: (1) to determine if there was a change in quartz content between transgressive and regressive dolomites of individual cycles and (2) to attempt a correlation from the Cane Creek No. 1 core, eastward across the basin toward the

Table 1: Table of the five samples used for QEMSCAN analysis.

Location	Depth (ft)	Cycle	Trans./Regres.	Lithology
Cane Creek Core	2134.8	2	Regressive	Silty Dolomite
Cane Creek Core	2184.0	2	Transgressive	Silty Dolomite
Cane Creek Core	2377.1	3	Regressive	Silty Dolomite
Cane Creek Core	2446.1	3	Transgressive	Silty Dolomite
Onion Creek	Outcrop	?	?	Silty Dolomite

Uncompahgre Uplift, to the Onion Creek area using the mineralogical composition (quartz and feldspar in particular) as the major correlative factor.

Sample preparation included using a diamond studded saw to cut each sample into proper sized sections, which were mounted in epoxy-resin and left to cure. The mounted samples were ground and polished using alcohol-based lubricants and suspensions to preserve water-sensitive materials like gypsum and halite. They were then carbon coated to establish an electrically conductive surface needed for the analysis. The QEMSCAN analysis machine uses x-rays and four detectors to examine each individual point on a grain or sample depending on the measurement size (25 and 10 microns were used for each sample). The data were then filtered through the QEMSCAN computer processors where a mineralogical spectrum was used to identify the mineral or mineral assemblage for that particular point. After the entire sample was scanned, a detailed picture of the sample including a mineralogical model was created.

QEMSCAN Analysis Results

The main purpose of testing the five dolomitic samples using the QEMSCAN analysis machine was to compare the mineralogical composition of each sample between transgressive and regressive sequences and to attempt a correlation across the basin.

Transgressive and Regressive Comparisons

Four samples from the Delhi-Taylor Oil Company Cane Creek No. 1 core were analyzed. The samples were from two evaporite cycles (cycles 2 and 3) and from both transgressive and regressive lithological units (Table 1). As first postulated by Raup and Hite (1992), there is a significant difference in the mineralogical composition between transgressive and regressive dolomites, particularly involving the amount of quartz. There is an abundant amount of quartz in each transgressive sample (Figures 29 and 30) compared to its regressive counterpart (Figures 31 and 32). In fact, there are increased amounts of plagioclase, alkali feldspar, muscovite, illite and kaolinite within the transgressive sequences (Figure 33 and Table 2). It is believed the increased amount of detrital grains is a result of rising water levels within the basin stirring up and collecting any material that had been deposited into the basin after halite deposition and before the start of the next sea-level transgression. It is also likely any loose material located along the edge of the basin, possibly from alluvial fans, would be collected and consumed by the incoming transgressive waters and thus deposited into basin.

Basin Correlation

In an attempt to correlate clastic zone mineralogical assemblages across the basin, the samples from the Cane Creek core (west)

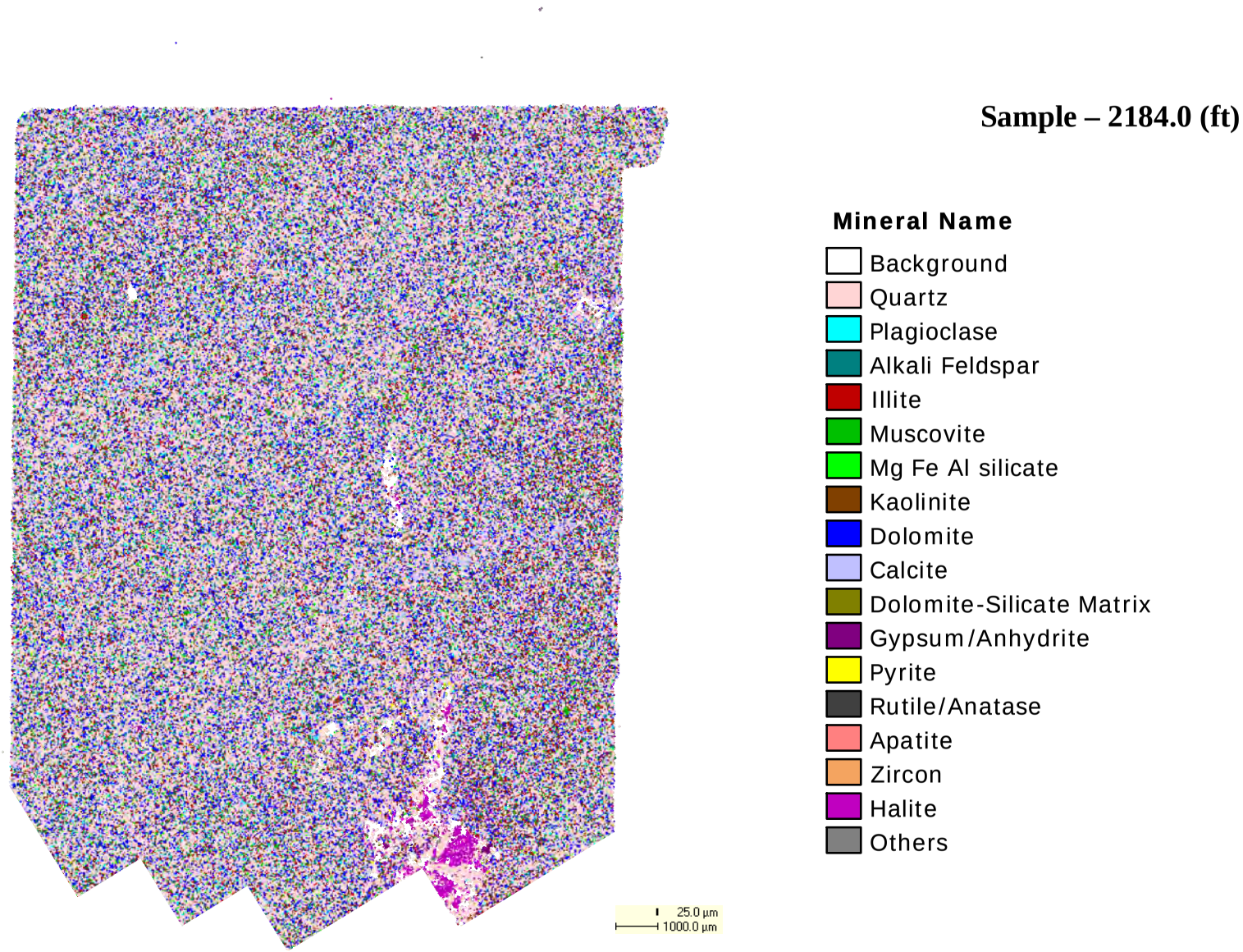

Figure 29: Figure showing the mineral compilation for transgressive sample 2184.0 (ft) (cycle 2) using a 25 µm measurement spacing. Background is equal to porosity.

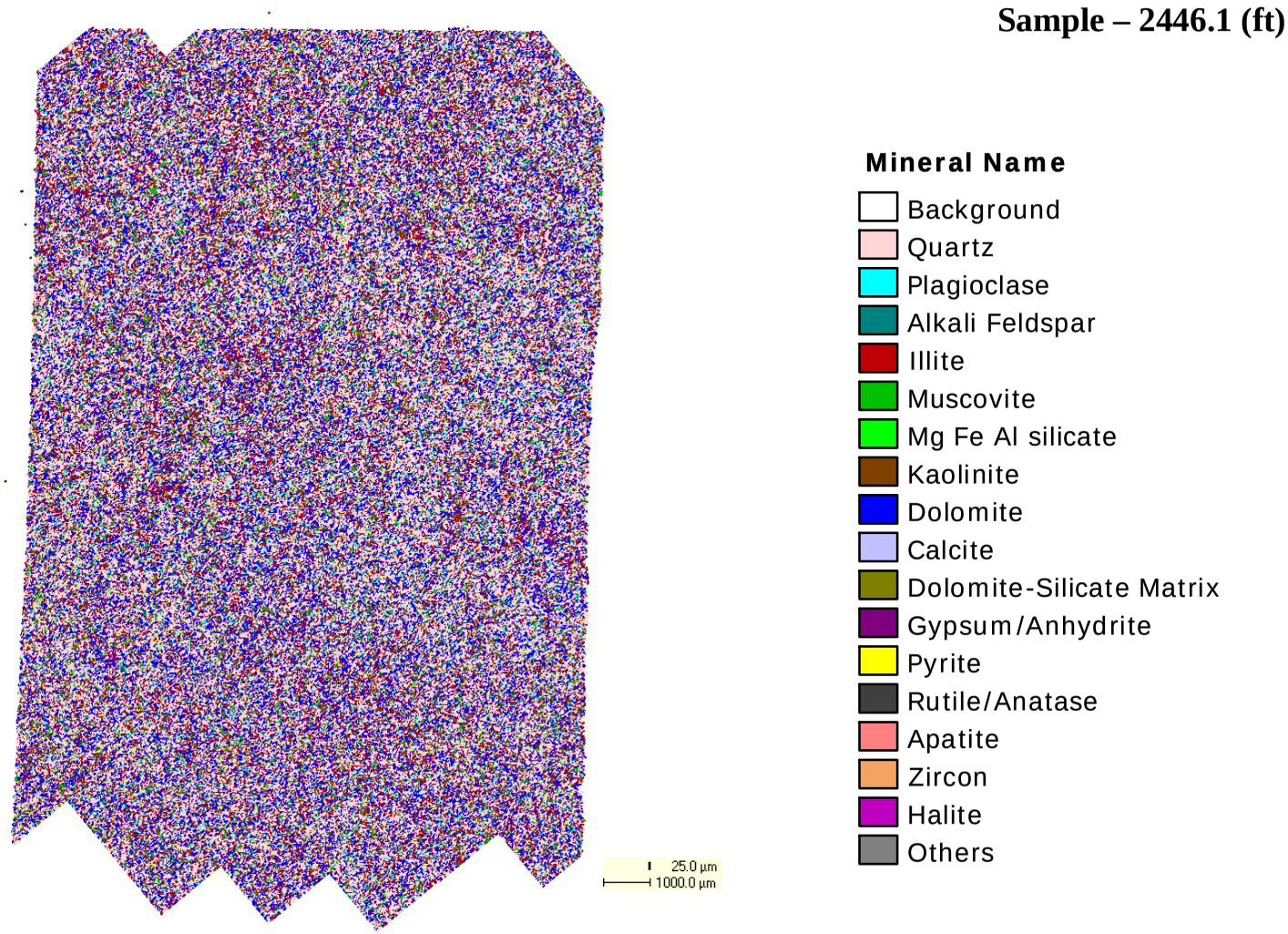

Figure 30: Figure showing the mineral compilation for transgressive sample 2446.1 (ft) (cycle 3) using a 25 µm measurement spacing. Background is equal to porosity.

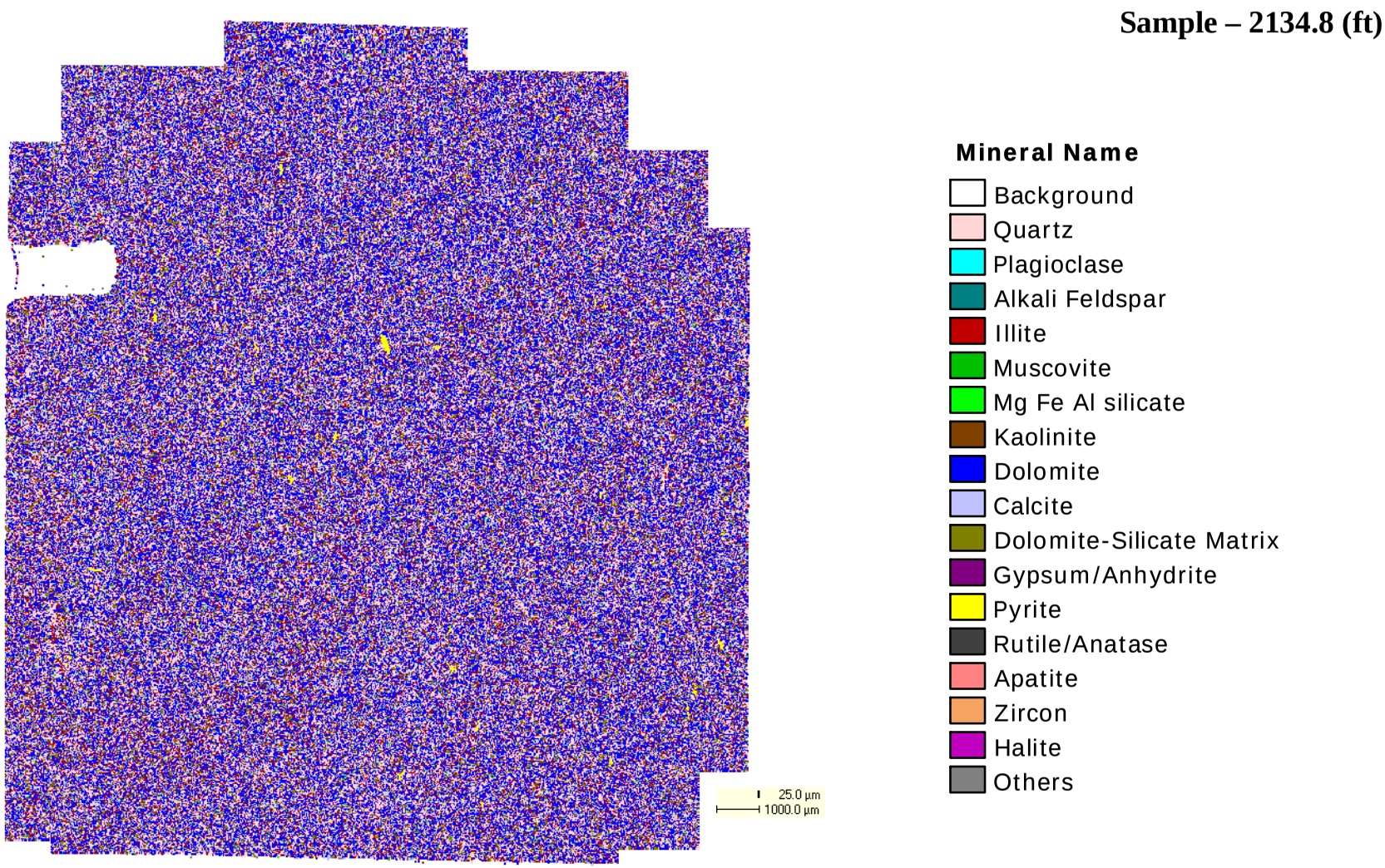

Figure 31: Figure showing the mineral compilation for regressive sample 2134.8 (ft) (cycle 2) using a 25 µm measurement spacing. Background is equal to porosity.

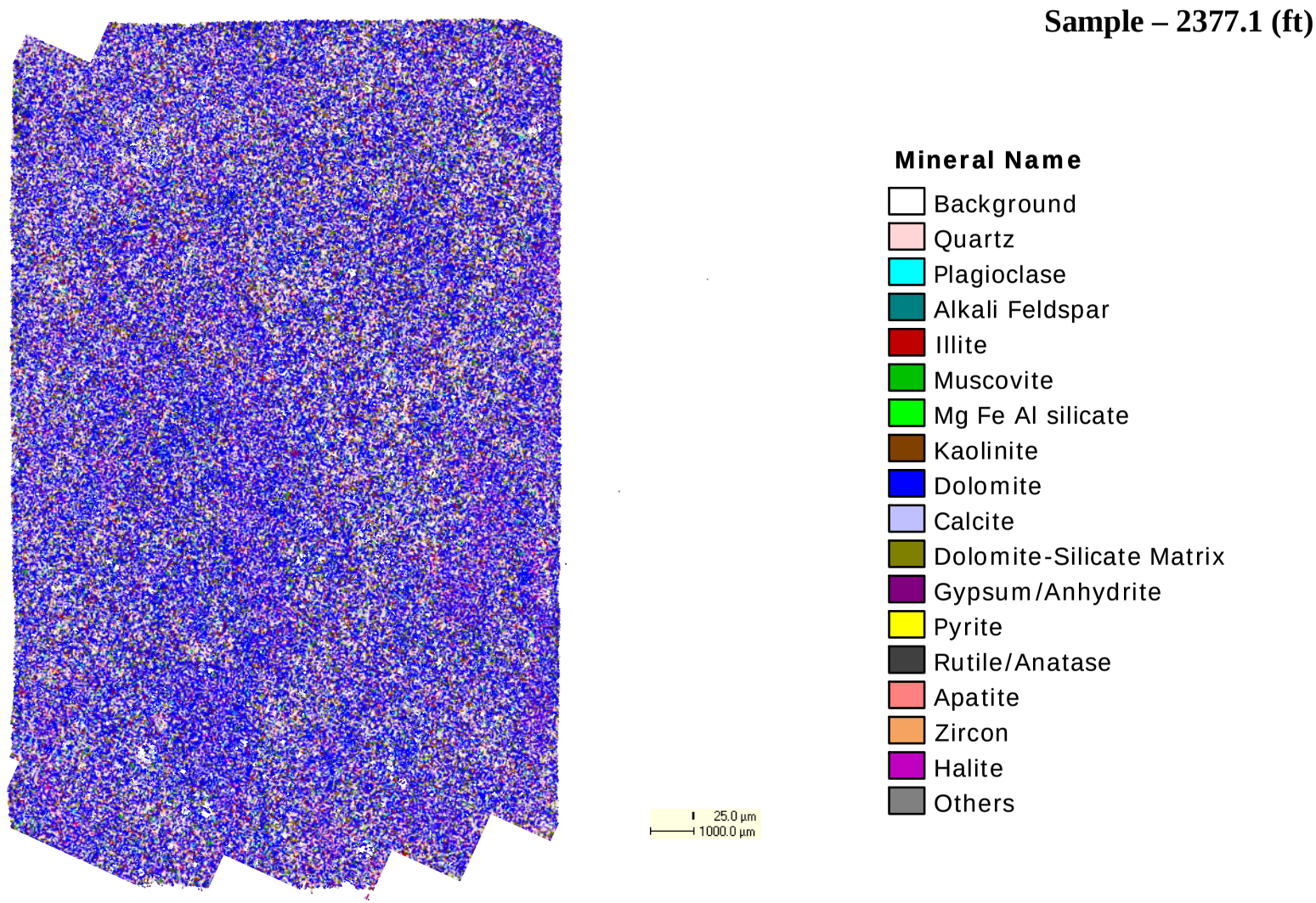

Figure 32: Figure showing the mineral compilation for regressive sample 2377.1 (ft) (cycle 3) using a 25 µm measurement spacing. Background is equal to porosity.

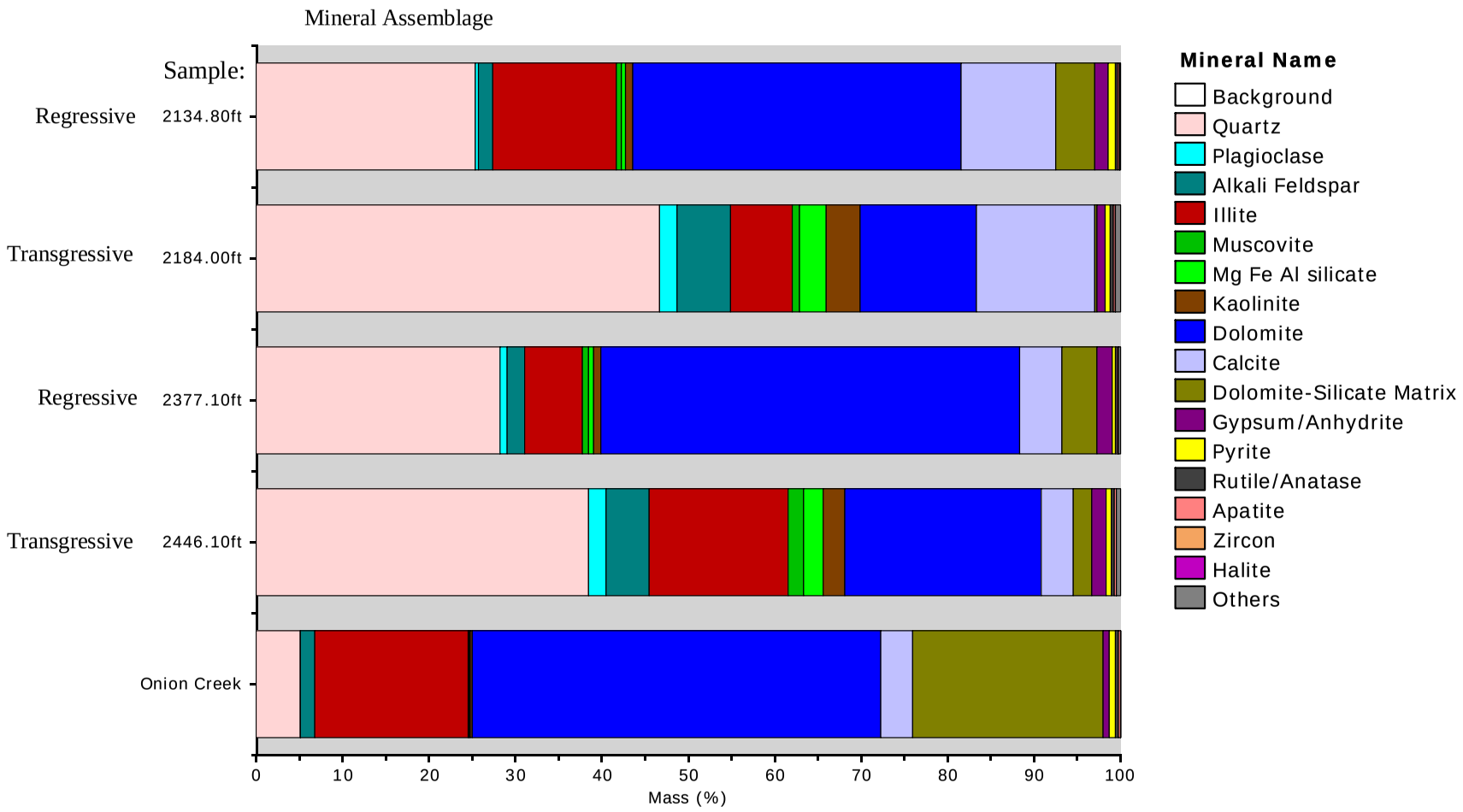

Figure 33: Figure graphically showing the mineral assemblage for the five QEMSCAN analyzed samples. Note the increased quartz, plagioclase, alkali feldspar, etc. content in the transgressive samples. Background is equal to porosity.

Table 2: A table displaying the mineral assemblages for the five QEMSCAN analyzed samples. The Mg Fe Al silicate mineral listing represents minerals like chlorite and serpentine.

	Samples (%)				
Minerals	**2134.8 (ft)**	**2184.0 (ft)**	**2377.1 (ft)**	**2446.1 (ft)**	**Onion Creek**
Quartz	25.4	46.7	28.2	38.4	5.2
Plagioclase	0.3	1.9	0.9	2.0	0.0
Alkali Feldspar	1.6	6.2	2.1	5.0	1.6
Illite	14.2	7.2	6.7	16.1	17.7
Muscovite	0.6	0.8	0.7	1.7	0.2
Mg Fe Al Silicate	0.5	3.1	0.5	2.3	0.0
Kaolinite	0.8	3.9	0.9	2.5	0.2
Dolomite	38.1	13.5	48.4	22.7	47.3
Calcite	10.9	13.7	5.0	3.8	3.7
Dolomite-Silicate Matrix	4.5	0.3	4.0	2.1	22.0
Gypsum/Anhydrite	1.6	0.9	1.7	1.7	0.8
Pyrite	0.8	0.6	0.3	0.6	0.7
Rutile/Anatase	0.3	0.4	0.2	0.4	0.2
Apatite	0.2	0.2	0.1	0.2	0.3
Zircon	0.0	0.1	0.0	0.0	0.0
Halite	0.0	0.0	0.0	0.0	0.0
Others	0.2	0.5	0.3	0.5	0.1
Total %	100.0	100.0	100.0	100.0	100.0

were compared to one outcrop sample collected from the Onion Creek diapir (east). The preliminary thinking, before the samples were analyzed, involved the Onion Creek sample comprising significant amounts of granitic material, compared to the samples from the Cane Creek core, if the detrital source was the nearby Uncompahgre Uplift. The results however, were rather inconclusive and can possibly be related to several problems involving the outcrop and rock/ sample characterization.

The Onion Creek sample composition compares best to the composition of the regressive dolomitic samples identified in cycles 2 and 3 of the Cane Creek core (Figures 33 – 35 and Table 2). It is composed of mostly of dolomite, illite and a dolomite-silicate matrix, which has been analyzed as an extremely fine-grained assortment of dolomite and quartz material. It is also the only sample of the five analyzed that displayed any identifiable laminations.

Several problems limit the effectiveness and accuracy of using the Onion Creek sample for a basin-wide comparison. The sample was collected from one of a very select few outcrops of the Paradox Formation in the northern half of the basin. In addition, the outcrop was highly altered and distorted

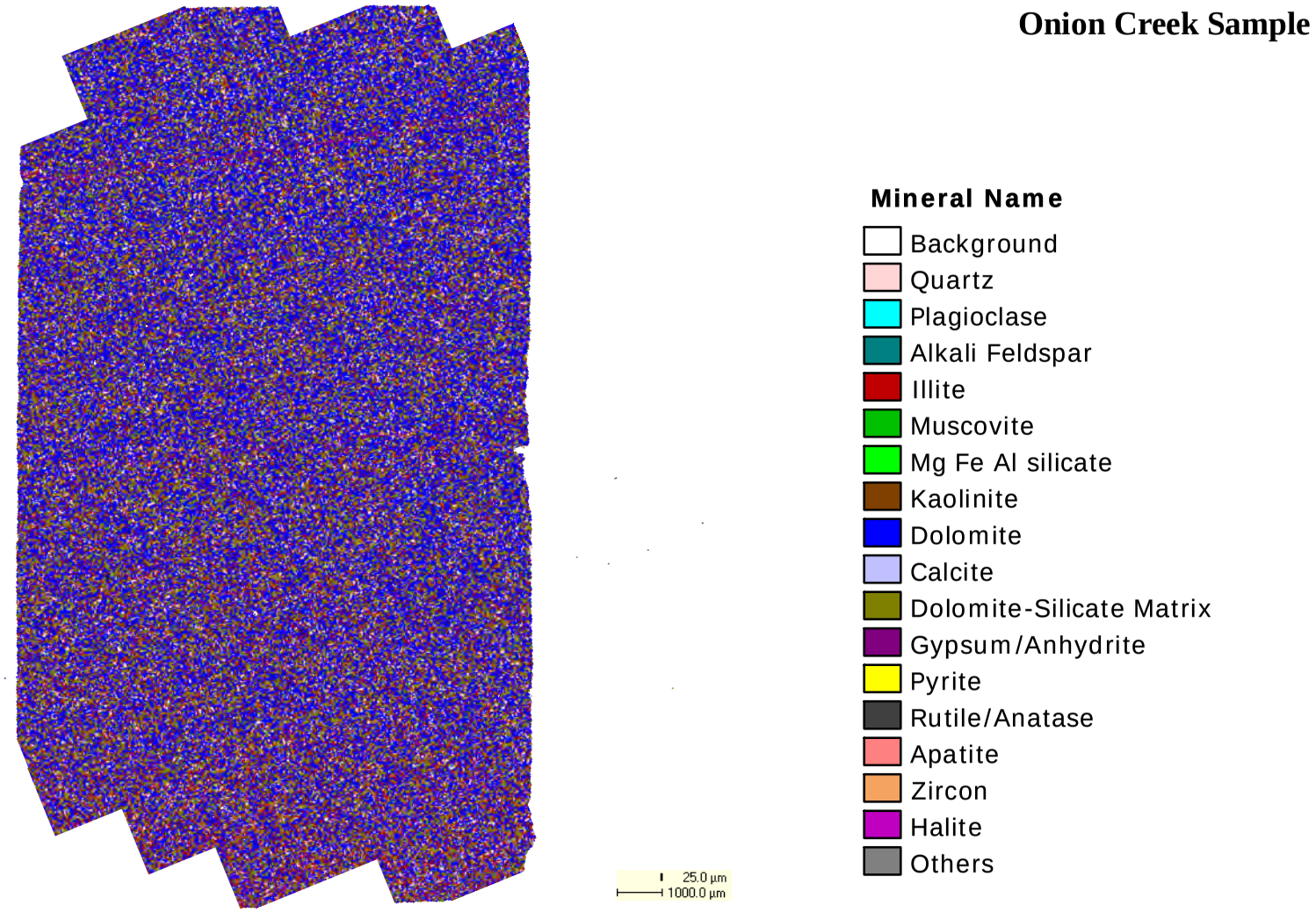

Figure 34: Figure showing the mineral compilation for the Onion Creek outcrop sample using a 25 µm measurement spacing. Background is equal to porosity.

Mineralogy – All Samples – 10.0 Micron Spacing

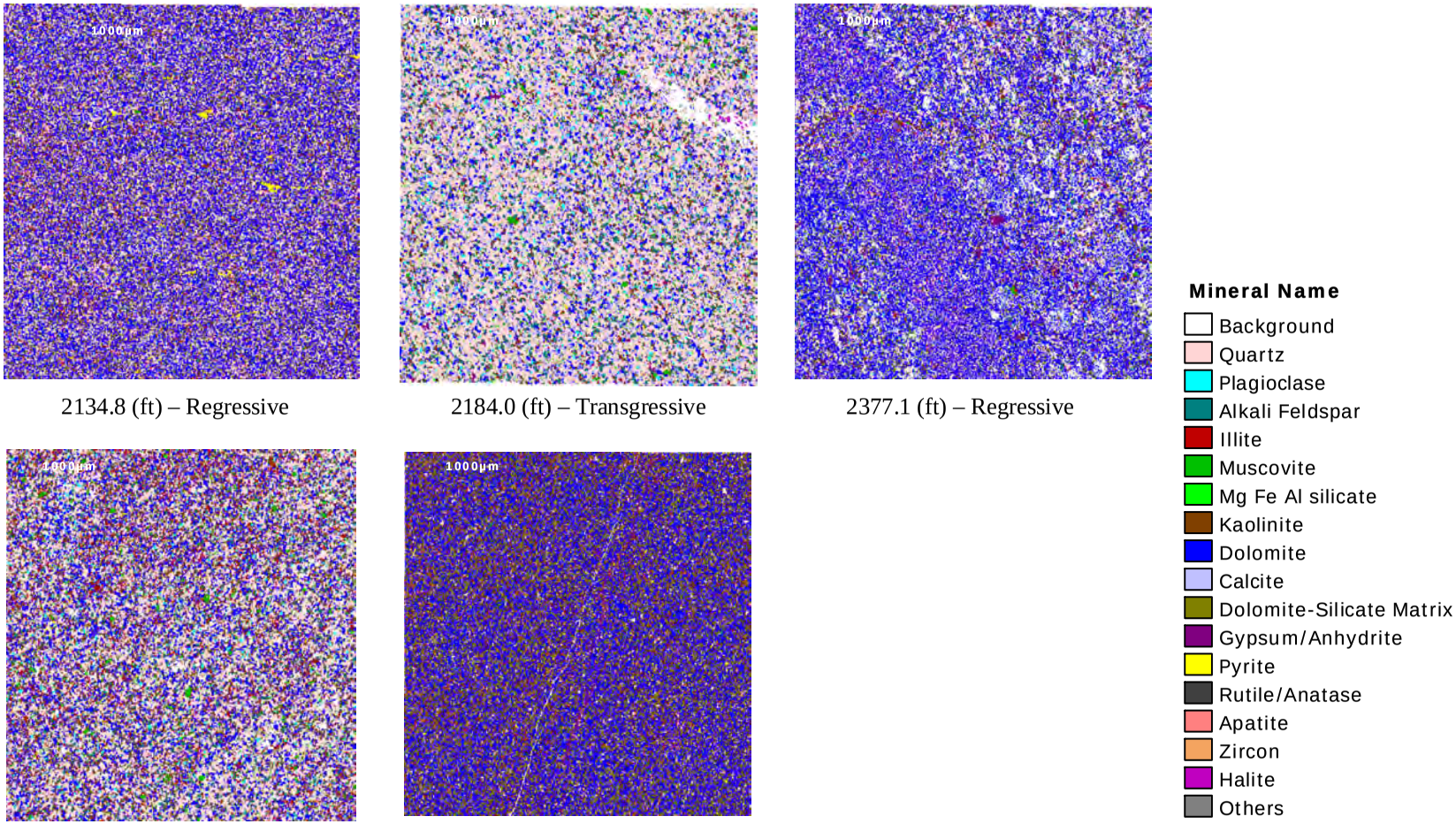

2134.8 (ft) – Regressive

2184.0 (ft) – Transgressive

2377.1 (ft) – Regressive

2446.1 (ft) – Transgressive

Onion Creek

Figure 35: Figure showing the mineral assemblage for all five samples using a 10 µm measurement spacing. Background is equal to porosity.

due to caprock formation processes. The sample was also selected from an atypical dolomitic bed (very thin) compared to the carbonate intervals sampled from the core. Finally, it is unclear which clastic zone, let alone evaporite cycle, the sample was taken. Because of the diapiric and caprock structural and chemical formation processes, it may not be possible to ascertain this vital information. Therefore, to create a better basin-wide correlation using the clastic zone mineral assemblages, the Onion Creek specimen should ideally be replaced by several samples taken from a cored interval located away from any major salt related structure.

Grain Size, Grain Density and Porosity Estimates

The average grain size, grain density, and an estimated porosity were calculated for all five samples. The average grain size for the transgressive samples is larger then the regressive samples (Figure 36). This supports the hypothesis that as the sea level rose, the incoming waters collected and distributed coarser grained material into the basin.

The grain density was calculated based on the mineral assemblage for each sample and is thus influenced by the most abundant minerals including quartz and dolomite (Figure 37). The grain density may have also been affected by several heavy minerals, like pyrite and zircon, boosting the sample density depending on representative percentages (Figure 38).

Porosity estimates were also conducted for the five samples, and the porosity ranges from 0.43 to 10.68 percent (Figure 39). Porosity has no clear correlation with transgressive or regressive samples. It is thought the porosity may be controlled by micro fractures, grain overgrowths and cement content and abundance.

In regressive sample 2134.8 (ft), bacterialy produced framboidal pyrite was identified. This indicates there was organic material deposited within at least the regressive dolomites.

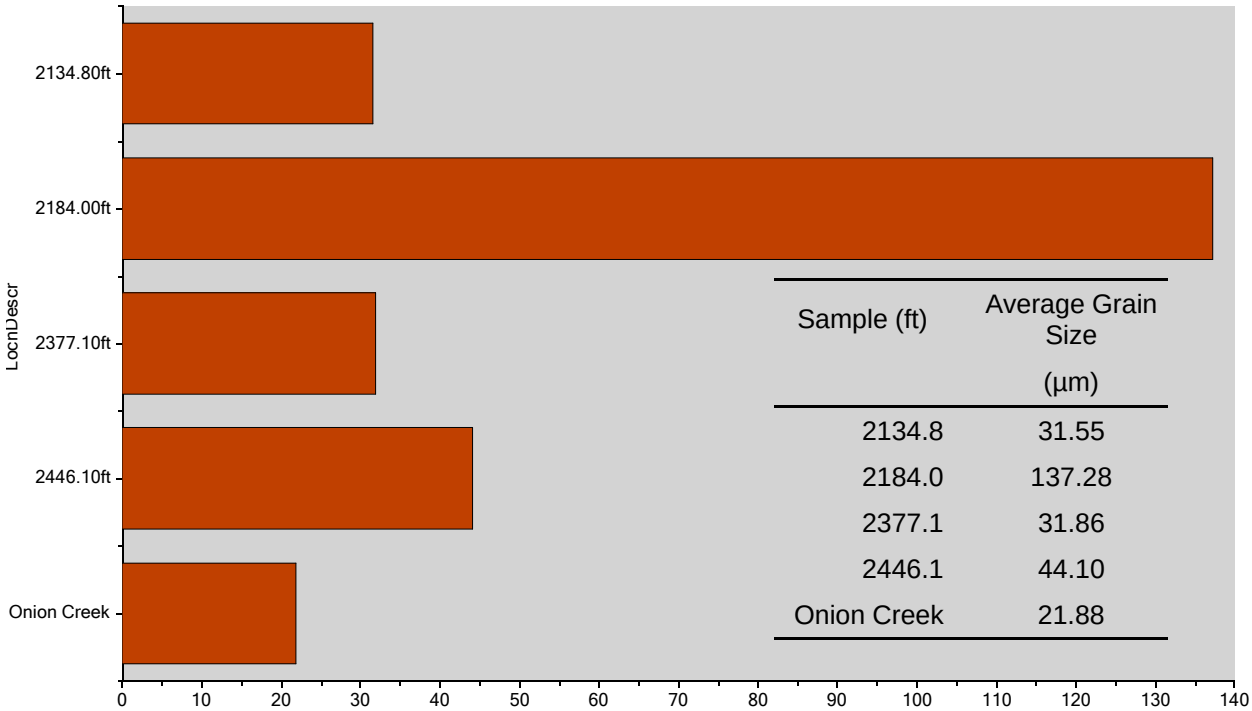

Sample (ft)	Average Grain Size (µm)
2134.8	31.55
2184.0	137.28
2377.1	31.86
2446.1	44.10
Onion Creek	21.88

Figure 36: Graph and table displaying the average grain size distribution for all five QEMSCAN analyzed samples. Note how the regressive samples (2134.8 (ft) and 2377.1 (ft)) tend to be finer grained.

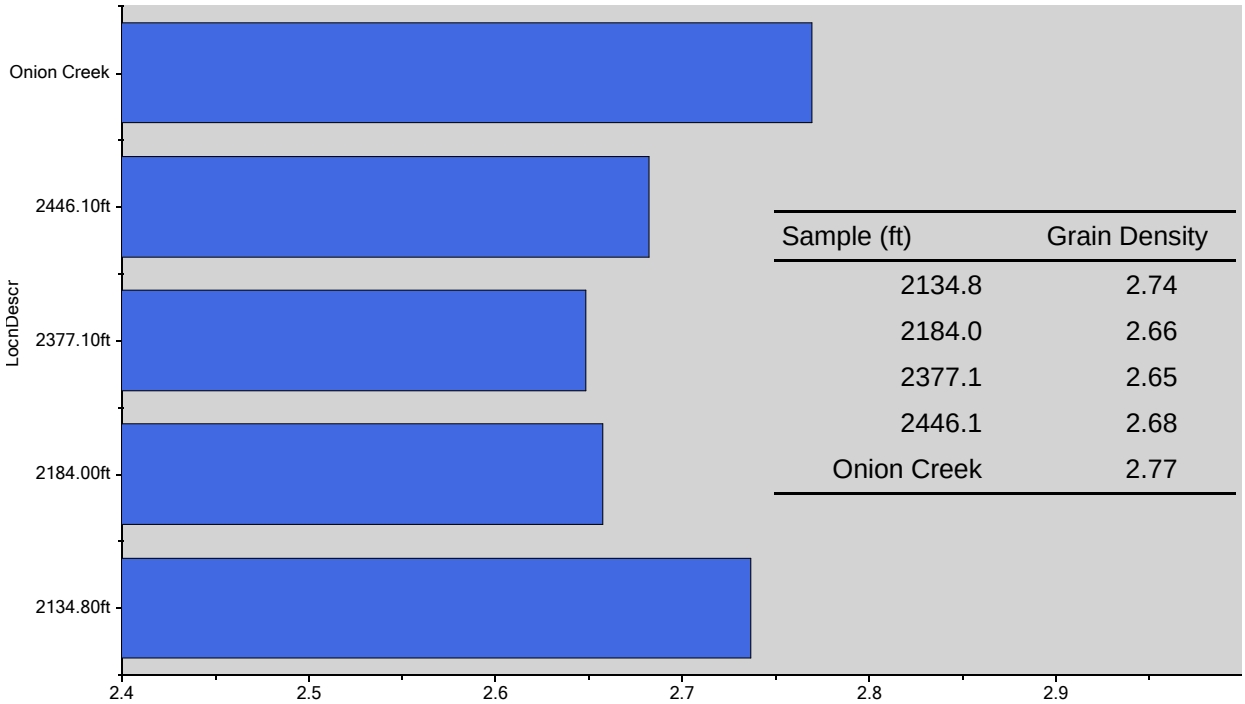

Sample (ft)	Grain Density
2134.8	2.74
2184.0	2.66
2377.1	2.65
2446.1	2.68
Onion Creek	2.77

Figure 37: Graph and table displaying the grain density distribution for all five QEMSCAN analyzed samples. The density calculations may be highly influenced by the amount of available pyrite.

EVAPORITE CYCLE ISOPACH MAPS AND ANALYSIS

To understand the spatial and correlative relationships of the Paradox Formation evaporite cycles, isopach maps were created for each individual evaporite sequence. These maps were created using *PETRA* (IHS) and incorporate both the halite and clastic intervals of each cycle.

Isopach Map Suite

Below is a suite of isopach maps for all 19 of the 29 evaporite cycles observed in the northern Paradox Basin (Figures 40– 58) that include both the halite zone and clastic interval. The maps are organized based on their depositional order where cycle 29 was deposited first followed by cycle 28 and so on. Isopach maps for all 29 cycles can be viewed in Appendix B. Principal observations and analysis of the following maps are discussed in further detail in the following section.

Map Analysis and Observations

Several key observations can be made from the 29 evaporite cycle isopach maps and are listed below.

1. Cycles 23, 20, 17, 13, 10 – 6 and 2 (Figures 46 – 49 and 52 – 57) all show a greater thickness beneath and along the northwest-southeast trend of the Cane Creek Anticline extending northwest towards Green River, Utah. These variations in thickness could be simply explained by post-depositional salt movement. However, Hite (1968) observed that Late Mississippian and Early Pennsylvanian (pre-Paradox Formation) age strata thicken slightly along the same regional zone, as do many of the individual clastic zones. This suggests that the area extending from the Cane Creek Anticline northwest towards the town of Green River, was a depositional low or

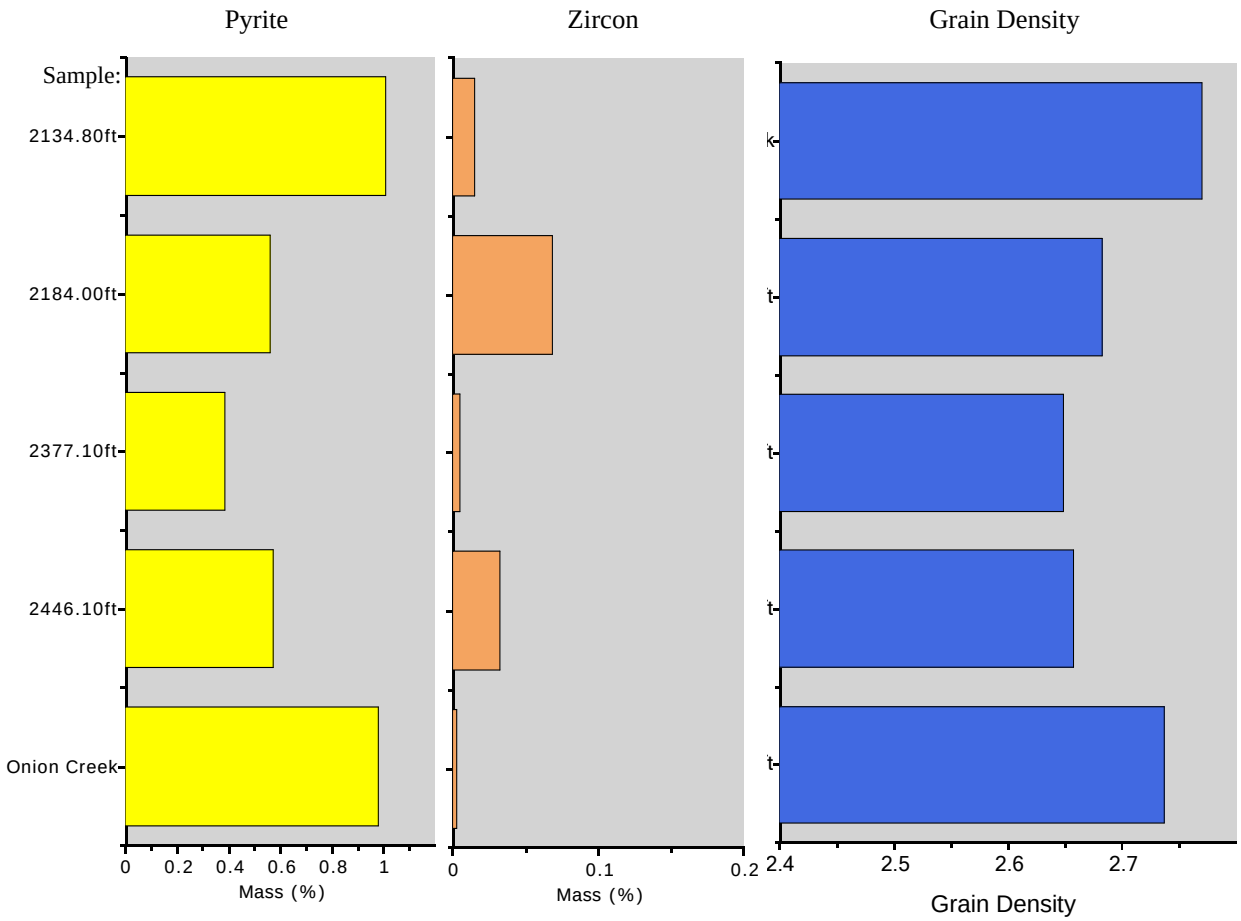

Figure 38: Figure comparing the pyrite content, zircon content and grain density for the five QEMSCAN analyzed samples. Note how an increased pyrite assemblage correlates to an increased grain density.

trough, flanked to the northeast and southwest by slightly positive structures (Hite, 1968). It is likely this trough was tectonically controlled and the controlling structures were active before the deposition of the first salt bed. The trough must have still been actively dropping down by at least the deposition of cycle 2 (Figure 57), but apparently stopped moving near or after the end of salt deposition. The conclusion of the down dropping might have also been caused by differential compaction over rigid fault blocks halting further movement.

2. The Cane Creek trough, described above, is also the only location where all of Hite's (1960) 29 cycles were deposited (Figures 59 – 62). In fact, several wells that were drilled down to the Mississippian encountered additional evaporite cycles numbering up through cycle 33.

3. Evaporite cycle 2 and specific rock units identified in the overlying Honaker Trail Formation are depositionally thinner over the Cane Creek Anticline, as first noticed by Hite (1968) (Figure 57). Hite attributes these thinner beds to folding and buckling of the upper salt beds into an anticlinal position that was likely a result of greater salt movement farther to the east, near the larger more abrupt salt walls.

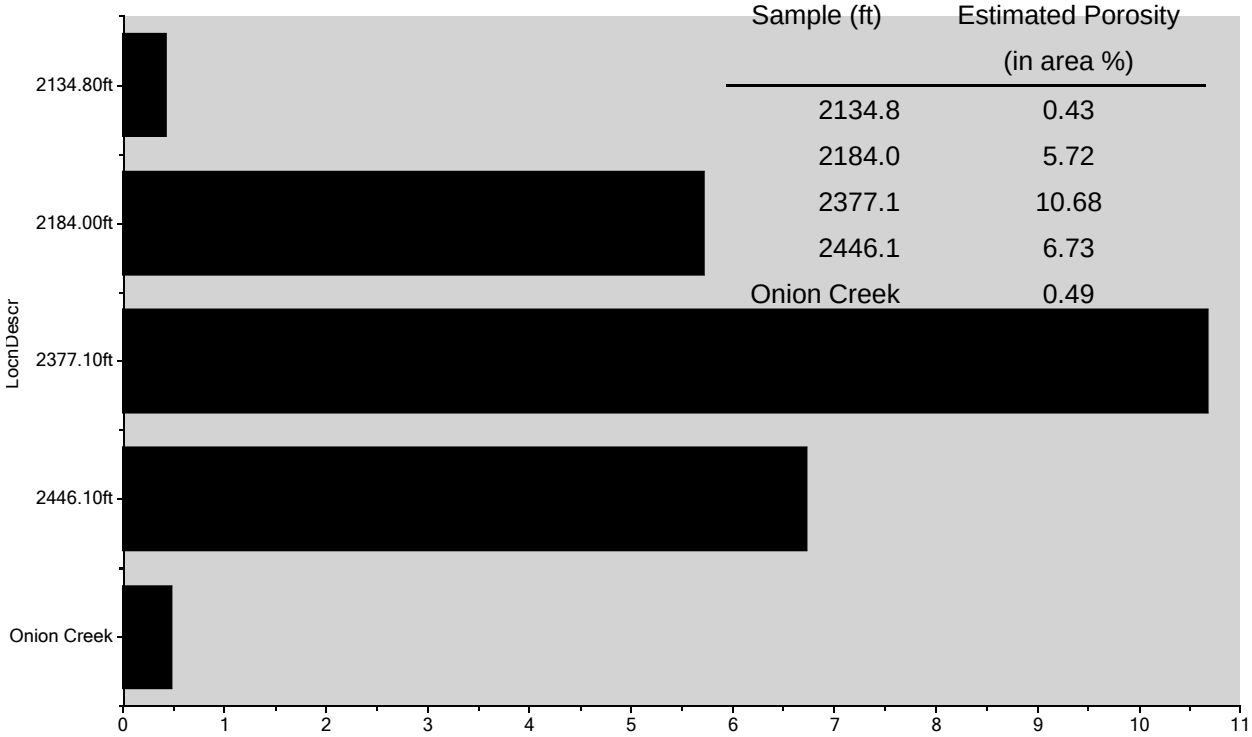

Sample (ft)	Estimated Porosity (in area %)
2134.8	0.43
2184.0	5.72
2377.1	10.68
2446.1	6.73
Onion Creek	0.49

Figure 39: Graph and table displaying the estimated porosity for all five QEMSCAN analyzed samples.

4. Many of the maps show a distinctive low along the western flank of the Salt Valley Anticline. Initial thoughts might suggest this low is solely attributed to salt evacuation into the growing salt wall (Crescent Unit #1 well, Figure 61). The resulting partial salt weld would therefore be misrepresentative of actual depositional cycle thicknesses. However, several of the isopach maps display thickening as they approach the salt wall. Well logs suggest there is considerable thinning along the western edge of the Salt Valley Anticline due to salt welding. The isopach maps that illustrate a thickening trend might be more representative of depositional thicknesses prior to salt tectonics.

5. An interesting relationship is observed with isopach maps involving cycles 29 – 24 (Figure 40 – 45). Cycle 29 thickens towards the east whereas the following cycle, 28, thickens to the west. This thickness reversal pattern continues through cycle 24, creating an oscillating depositional pattern. We interpret that local tectonics (possibly the same basement faulting that controlled the deposition within the Cane Creek trough) are responsible for these thickness fluctuations within the early evaporite cycles.

6. The Mississippian Leadville Limestone and the Pennsylvanian Pinkerton Trail Formation display a regional dip to the east into the deepest part of the Paradox Basin, but are abruptly interrupted by the Uncompahgre Uplift . This regional down dropping was a result of basin subsidence along the Uncompahgre Front. The Paradox Formation

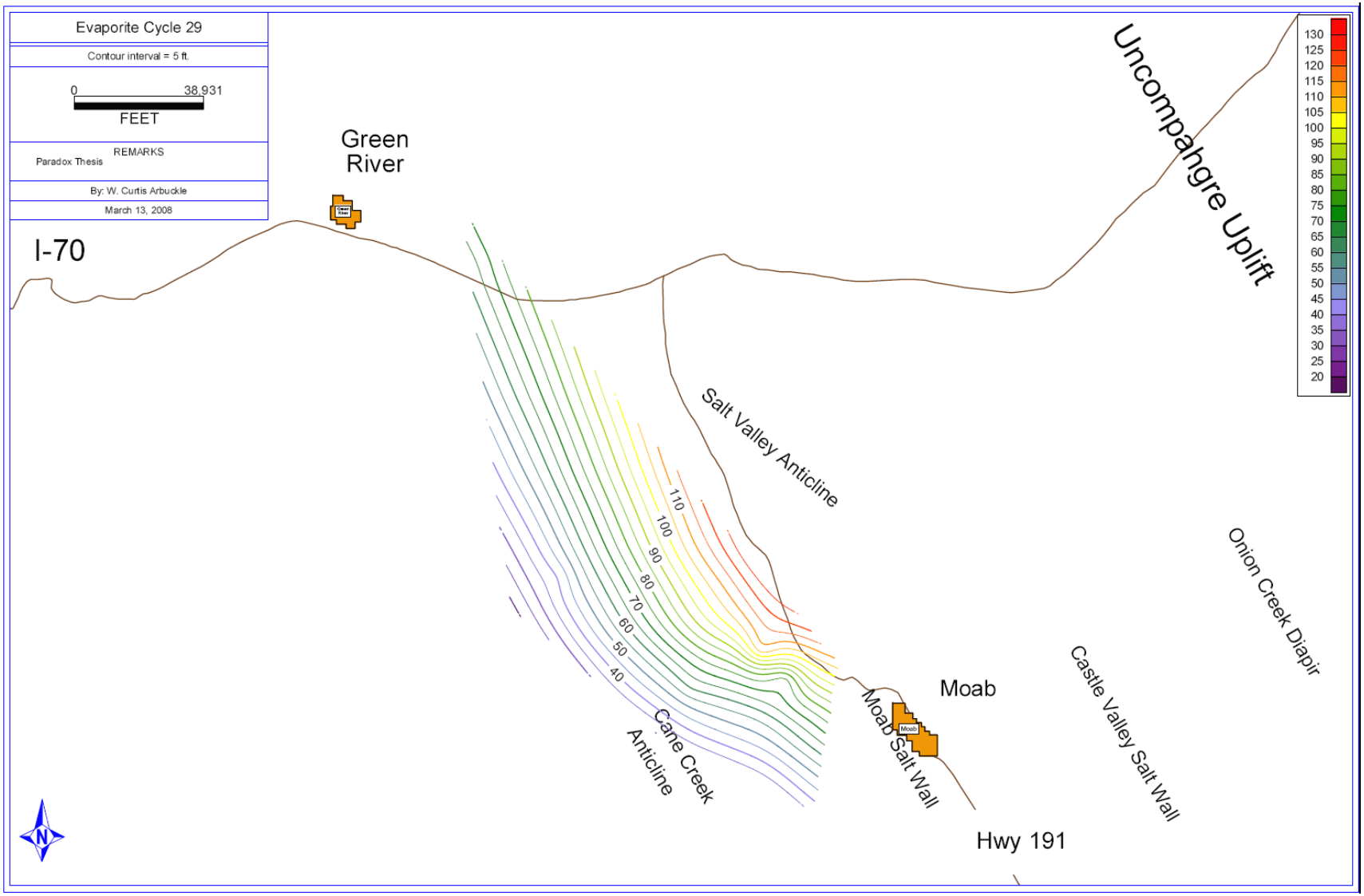

Figure 40: Isopach map of evaporite cycle 29 within the Paradox Formation. See text for analysis. Contour interval = 5 feet (1.52 m).

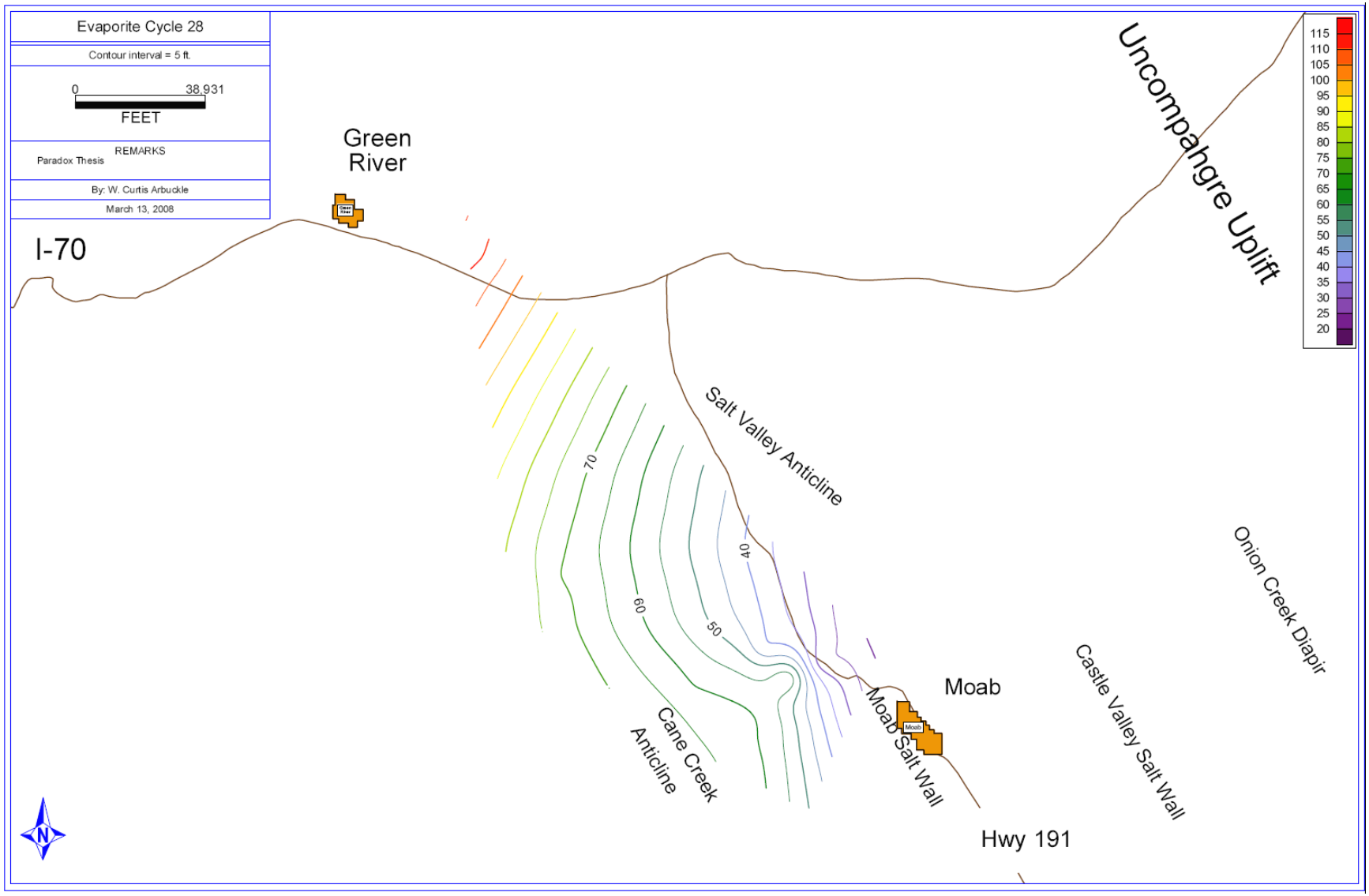

Figure 41: Isopach map of evaporite cycle 28 within the Paradox Formation. See text for analysis. Contour interval = 5 feet (1.52 m).

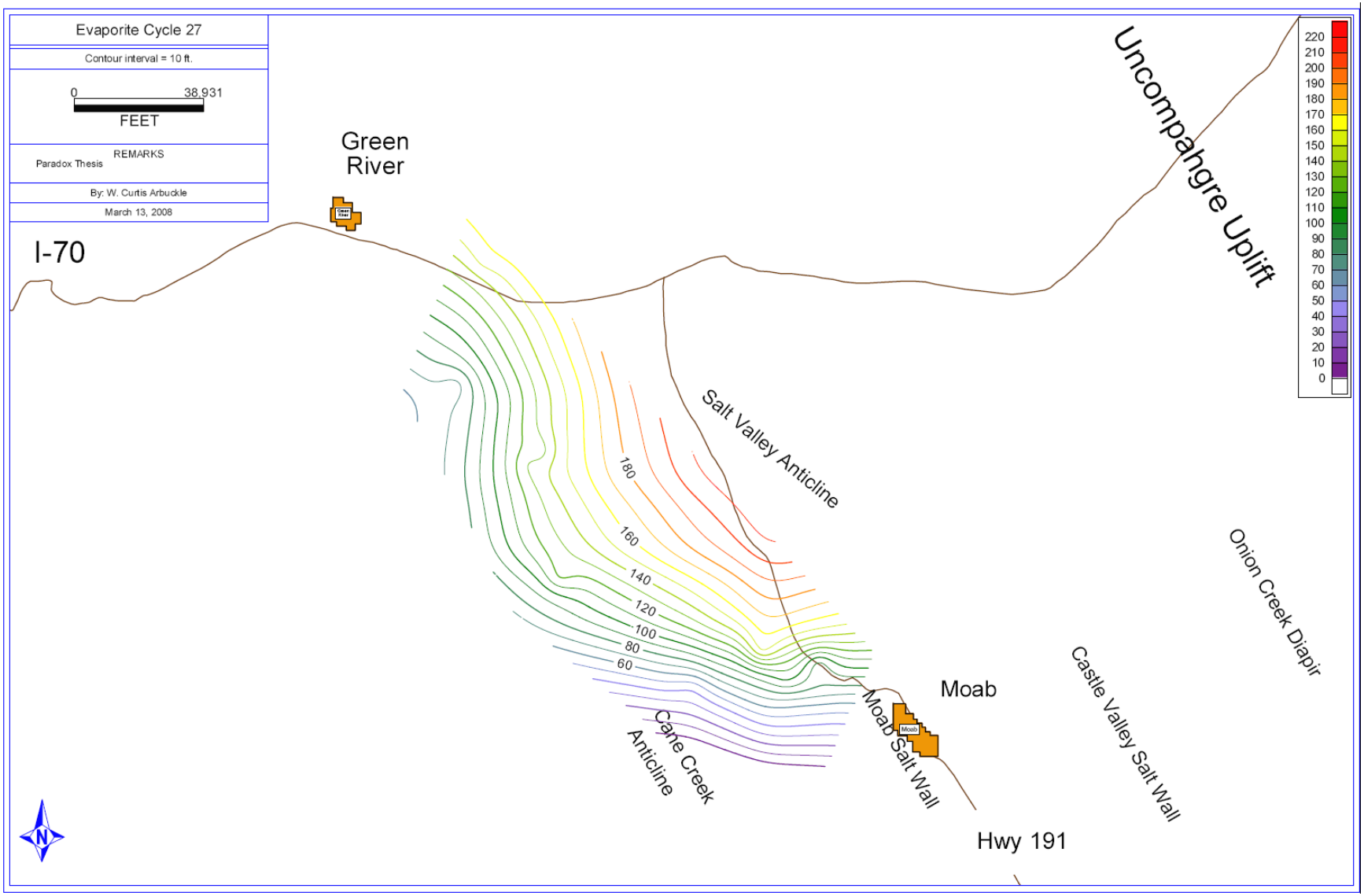

Figure 42: Isopach map of evaporite cycle 27 within the Paradox Formation. See text for analysis. Contour interval = 10 feet (3.05 m).

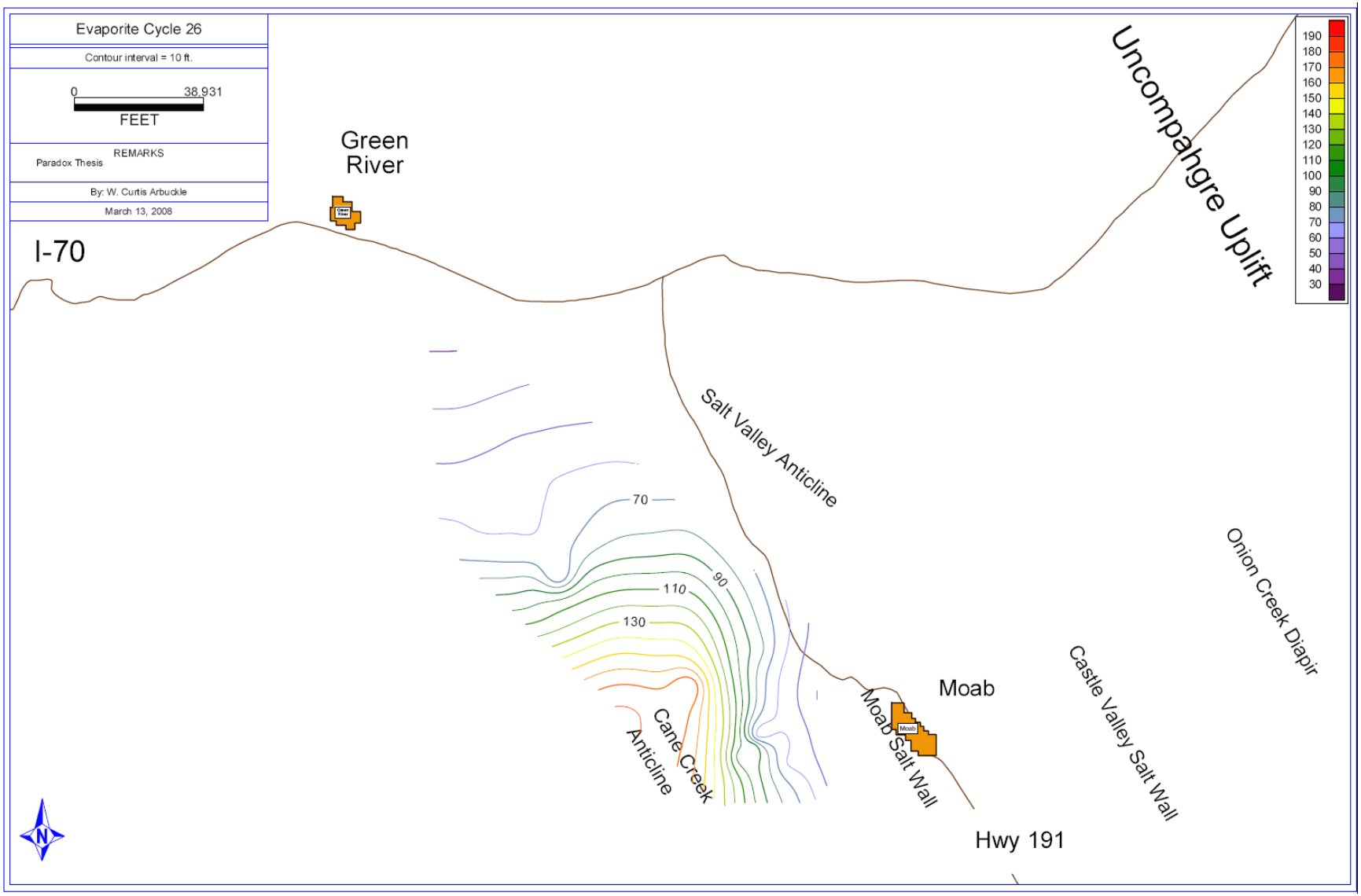

Figure 43: Isopach map of evaporite cycle 26 within the Paradox Formation. See text for analysis. Contour interval = 10 feet (3.05 m).

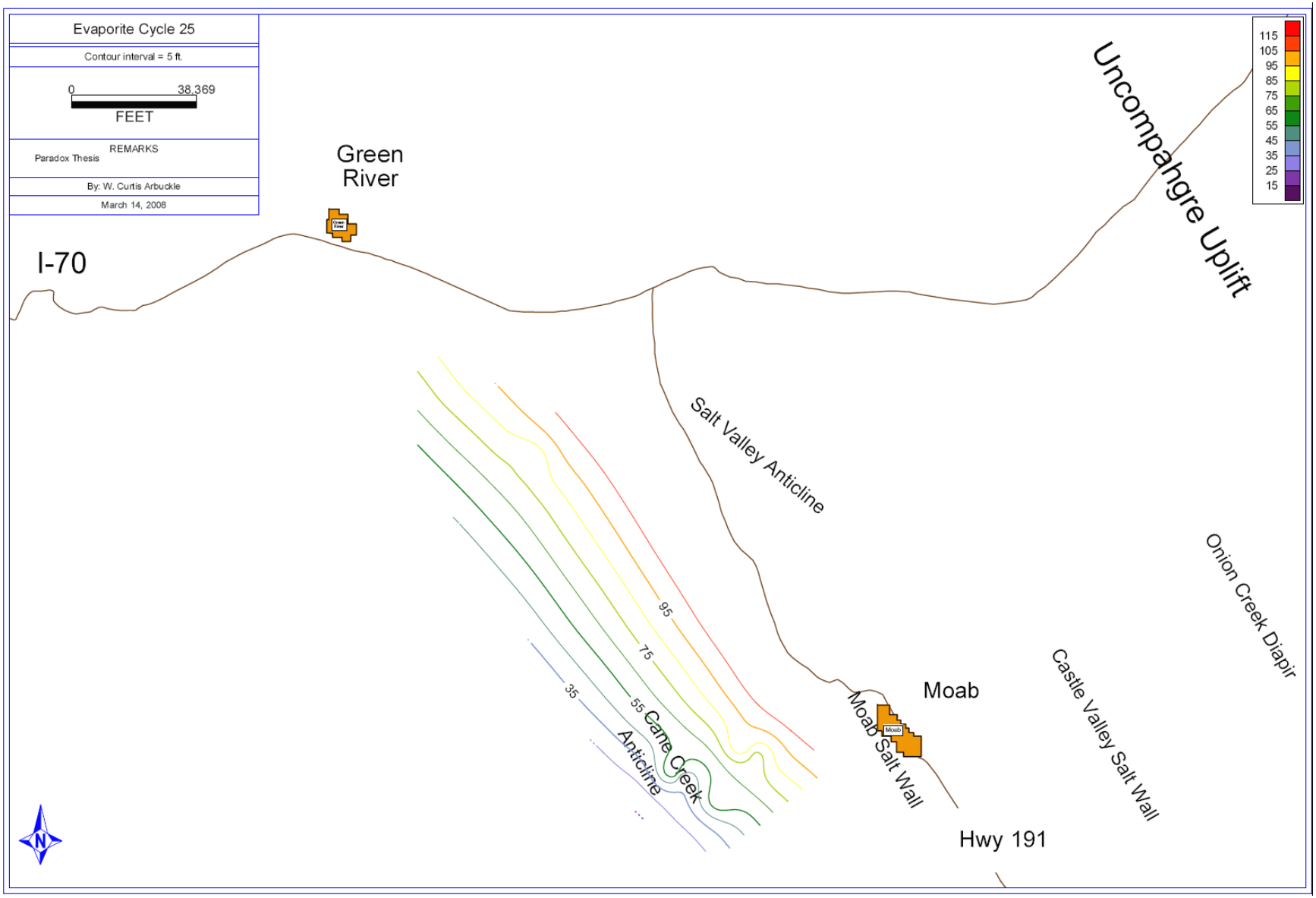

Figure 44: Isopach map of evaporite cycle 25 within the Paradox Formation. See text for analysis. Contour interval = 5 feet (1.52 m).

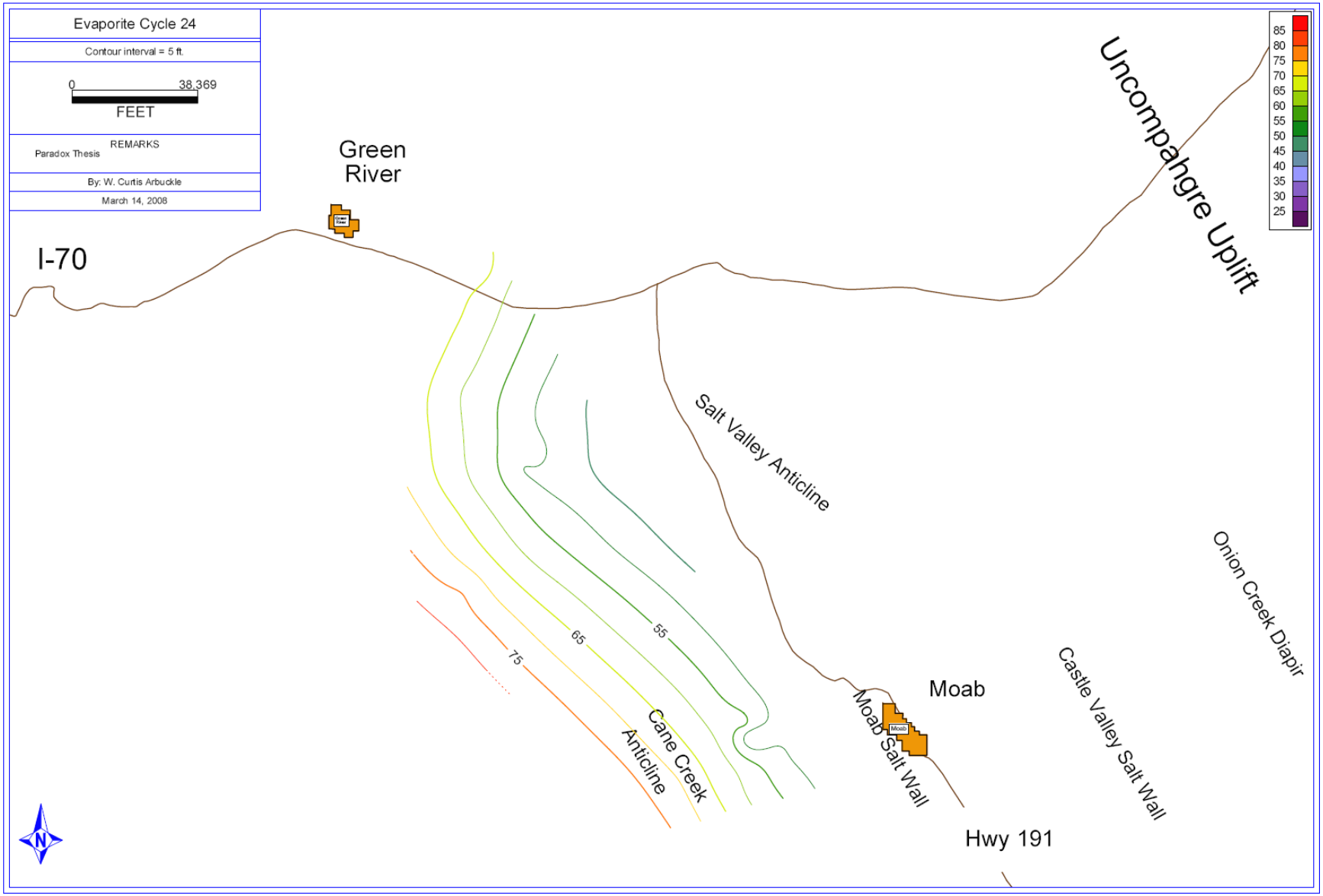

Figure 45: Isopach map of evaporite cycle 24 within the Paradox Formation. See text for analysis. Contour interval = 5 feet (1.52 m).

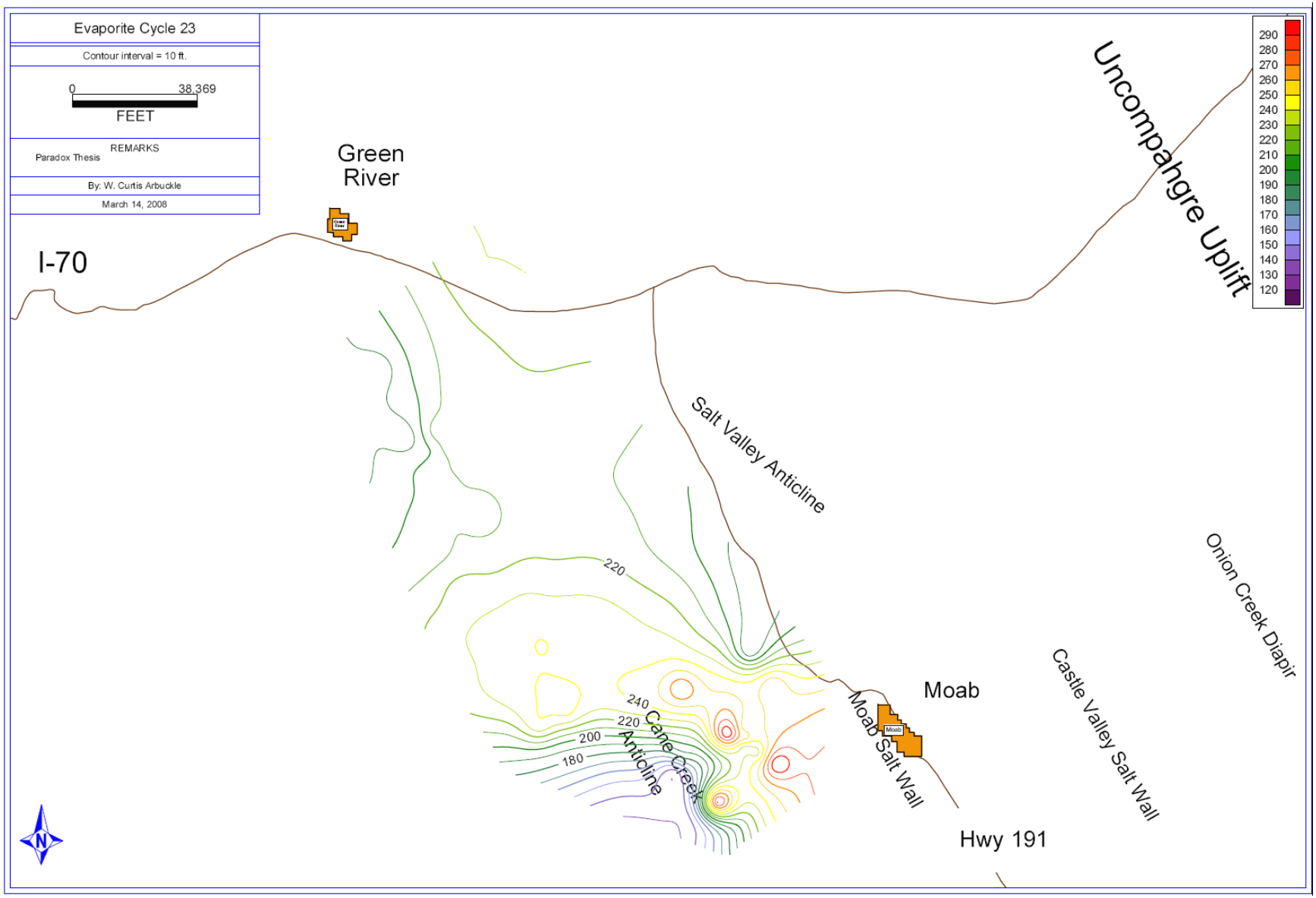

Figure 46: Isopach map of evaporite cycle 23 within the Paradox Formation. See text for analysis. Contour interval = 10 feet (3.05 m).

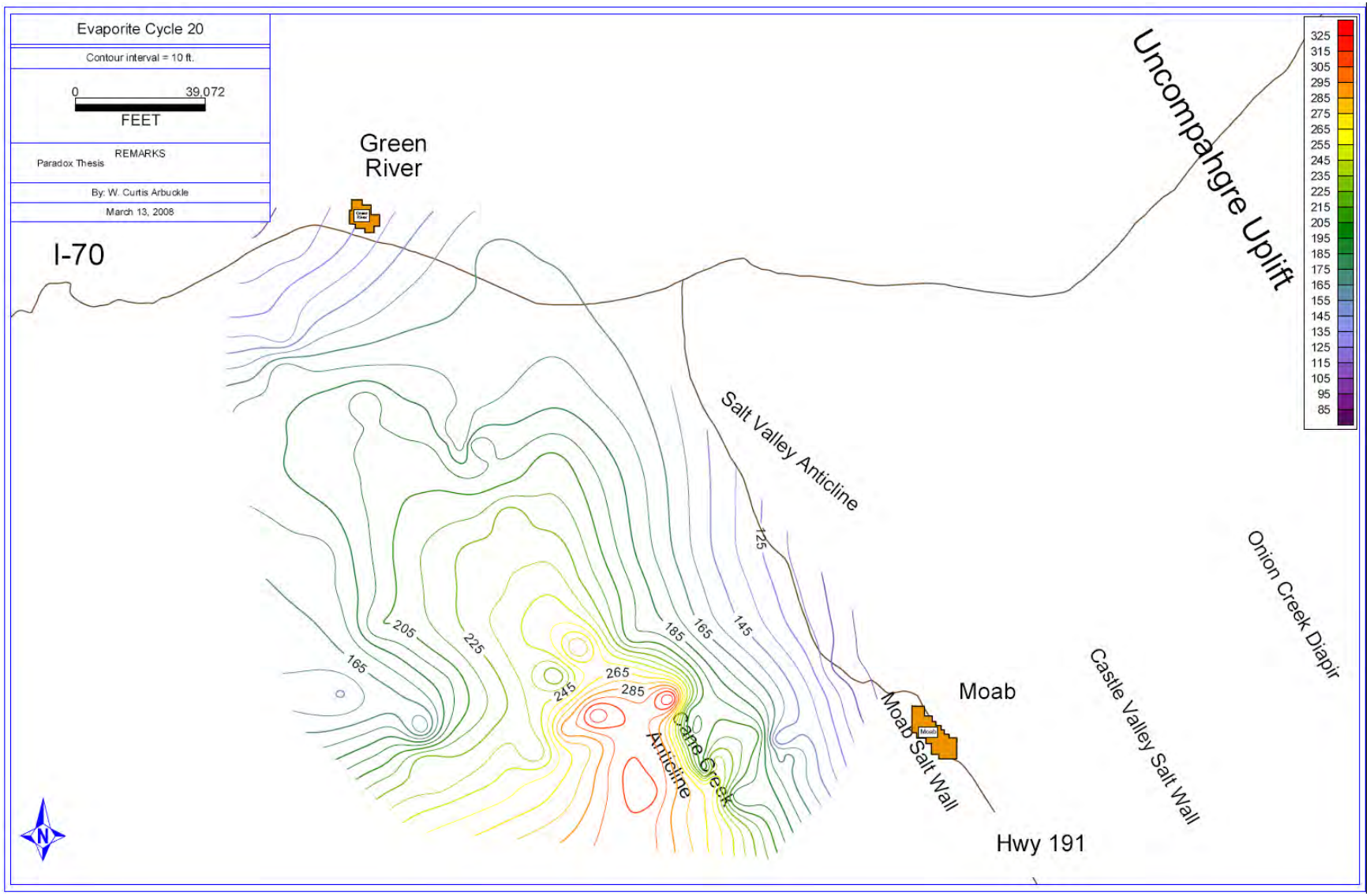

Figure 47: Isopach map of evaporite cycle 20 within the Paradox Formation. See text for analysis. Contour interval = 10 feet (3.05 m).

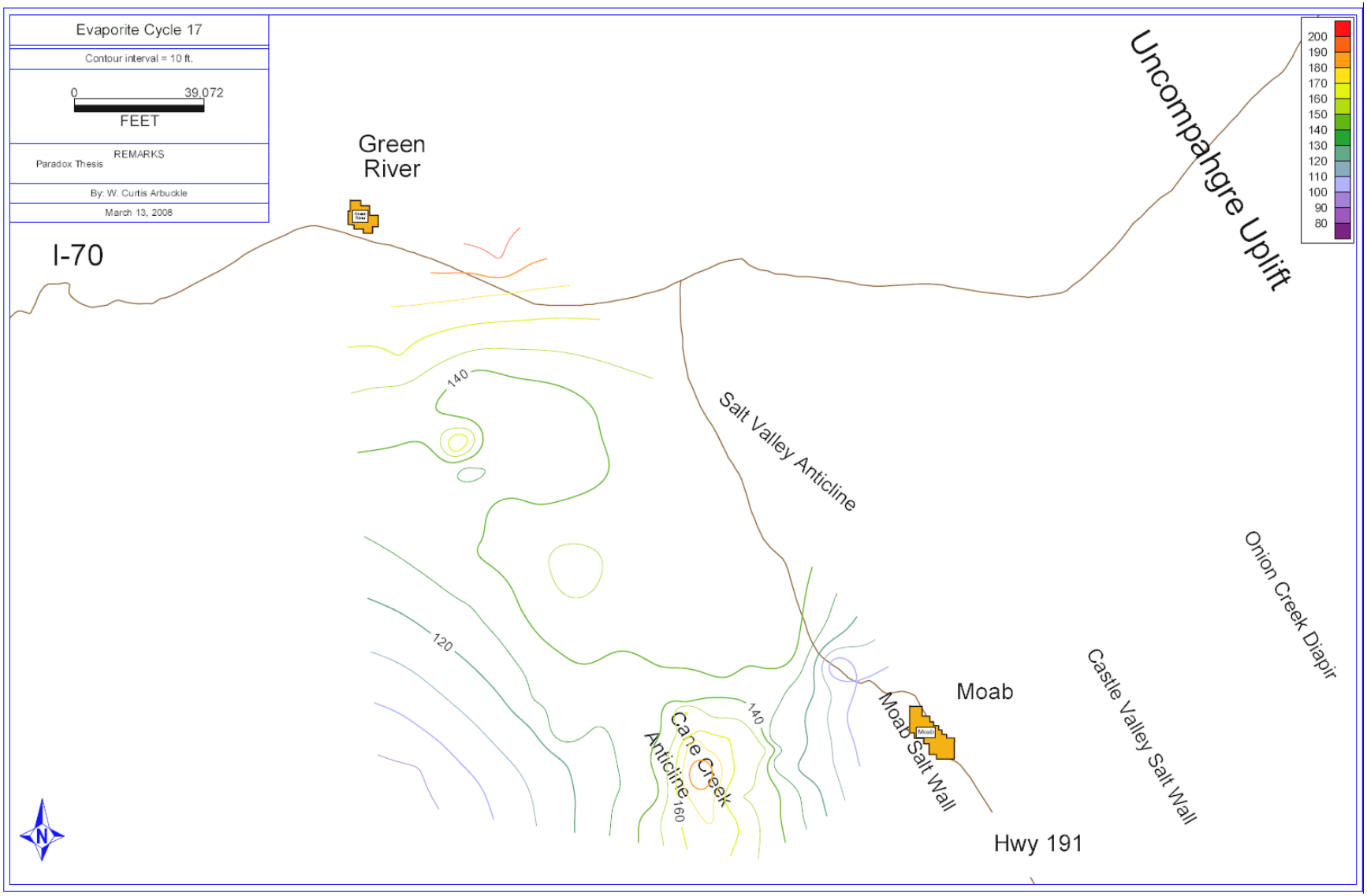

Figure 48: Isopach map of evaporite cycle 17 within the Paradox Formation. See text for analysis. Contour interval = 10 feet (3.05 m).

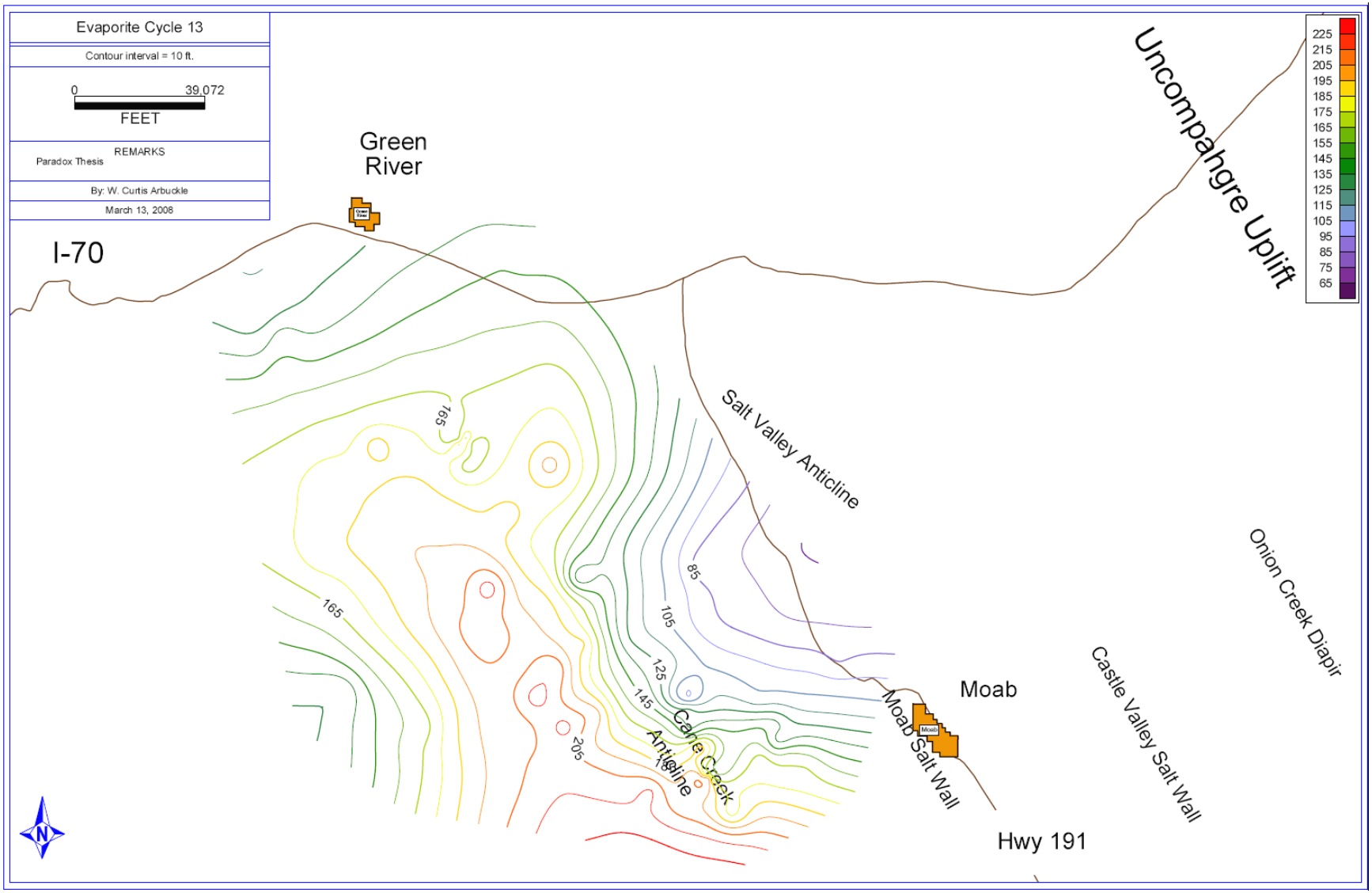

Figure 49: Isopach map of evaporite cycle 13 within the Paradox Formation. See text for analysis. Contour interval = 10 feet (3.05 m).

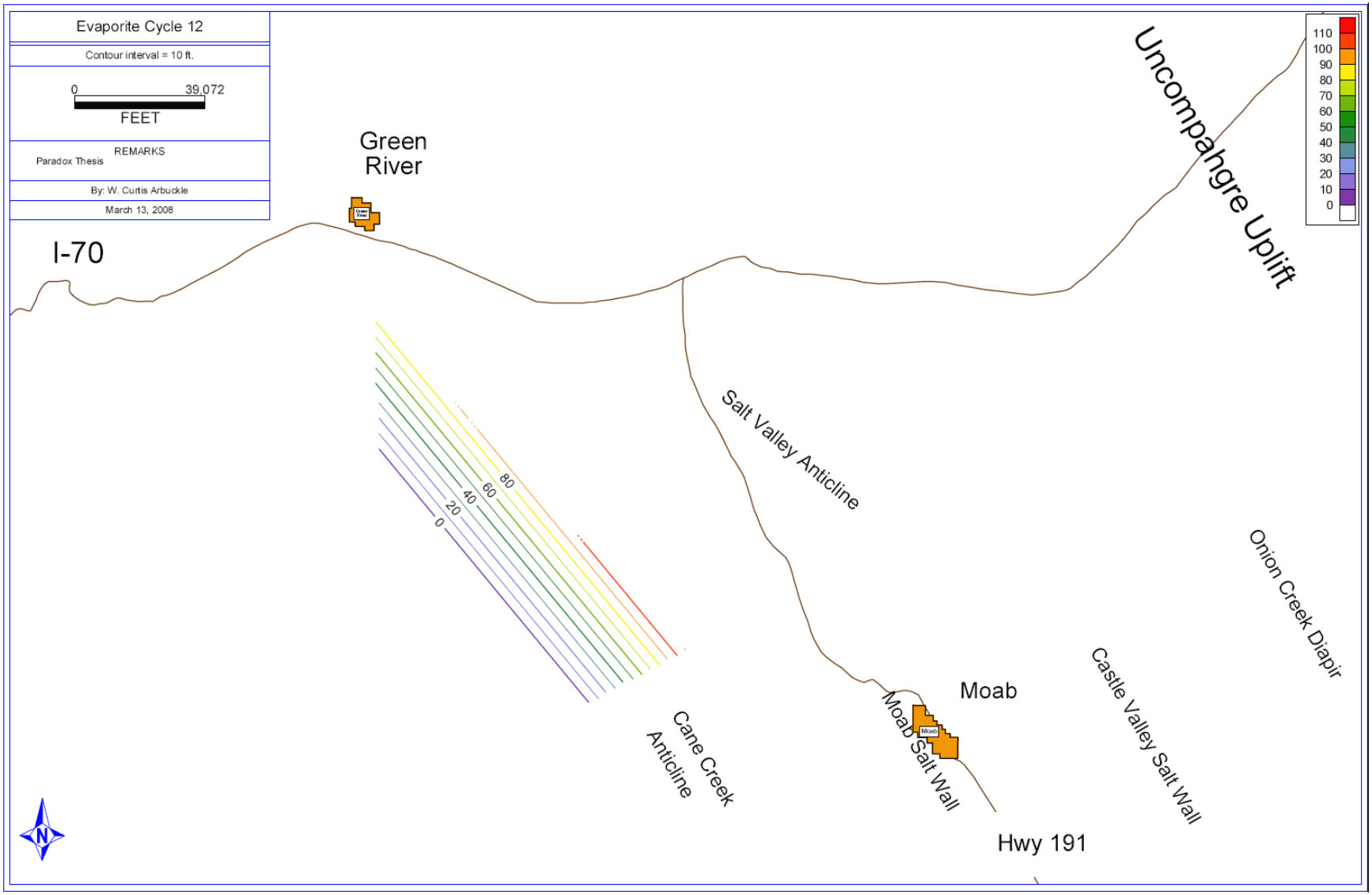

Figure 50: Isopach map of evaporite cycle 12 within the Paradox Formation. See text for analysis. Contour interval = 10 feet (3.05 m).

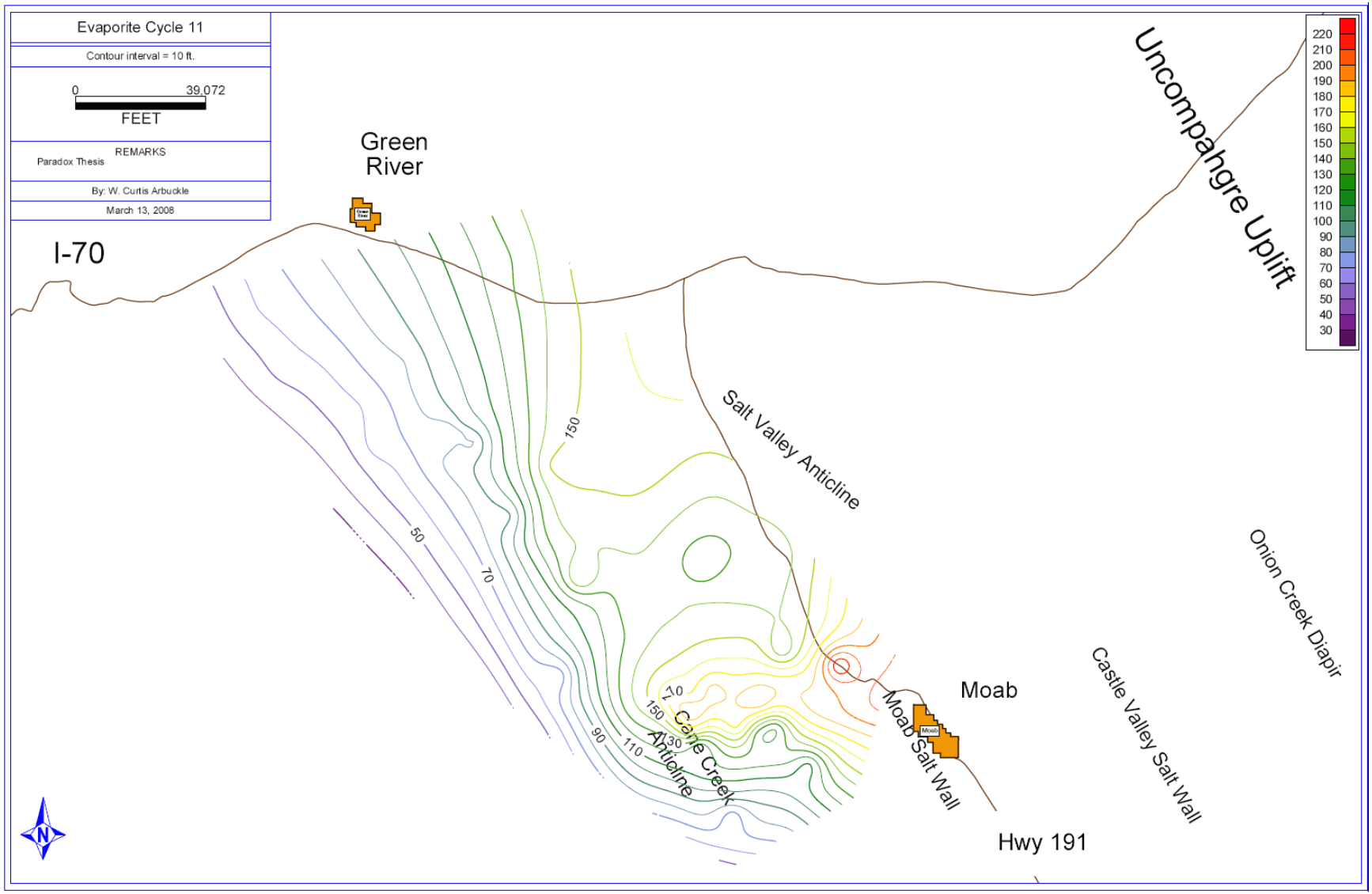

Figure 51: Isopach map of evaporite cycle 11 within the Paradox Formation. See text for analysis. Contour interval = 10 feet (3.05 m).

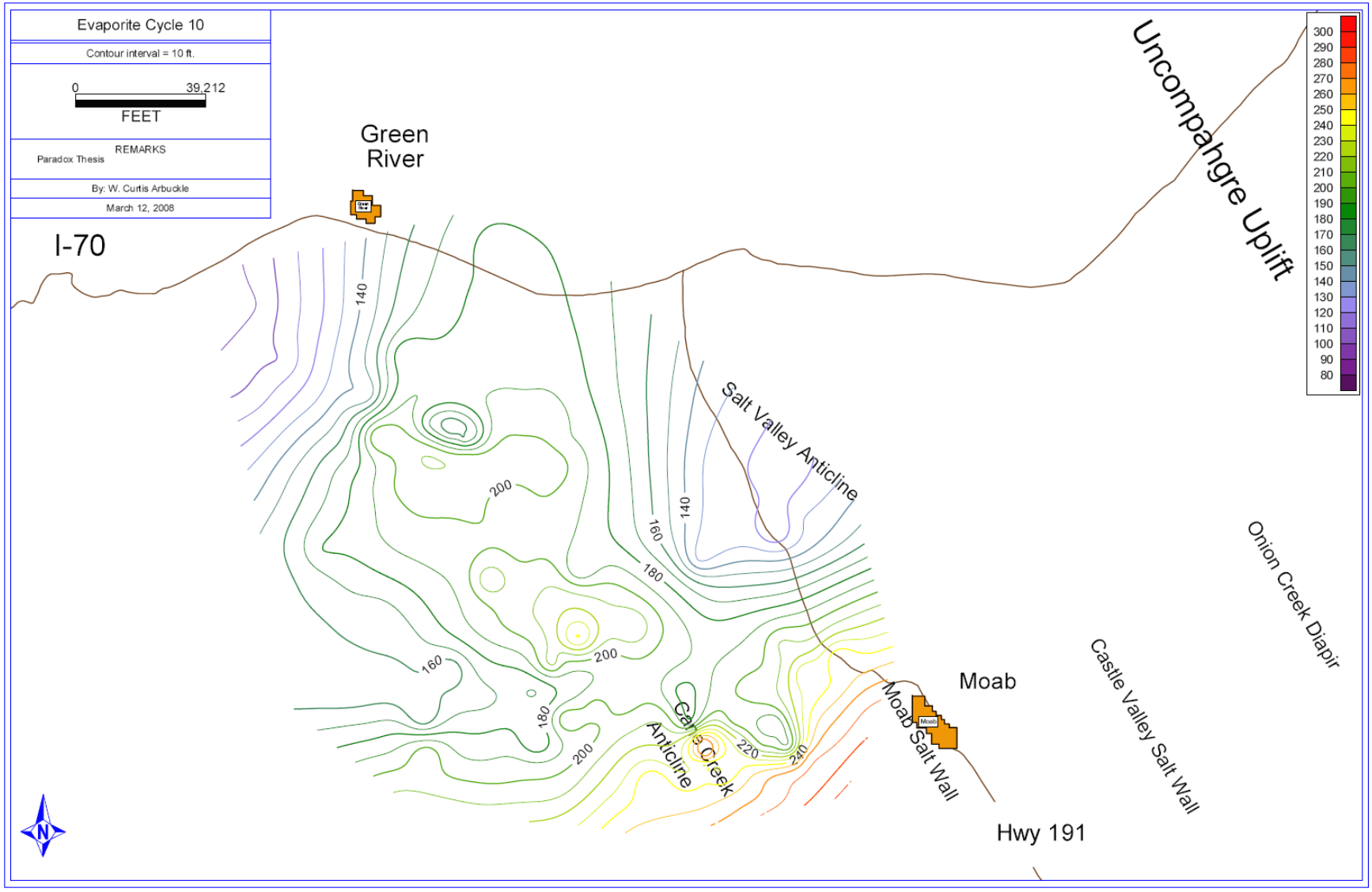

Figure 52: Isopach map of evaporite cycle 10 within the Paradox Formation. See text for analysis. Contour interval = 10 feet (3.05 m).

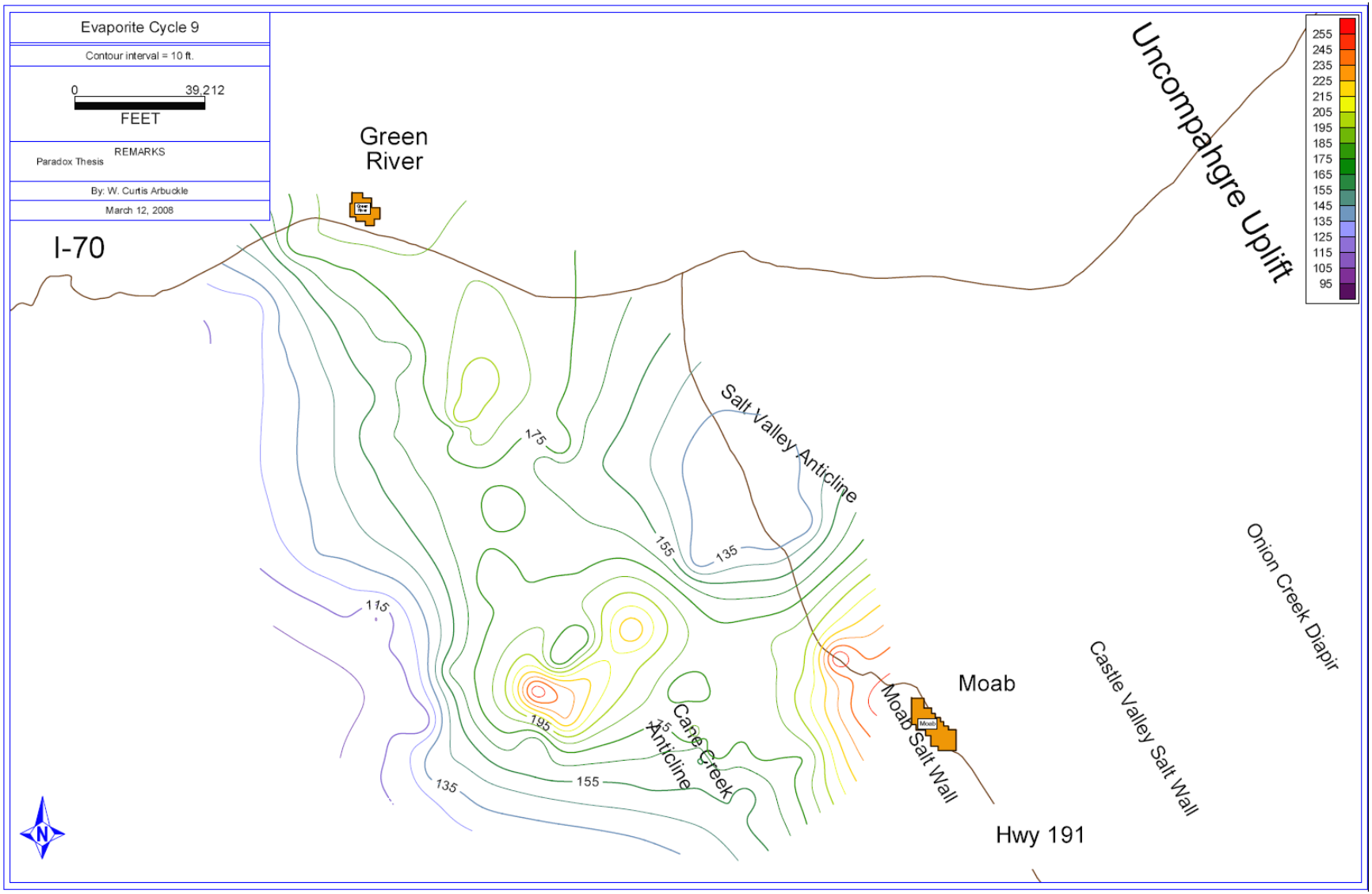

Figure 53: Isopach map of evaporite cycle 9 within the Paradox Formation. See text for analysis. Contour interval = 10 feet (3.05 m).

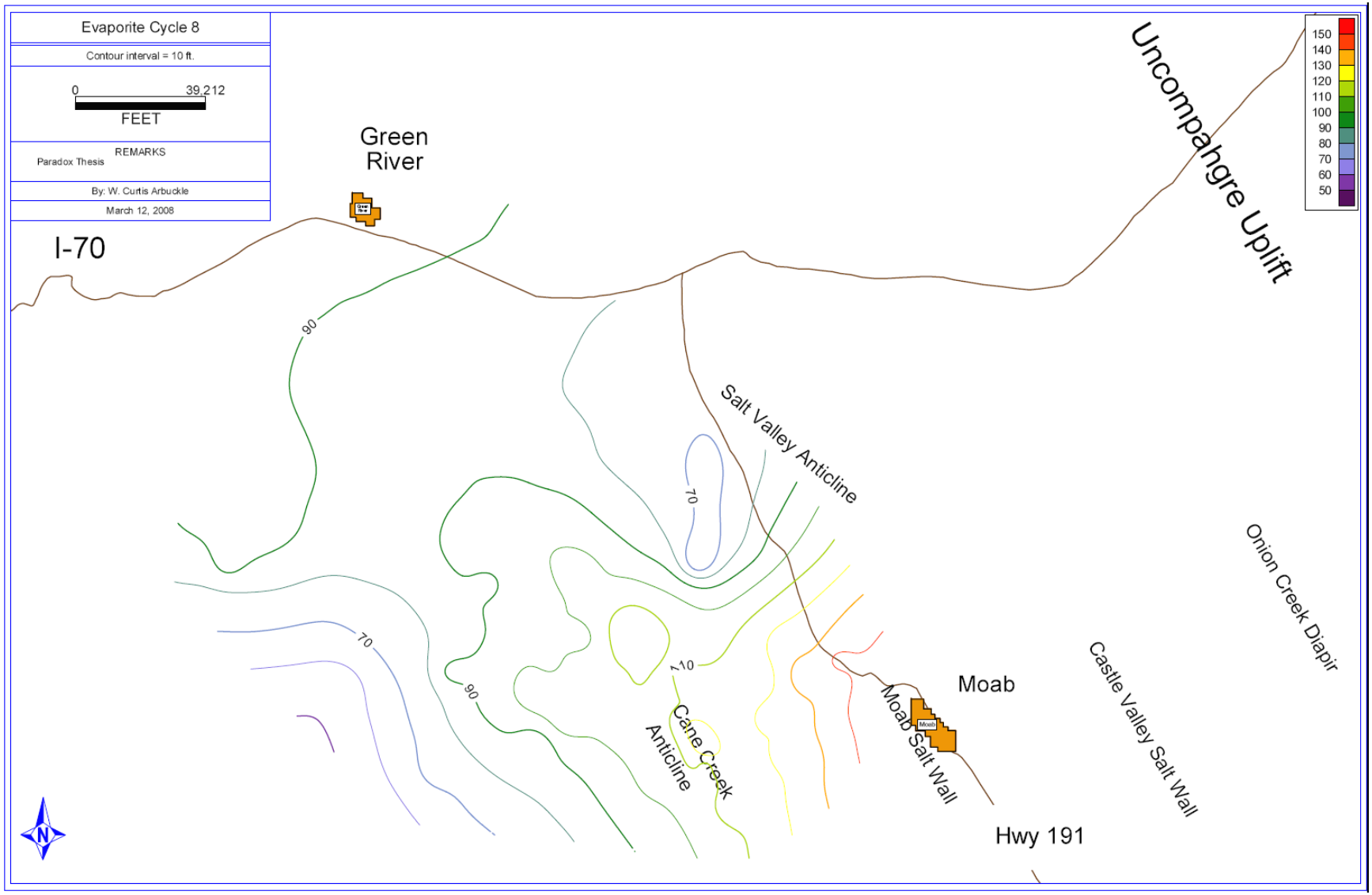

Figure 54: Isopach map of evaporite cycle 8 within the Paradox Formation. See text for analysis. Contour interval = 10 feet (3.05 m).

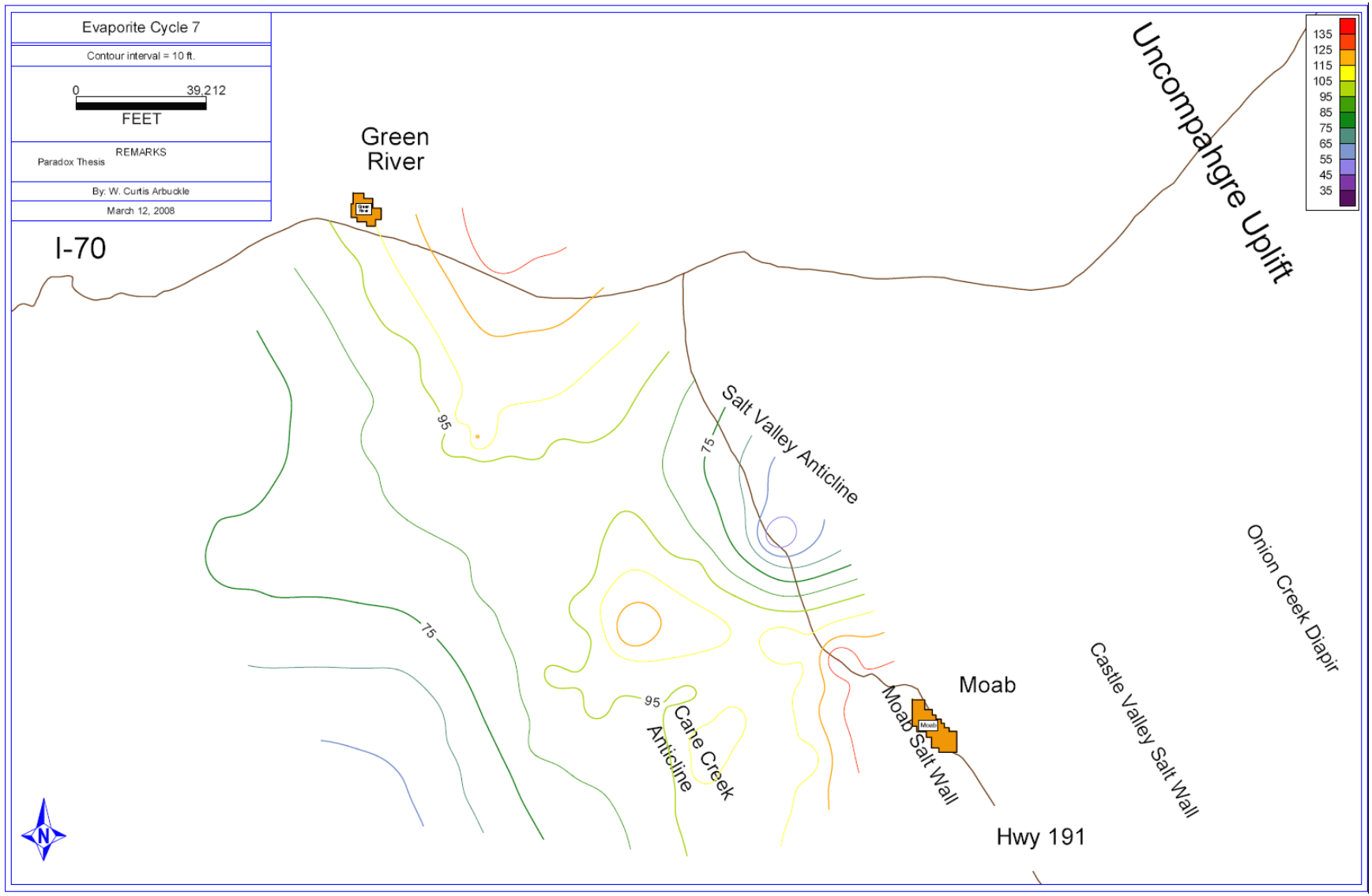

Figure 55: Isopach map of evaporite cycle 7 within the Paradox Formation. See text for analysis. Contour interval = 10 feet (3.05 m).

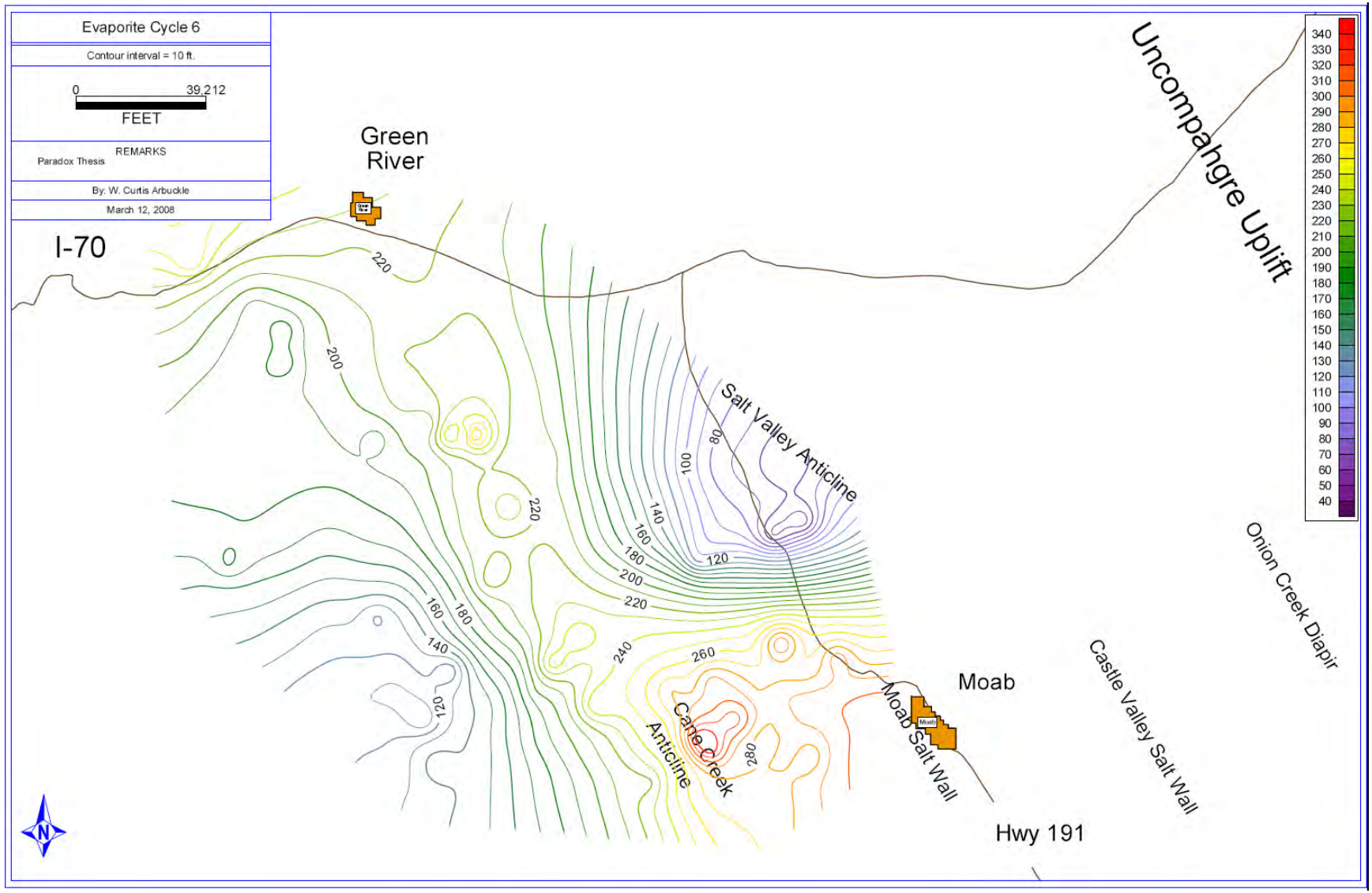

Figure 56: Isopach map of evaporite cycle 6 within the Paradox Formation. See text for analysis. Contour interval = 10 feet (3.05 m).

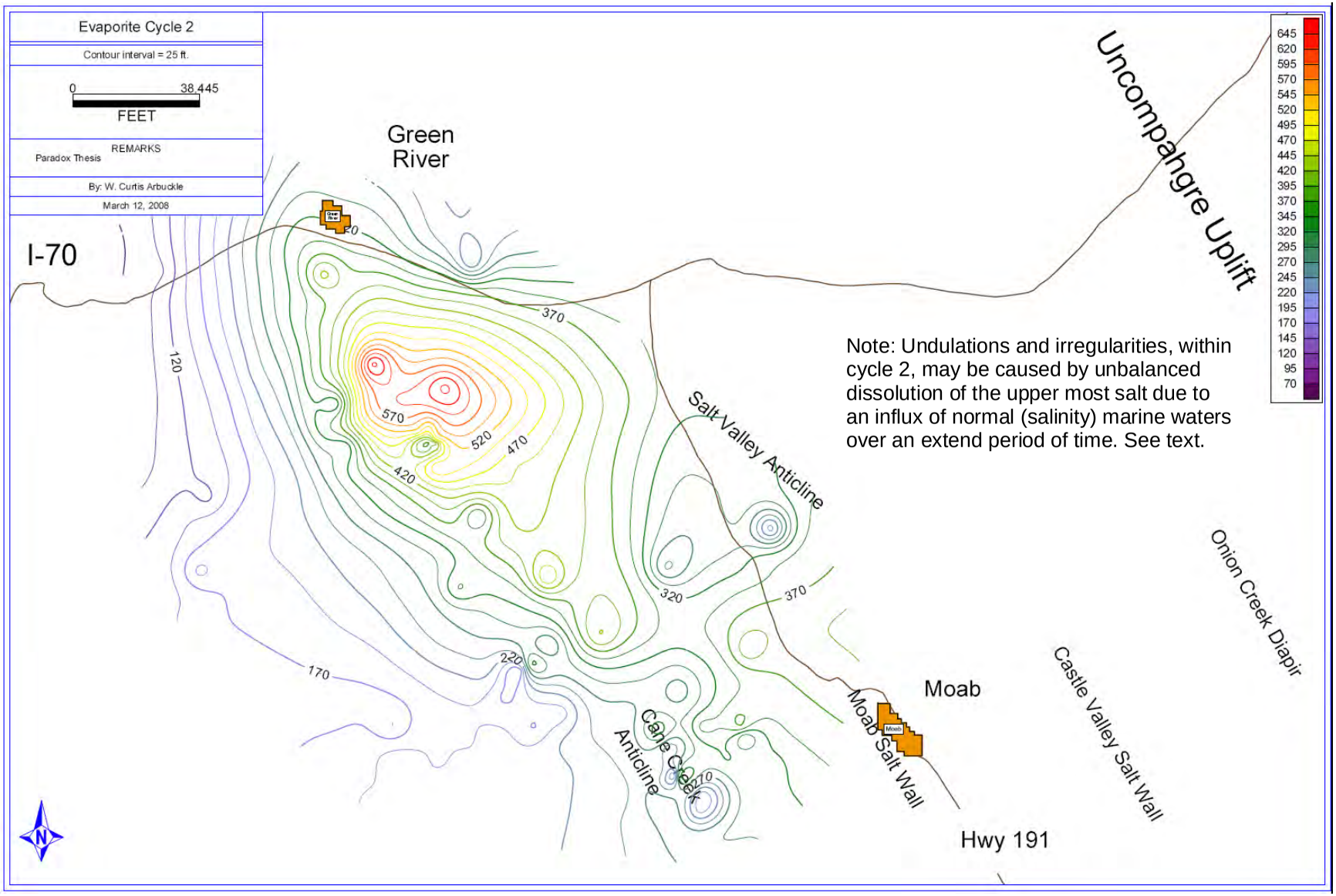

Figure 57: Isopach map of evaporite cycle 2 within the Paradox Formation. See text for analysis. Contour interval = 25 feet (7.62 m).

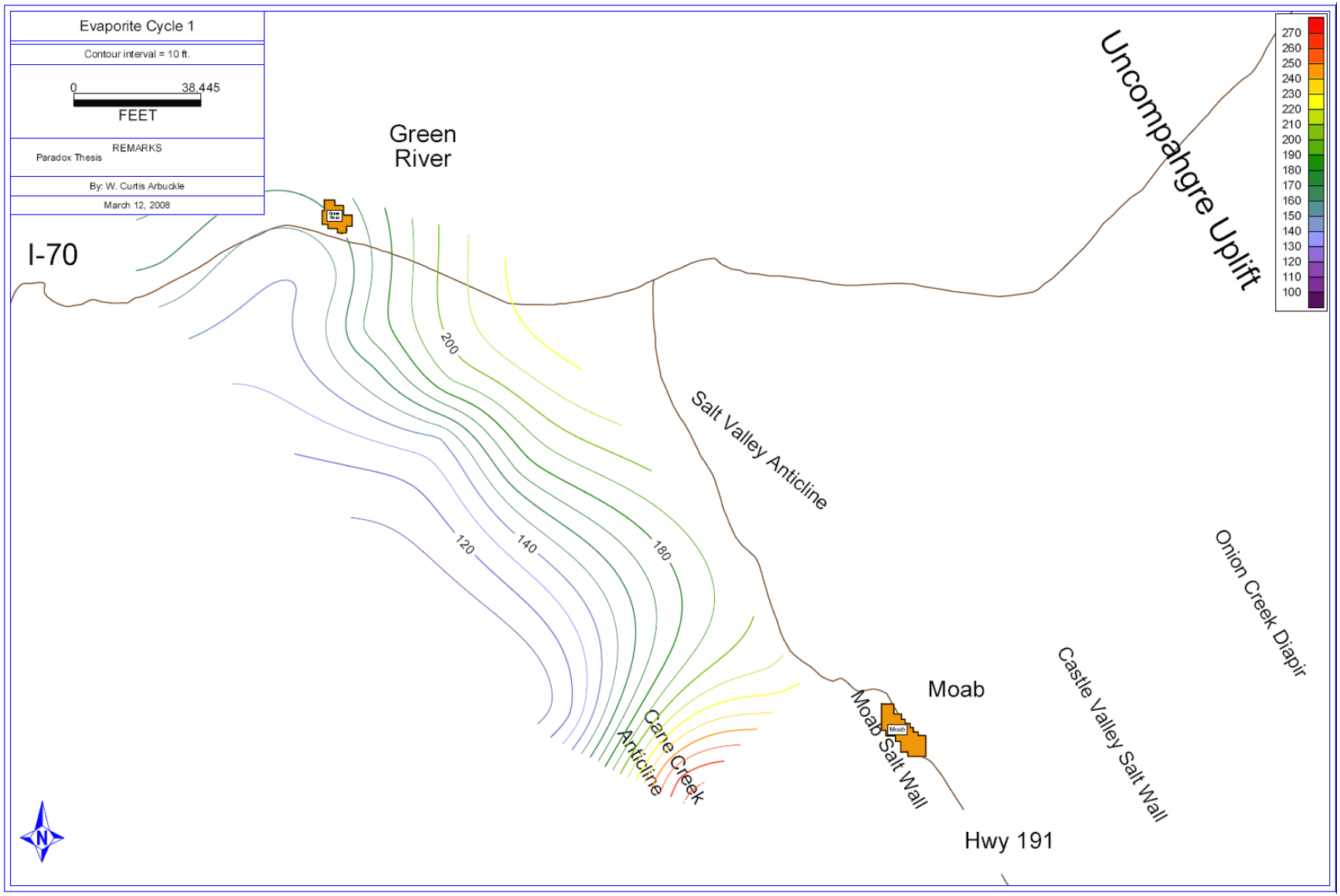

Figure 58: Isopach map of evaporite cycle 1 within the Paradox Formation. See text for analysis. Contour interval = 10 feet (3.05 m).

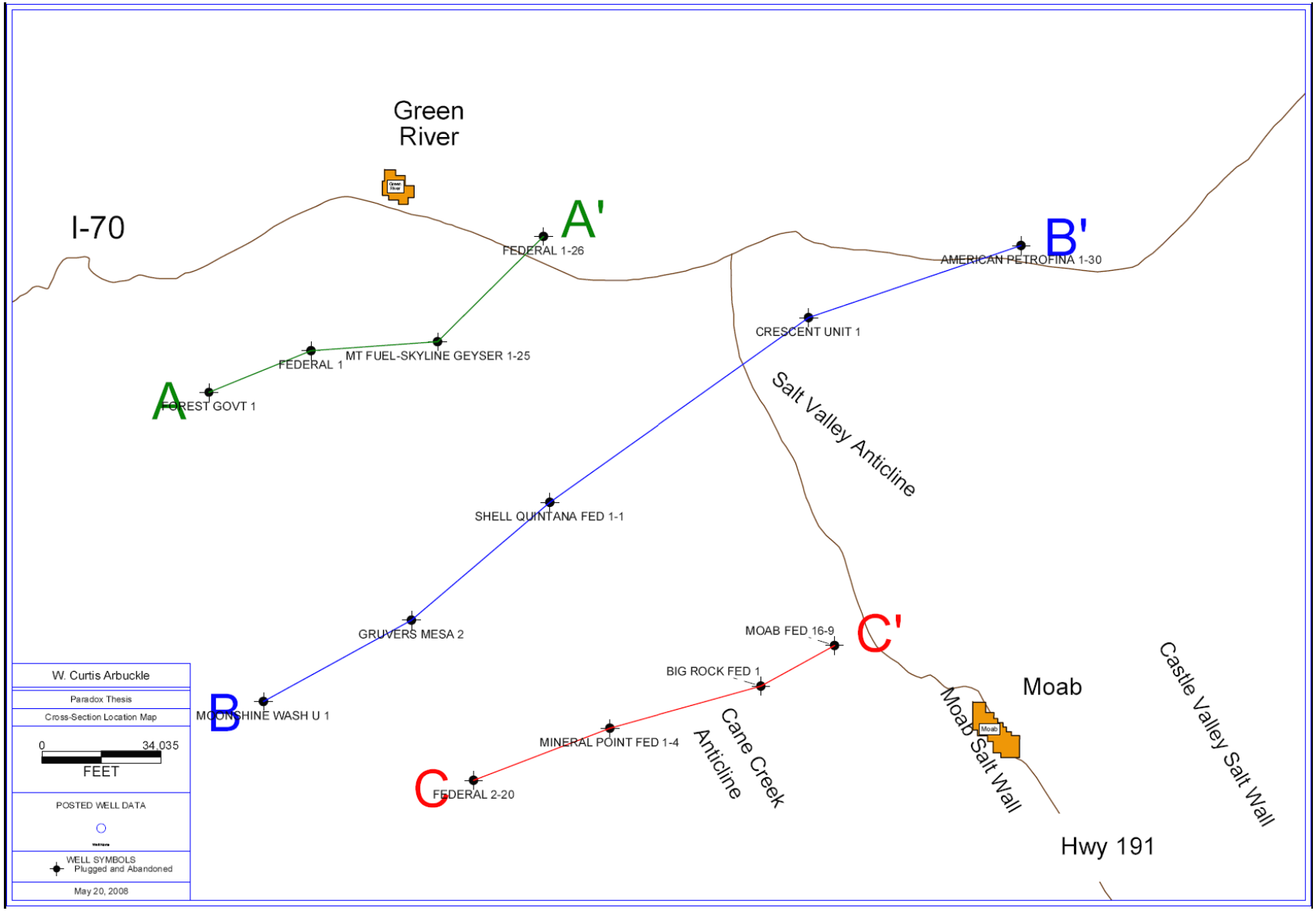

Figure 59: Map showing the location of cross sections A-A', B-B' and C-C'.

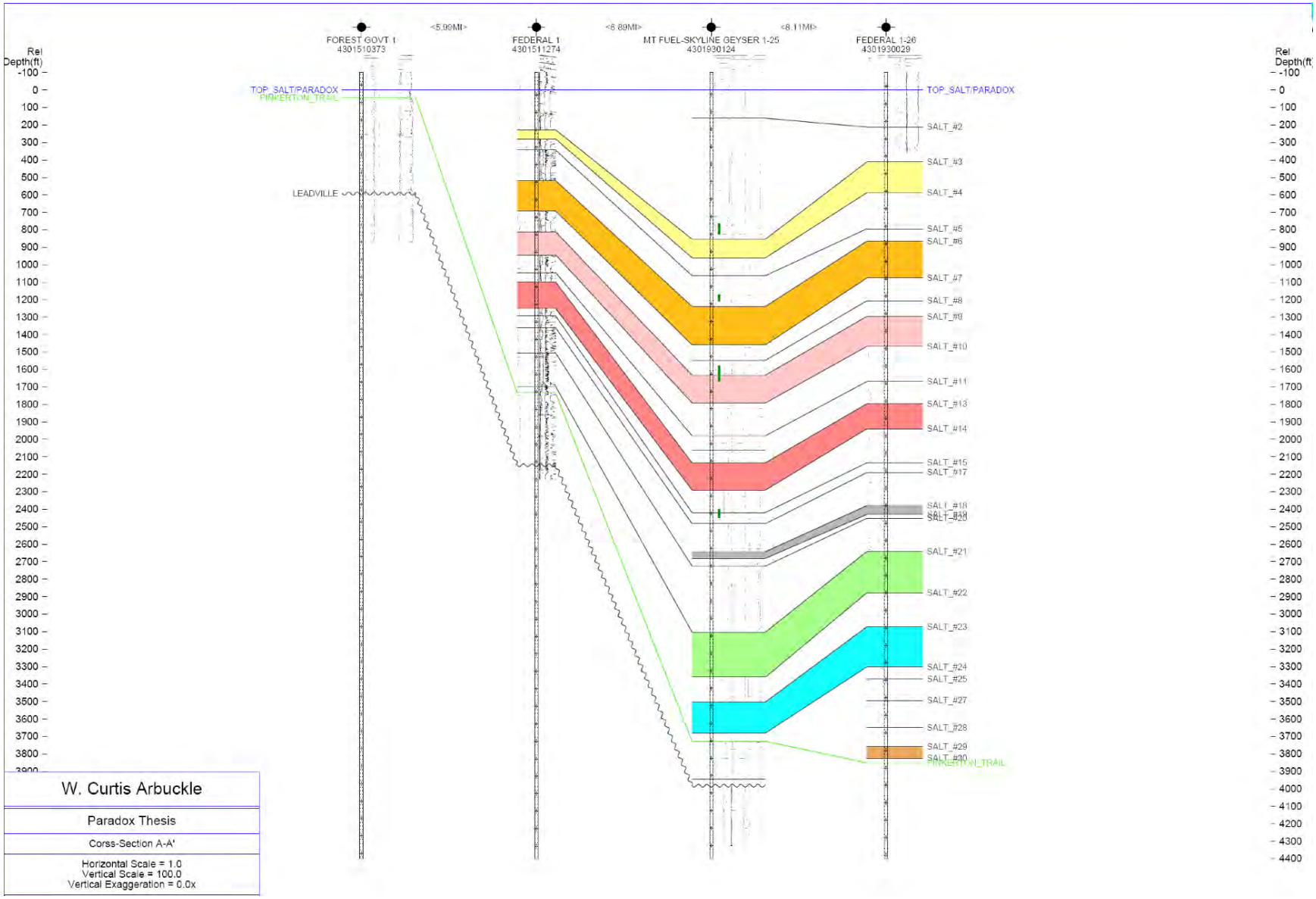

Figure 60: Well cross section A-A' (for location see Figure 59).

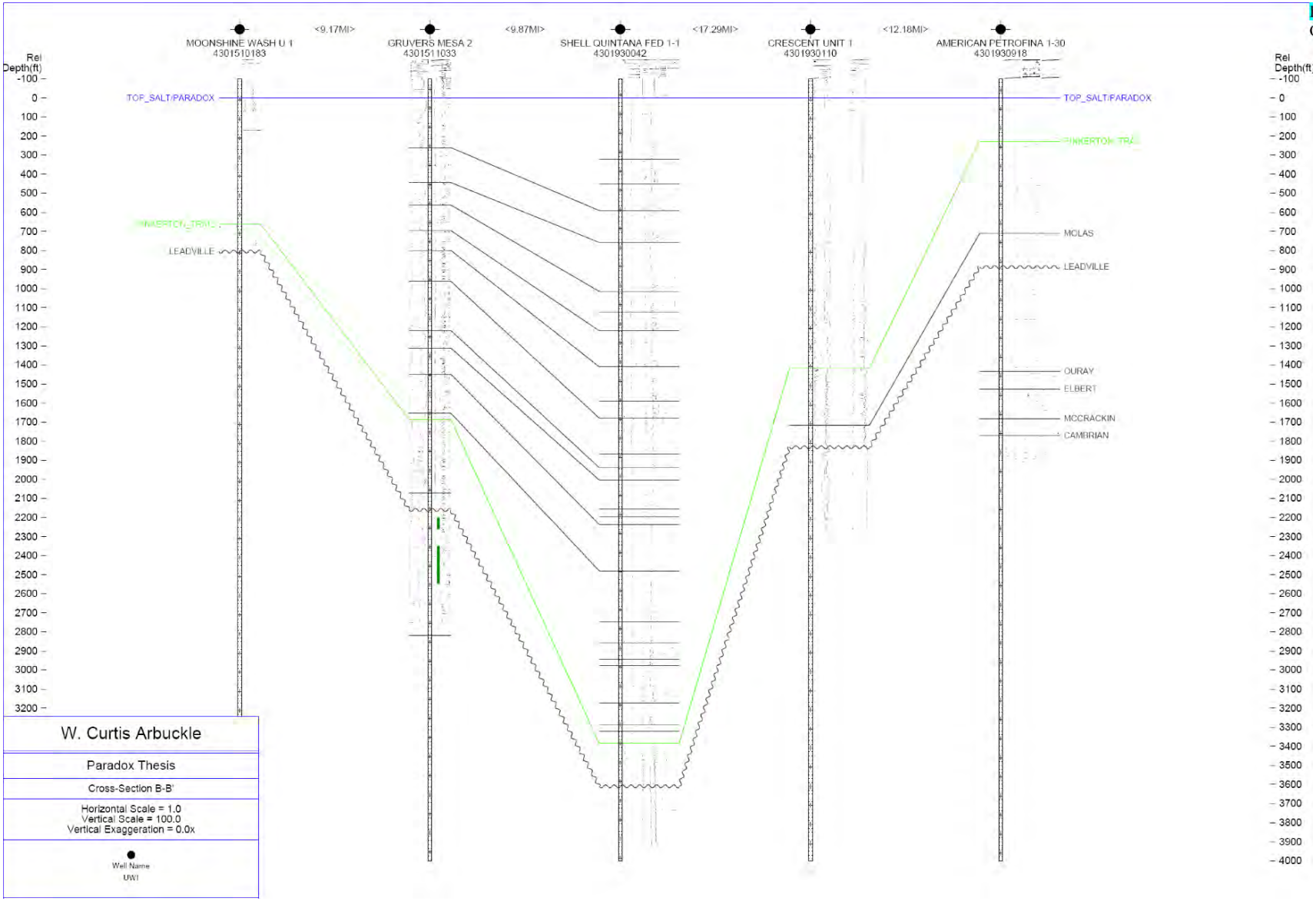

Figure 61: Well cross section B-B' (for location see Figure 59).

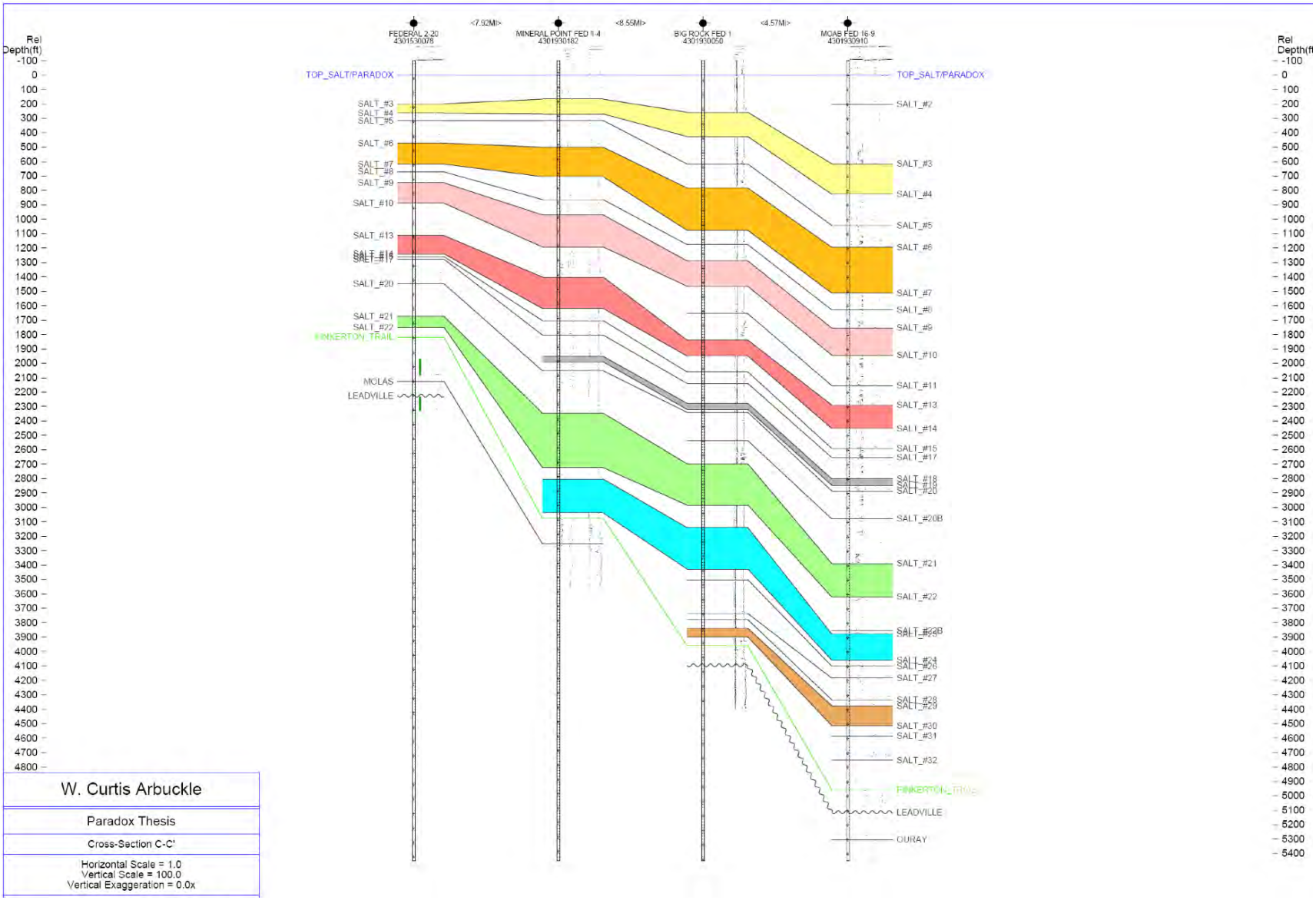

Figure 62: Well cross section C-C' (for location see Figure 59).

evaporite cycles generally don't follow the same depositional patterns as most clastic rocks and instead were precipitated in depressions where brine concentrations reached salt saturations. Therefore, observing the same basin subsidence trend with the Paradox salt, while considering salt movement/tectonics, becomes difficult. The overlying Honaker Trail Formation (Figure 63) also displays little evidence of basin subsidence. This is partly caused by the significant amount of coarse clastic material shed from the Uncompahgre Uplift into the basin. The resulting salt walls further shroud any detailed evidence of ongoing subsidence during the Pennsylvanian time.

7. The accuracy of the isopach maps involving cycles 1 and 2 is somewhat questionable. For cycle 1 (Figure 58), its areal extent does not cover the entire study area, particularly where the data are available west of the Salt Valley Anticline. The thickest accumulations were deposited along depositional lows, mainly in an area just south of the town of Green River, Utah and along the Cane Creek Anticline (Figure 58). The subsequent isopach map is more of an interpretation between these two areas then an accurate representation.

   Cycle 2 (with the exception of cycle 1) is the upper most evaporate-bearing sequence (Figure 57). Because cycle 2 is the last main, widely deposited evaporite interval, it was probably in contact with open marine waters longer than most of the previous cycles. This change from a penesaline environment (Paradox Formation) to a marine environment (Honaker Trail Formation) (Hite, 1960) may have caused the upper section of cycle 2 (and/or cycle 1) to be eroded and dissolved away. It would be very difficult to estimate the loss in thickness due to this process and the resulting map is full of undulations that don't appear to be depositionally controlled.

8. Isopach maps involving cycles 12 – 10 (Figures 50 – 52) are very complex. For many of the wells within the database, cycles 11 and 12 are incomplete and lack a halite zone. Arguably, it can be considered that any clastic material deposited (without an associated halite zone) during these two cycles would be added to the assemblage of the previous cycle. For example, if cycle 11 was void of any related halite, any clastic material deposited during cycle 11 would be grouped into cycle 10. This creates correlation and thickness problems particularly where cycle 10 becomes locally much thicker in the absence of both the halite beds of cycles 11 and 12. These two cycles were restricted to a small area north of the Cane Creek Anticline, especially cycle 12 (Figure 50). The same situation applies to cycles 16 and 15 (Figures B-14 and B-15), where cycle 16 was not widely deposited.

Mapping Problems and Potential Sources of Error

Unfortunately, there are several problems when correlating and mapping the evaporite cycles across the northern part of the basin. The most prolific issue involves the salt walls and anticlines. As the salt was evacuated into the deformed structures we observe today, the clastic zones within the salt were also forced upward. During this process, the clastic

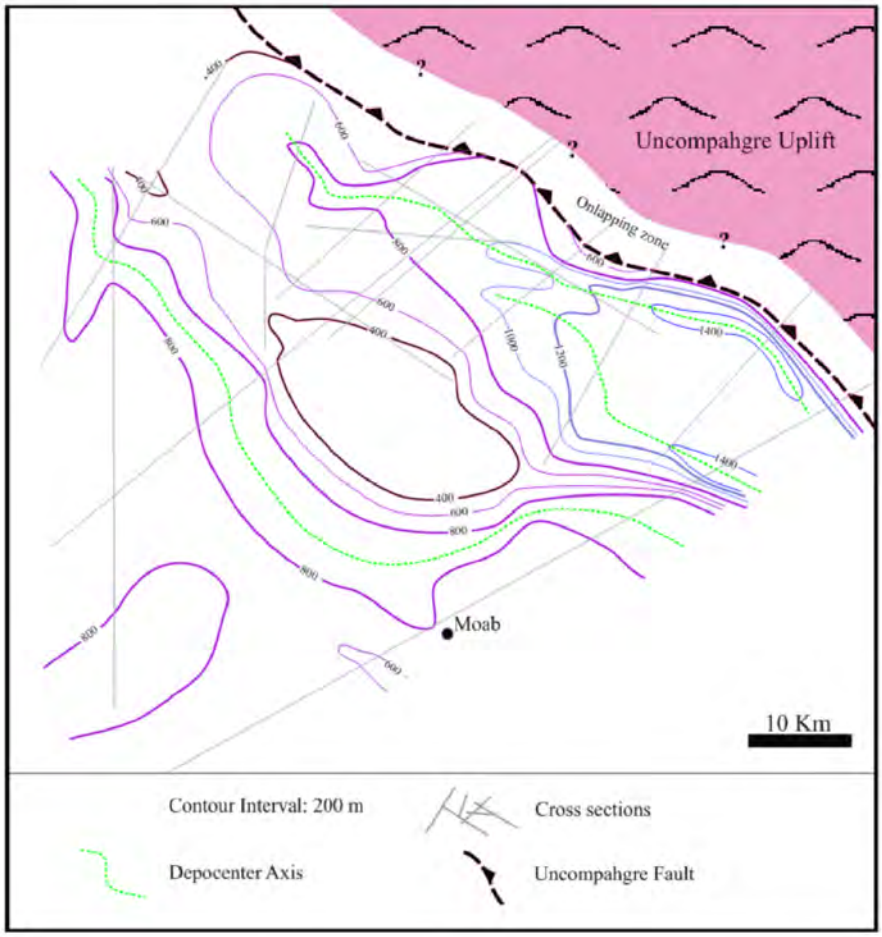

Figure 63: A paleogeographic and isopach map of the Honaker Trail Formation. Notice how the formation thins atop the Salt Valley salt wall (center of figure) but is much thicker along the flanks of the structure. These depocenters are also areas of significant salt movement and welding. West of the Salt Valley salt wall, the thickness of the Honaker Trail Formation is rather continuous (Paz Cuellar, 2006).

intervals became distorted, broken, and lost any recognizable orientation needed for correlation. Another correlation problem involving the salt wall structures is the associated synclines located adjacent to the salt walls (an example being the Courthouse Syncline). These synclines are areas where the present day thickness of the salt is thinner, but they don't necessarily represent areas of thinner deposition. It is more likely the lack of salt is caused by the formation of the salt walls where any available salt was evacuated, creating partial salt weld on either side of the structure. These problems involving salt movement become particularly relevant when attempting to correlate from the western side of the study area, across the Salt Valley Anticline (and Courthouse Syncline), to the eastern portion of the study area. Correlations west of the anticline are relatively straight forward whereas the opposite can be said along the salt structure. East of the Salt Valley salt wall, correlations are also rather complex, mainly due to a lack of sufficient well data, salt welding, and a large increase in coarse clastic material not observed west of the Salt Valley Anticline.

Another problem that arises when attempting to correlate the evaporite cycles involves the depositional relationships between each cycle. Because consecutive cycles are deposited on top of each other in a more or less sequential order, topographical variations in underlying cycles affect overlying depositional units. For example, if there was a local depression following the deposition of cycle 'X', it would be filled in by the overlying cycle 'Y' thus allowing for cycle 'Y' to be locally thicker. Therefore, correlations across areas of local thickness

change are at times difficult to interpret and understand. It is also unclear how or why these local depressions or highs form, but correlations suggest salt movement and tectonics play an important role. Evidence for these types of occurrences becomes apparent within the evaporite cycles of the Paradox Basin.

Also, since the boundaries between cycles are deemed as solution unconformities, it is likely at least some of the uppermost section of each cycle would be removed or dissolved by the first transgressive waters entering the basin. Estimating how much of each cycle was lost is nearly impossible given the list of variables that includes water depth, water temperature, water flow direction, water velocity, local and regional topography, clastic and organic material, and the chemical makeup of the inflowing waters. If some areas of the basin experienced more of these formation-changing variables compared to other areas, then the post-depositional dissolution can vary greatly with location. This makes accurate correlation difficult.

Well data used for mapping of cycles 29 – 24 (Figures 40 – 45) are inadequate. Many of the wells drilled east of Salt Valley targeted the Cane Creek shale (clastic zone 23) and were not drilled any deeper. Only six wells drilled through all 29 evaporite cycles of the Paradox Formation into underlying strata. These six wells (and thus data points) are enough to create isopach thickness maps of each interval, but prove to be an inadequate representation due to the expanse of the mappable area.

DISCUSSION

Pennsylvanian Cyclicity of the Northern Paradox Basin – Paradox Formation

Cyclicity can be controlled by a number of factors including tectonic, sedimentary, climatic and eustatic controls, and it is likely many of these factors contribute to the level and persistence of any cyclical patterns. Hite and Buckner (1981) concluded the cyclicity observed in the Paradox Basin evaporites was caused by periodic sea-level changes because of glacio-eustatic fluctuations involving Gondwanaland ice sheets during Pennsylvanian time. An increase of ice volume would have caused a lowering of global sea level, thus isolating the basin from open marine waters. This would result in a rise of brine salinities leading to the deposition of the Paradox Formation evaporites. In contrast, a retreat of Gondwanaland glaciers would cause a rise in sea level allowing marine waters to flood and circulate within the Paradox Basin. The fresher water would cause some dissolution of the already deposited, uppermost halite layers creating a solution disconformity. During this time of higher sea level, the clastic intervals would have been deposited.

It is possible that the glacio-eustatic driven evaporite cycles of the Paradox Formation might correlate with the cyclothems from the Mid-continent of the United States, even down to fourth and fifth-order composite cycles (Raup and Hite, 1992; Olszewski and Patzkowsky, 2003). Cycles and cyclothems of glacio-eustatic origin should be synchronous and correlative with other basins throughout the world (Dickinson *et al*., 1994). However, problems exist in making definitive correlations. The main problem is assuming that each major glacial-eustatic event left the same imprint and was of the same magnitude within any given basin. This is not observed within cycles documented during the Pleistocene and should be discounted for cycles formed during the Pennsylvanian (Nadon and Kelly, 2004). The presence of paleosols between cycles during the Pennsylvanian suggests that deposition and exposure took place at slightly different times in many locations around the Mid-continent, Appalachian, and Illinois

basins (Olszewski and Patzkowsky, 2003; Nadon and Kelly, 2004). This implies there could be missing cycles that are thus non-correlative between basins, especially if one was to include the Paradox Basin. These factors prevent high-resolution correlation of cycles between basins of roughly the same age and presumably affected by the same glacio-eustatic cyclical processes.

Tectonic controls on the cyclicity within the northern Paradox Basin are somewhat difficult to constrain during the late Pennsylvanian. The Uncompahgre Uplift was at least mildly positive during the late stages of the deposition of the evaporites and was the source of at least some of the clastic material found within the cycles. The uplift may have also been the major cause of basin subsidence, therefore creating accommodation space needed for each successive cycle. However, the Uncompahgre alone could not have caused the cyclicity observed within the evaporites, unless it was directly influencing the pathway and flow of seawater into the basin (Hite and Buckner, 1981). However, the regional tectonics of the Ancestral Rocky Mountains must have had some influence on cyclical deposition, but the effects are often overshadowed by evidence supporting strong glacio-eustatic control (Houck, 1997).

Other climate driven causes for cycles should also be considered for the Paradox Basin. A change in the aridity of the climate would alter depositional patterns involving evaporation rates and seasonal precipitation (Hite and Buckner, 1981). These changes are considered minor compared to the much larger-scale glacio-eustatic changes described above, but they would still alter any cyclical pattern to some degree.

Sequence Stratigraphy and Palynomorphs Relating to Milankovitch Periodicity

Sequence stratigraphic cycles in the southern part of the Paradox Basin were identified by Weber *et al*. (1995). They were able to divide the Paradox and lower Honaker Trail formations into five, third-order stratigraphic sequences, or composite cycles, based on stratigraphic rock relationships (see Figure 64). The older four sequences are entirely within the Paradox Formation, where each individual evaporite cycle is considered a fourth-order sequence. These fourth-order sequences range in duration from 100,000 – 500,000 years (Weber *et al*., 1995), which closely mimics the eccentricity cycle durations defined in the Milankovitch theory.

Palynomorph data identified within the evaporite cycles gives several clues to the climate, age, depositional environment, and cyclicity of the Paradox Basin. The presence of palynomorphs generally associated with Middle Pennsylvanian coal deposits outside the Paradox Basin indicates that locally the environment may have supported large, arborescent plants typically found in swamp-like environments during periods of highstand (Reuger, 1996). A lack of such pollen grains identified within regressive and lowstand rocks of the Paradox Basin indicates there was climatic variability during the deposition of the cycles. This evidence supports the theory that the cyclicity of the Paradox Formation was at least partially controlled by glacio-eustatic processes on roughly a 100,000 year (Milankovitch) succession.

Comparing Sequence Stratigraphy and Palynomorph Cycle Boundaries

Rueger (1996) identified and categorized palynomorph data taken from the Paradox Formation into four biostratigraphic zones based on sharp changes in taxa percentages . When compared to the third-order sequences defined by Weber *et al*. (1995), a tentative correlation can be made (Figure 64). Interestingly, many of the unit boundaries identified by both authors align and compare very well, especially since one is based on

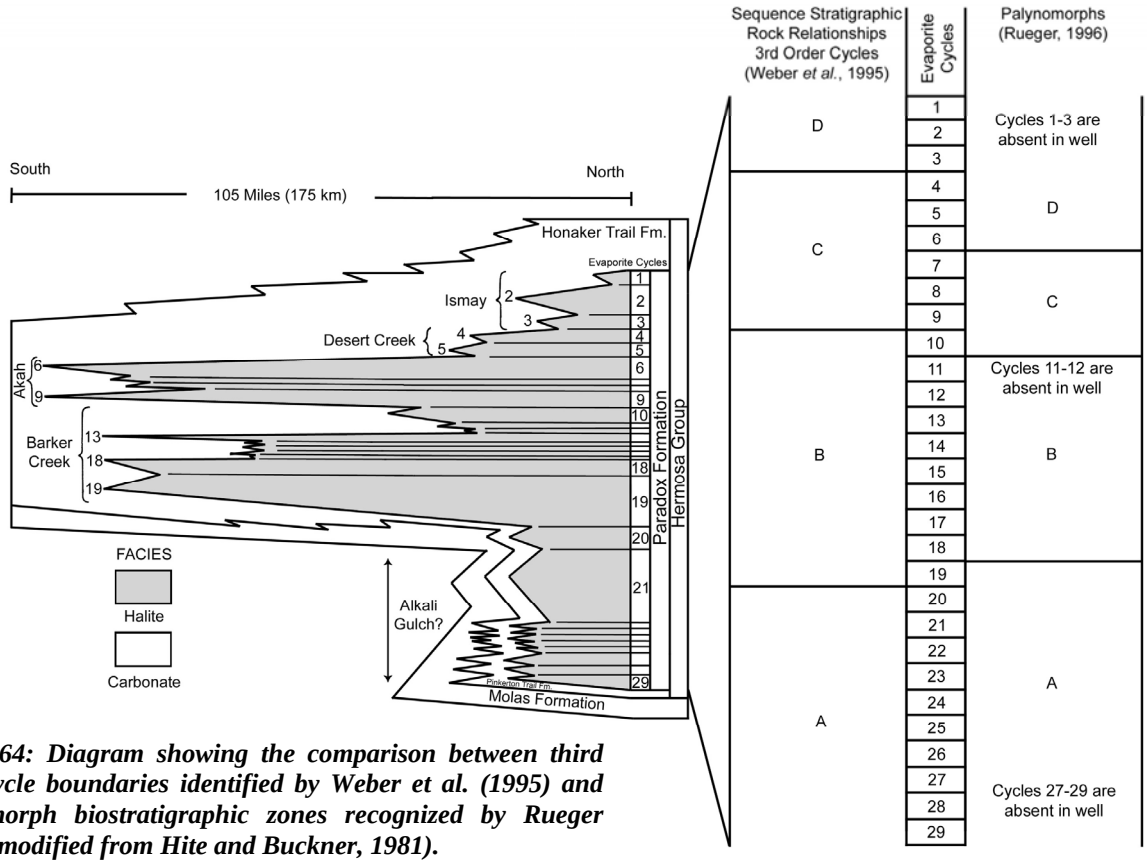

Figure 64: Diagram showing the comparison between third order cycle boundaries identified by Weber et al. (1995) and palynomorph biostratigraphic zones recognized by Rueger (1996) (modified from Hite and Buckner, 1981).

sequence stratigraphic rock relationships and the other from floral successions. What the agreement suggests is that these boundaries mark significant climatic changes within the basin on at least a third order cyclical level.

Paradox Formation – Depositional Age and Timing

An important aspect of this study is to understand the timing and formation of the northern Paradox Basin with relation to the Uncompahgre Uplift. To achieve this goal, an age estimate calculated from the depositional duration of the Paradox Formation would provide a rough time for basin formation and evolution. The Paradox Formation is thought to have been mostly deposited during the Desmoinesian (309.4 – 305.5 Ma according to Gradstein *et al*., (2004). By Late Desmoinesian time, and the end of Paradox deposition, massive amounts of coarse arkosic material were being shed from the Uncompahgre Uplift located to the northeast (Baars and Stevenson, 1981). This presents an approximate time boundary estimate for the deposition of the Paradox Formation and timing of the Uncompahgre Uplift.

To calculate the age of the Paradox Formation, thicknesses of individual lithology types were tallied for 10 wells. These thicknesses were then multiplied by annual sedimentation rates, also unique to each lithology type, resulting in age duration estimates for individual evaporite cycles and for the entire Paradox Formation. Age correlations can then be made from east to west across the basin and can be related to global and local climate changes. It is however difficult to estimate the time of non-deposition during each cycle, although it can be estimated and included into the calculations.

Sedimentation Rates

It is often difficult to estimate halite sedimentation rates. The regularity of bromide profiles for the halite beds within the Paradox Basin suggests there was relatively continuous, uninterrupted deposition (Raup and Hite, 1992). Wardlaw and Schwerdtner (1966) analyzed several evaporite depositional provinces, each having different halite sedimentation rates ranging from 0.4 – 59 inches (1 – 150 cm) per year. They closely examined the Middle Devonian Prairie Evaporite Formation in Saskatchewan, Canada, and concluded that a halite sedimentation rate of 2.0 inches (5 cm) per year was reasonable. Similar rates were recorded in the tectonic setting of the Permian Zechstein Basin in Germany ranging from 1.18 – 4.0 inches (3 – 10 cm) per year (Borchert, 1969). Annual halite intervals measured between anhydrite laminae of the Delhi-Taylor Oil Company Cane Creek No. 1 core (T 26S, R 20E, sec. 25) averaged 1.57 inches (4 cm) in thickness per year and represent a good estimate of halite sedimentation rates within the Paradox Basin.

The thickest, consistent, in situ salt zone within the northern Paradox Basin is the halite section of cycle 6 at around 330 feet (100 m). Considering an average salt sedimentation rate of 1.57 inches (4 cm) per year, this bed would have been deposited in roughly 2,500 years. On a larger scale, a total of 5,000 – 6,000 feet (1,500 – 1,800 m) of depositional evaporites were precipitated within the Paradox Basin. Using the same average sedimentation rate, the total accumulation of evaporites would have been deposited in roughly 37,500 to 45,000 years. Therefore, the bulk of the depositional time for each individual evaporite cycle, and thus the entire formation, is governed by the clastic intervals. With much slower sedimentation rates, the black shales, anhydrites and silty dolomites become extremely important in the age estimate for each cycle and the formation in its entirety (Table 3).

Total Age of the Paradox Formation

The total age estimate for the entire Paradox Formation can be calculated using the sedimentation rates featured in Table 3 and utilizing the total thickness of each individual rock type (Appendix C, Table C-1). The age estimates for the 10 selected wells range from about 600,000 years to over 1.5 million years (Table 4). These estimates however, only account for periods of deposition and do not incorporate episodes of non-deposition, which could have lasted much longer than the total time of salt and clastic deposition combined. Unfortunately, it is very difficult to determine the length of these periods of non-deposition, which are

Table 3: Table showing the depositional rates for each lithology within an ideal evaporite cycle of the Paradox Formation.

Phase	Lithology	Average Annual Rate of Deposition (inches)	(mm)
Regressive	Halite	1.575	40.00
	Anhydrite	0.031	0.80
	Silty Dolomite	0.007	0.17
----------	Black Shale	0.020 - 0.121	0.51 - 3.08
Transgressive	Silty Dolomite	0.008	0.20
	Anhydrite	0.031	0.80

Table 4: A table showing the duration of Paradox Formation deposition for 10 wells based on calculations using lithology thicknesses and sedimentation rates. The table does not include estimated time of non-deposition. A maximum and minimum were calculated based on black shale sedimentation rates of 0.020 to 0.121 inches (0.51 to 3.08 mm) per year.

No.	API #	Operator	Well Name	Age (years)	
				(max.)	(min.)
1	4301511182	SUPERIOR OIL COMPANY	GRAND FAULT UNIT 14	1,544,000	1,476,000
2	4301530079	MEGADON ENTERPRISES	GEYSER DOME 1-14	873,000	830,000
3	4301930124	MOUNTAIN FUEL SUPPLY	MT FUEL-SKYLINE GEYS	1,181,000	1,089,000
4	4301930282	RESERVE OIL & GAS	SALT WASH NORTH 1	1,125,000	1,055,000
5	4301930688	MEGADON ENTERPRISES	FEDERAL 1-26	1,092,000	1,014,000
6	4301930050	GENERAL CRUDE OIL CO	BIG ROCK FED 1	1,203,000	1,116,000
7	4301930910	CHANDLER & ASSOCIATE	MOAB FED 16-9	1,104,000	1,023,000
8	4301530145	DAVIS OIL COMPANY	POOL UNIT 1	636,000	602,000
9	4301931190	COORS ENERGY	COORS USA 1-10LC	923,000	817,000
10	4301910767	MURPHY CONSTRUCTION	LITTLE VALLEY-FED 1	843,000	714,000

generally considered to be at the end of each subsequent cycle (following the last period of the halite/potash precipitation). If we consider the total time of non-deposition to be at least twice as long as the total time of complete deposition/precipitation, then the total age estimates for the Paradox Formation are recalculated to range from 1.8 million years to over 4.5 million years. These estimates therefore fit within the time period of the Desmoinesian further quantifying that the Paradox Formation could have been completely deposited during the time interval of about 309.4 – 305.5 Ma (Gradstein *et al*., 2004).

When the estimated ages for the 10 wells are plotted and contoured, very interesting relationships are established areally (Figure 65). Moving west to east towards the Uncompahgre Uplift, and thus the deepest part of the basin, the total age of deposition for the Paradox Basin becomes greater. This indicates several key factors related to basin evolution. First, since the bulk of the age estimate is based on the clastic intervals (much slower sedimentation rates compared to halite), it is clear farther to the east, more clastic material is present. This signifies there was more clastic material supplied from the eastern (possibly from the Uncompahgre Uplift) side of the basin than from the west. It also might suggest there was a greater amount of accommodation in the east (i.e., the deepest part of the basin) possibly caused by basin subsidence in relation to the crustal flex of the rising Uncompahgre Uplift. Secondly, it is interesting to note how the sediments east of the Cane Creek Anticline were deposited over a progressively shorter duration of time moving farther to the east (Figure 65). This might suggest that salt tectonics was active by at least the end of the Paradox salt deposition. Since the age estimates are based heavily on the clastic material and non-depositional periods are almost impossible to ascertain, the Cane Creek Anticline may have started to become a more positive feature sometime during the Desmoinesian. The final few cycles appear to have been depositionally thinner over this structure.

Duration Per Individual Depositional Cycle

If the sedimentation rates (Table 4) are applied to the sequence of rock types, in evaporite cycle 2 for example, the calculations suggest a depositional time interval of roughly 100,000 years (Table 5).

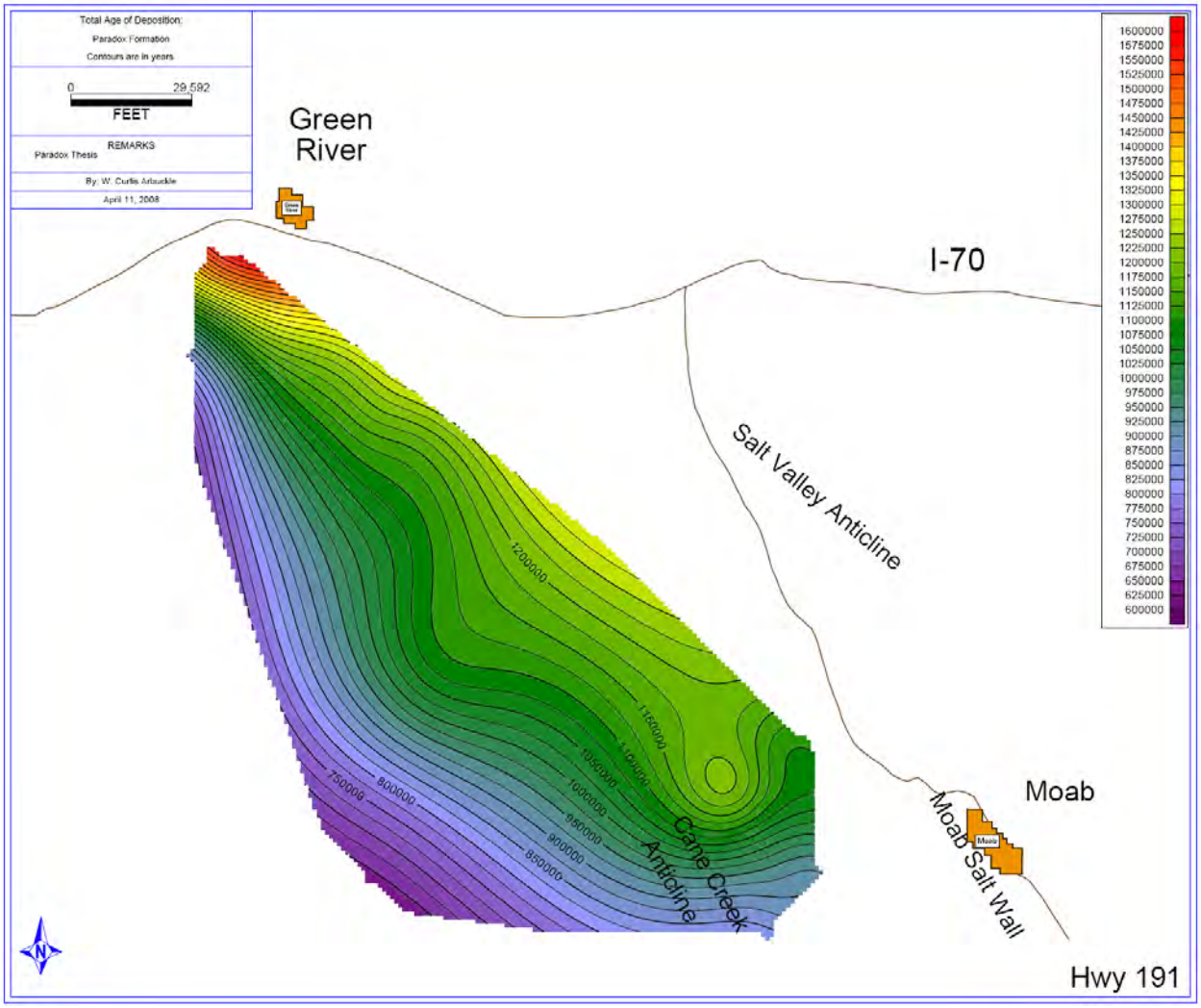

Figure 65: Map showing the total duration estimate for the depositional units within the Paradox Formation. These times were calculated using thicknesses tallied from well logs and sedimentation rates for each individual lithology. Contour intervals are in years.

Table 5: Table showing the estimated rates of sedimentation and age duration of deposition for evaporite cycle 2 of the Coors Energy, Coors USA 1-10LC well (T 26S, R 20E, sec. 10). (R) = regressive; (T) = Transgressive.

Lithology	Annual Rate of Deposition		Thickness		Age
	(inches)	(mm)	(feet)	(meters)	(years)
Halite	1.575	40.00	217.1	66.17	1,654
Anhydrite (total)	0.031	0.80	31.9	9.72	12,154
Silty Dolomite (R)	0.007	0.17	22.05	6.72	39,534
Black Shale	0.020-0.121	0.51-3.08	18.3	5.58	10,937 - 1,811
Silty Dolomite (T)	0.008	0.20	24.95	7.60	38,024
		Totals	314.3	95.8	102,303 - 93,177

This duration of deposition fits the 100,000 year eccentricity Milankovitch periodicity. Unfortunately, the age estimate for many of the other cycles, including cycle 2, 3, 5, 9 and 10 in several other wells, sometimes falls short of this 100,000 year period (Appendix C, Tables C-2 – C-5). Because there is such variability in the duration of the evaporite cycles, other processes and factors must have influenced timing and rate of sedimentation. It is also important to note the duration of the cycles become increasing longer as the cycles become younger. For example, cycle 9 has an average duration of 50 – 54,000 years where as cycle 3 ranges from 70 – 79,000 years. There are many reasons that could limit the duration of each cycle and probably include a combination of fluctuating periods of localized tectonic activity, relative and eustatic sea-level changes, basin isolation, plate tectonics, subsidence, the influence of meteoric groundwater or seepage, varying periods of non-deposition, irregular erosional patterns, etc.

Subsidence

Subsidence in a present-day, tectonically active region can be extremely variable making the calculation of subsidence rates difficult. Therefore, establishing a subsidence rate for the Paradox Basin, which formed roughly 300 millions of years ago, is a difficult task. Donovan *et al*. (1985) estimated subsidence rates of 0.0004 – 0.02 inches (0.01 – 0.5 mm) per year for several geotectonic settings in Oklahoma during the Paleozoic. However, there are examples of subsidence rates in collapsing basins of 16 – 19 feet (5 – 6 m) per 1,000 years, which is about equal to 0.24 inches (6 mm) per year (Sonnenfeld, 1984).

If a subsidence rate of 0.04 inches (1 mm) per year is applied to the Paradox Basin, it is apparent that the average salt sedimentation rate of 1.57 inches (4 cm) per year far exceeds any subsidence totals. Therefore, the basin must have been deep enough to accommodate the deposition of each subsequent cycle and/ or have a high enough rate of subsidence to accommodate such rapid rates of precipitation. To summarize, the thickest salt accumulations would be located in areas with the greatest rates of subsidence (Sonnenfeld, 1984). Also at this time the basin would have been relatively isolated from any open marine waters that would hinder the deposition of evaporites, but still have enough marine water influx to fuel and re-supply the brine with salt minerals.

One must also consider that when precipitation rates exceed basin subsidence rates, after halite saturation, the basin floor typically levels out creating a broad flat surface at the end of each cycle (Sonnenfeld, 1984). Therefore, any localized thickness changes within the halite interval of a cycle, could be explained by tectonic processes, which include periods of rapid subsidence coupled with rapid uplift.

The Formation and Timing of the Uncompahgre Uplift and Paradox Basin

The Uncompahgre and San Luis uplifts were a continuous Pennsylvanian tectonic highland stretching from southwestern Colorado to central-eastern Utah, and formed during the Late Paleozoic as part of the ARM.

By the end of Mississippian time, there were probably several hundreds to thousands of feet of early and middle Paleozoic age strata that extended across the current location of the Paradox Basin and Uncompahgre Uplift. Based on lithofacies data and stratigraphic relationships, the Uncompahgre and San Luis uplifts first became positive in the southern extremities by early Pennsylvanian time (Wengerd, 1958; Fetzner, 1960).

It is believed that by middle Pennsylvanian (Desmoinesian) time the

Uncompahgre front in the northern and eastern sections of the basin was in existence, but was not as tectonically active as the San Luis complex farther to the south. At this time, the Uncompahgre probably was not significantly elevated above local sea level, if at all. However, the uplift itself and the associated trough or foredeep still affected the depositional patterns of the Paradox Formation. This will be discussed further in the next section.

A significant pulse of uplift along the central part of the Uncompahgre (in the vicinity of the Colorado-Utah state line) occurred near the end of evaporite deposition (Elston and Shoemaker, 1960). This pulse is marked by arkosic and granitic material (as coarse as boulder size) interbedded with the upper part of the Paradox Formation in Sinbad Valley (Elston *et al*., 1962). Further tectonic pulses followed giving rise to the Uncompahgre Uplift, which by Late Desmoinesian/Early Missourian time, had become a strongly positive feature shedding arkosic material at least 20 miles (32.2 km) into the basin (Elston and Shoemaker, 1960).

The Uncompahgre experienced its most significant uplifting episode near the end of the Pennsylvanian and into Permian time. An abundant influx of arkosic material into the Uncompahgre trough (undifferentiated Cutler Group) is evidence of this important period of uplift. Several other tectonic pulses have been documented following the major uplifting episode in Early Permian time. The deposition of the Late Triassic Moenkopi Formation marks the end of any further uplift or significant movement along the Uncompahgre.

The Uncompahgre Uplift and its Impact on the Northern Paradox Basin

There is strong evidence supporting the idea that the San Luis Uplift experienced greater amounts of uplift and tectonic activity before the northern part of the Uncompahgre became a positive feature. However, even if the structure wasn't elevated significantly above local sea level, it still could have influenced sedimentation patterns.

A lack of an abundant amount of arkosic material located in the oldest evaporite cycles suggests the Uncompahgre was not exposed above sea level and thus subject to typical erosion processes. However, the Uncompahgre may have already begun thrusting upwards, but the majority of it remained below sea level (Figure 66). A submerged Uncompahgre structure, and the immediate surrounding area, could have been an ideal location for increased carbonate accumulations. Paz Cuellar (2006) observed this in an area east of Onion Creek where there was a lack of significant arkosic material in Middle Pennsylvanian strata (and thus a greater accumulation of non-evacuated salt) and increased amounts of carbonates. Personal communication with Gary Nydegger (2007) also supports this conclusion; he noted there were increased carbonate accumulations within the Paradox Basin #1 well that are typically not found that far west into the basin. A re-interpretation of the Paradox Formation lithology in the American Petrofina Elba Flats Unit No. 1-30 well further implies a greater mix of carbonates with the abundant clastic material.

Also, if the Uncompahgre was a low relief feature, or submerged below relative sea level (Figure 66), there still would have been significant amounts of subsidence adjacent to the uplift. Basin subsidence probably began near the end or shortly after the deposition of the Pinkerton Trail Formation as illustrated by the consistent and continuous structural dip of the formation. By middle Desmoinesian time, the Uncompahgre was at or near sea level and had enough associated subsidence to create the initial stages of the foredeep we observe today. As the uplift became much more of a positive structure by the end of the

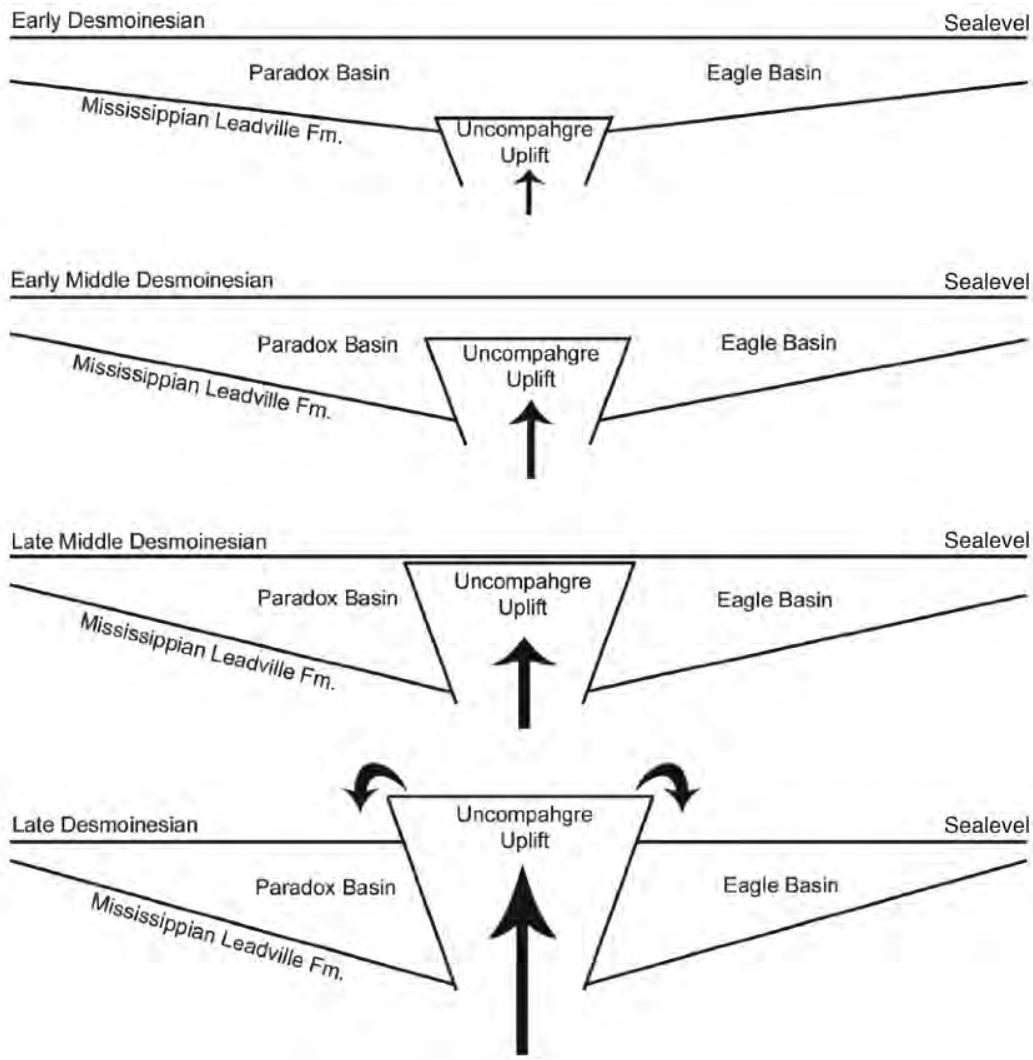

Figure 66: A schematic diagram illustrating the possible progression of the Uncompahgre Uplift throughout Desmoinesian time. Notice that although the uplift was not above sea level during early Desmoinesian time, it was still affecting basin subsidence. This diagram also suggests the Paradox Basin and the Eagle Basin (Eagle Valley evaporites) were once connected early in the basin(s) evolution.

Pennsylvanian, the foredeep had subsided over 12,000 feet (3,650 m).

Uncompahgre Uplift – Unanswered Questions

Questions remain about the rise of the Uncompahgre Uplift. Wells drilled in the northeastern section of the basin contain significant amounts of arkosic material in what are interpreted as age-equivalent Paradox Formation strata. One could argue that the majority of salt has been evacuated from this part of the basin, and that the overlying arkosic material is not part of the Paradox Formation but rather Late Pennsylvanian in age, or part of the Cutler Formation (Permian). If indeed the clastic material was deposited as part of the Paradox Formation, then there must have been a local, positive, granitic structure shedding material into the basin. The GCRL Energy LTD Seismosaur Federal #1 well (T 21S, R 20E, sec. 20) is an interesting datapoint (Figure 67). This unusual well penetrates clastic intervals between salt zones that over 500 feet

Figure 67: Map showing the location of the GCRL Energy Ltd. Seismosaur Federal #1 well. Image modified from Google Earth (2007).

(152 m) thick (Utah Division of Oil, Gas and Mining, 2007). These intervals are also composed of sandstones, limestones, shales, dolomites, marlstones as well as glauconite, which is altered from detrital biotite in shallow marine waters under reducing conditions (Nesse, 2000). This again suggests there was a local positive granitic structure that sourced these clastic zones. It is possible there were some parts of the Uncompahgre Uplift that were above relative sea level, creating islands that were able to shed this localized clastic material.

Early Clastic Sediment Supply

The depositional processes responsible for much of the clastic material in the lower, older, evaporite cycles is uncertain. Within the silty dolomite interbeds (transgressive and regressive), there are abundant amounts of quartz and feldspar (near 40 percent of the total mineralogy). These grains are well sorted and very fine to fine grained much like the hosting dolomite. It is unclear how and why these detrital grains were deposited with the dolomite and how they reached such a distance from the available and known source areas.

There were two known main source areas for the clastic material during the time of deposition; the Uncompahgre Uplift to the east, and the shelf margin in the southwest. Undoubtedly both sources supplied clastic material to the basin synchronously by the end of the Pennsylvanian.

The quartz and other related minerals might have reached the center of the basin by density currents (or low-density turbidites) over the top of dense salinity brines circulating down to the bottom of the basin. Raup and Hite (1992) suggest these currents may have collected clastic material as they advanced along the rising shoreline and past the arkosic alluvial fans that formed adjacent to the rising Uncompahgre Uplift. Such movement across significant distances may have led to the high degree of sorting of the clastic grains. Harms and Williamson (1988) propose a similar mechanism of transport into deep water involving the Delaware Mountain Group in the Delaware Basin, Texas and New Mexico. The extreme level of sorting might also suggest the clastic grains are eolian in origin.

Most of the sandstones, sometimes classified as turbidites, are located in the northern part of the basin. If the Uncompahgre was not a strongly positive feature during sandstone deposition, an alternative source is required. These sandstones may have been transported into the basin via the Freemont embayment or through the Oquirrh passageway (see figure 13).

Paradox Basin and Uncompahgre Uplift Formation Model Comparison

There is no doubt the Paradox Basin and Uncompahgre Uplift shared a complex relationship during their respective formation. Whether or not they formed as a linked tectonic system is highly debatable and contested. Existing evidence supports various models including 1) pull-apart tectonics, 2) basin-wide flexural models, 3) the development of the Uncompahgre Uplift after the formation of the basin, and 4) the presence of glacial-ice atop the uplift.

The Paradox Basin: A Pull-apart Basin

Stevenson and Baars (1986) believe the Paradox Basin and ARM formed due to extensional and pull-apart tectonics. East-west extension during the Middle Pennsylvanian was caused by an intersection of regional and local basement faults and fracture zones. Strike-slip faulting along the Uncompahgre front created a bend between the Uncompahgre and San Luis uplift(s). This bend released an area of strike-slip offset and

extension creating basin subsidence (Stevenson and Baars, 1986). Sub-basins formed in response to the local extension along the local fault lineaments, each having a varied amount of subsidence where the greatest occurred closer to the major controlling faults along the Uncompahgre front. The basin was deepened several times during the Middle Pennsylvanian due to further extensional basement faulting but subsidence slowed during the Late Desmoinesian (Desert Creek stage) (Stevenson and Baars, 1986). At this juncture, minor amounts of wrench faulting created shoaling conditions in the southern part of the basin where the algal-carbonate mounds formed. Also, further basin subsidence occurred in the northern and eastern sections of the basin resulting in the deposition of marine and non-marine sediments by Early Permian time (Stevenson and Baars, 1986).

Based on the shape, structure and areal evidence presented by Stevenson and Baars (1986), accepting that the Paradox Basin and Uncompahgre Uplift were products of strike-slip extensional basement faulting seems plausible. Structural and tectonic features, including the local northeast-southwest and northwest-southeast trending basement faults and uplifts, support their theory. Resulting sub-basins and key evidence of a stress releasing bend/break in the Uncompahgre and San Luis uplift(s) compare well to other basins formed due to pull-apart tectonics.

Unfortunately, little data based on stratigraphical relationships were used in Stevenson and Baars' (1986) analysis. Utilizing well and seismic data could help support their theory, which is primarily centered on tectonic associations. Some stratigraphic and structural reconstructions, (Kluth and DuChene, 2007) clearly don't support the Stevenson and Baars (1986) model.

The Paradox Basin: A Flexural Model

Barbeau (2003) interpreted the Paradox Basin as an intraforeland flexural basin formed due to flexural subsidence associated with the rise of the Uncompahgre Uplift. Barbeau's model utilized subsidence history, shape, structural relationships and facies architecture to justify the idea of a foredeep zone that formed adjacent to the uplift as a result of crustal flexure (Figure 7). Barbeau (2003) also noted there should be a positive crustal rebound structure called a forebulge that would form opposite of the foredeep. His model suggests this bulge is associated with the carbonate shelf located at the southern edge of the basin.

Barbeau's (2003) model contrasts with the previous pull-apart/extensional interpretations made by Stevenson and Baars (1986) noting a lack of strike-slip offset. Barbeau (2003) also explains that the northwest-southeast trend of the Uncompahgre Uplift and the Paradox Basin suggest the two structures were formed together as a result of northeast-southwest shortening, again contrary to what Stevenson and Baars (1986) hypothesized.

Barbeau (2003) also compared the Paradox Basin with other flexural-isolated foreland basins and the more closely related ARM basins. Barbeau explained how the northwest-southeast orientation of the Paradox Basin, combined with the major thrust fault system in the east (the Uncompahgre thrust) and the foreland basin facies architecture exhibited along the foredeep and forebulge, are analogous to other ARM basins. Furthermore, Barbeau implies that any model illustrating the formation of the ARM would consist of a system showing northeast-southwest contraction.

Barbeau's (2003) model raises several concerns including whether or not the Ouachita-Marathon thrust belt resulted in enough stress to exhibit shortening in the

ARM uplifts and basins. The model and representative cross section (Figure 7) strike roughly about 35 degrees south of perpendicular from strike of the Uncompahgre Uplift. Although this cross section summarizes and fits the proposed model, it fails to incorporate much of the northern half of the basin. The northern half is by far the deepest and thus displays the greatest amount of subsidence. Therefore, to ignore these important features suggests the model may not be representative for the northern part of the basin. Additionally, a lack of strong evidence supporting a forebulge (which is structurally controlled) in the northwestern section of the basin is lacking, raising further questions about the accuracy of a flexural model for at least the northern Paradox Basin.

The Paradox Basin and Eagle Valley Evaporites – A New Perspective

Recently, several authors including Kluth and DuChene (2006, 2007), Rasmussen (2006) and Kluth (2008) have speculated the Paradox Basin and the Eagle Valley evaporites were once connected, before the rise of the Uncompahgre Uplift. Rasmussen (2006) uses stratigraphic relationships, of inter-layered evaporites and carbonates abutting against the Uncompahgre Uplift, to recognize that the siliciclastics do not terminate against the uplift. This would only be possible if the Uncompahgre was not a positive feature at the beginning of Paradox Formation deposition. However, by late Desmoinesian and into Permian time, coarse arkosic material was being shed from the Uncompahgre Uplift into the basin. This suggests the uplift began to develop sometime during the Desmoinesian and escalated fast enough to erode the abundant amount of arkosic material into the basin by at least the beginning of Permian time.

Kluth and DuChene (2007) created several restorations of the Paradox Basin based upon one seismic line striking northeast-southwest across the Lisbon Valley, Gypsum Valley, Paradox Valley and Sinbad/ Onion Creek salt structures. Their restorations involve removing the sediment load of the overlying Honaker Trail Formation and Cutler Group, both of which caused significant differential loading and ultimately led to salt wall/structure growth. Again, similar to Rasmussen (2006, the restorations illustrate that the Uncompahgre Uplift was not a positive feature at the start of salt deposition, once more suggesting the Paradox Basin and Eagle Valley evaporites were connected.

Kluth (2008) suggested the San Luis Highlands were uplifted (Middle Pennsylvanian Desmoinesian time) before the Uncompahgre Uplift noting how some of the arkosic material shed from the highlands interfingers with several salt intervals in the southeastern section of the basin. Soon thereafter, the Uncompahgre began to develop further to the north, but only after a significant percentage of the Paradox Formation, and maybe the Honaker Trail Formation, was already deposited.

The evidence presented by the authors described above is strikingly convincing, however there are several important questions that were not addressed and/or remain inconclusive. From what Kluth and DuChene (2007) presented in their restorations, there was no indication that basin-wide subsidence was incorporated into their model. Without this information, it is hard to determine the timing, duration and thus evolution of the basin and Uncompahgre Uplift. Rasmussen (2006), Kluth and DuChene (2007) and Kluth (2008) together also fail to present any significant explanation(s) regarding basin formation prior to the development of the Uncompahgre Uplift. Their model therefore lacks, at least in the author's opinion, an important aspect of the Paradox Basins evolution.

Late Paleozoic Glacial Evidence on the Uncompahgre Plateau

Soreghan *et al*. (2007) published an extensive study on the processes, timing and formation of Unaweep Canyon. Unaweep Canyon is about 0.62 miles (1 km) deep and 3.73 miles (6 km) wide and cuts perpendicular to the northwest-southeast trending Uncompahgre Uplift (Figure 68). It has been suggested that the ancient Gunnison River or the Colorado River once flowed through the area carving out the canyon, but a lack of (a large quantity of) typical river sediments and gravels poses additional questions.

Recent paleomagnetic, palynology and provenance data hint that the canyon fill is of late Paleozoic age (Soreghan *et al*., 2007). Further evidence of apparent Permo-Pennsylvanian glacial deposits (dropstones) within the canyon suggests the canyon itself was formed due to glacial processes (Soreghan and Soreghan, 2003). This implies there was ice at the equator (roughly) during canyon formation, thus appearing inconsistent with the late Paleozoic setting typically characterized for the region. If the climate of the late Paleozoic experienced rapid changes, then low-elevation glaciation could be possible. This however seems rather extreme based on global and regional climate studies and relationships. A more likely, but still unproven, hypothesis is that the Uncompahgre Uplift was much higher in elevation than

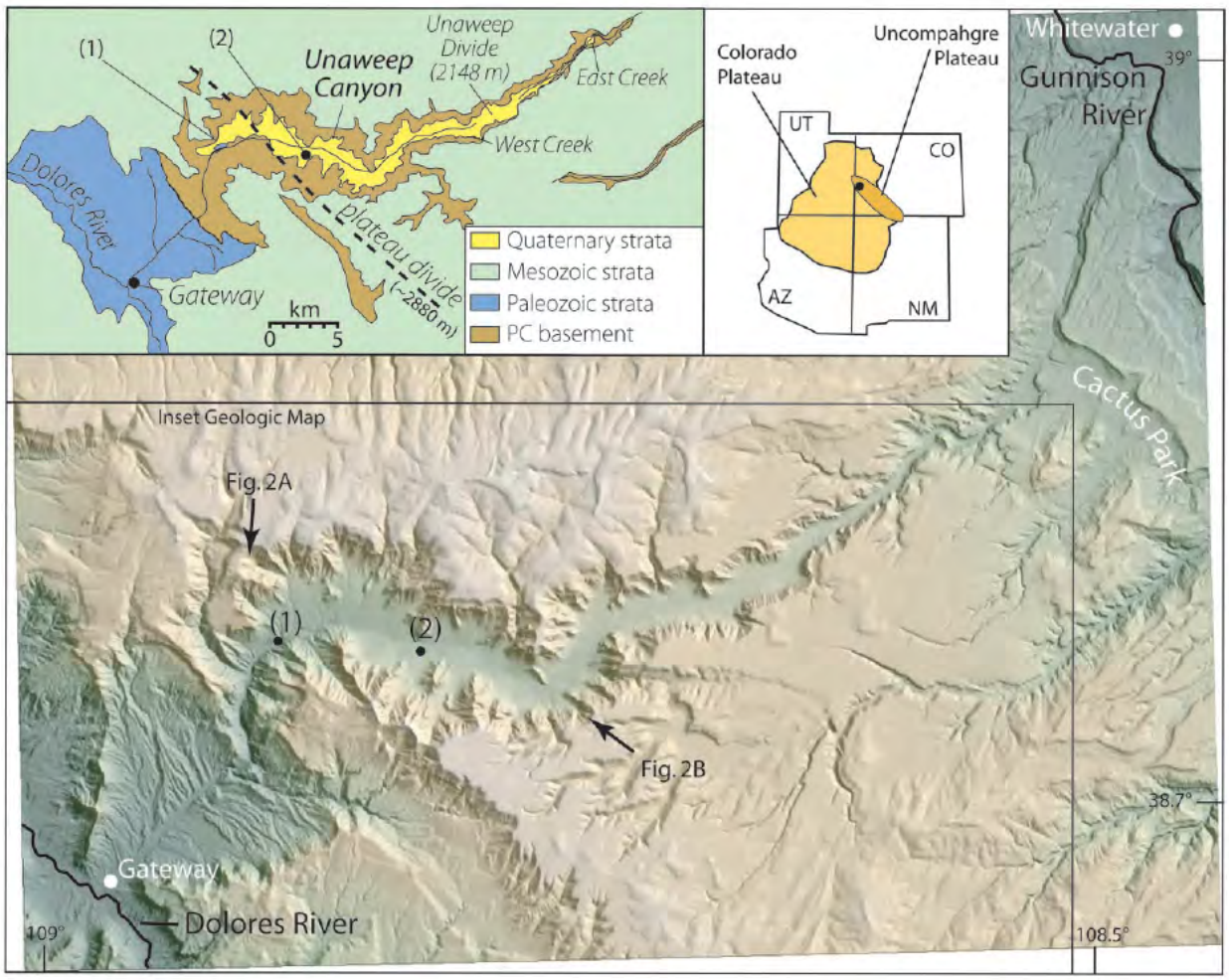

Figure 68: Figure and map showing the location and strata of Unaweep Canyon (after Soreghan et al., 2007).

previously thought. For modern tropical glaciation to occur, an elevation of 13,100 – 16,400 feet (4,000 – 5,000 m) is required (Soreghan *et al*., 2007). Although this is reasonable in theory, it may be implausible requiring a significant orogenic collapse of the Uncompahgre, following the conclusion of uplift, which has yet to be observed structurally (Soreghan *et al*., 2007).

Hydrocarbon Exploration – Economic Potential

The hydrocarbon potential of the Pennsylvanian age rocks within the northern Paradox Basin is once again being recognized. Increased leasing and drilling activity, may identify new economic hydrocarbon accumulations. Recently, Delta Petroleum has drilled several wells targeting the clastic intervals within the Paradox Formation (Delta Petroleum, 2008) and Golden State Resources has completed a successful well targeting what appear to be carbonate reservoirs within the upper Paradox Formation (Golden State Resources, 2002).

Carbonate Reservoirs

Carbonate reservoirs in the northwestern portion of the basin are currently being explored. Golden State Resources drilled the Paradox Basin #1 well (T 23S, R 23E, sec. 16) on top of an up-thrown basement fault block (Figures 69 and 70). Their targeted intervals included sub-Pennsylvanian reservoirs, but encountered shows within Pennsylvanian aged strata. Most of these shows are thought to be within carbonate rocks and/or within carbonate buildups (Figure 78) (Golden State Resources, 2002). The absence of major salt accumulations (either non-depositional or welded) (Gary Nydegger, 2007, personal communication) and the presence of significant thicknesses of carbonates, highlight the possibility of considerable hydrocarbon accumulations atop these fault blocks.

Fine Grained Sands – Turbidites

The fine-grained sands facies, which have often been characterized as turbidites, could be highly significant to hydrocarbon exploration. These sands are potentially favorable reservoirs for hydrocarbons generated from the organic-rich, black shale source rocks. However, most of these sands tend to be thin and of limited lateral extent, making exploration and identification difficult. Further petroleum exploration near the Uncompahgre Uplift would provide a better understanding of the economic potential of the turbidites.

CONCLUSIONS AND RECOMMENDATIONS

The dynamic evolution of the northern Paradox Basin controlled the cyclicity and deposition of the Pennsylvanian Paradox Formation. The following are conclusions from this study:

Periodicity and Mechanisms Involving Pennsylvanian Cyclicity – Paradox Formation

1. The cyclicity observed within the Paradox Formation is a result of several related factors including regional and local tectonics, subsidence, sediment availability and supply, climate, and finally glacio-eustatic sea-level fluctuations.

2. We believe the evidence presented indicates that Gondwanaland glaciations ultimately caused the eustatic sea-level fluctuations, and were the main factor influencing Paradox Formation cyclicity.

3. Stratigraphic rock relationships and palynomorph data both indicate there are five third order sequences

comprising the Paradox and lower Honaker Trail formations. Therefore, it is deemed that each individual evaporite cycle was roughly deposited as a fourth order sequence having 100,000 – 500,000 year duration.

4. Unfortunately, there is not undisputable evidence that Milankovitch cyclicity solely controlled the cyclic depositional patterns observed in the Paradox Basin. However, it is clear that orbitally forced cycles strongly influenced sedimentation within the basin. Perhaps such a short interval of 100,000 years, or less, makes reliable identification and correlation of like cycles too problematic.

5. Age estimates for the entire Paradox Formation are highly dependent on the thickness and lithology types of the clastic zones. Greater thicknesses within the clastic zones (particularly with the black shales and dolomites) indicate longer depositional sequences and thus provide further indication about sediment source and supply.

6. Age estimates of individual cycles calculated based on sedimentation rates indicate the cycle durations ranged upwards of 100,000 years further concurring with Milankovitch influenced cyclicity. Transgressive and regressive lithologies also give clues to the amount and length of each individual cycle.

Basin Formation and the Evolution of the Uncompahgre Uplift

1. Isopach thickness maps of individual evaporite cycles clearly illustrate the northern Paradox Basin formed due to several dynamic processes. The maps suggest the basin was somewhat tectonically active even before Pennsylvanian time. They also indicate there could have been salt movement as early as the end of the Desmoinesian, implying there was greater salt movement farther to the east as a result of early Cutler deposition (sediment loading).

2. The northern Paradox Basin experienced an eight million year period (308 – 300 Ma) of relatively rapid subsidence. The start of this time interval coincides with at least the beginning of the Desmoinesian and therefore occurred during the deposition of the Paradox Formation. Major subsidence appears to end by Early Permian time.

3. The Uncompahgre Uplift was slower to develop compared to the San Luis Uplift farther to the south. However, even though the Uncompahgre was not areally exposed until near the end of the Pennsylvanian, it still influenced depositional patterns and was accompanied by significant basin subsidence. Further, evidence of early eroded arkosic material suggests the Uncompahgre went through several stages or pulses of uplift with the largest occurring near the end of Desmoinesian time.

4. Several basin formation models propose different ideas involving the relationship between basin formation and the development of the Uncompahgre Uplift. Each model uses convincing evidence to support its conclusions, however, it is unlikely all of the models are entirely correct since each has conflicting results. Therefore, it is more reasonable to conclude that each model is accurate to some extent

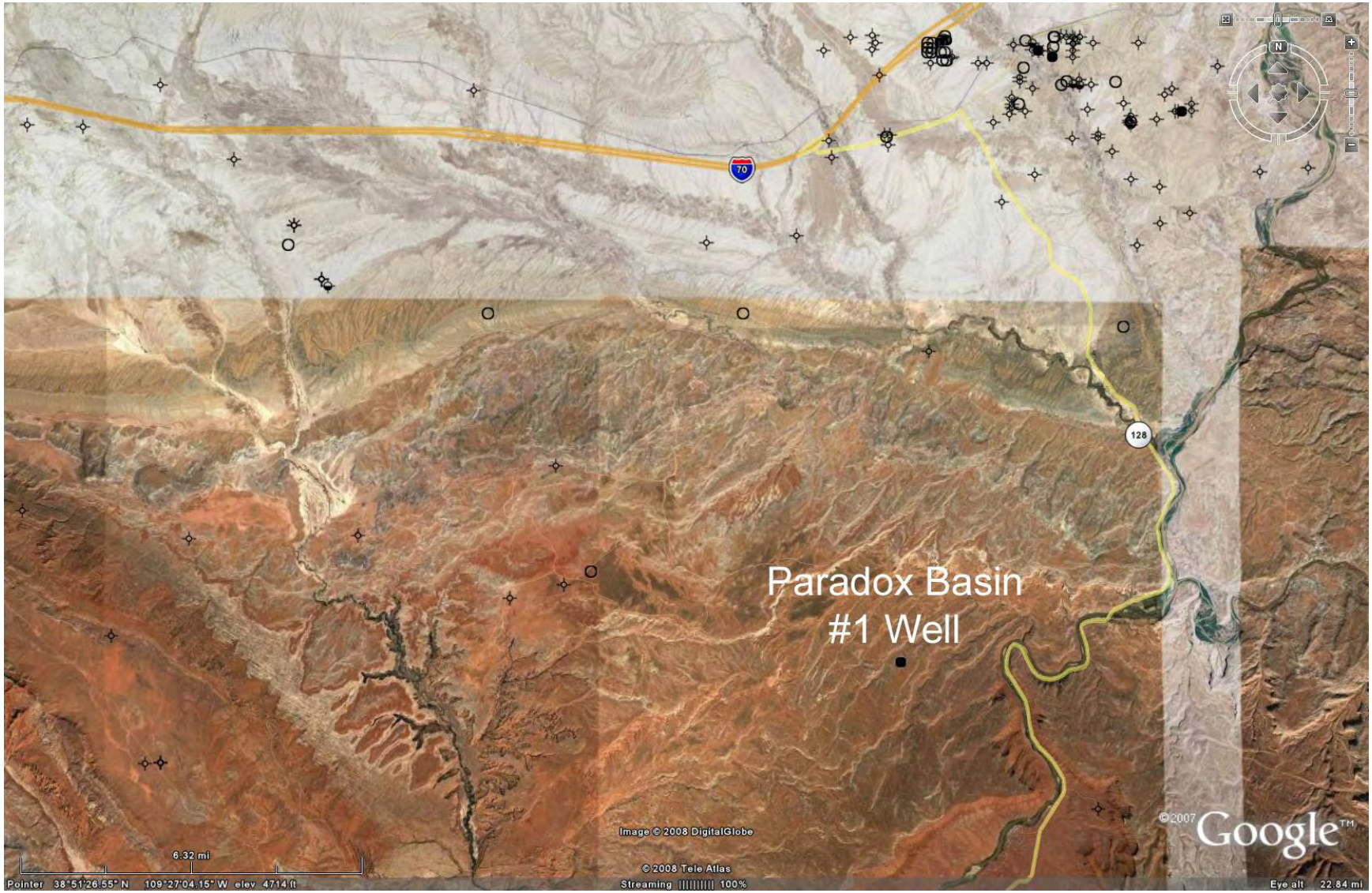

Figure 69: Map showing the location of the Paradox Basin #1 well. Image modified from Google Earth (2007).

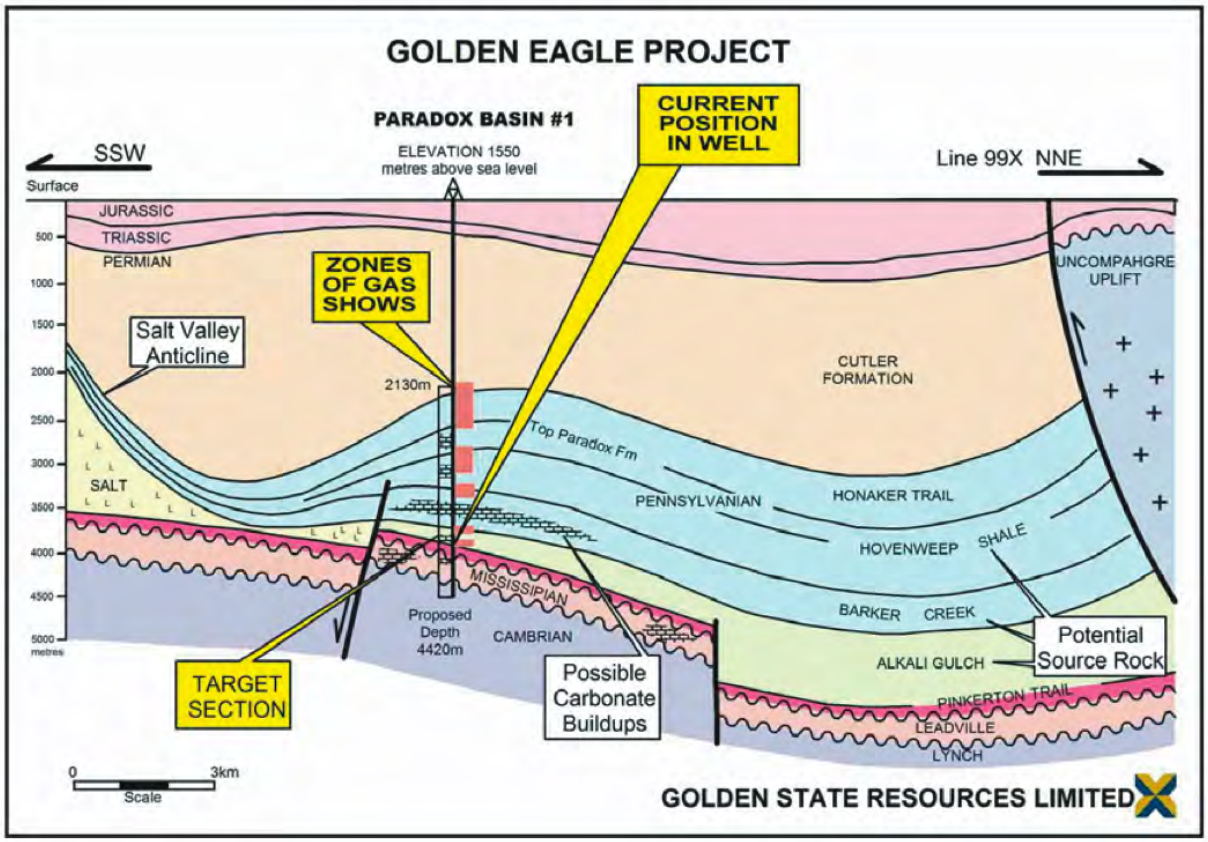

Figure 70: Illustration of the expected lithologies encountered by the Golden State Resources Paradox Basin #1 well (Golden State Resources, 2007).

and that a combination of these models probably creates a more complete and accurate representation. We believe the Paradox and Eagle basins were connected early, during the initial cycles of salt deposition. The Uncompahgre Uplift developed early in the basin history, but never reached any significant height above sea level (for long durations of time) until near the end of Pennsylvanian time.

5. Estimates of the duration of Paradox Formation sedimentation in different parts of the basin further support a conclusion that the eastern half of the basin is much older, deeper and started to develop earlier then the rest of the basin (possibly starting in Late Atokan or Early Desmoinesian time).

6. The two main sources of sediment supply into the basin are the Uncompahgre Uplift to the east and the San Luis Uplift near the southern margin of the basin. Evidence suggests both sources added substantial material into the depths of the basin. However, once the Uncompahgre became a strongly positive structure, it had by far a greater impact on clastic supply, at least in the northern half of the basin.

Recommendations for Future Work

1. To help compliment and complete a northern Paradox Basin correlation based upon rock type lithologies, additional samples from drill cores or cuttings from the easternmost section

of the basin are needed. These samples would allow for better correlations of individual evaporite cycles and/or transgressive regressive sequences unlike what is available in outcrop and used for the QEMSCAN analysis in this study.

2. Additional detailed analysis on fine-grained clastic sediments within the clastic zones of the evaporite cycles would help identify the provenance for these detrital sediments. Only then could their source be identified.

3. Many of the wells drilled within the northern Paradox Basin, and used in this study, have unreliable formation top picks for the Honaker Trail Formation, which are often confused with beds from the lower Cutler Group. Accurate top information would provide additional details on salt movement, timing, and give clues to when the Cutler was deposited in relation to the formation of the Uncompahgre Uplift.

4. Additional interpreted seismic lines across the Uncompahgre may provide further insight to the correlativeness of the genetic relationship between the Paradox and Eagle basins.

REFERENCES

Baars, D. L., 1962, Permian systems of Colorado Plateau, American Association of Petroleum Geologists Bulletin, vol. 46, no. 2, pages 149-218.

Baars, D. L., 1966, Pre-Pennsylvanian paleotectonics – key to basin evolution and petroleum occurrences in Paradox Basin, Utah and Colorado, American Association of Petroleum Geologists Bulletin, vol. 50, no. 10, October, pages 2082-2111.

Baars, D. L., 1987, Paleozoic rocks of Canyonlands country, *in* J. A. Campbell, ed., Geology of Cataract Canyon and vicinity, A field symposium – guidebook of the Four Corners Geological Society, Tenth Field Conference, May 14th-17th, pages 11-17.

Baars, D. L., J. W. Parker, and J. Chronic, 1967, Revised stratigraphic nomenclature of Pennsylvanian system, Paradox Basin, American Association of Petroleum Geologists Bulletin, vol. 51, no. 3, March, pages 393-403.

Baars, D. L., and G. M. Stevenson, 1981, Tectonic evolution of the Paradox Basin, Utah & Colorado, *in* D. L. Wiegand, ed., Geology of the Paradox Basin, Rocky Mountain Association of Geologists, 1981 Field Conference, pages 23-31.

Baars, D. L., and G. M. Stevenson, 1982, Subtle stratigraphic traps in Paleozoic rocks of Paradox Basin, American Association of Petroleum Geologists Special Volumes, M32, The deliberate search for the subtle trap, pages 131-158.

Baker, F., 1969, Precambrian geology of the Needle Mountains, southwestern Colorado, United States Geological Survey Professional Paper 644-A, 35 pages.

Barbeau, D. L., 2003, A flexural model for the Paradox Basin: implications for the tectonics of the Ancestral Rocky Mountains, Basin Research, vol. 15, pages 97-115.

Beloussov, V. V., 1962, Basic problems in geotectonics, New York, McGraw-Hill Book Company, Inc., 816 pages.

Berger, A., 1984, Accuracy and frequency stability of the earth's orbital elements during the Quaternary, *in* A. Berger, J. Imbrie, J. Hays, G. Kukla, B. Saltzman, eds., Milankovitch and climate: part 1, D. Reidel Publishing Company, Dordrecht, Netherlands, pages 3-39.

Berger, A., M. F. Loutre, and V. Dehant, 1989, Influence of the changing lunar orbit on the astronomical frequencies of pre-Quaternary insolation patterns, Paleoceanography, vol. 4, no. 5, October, pages 555-564.

Berman, A. E., D. Poleschook Jr., and T. E. Dimelow, 1980, Jurassic and Cretaceous systems of Colorado, *in* H. C. Kent, and K. W. Porter, eds., Colorado Geology, Rocky Mountain Association of Geologists, Denver Colorado, pages 111-128.

Blakey, R., 2007, Paleogeography and tectonic evolution of late Paleozoic sedimentary basins, southwestern North America, < http://jan.ucc.nau.edu/~rcb7/>, accessed March 25, 2008.

Borchert, H., 1969, Principles of oceanic salt deposition and metamorphism, Geological Society of America Bulletin, vol. 80, no. 5, May, pages 821-864.

Borchert, H., and R. O. Muir, 1964, Salt deposits: the origin, metamorphism and deformation of evaporites, D. Van Nostrand Company, LTD., London, 333 pages.

Bouma, A. H., 2000, Fine-grained, mud-rich turbidite systems: model and comparison with coarse-grained, sand-rich systems, *in* A. H. Bouma and C. G. Stone, eds., Fine-grained turbidite systems, American Association of Petroleum Geologists Memoir 72, Society of Sedimentary Geology Special Publication, no. 68, pages 9-20.

Bradish and Clair, 1956, Geological report, Paradox Basin and related areas: Part 1, Subsurface geology of the Paradox Basin, prepared for Vega Corporation, Denver, Colorado, 38 pages.

Braitsch, O., 1971, Salt deposits; their origin and composition, Springer-Verlag, New York, 297 pages.

Brambach, R. K., C. R. Scotese, and A. M. Zeigler, 1980, Before Pangea: the geographies of the Paleozoic World, American Scientist, vol. 68, no. 1, January-February, pages 26-38.

Brown, H. H., 1960, Pennsylvanian of the Paradox Basin salt structure area, *in* Geology of the Paradox Basin fold and fault belt, Four Corners Geological Society – Guidebook, Third Field Conference, page 79.

Cater, F. W., 1970, Geology of the Salt Anticline region in southwestern Colorado, Geological Survey Professional Paper 637, United States Atomic Energy Comission, Washington, 80 pages.

Cater, F. W., and D. P. Elston, 1963, Structural development of salt anticlines of Colorado and Utah, American Association of Petroleum Geologists, Memoir 2, Backbone of the Americas, pages 152-159.

Condon, S. M., 1995, Geology of pre-Pennsylvanian rocks in the Paradox Basin

and adjacent areas, southeastern Utah and southwestern Colorado, United States Geological Survey Bulletin 2000-G, 53 pages.

Condon, S. M., 1997, Geology of the Pennsylvanian and Permian Cutler Group and Permian Kaibab Limestone in the Paradox Basin, southeastern Utah and southwestern Colorado, United States Geological Survey Bulletin 2000-P, 46 pages.

Currie, B. S., 1998, Upper Jurassic-Lower Cretaceous Morrison and Cedar Mountain formations, NE Utah-NW Colorado: relationships between nonmarine deposition and early cordilleran foreland-basin development, Journal of Sedimentary Research, vol. 68, no. 4, July, pages 632-652.

Delta Petroleum, 2008, Delta Petroleum Corporation, < http://www.deltapetro.com/rockymountainregion.html>, accessed February 10, 2008.

Denver Earth Resources Library, 2007, 730 17th St # B1, Denver, CO 80202, (303) 825-5614.

Dickinson, W. R., G. S. Soreghan, and K. A. Giles, 1994, Glacio-eustatic origin of Permo-Carboniferous stratigraphic cycles: evidence from the southern cordilleran foreland region, Tectonic and Eustatic Controls on Sedimentary Cycles, SEPM Concepts and Paleontology #4, pages 25-34.

Doelling, H. H., 1983, Observations on Paradox Basin salt anticlines, *in* W. R. Averett, ed., Northern Paradox Basin Uncompahgre Uplift, Grand Junction Geological Society Field Trip, pages 81-90.

Doelling, H. H., 1988, Geology of Salt Valley Anticline and Arches National Park, Grand County, Utah, *in* H. H. Doelling, C. G. Oviatt, and P. W. Huntoon, Salt deformation in the Paradox region, Utah Geological and Mineral Survey Bulletin 122, 58 pages.

Doelling, H. H., 2001, Geologic map of the Moab and eastern part of the San Rafael Desert 30’ X 60’ quadrangles, Grand and Emery counties, Utah, and Mesa county Colorado, Utah Geological Survey Map 180, scale 1:100,000.

Donovan, R. N., W. Beachamp, T. Ferraro, C. Lajek, D. McConnell, M. Munsil, D. Ragland, B. Sweet, and D. Taylor, 1985, Subsidence rates in Oklahoma during the Paleozoic, Oklahoma City Geological Society, The Shale Shaker Digest XI, vol. XXXIII-XXXV (1982-1985), pages 14-16.

Draut, A. E., 2005, The geology of central and southeastern Utah: itinerary for a one-day field trip, Geological Society of America, Penrose Conference Field Trip Guide – Lessons in tectonics, climate, and eustasy from the stratigraphic record in arc collision zones, Price, Utah, 10-14 October, 20 pages.

Dutton, S. P., and C. W. Kreitler, 1980, Caprock formation and diagenesis, Gyp Hill Salt Dome, south Texas, Gulf Coast Association of Geological Societies Transactions, vol. 30, pages 333-339.

Dutton, S. P., C. W. Kreitler, and B. R. Bracken, 1982, Formation and diagenesis of salt-dome cap rock, Texas Gulf Coast, *in* C. R. Handford, R. G. Loucks, and G. R. Davies, eds., Depositional and diagenetic spectra of evaporites – a core workshop, Society for Sedimentary

Geology core workshop no. 3, Calgary, Canada, June 26-27, pages 100-129.

Elston, D. P., and E. M. Shoemaker, 1960, Late Paleozoic and Early Mesozoic structural history of the Uncompahgre Front, *in* Geology of the Paradox Fold and Fault Belt, Four Corners Geological Society – Guidebook, Third Field Conference, pages 47-55.

Elston, D. P., E. M. Shoemaker, and E. R. Landis, 1962, Uncompahgre Front and salt anticline region of Paradox Basin, Colorado and Utah, American Association of Petroleum Geologists Bulletin, vol. 46, no. 10, October, pages 1857-1878.

Epis, R. C., G. R. Scott, R. B. Taylor, and C. E. Chapin, 1980, Summary of Cenozoic geomorphic, volcanic and tectonic features of central Colorado and adjoining areas, *in* H. C. Kent, and K. W. Porter, eds., Colorado Geology, Rocky Mountain Association of Geologists, Denver Colorado, pages 135-156.

Fetzner, R. W., 1960, Pennsylvanian paleotectonics of Colorado Plateau, American Association of Petroleum Geologists Bulletin, vol. 44, no. 8, August, pages 1371-1413.

Fischer, A. G., 1984, The two Phanerozoic supercycles, *in* W. A. Berggren and J. A. Van Couvering, eds., Princeton University Press, Princeton, New Jersey, pages 129-150.

Frahme, C. W., and E. B. Vaughn, 1983, Paleozoic geology and seismic stratigraphy of the northern Uncompahgre Front, Grand County, Utah, *in* J. D. Lowell, and R. Gries, Rocky Mountain foreland basins and uplifts, Rocky Mountain Association of Geologists, pages 201-211.

Friedman, G. M., 1982, Evaporites as source rock for petroleum, *in* C. R. Handford, R. G. Loucks, and G. R. Davies, eds., Depositional and diagenetic spectra of evaporites – a core workshop, SEPM Core Workshop No. 3, Calgary, Canada, June 26-27, pages 385-395.

Golden State Resources, 2002, Golden State Resources Limited, < http://www.goldenstate.com.au>, accessed April 16, 2008.

Goldsmith, L. H., 1969, Concentration of potash salts in saline basins, American Association of Petroleum Geologists Bulletin, vol. 53, no. 4, April, pages 790-797.

Goggle Earth, 2007, Google Earth, *in* <http:// earth.google.com/>.

Gradstein, F. M., J. G. Ogg, A. G. Smith, F. P. Agterberg, W. Bleeker, R. A. Cooper, V. Davydov, P. Gibbard, L. A. Hinnov, M. R. House, L. Lourens, H. P. Luterbacher, J. McArthur, M. J. Melchin, L. J. Robb, J. Shergold, M. Villeneuve, B. R. Wardlaw, J. Ali, H. Brinkhuis, F. J. Hilgen, J. Hooker, R. J. Howarth, A. H. Knoll, J. Laskar, S. Monechi, K. A. Plumb, J. Powell, I. Raffi, U. Röhl, P. Sadler, A. Sanfilippo, B. Schmitz, N. J. Shackleton, G. A. Shields, H. Strauss, J. Van Dam, T. van Kolfschoten, J. Veizer, and D. Wilson, 2004, A Geologic Time Scale 2004, Cambridge University Press, Cambridge, United Kingdom, 589 pages.

Gustafson, V. O., 1981, Petroleum geology of the Devonian and Mississippian rocks of the Four Corners region, *in* D. L. Wiegand, ed., Geology of the Paradox Basin, Rocky Mountain Association of Geologists, 1981 Field Conference, pages 101-109.

Hallam, A., 1992, Phanerozioc sea-level changes, Columbia University Press, New York, 266 pages.

Harms, J. C., and C. R. Williamson, 1988, Deep-water density current deposits of Delaware Mountain Group (Permian), Delaware Basin, Texas and New Mexico, American Association of Petroleum Geologists Bulletin, vol. 72, no. 3, March, pages 299-317.

Harrison, T. S., 1927, Colorado-Utah salt domes, American Association of Petroleum Geologists Bulletin, vol. 11, no. 2, February, pages 111-133.

Heckel, P. H., 1986, Sea-level curve for Pennsylvanian eustatic marine transgressive-regressive depositional cycles along mid-continent outcrop belt, North America, Geology, vol. 15, April, pages 330-334.

Herman, G., and C. A. Barkell, 1957, Pennsylvanian stratigraphy and productive zones, Paradox salt basin, American Association of Petroleum Geologists, vol. 41, no. 5, May, pages 861-881.

Hite, R. J., 1960, Stratigraphy of the saline facies of the Paradox Member of the Hermosa Formation of southeastern Utah and southwestern Colorado, *in* Geology of the Paradox Basin fold and fault belt, Four Corners Geological Society – Guidebook, Third Field Conference, pages 86-89.

---1968, Salt deposits of the Paradox Basin, southeast Utah and southwest Colorado, *in* R. B. Mattox, ed., Saline deposits: A symposium based on papers from the international conference on saline deposits, Houston, Texas, 1962, Geological Society of America Special Papers 88, pages 319-330.

Hite, R. J., 1983, Preliminary mineralogical and geochemical data from the Department of Energy Gibson Dome corehole no. 1, San Juan County, Utah, U.S. Geological Survey Open-File Report 83-780, 57 pages.

Hite, R. J., 1985, The sulfate problem in marine evaporites, *in* B. C. Schreiber and H. L. Harner, eds., Sixth International Symposium On Salt, vol. 1, pages 217-230.

Hite, R. J., and D. H. Buckner, 1981, Stratigraphic correlations, facies concepts, and cyclicity in the Paradox Basin, *in* D. L. Wiegand, ed., Geology of the Paradox Basin, Rocky Mountain Association of Geologists, 1981 Field Conference, pages 147-159.

Hite, R. J., D. E. Anders, and T. G. Ging, 1984, Organic-rich source rocks of Pennsylvanian age in the Paradox Basin of Utah and Colorado, *in* J. Woodward, F. F. Meissner, and J. L. Clayton, eds., Hydrocarbon source rocks of the greater Rocky Mountain region, Rocky Mountain Association of Geologists, pages 255-274.

Houck, K. J., 1997, Effects of sedimentation, tectonics, and glacio-eustasy on depositional sequences, Pennsylvanian Minturn Formation, north-central Colorado, American Association of Petroleum Geologists Bulletin, vol. 81, no. 9, September, pages 1510-1533.

House, M. R., 1995, Orbital forcing timescales: an introduction, *in* M. R. House and A. S. Gale, eds., Orbital forcing timescales and cyclostratigraphy, Geological Society Special Publication No. 85, pages 1-18.

Intrepid Mining, 2006, Intrepid Potash,

Intrepid Mining, LLC, < http://www.intrepidpotash.com/index.html>, accessed on March 11, 2008.

Jenyon, M. K., 1986, Salt tectonics, Elsevier Applied Science Publishers, London and New York, 191 pages.

Joesting, H. R., J. E. Case, and D. Plouff, 1966, Regional geophysical investigations of the Moab-Needles area, Utah, Geological Survey Professional Paper 516-C, 21 pages.

Jones, R. W., 1958, Origin of salt anticlines of Paradox Basin, American Association of Petroleum Geologists Bulletin, vol. 43, no. 8, August, pages 1869-1895.

Kamola, D. L., and M. A. Chan, 1988, Coastal dune facies, Permian Cutler Formation (White Rim Sandstone), Capital Reef National Park area, southern Utah, Sedimentary Geology, vol. 56, Elsevier Science Publishers B. V., Amsterdam, Netherlands, pages 341-356.

Kelley, V. C., 1955, Regional tectonics of the Colorado Plateau and relationship to the origin and distribution of uranium, University of New Mexico Press, Albuquerque, 120 pages.

Kelley, V. C., 1958, Tectonics of the region of the Paradox Basin, *in* A. F. Sanborn, ed., Guidebook to the geology of the Paradox Basin, Intermountain Association of Petroleum Geologists, Ninth Annual Field Conference, pages 31-38.

Kirkland, D. W., and R. Evans, 1981, Source-rock potential of evaporitic environment, American Association of Petroleum Geologists Bulletin, vol. 65, no. 2, pages 181-190.

Klein, C., 2002, Mineral science, John Wiley and Sons, Inc., New York, 641 pages.

Klingspor, A. M., 1966, Cyclic deposits of potash in Saskatchewan, Canadian Petroleum Geology Bulletin, vol. 14, no. 2, June, pages 193-207.

Kluth, C. F., 1986, Plate tectonics of the Ancestral Rocky Mountains, *in* J. A. Peterson, ed., Paleotectonics & sedimentation in the Rocky Mountain region, United States, American Association of Petroleum Geologists, Memoir 41, Tulsa Oklahoma, pages 353-369.

---2008, A new look at the Ancestral Rocky Mountains, Rocky Mountain Association of Geologists Friday Luncheon Lecture Series, April 18th, 2008.

Kluth, C. F., and H. R. DuChene, 2006, The geometry and tectonics of the Uncompahgre mountain front, western Colorado, abstract, Geological Society of America abstract with programs, vol. 38, no. 6, page 29.

---2007, The tectonic development of the Uncompahgre Uplift and the Paradox Basin, Utah and Colorado, Geological Society of America Annual Meeting Denver, October 28-31, Poster.

Kosanke, R. M., 1995, Palynology of part of the Paradox and Honaker Trail formations, Paradox Basin, Utah, United States Geological Survey Bulletin 2000-L, 9 pages.

Kupfer, D. H., 1989, Gypsum dehydration, agent of salt diapirism, Gulf Coast Association of Geological Societies Transactions, vol. 39, Pages 171-181.

Lockridge, J. P., 1958, Alkali Gulch gas field, La Plata County, Colorado, *in* A. F. Sanborn, ed., Guidebook to the geology of the Paradox Basin, Intermountain Association of Petroleum Geologists, Ninth Annual Field Conference, pages 245-246.

Loope, D. B., and G. B. Kuntz, 1987, Evidence of evaporate growth within marine limestones of the upper member of the Hermosa Formation (Pennsylvanian), Cataract Canyon, southeastern Utah, *in* J. A. Campbell, ed., Geology of Cataract Canyon, Four Corners Geological Society Guidebook, Tenth Field Conference, pages 75-79.

Magaritz, M., 1987, A new explanation for the cyclic deposition in marine evaporite basins: meteoric water input, Chemical Geology, vol. 62, pages 239-250.

Malin, W. J., 1958, A preliminary informal system of nomenclature for a part of the Pennsylvanian of the Paradox Basin, *in* A. F. Sanborn, ed., Guidebook to the geology of the Paradox Basin, Intermountain Association of Petroleum Geologists, Ninth Annual Field Conference, pages 135-137.

Martin, G. W., 1981, Patterson Field, *in* D. L. Wiegand, ed., Geology of the Paradox Basin, Rocky Mountain Association of Geologists, 1981 Field Conference, pages 61-69.

Maughan, E. K., and W. J. Perry Jr., 1986, Lineaments and their tectonic implications in the Rocky Mountains and adjacent plains region, *in* J. A. Peterson, ed., Paleotectonics & sedimentation in the Rocky Mountain region, United States, American Association of Petroleum Geologists, Memoir 41, Tulsa Oklahoma, pages 41-53.

Merrill, W. M., and R. M. Winar, 1958, Molas and associated formations in San Juan Basin-Needle Mountains area, southwestern Colorado, American Association of Petroleum Geologists Bulletin, vol. 42, no. 9, September, pages 2107-2132.

Molenaar, C. M., 1981, Mesozoic stratigraphy of the Paradox Basin – an overview, *in* D. L. Wiegand, ed., Geology of the Paradox Basin, Rocky Mountain Association of Geologists, 1981 Field Conference, pages 119-127.

Moore, R. C., 1936, Stratigraphic classification of the Pennsylvanian rocks of Kansas, State Geological Survey of Kansas Bulletin 22, 256 pages.

Nadon, G. C., and R. R. Kelly, 2004, The constraints of glacial eustatic and low accommodation on sequence-stratigraphic interpretations of Pennsylvanian strata, Conemaugh Group, Appalachian Basin, U.S.A., *in* J. C. Pashin, and R. A. Gastaldo, eds., Sequence stratigraphy, paloeclimate, and tectonics of coal-bearing strata, American Association of Petroleum Geologists Studies in Geology 51, pages 29-44.

National Park Service, 2007, Arches National Park, <http://www.nps.gov/arch/>, accessed March 9, 2008.

Neff, A. W., 1960, Comparisons between the salt anticlines of south Persia and those of the Paradox Basin, *in* Geology of the Paradox Basin fold and fault belt, Four Corners Geological Society – Guidebook, Third Field Conference, pages 56-64.

Nesse, W. D., 2000, Introduction to mineralogy, Oxford University Press, Inc., New York, 442 pages.

Nuccio, V. F., and S. M. Condon, 1996, Burial and thermal history of the Paradox Basin, Utah and Colorado, and petroleum potential of the Middle Pennsylvanian Paradox Formation, United States Geological Survey Bulletin 2000-O, 47 pages.

Okszewski, T. D., and M. E. Patzkowsky, 2003, From cyclothems to sequences: the record of eustasy and climate on an icehouse epeiric platform (Pennsylvanian-Permain, North America Midcontinent), Journal of Sedimentary Research, vol. 73, no. 1, January, pages 15-30.

Paz Cuellar, M. G., 2006, Restoration of mountain front and salt structures in the northern Paradox Basin, Colorado School of Mines masters thesis, 142 pages.

Pekarek, A. H., 2001, Solar forcing of earth's climate, *in* L. C. Gerhard, W. E. Harrison and B. M. Hanson, eds., Geological perspectives of global climate change, pages 19-34.

Peterson, J. A., 1966, Genesis and diagenesis of Paradox Basin carbonate mound reservoirs, *in* Symposium on Recently Developed Geologic Principles and Sedimentation of the Permo-Pennsylvanian of the Rocky Mountains, Wyoming Geological Association, Twentieth Annual Conference, Casper College, Casper, Wyoming, August to September, pages 67-86.

Prommel, H. W. C., and H. E. Crum, 1927, Salt domes of Permian and Pennsylvanian age in southeastern Utah and their Influence on oil accumulation, American Association of Petroleum Geologists Bulletin, vol. 11, no. 4, April, pages 373-393.

Raup, O. B., and R. J. Hite, 1992, Lithology of evaporite cycles and cycle boundaries in the upper part of the Paradox Formation of the Hermosa Group of Pennsylvanian age in the Paradox Basin, Utah and Colorado, United States Geological Survey Bulletin 2000-B, 37 pages.

Rasmussen, D. L., 2006, Escalation of Pennsylvanian-Permian Uncompahgre Uplift revealed by progression of siliciclastic wedges in the Paradox Basin, Colorado and Utah, abstract, Geological Society of America abstract with programs, vol. 38, no. 6, page 29.

Reid F. S., and C. E. Berghorn, 1981, Facies recognition and hydrocarbon potential of the Pennsylvanian Paradox Formation, *in* D. L. Wiegand, ed., Geology of the Paradox Basin, Rocky Mountain Association of Geologists, 1981 Field Conference, pages 111-117.

Reuger, B. F., 1996, Palynology and its relationship to climatically induced depositional cycles in the Middle Pennsylvanian (Desmoinesian) Paradox Formation of southeastern Utah, United States Geological Survey Bulletin 2000-K, 30 pages.

Schwarzacher, W., 1993, Cyclostratigraphy and the Milankovitch theory, Developments in Sedimentology 52, Elesevier Science Publishers B. V., Amsterdam, Netherlands, 225 pages.

Shoemaker, E. M., J. E. Case, and D. P. Elston, 1958, Salt anticlines of the Paradox Basin, *in* A. F. Sanborn, ed., Guidebook to the geology of the Paradox Basin, Intermountain Association of Petroleum Geologists, Ninth Annual Field Conference, pages 39-59.

Sonnenfeld, P., 1984, Brines and evaporites, Academic Press Inc., Orlando, 613 pages.

Sonnenfeld, P., and P. P. Hudec, 1985, Clay laminations: their cause and effect, *in* B. C. Schreiber and H. L. Harner, eds., Sixth International Symposium On Salt, vol. 1, pages 51-56.

Soreghan, M.J., and G.S. Soreghan, 2003, Ice at the equator: a Paleozoic Yosemite lurking in western Colorado?, Earth Scientist Magazine, University of Oklahoma, pages 28-31.

Soreghan, G. S., D. E. Sweet, K. R. Marra, C. F. Eble, M. J. Soreghan, R. D. Elmore, S. A. Kaplan, and M. D. Blum, 2007, An exhumed Late Paleozoic canyon in the Rocky Mountains, The Journal of Geology, vol. 115, pages 473-481.

Stevenson, G. M., and D. L. Baars, 1986, The Paradox: A pull-apart basin of Pennsylvanian age *in* J. A. Peterson, ed., Paleotectonics & sedimentation in the Rocky Mountain region, United States, American Association of Petroleum Geologists, Memoir 41, Tulsa Oklahoma, pages 513-539.

Stewart, F. H., 1963, Chapter Y: marine evaporites, *in* M. Fleischer, ed., Data of geochemistry-sixth edition, United States Geological Survey Professional Paper 440-Y, Y52 pages.

Stokes, W. L., 1948, Geology of the Utah-Colorado salt dome region with emphasis on Gypsum Valley, Colorado, Guidebook to the Geology of Utah, no. 3, Utah Geological Survey, 50 pages.

Tillman, R. W., 1971, Petrology and paleoenvironments, Robinson Member, Minturn Formation (Desmoinesian), Eagle Basin, Colorado, American Association of Petroleum Geologists Bulletin, vol. 55, no. 4, April, pages 593-620.

Tissot, B. P., and D. H. Welte, 1984, Petroleum formation and occurrence, second revised and enlarged edition, Springer-Verlag, Berlin, Heidelberg, New York, Tokyo, 699 pages.

Trudgill, B., N. Banbury, and J. Underhill, 2004, Salt evolution as a control on structural and stratigraphic systems: Northern Paradox foreland basin, SE Utah, USA, in GCSSEPM 24th Annual Research Conference.

Tucker, M. E., and V. P. Wright, 1990, Carbonate sedimentology, Blackwell Science Ltd., London, 482 pages.

Tweto, O., 1980a, Precambrian geology of Colorado, *in* H. C. Kent, and K. W. Porter, eds., Colorado Geology, Rocky Mountain Association of Geologists, Denver Colorado, pages 37-46.

Tweto, O., 1980b, Tectonic history of Colorado, *in* H. C. Kent, and K. W. Porter, eds., Colorado Geology, Rocky Mountain Association of Geologists, Denver Colorado, pages 5-9.

Tweto, O., 1980c, Summary of the Laramide Orogeny in Colorado, *in* H. C. Kent, and K. W. Porter, eds., Colorado Geology, Rocky Mountain Association of Geologists, Denver Colorado, pages 129-134.

Tweto, O., 1987, Rock units of the Precambrian basement in Colorado, United States Geological Survey Professional Paper 1321-A, 54 pages.

Utah Division of Oil, Gas and Mining, 2007, Utah Department of Natural Resources Division of Oil, Gas and Mining, <http://oilgas.ogm.utah.gov/index.htm>, last accessed April 23, 2008.

Vail, P. R., R. M. Mitchum Jr., and S. Thompson III, 1977, Seismic stratigraphy and global changes of sea level, Part 4: Global cycles of relative changes of sea level, American Association of Petroleum Geologists Memoir 26: Seismic stratigraphy – applications to hydrocarbon exploration, pages 83-97.

Veevers, J. J., and C. McA. Powell, 1987, Late Paleozoic glacial episodes in Gondwanaland reflected in transgressive-regressive depositional sequences in Euramerica, Geological Society of America Bulletin, vol. 98, April, pages 475-487.

Ver Planck, W. E., 1958, Salt in California, California Division of Mines Bulletin, vol. 175, 168 pages.

Wanless, H. R., and F. P. Shepard, 1936, Sea level and climatic changes related to late Paleozoic cycles, Geological Society of America Bulletin, vol. 47, no. 8, pages 1177-1206.

Wardlaw, N. C., and W. M. Schwerdtner, 1966, Halite-anhydrite seasonal layers in the Middle Devonian Prairie Evaporite Formation, Saskatchewan, Canada, Geological Society of America Bulletin, vol. 77, April, pages 331-342.

Warner, L. A., 1978, The Colorado Lineament: a middle Precambrian wrench fault system, Geological Society of America Bulletin, vol. 89, pages 161-171.

---1980, The Colorado Lineament, *in* H. C. Kent, and K. W. Porter, eds., Colorado Geology, Rocky Mountain Association of Geologists, Denver Colorado, pages 11-21.

Warren, J. K., 1985, On the significance of evaporite laminations, *in* B. C. Schreiber and H. L. Harner, eds., Sixth International Symposium On Salt, vol. 1, pages 161-170.

---1989, Evaporite sedimentology, Prentice Hall, New Jersey, 285 pages.

---1999, Evaporites: Their evolution and economics, Blackwell Science Ltd., Oxford, 438 pages.

Weber, L. J., J. F. (Rick) Sarg, and F. M. Wright, 1995, Sequence stratigraphy and reservoir delineation of the Middle Pennsylvanian (Desmoinesian), Paradox Basin and Aneth Field, southwestern USA, *in* Milankovitch sea level changes, cycles and reservoirs on carbonate platforms in greenhouse and ice-house worlds, SEPM short course notes, no. 35, pages 1-81.

Weir, G. W., and W. P. Puffett, 1981, Incomplete manuscript on stratigraphy and structural geology and uranium-vanadium and copper deposits of Lisbon Valley area, Utah-Colorado, United States Geological Survey, open-file report 81-39, 292 pages.

Wengerd, S. A., 1958, Pennsylvanian stratigraphy, southwest shelf, Paradox Basin, *in* A. F. Sanborn, ed., Guidebook to the geology of the Paradox Basin, Intermountain Association of Petroleum Geologists, Ninth Annual Field Conference, pages 109-134.

---1962, Pennsylvanian sedimentation in

Paradox Basin, Four Corners Region, *in* Pennsylvanian systems in the United States, American Association of Petroleum Geologists, Special Volumes 23, pages 264-330.

Wengerd, S. A., and J. W. Strickland, 1954, Pennsylvanian stratigraphy of Paradox salt basin, Four Corners region, Colorado and Utah, American Association of Petroleum Geologists Bulletin, vol. 38, no. 10, October, pages 2157-2199.

White, M. A., and M. I. Jacobson, 1983, Structures associated with the southwest margin of the Ancestral Uncompahgre Uplift, *in* W. R. Averett, ed., Northern Paradox Basin-Uncompahgre Uplift, Grand Junction Geological Society Field Trip, October 1-2, pages 33-39.

Wright, J. C., D. R. Shawe, and S. W. Lohman, 1962, Definition of members of Jurassic Entrada Sandstone in east-central Utah and west-central Colorado, American Association of Petroleum Geologists Bulletin, vol. 46, no. 11, November, pages 2057-2070.

Yang, W., 2000, Carbonate sedimentation rates in mixed siliciclastic and carbonate cycles, Cisco Group (Virgillian and Wolfcampian), eastern shelf, Texas, American Association of Petroleum Geologists Annual Meeting Abstract, New Orleans, Louisiana, April 16-19.

Young, R. G., 1983, Petroleum in northeastern Grand County, Utah, *in* W. R. Averett, ed., Northern Paradox Basin-Uncompahgre Uplift, Grand Junction Geological Society Field Trip, October 1-2, pages 1-7.

Zharkov, M. A., 1981, History of Paleozoic salt accumulation, Springer-Verlag, Berlin, 309 pages.

APPENDIX A

Table A-1: Wells with available well log information used for maps, cross sections and correlations. Well logs were obtained through the Utah Division of Oil, Gas and Mining (2007) Website.

No.	API #	Operator	Well Name	Township	Range	Section
1	4301510928	PLACID OIL COMPANY	MARSH FLAT UNIT 1	17S	14E	29
2	4301520053	DIAMOND SHAMROCK EXP	WITTER FED 1	18S	15E	19
3	4301530014	CHEVRON USA INC	NORRIS FED 1	18S	16E	8
4	4301530001	CALIFORNIA-TIME PET	BARRIER BANK 1	19S	14E	11
5	4301510504	HUMBLE OIL & REFININ	SPHINX UNIT 1A	19S	14E	35
6	4301530003	TOLEDO MINING CO	TOLEDO FEDERAL 1	20S	14E	33
7	4301530018	DENISON MINES LTD	DENISON MINES-SKYLIN	21S	14E	5
8	4301530089	MEGADON ENTERPRISES	SALERATUS FED ST 2-3	21S	14E	36
9	4301511182	SUPERIOR OIL COMPANY	GRAND FAULT UNIT 14	21S	15E	24
10	4301511138	TEXAS EASTERN SKYLIN	GREEN RIVER UNIT 1	21S	16E	33
11	4301930029	SHELL OIL COMPANY	FEDERAL 1-26	21S	17E	26
12	4301931357	GCRL ENERGY LTD	GCRL SEISMOSAUR FED	21S	20E	20
13	4301911485	PACIFIC WESTERN OIL	THOMPSON 1	21S	21E	33
14	4301930328	TXO PRODUCTION CORP	KLOTZ FEDERAL 1	21S	22E	11
15	4301930918	MOBIL OIL CORPORATION	AMERICAN PETROFINA 1	21S	22E	30
16	4301510021	AMAX PETROLEUM CORP	GREEN RIVER DESERT U	22S	15E	9
17	4301530079	MEGADON ENTERPRISES	GEYSER DOME 1-14	22S	15E	14
18	4301511274	TEXAS EASTERN TRANS	FEDERAL 1	22S	15E	26
19	4301520342	EQUITY OIL COMPANY	FEDERAL 1	22S	15E	28
20	4301910030	KERN COUNTY LAND CO	AMERADA GREEN RIVER	22S	16E	2
21	4301930074	FERGUSON OIL CO	U-TEX ET AL 1-14	22S	16E	14
22	4301930124	MOUNTAIN FUEL SUPPLY	MT FUEL-SKYLINE GEYS	22S	16E	25
23	4301911188	SUPERIOR OIL COMPANY	SALT WASH UNIT 22-34	22S	17E	34
24	4301930110	CONOCO INC	CRESCENT UNIT 1	22S	20E	17
25	4301510373	FOREST OIL CORP	FOREST GOVT 1	23S	14E	11
26	4301511030	SHELL OIL COMPANY	CHAFFIN UNIT 1	23S	15E	21
27	4301510736	MOBIL OIL CORPORATION	JAKEY'S RIDGE 12-3	23S	16E	3
28	4301510737	MOBIL OIL CORPORATION	JAKEY'S RIDGE 34-15	23S	16E	15
29	4301930282	RESERVE OIL & GAS	SALT WASH NORTH 1	23S	17E	9
30	4301910086	BELCO DEVELOPMENT CO	FLOY UNIT 1	23S	17E	11
31	4301910831	PAN AMERICAN PETROLE	SALT WASH UNIT 1	23S	17E	15
32	4301930752	MEGADON ENTERPRISES	FEDERAL 1-15	23S	17E	15
33	4301910832	PAN AMERICAN PETROLE	SUNILAND STATE A 1	23S	17E	16
34	4301910833	S W ENERGY CORP	SUNILAND STATE A-2	23S	17E	16
35	4301915819	SMOOT, RICHARD P	CF&I 22-16	23S	17E	16
36	4301915820	SMOOT, RICHARD P	CF&I 42-16	23S	17E	16
37	4301930783	S W ENERGY CORP	STATE 1-16A	23S	17E	16
38	4301916047	S W ENERGY CORP	GOVT SMOOT 1	23S	17E	17
39	4301930044	S W ENERGY CORP	GOVT SMOOT 3	23S	17E	17
40	4301930679	S W ENERGY CORP	GOVT 18-2	23S	17E	18
41	4301930327	PEASE OIL & GAS COMP	FEDERAL SKYLINE 1A S	23S	17E	21
42	4301930647	CITIES SERV OIL & GA	FEDERAL DE-1	23S	18E	20
43	4301930038	SHELL OIL COMPANY	MT FUEL FEDERAL 1-21	23S	18E	21
44	4301930251	HILLIARD OIL & GAS	KLONDIKE U 1	23S	18E	24
45	4301920146	UNION OIL CO OF CALI	DEVILS GARDEN USA 1	23S	21E	5

Table A-1: continued.

No.	API #	Operator	Well Name	Township	Range	Section
46	4301930055	QUINTANA PETROLEUM	YELLOW CAT USA 1-9	23S	22E	9
47	4301910980	ARCO OIL & GAS COMPA	ONION CREEK U 1	23S	24E	31
48	4301510116	GENERAL PETROLEUM CO	45-56	24S	15E	5
49	4301530235	COORS ENERGY	FEDERAL 1-29MW	24S	15E	29
50	4301511031	SHELL OIL COMPANY	GRUVERS MESA 1	24S	16E	19
51	4301930042	SHELL OIL COMPANY	SHELL QUINTANA FED 1	24S	17E	1
52	4301930688	MEGADON ENTERPRISES	FEDERAL 1-26	24S	17E	26
53	4301930276	LADD PETROLEUM CORPO	FEDERAL 1-27U	24S	18E	27
54	4301930272	MOUNTAIN FUEL SUPPLY	KLONDIKE UNIT 2	24S	19E	22
55	4301930455	TIGER OIL CO	STATE 12-11	24S	20E	11
56	4301931112	LADD PETROLEUM CORP	SALT VALLEY 1	24S	20E	16
57	4301910905	PHILLIPS PETROLEUM	ONION CREEK UNIT 2	24S	23E	13
58	4301931180	CONOCO INC	CONOCO FED 31 1	24S	23E	31
59	4301930206	MOBIL OIL CORPORATION	FEDERAL SECTION 7-1	24S	25E	7
60	4301930937	EXXON CORPORATION	ONION CREEK FED 1	24S	25E	18
61	4301511184	SUPERIOR OIL COMPANY	N SPRING WASH 31-15	25S	15E	15
62	4301510229	CONTINENTAL OIL CO	MOONSHINE WASH U 2	25S	15E	22
63	4301510183	STANDARD OIL CO	MOONSHINE WASH U 1	25S	15E	32
64	4301511033	SHELL OIL COMPANY	GRUVERS MESA 2	25S	16E	10
65	4301510182	STANDARD OIL CO	LOOKOUT POINT UNIT 1	25S	16E	29
66	4301911187	SUPERIOR OIL COMPANY	BOWKNOT UNIT 43-20	25S	17E	20
67	4301910715	MCRAE OIL & GAS CORP.	MCRAE-FEDERAL 1	25S	18E	10
68	4301931331	INTREPID OIL & GAS	KANE SPRINGS FED 10	25S	18E	10
69	4301931341	INTREPID OIL & GAS	KANE SPRINGS 16-1	25S	18E	16
70	4301930043	SHELL OIL COMPANY	FEDERAL 1-20	25S	18E	20
71	4301930033	SHELL OIL COMPANY	FEDERAL 1-21	25S	18E	21
72	4301930170	READ & STEVENS INC	SH. BOWKNOT 1	25S	18E	21
73	4301910368	FEDERAL OIL CO	FED BOWKNOT 1	25S	18E	30
74	4301930045	SHELL OIL COMPANY	SHELL-QUINTANA FED 1	25S	18E	35
75	4301931363	HUNT PETROLEUM AEC	CANE CREEK FED 7-1	25S	19E	7
76	4301930050	GENERAL CRUDE OIL CO	BIG ROCK FED 1	25S	19E	26
77	4301910154	CALVERT EXPLORATION	BIG FLAT UNIT 6	25S	19E	27
78	4301911333	UNION OIL CO OF CALI	BIG FLAT UNIT 5	25S	19E	27
79	4301930379	HUSKY OIL COMPANY	FED BARTLETT FLAT 10	25S	19E	27
80	4301931310	INTREPID OIL & GAS	KANE SPRINGS FED 27	25S	19E	27
81	4301931325	INTREPID OIL & GAS	KANE SPRINGS FED 28	25S	19E	28
82	4301931334	INTREPID OIL & GAS	KANE SPRINGS FED 25	25S	19E	34
83	4301930910	CHANDLER & ASSOCIATE	MOAB FED 16-9	25S	20E	9
84	4301930810	DAVIS OIL COMPANY	GOLD BAR UNIT 2	25S	20E	23
85	4301930795	DAVIS OIL COMPANY	GOLD BAR UNIT 1	25S	20E	29
86	4301931018	SAMSON RESOURCES CO	ARCHES FEDERAL 1	25S	21E	18
87	4301910397	GOLD BAR RESOURCES	CASTLE VALLEY U 1	25S	23E	16
88	4301530205	BOSWELL ENERGY CORP	N SPRING CREEK FED 1	26S	15E	21
89	4301530010	HUNT PETROLEUM CORP	USA FED 1	26S	16E	31
90	4301511181	SUPERIOR OIL COMPANY	BOW KNOT UNIT 14-5	26S	17E	5

Table A-1: continued.

No.	API #	Operator	Well Name	Township	Range	Section
91	4301530145	DAVIS OIL COMPANY	POOL UNIT 1	26S	17E	17
92	4301530078	MEGADON ENTERPRISES	FEDERAL 2-20	26S	17E	20
93	4301930182	GRYNBERG, JACK J	MINERAL POINT FED 1	26S	18E	4
94	4301911335	PURE OIL CO	MINERAL POINT USA 1	26S	18E	7
95	4301931119	EP OPERATING COMPANY	MINERAL CANYON FED 1	26S	19E	3
96	4301911565	RUBY, GLEN ET AL	GLEN M RUBY 1-A	26S	19E	11
97	4301911578	TIDEWATER OIL CO	TIDEWATER OIL CO 74	26S	19E	11
98	4301920409	KING OIL CO	KING OIL COMPANY 1 R	26S	19E	11
99	4301931364	INTREPID OIL & GAS	CANE CREEK FED 11-1	26S	19E	11
100	4301911002	RUBY, GLEN ET AL	BIG FLAT UNIT 2	26S	19E	14
101	4301915777	RUBY, GLEN ET AL	BIG FLAT UNIT 1	26S	19E	14
102	4301930357	ENERGY RESERVES GR	SUNBURST 1	26S	19E	14
103	4301931156	EP OPERATING COMPANY	MINERAL CANYON U 1-1	26S	19E	14
104	4301931332	INTREPID OIL & GAS	KANE SPRINGS FED 20	26S	19E	20
105	4301911332	UNION OIL CO OF CALI	BIG FLAT UNIT 4	26S	19E	23
106	4301915778	RUBY, GLEN ET AL	BIG FLAT UNIT 3	26S	19E	23
107	4301930620	DAVIS OIL COMPANY	MATTHEW FED 1	26S	20E	4
108	4301930823	DAVIS OIL COMPANY	MATTHEW FED 2	26S	20E	4
109	4301930796	DAVIS OIL COMPANY	SKYLINE UNIT 1	26S	20E	5
110	4301910155	CALVERT EXPLORATION	BIG FLAT UNIT 7	26S	20E	6
111	4301930273	MINERALS MANAGEMENT	SKYLINE FEDERAL 8-44	26S	20E	8
112	4301911143	SOUTHERN NATURAL GAS	LONG CANYON UNIT 2	26S	20E	9
113	4301915925	INTREPID OIL & GAS	LONG CANYON 1	26S	20E	9
114	4301931190	COORS ENERGY	COORS USA 1-10LC	26S	20E	10
115	4301910987	MOAB OIL CO	WHITE CLOUD 1	26S	20E	14
116	4301910767	MURPHY CONSTRUCTION	LITTLE VALLEY-FED 1	26S	20E	29
117	4301911336	PURE OIL CO	HOBSON USA 1	26S	20E	30
118	4301910145	CABEEN EXPLORATION	BIG FLAT-GOVT 1	26S	20E	31
119	4301930076	UNION OIL CO OF CALI	BURKHOLDER UNIT 1-G	26S	22E	1
120	4301930113	CITIES SERV OIL & GA	CSO-FED WEAVER 1	26S	22E	28
121	4301910830	PAN AMERICAN PETROLE	PACE STATE 1	26S	25E	12
122	4301931157	AMOCO PRODUCTION CO	TAYLOR CREEK U 2	26S	25E	12

Table A-2: List of wells used for lithology classification and age estimate relationships.

No.	API #	Operator	Well Name	Township	Range	Section
1	4301511182	SUPERIOR OIL COMPANY	GRAND FAULT UNIT 14	21S	15E	24
2	4301530079	MEGADON ENTERPRISES	GEYSER DOME 1-14	22S	15E	14
3	4301930124	MOUNTAIN FUEL SUPPLY	MT FUEL-SKYLINE GEYS	22S	16E	25
4	4301930282	RESERVE OIL & GAS	SALT WASH NORTH 1	23S	17E	9
5	4301930688	MEGADON ENTERPRISES	FEDERAL 1-26	24S	17E	26
6	4301930050	GENERAL CRUDE OIL CO	BIG ROCK FED 1	25S	19E	26
7	4301930910	CHANDLER & ASSOCIATE	MOAB FED 16-9	25S	20E	9
8	4301530145	DAVIS OIL COMPANY	POOL UNIT 1	26S	17E	17
9	4301931190	COORS ENERGY	COORS USA 1-10LC	26S	20E	10
10	4301910767	MURPHY CONSTRUCTION	LITTLE VALLEY-FED 1	26S	20E	29

APPENDIX B

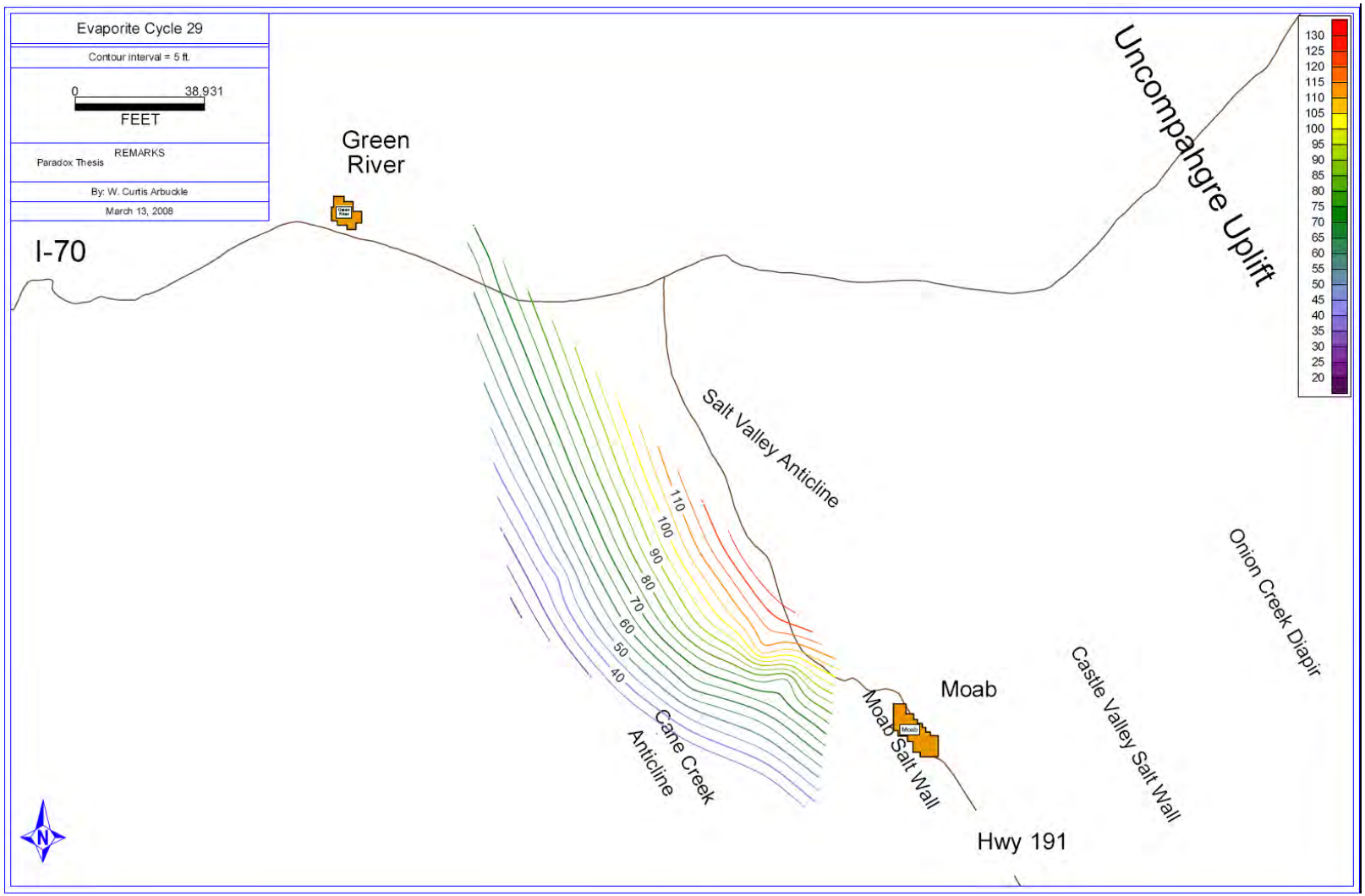

Figure B-1: ***Isopach map of evaporite cycle 29 within the Paradox Formation. See text for analysis. Contour interval = 5 feet (1.52 m).***

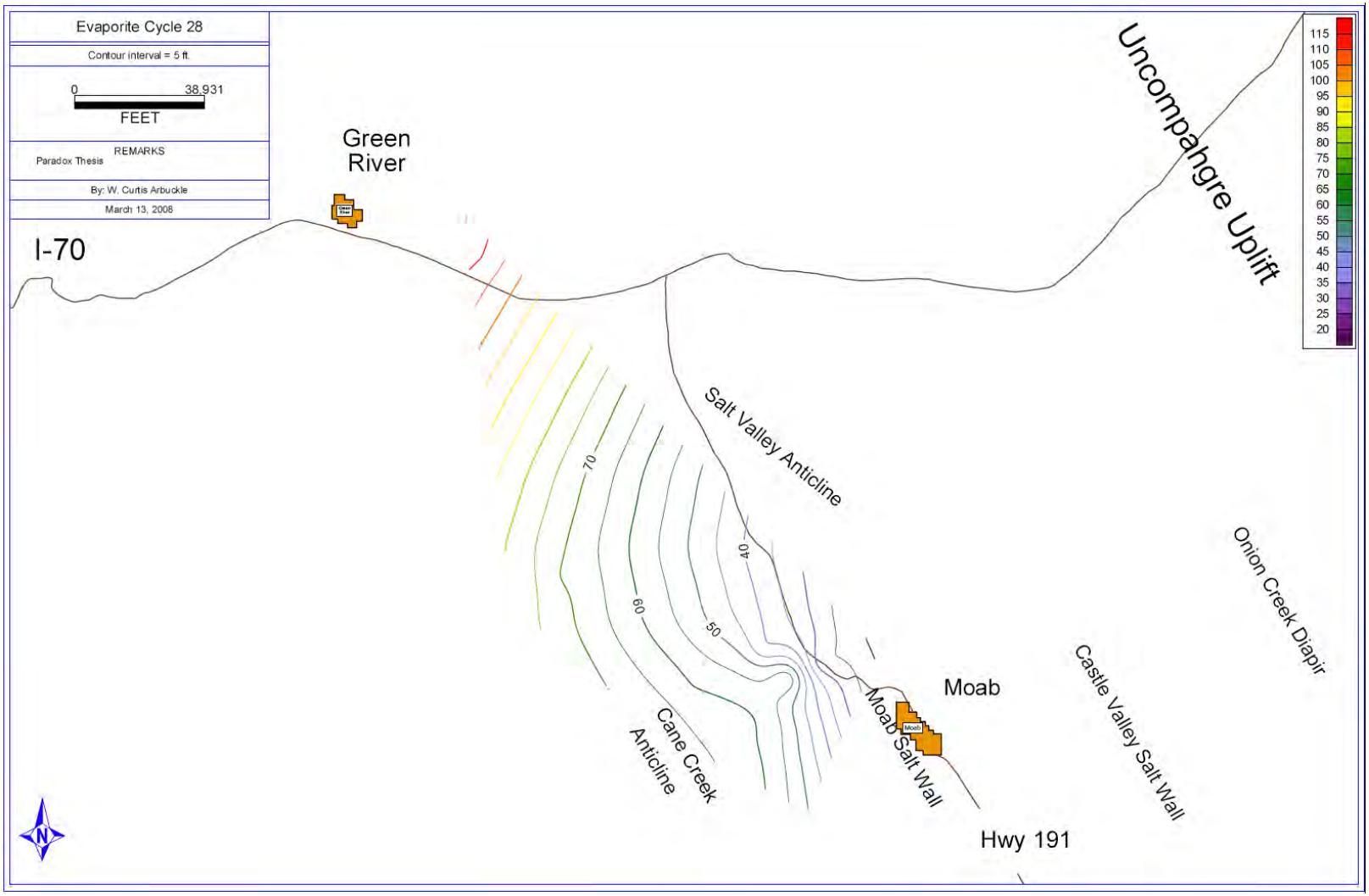

Figure B-2: ***Isopach map of evaporite cycle 28 within the Paradox Formation. See text for analysis. Contour interval = 5 feet (1.52 m).***

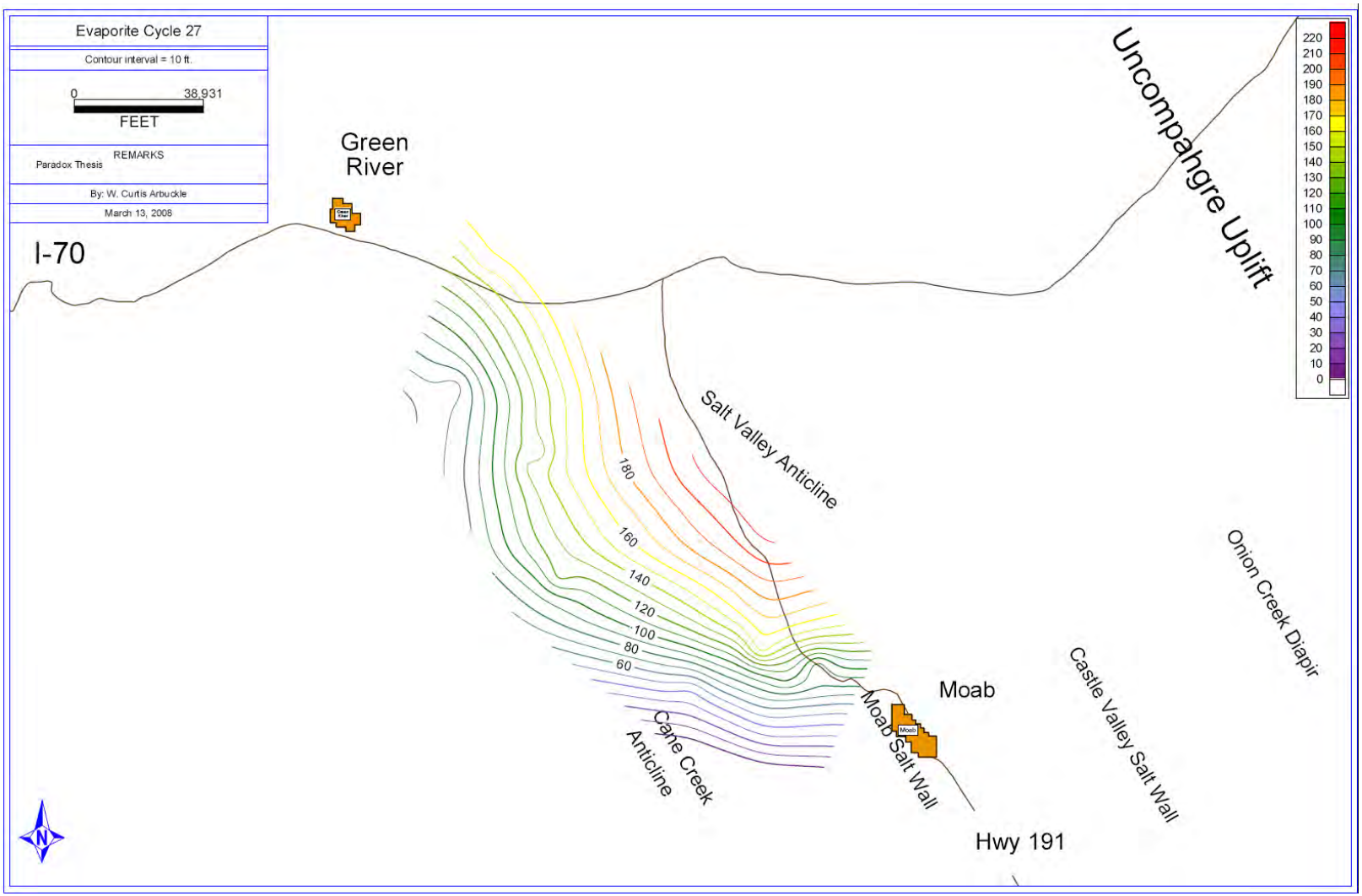

Figure B-3: ***Isopach map of evaporite cycle 27 within the Paradox Formation. See text for analysis. Contour interval = 10 feet (3.05 m).***

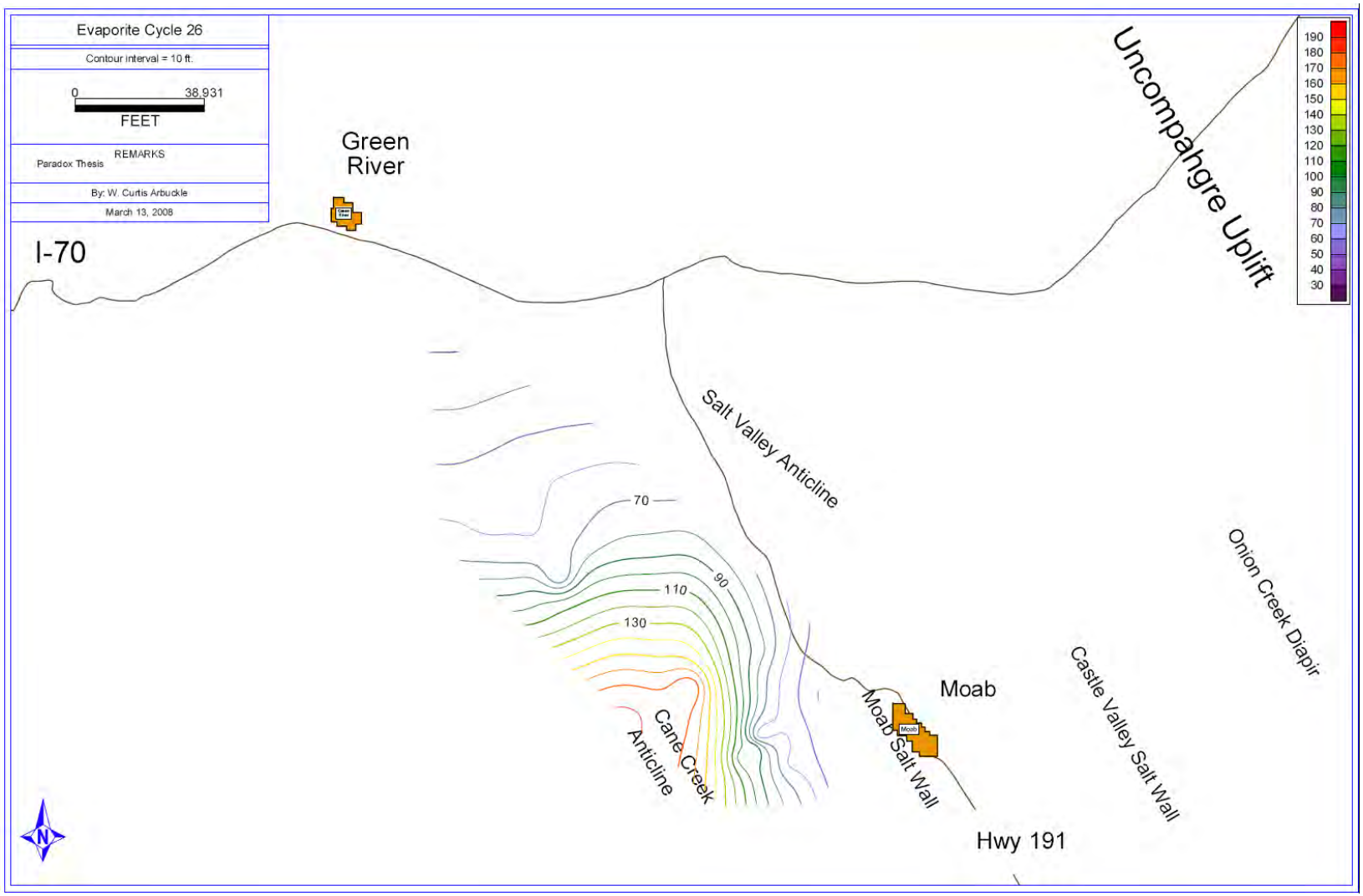

Figure B-4: ***Isopach map of evaporite cycle 26 within the Paradox Formation. See text for analysis. Contour interval = 10 feet (3.05 m).***

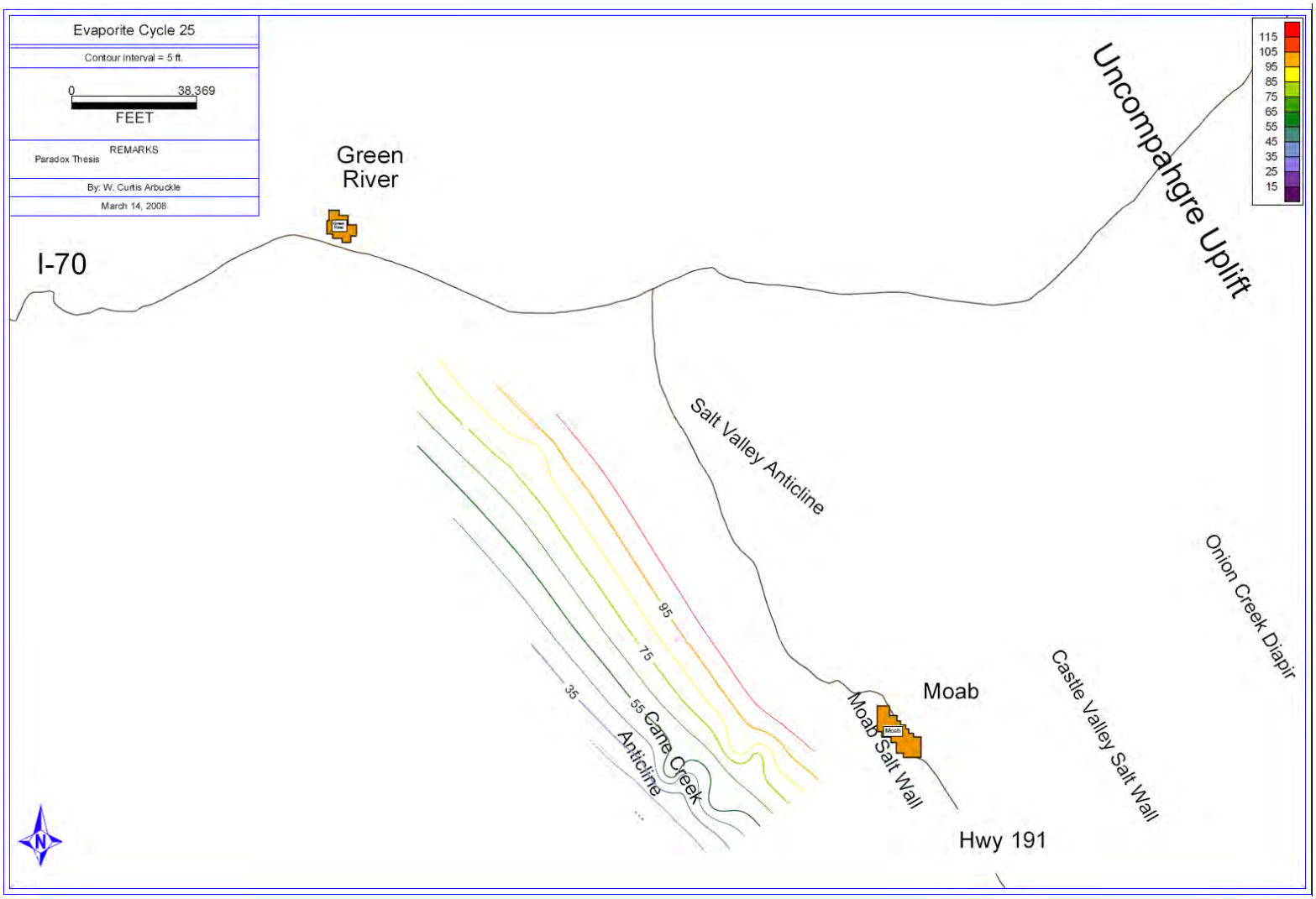

Figure B-5: ***Isopach map of evaporite cycle 25 within the Paradox Formation. See text for analysis. Contour interval = 5 feet (1.52 m).***

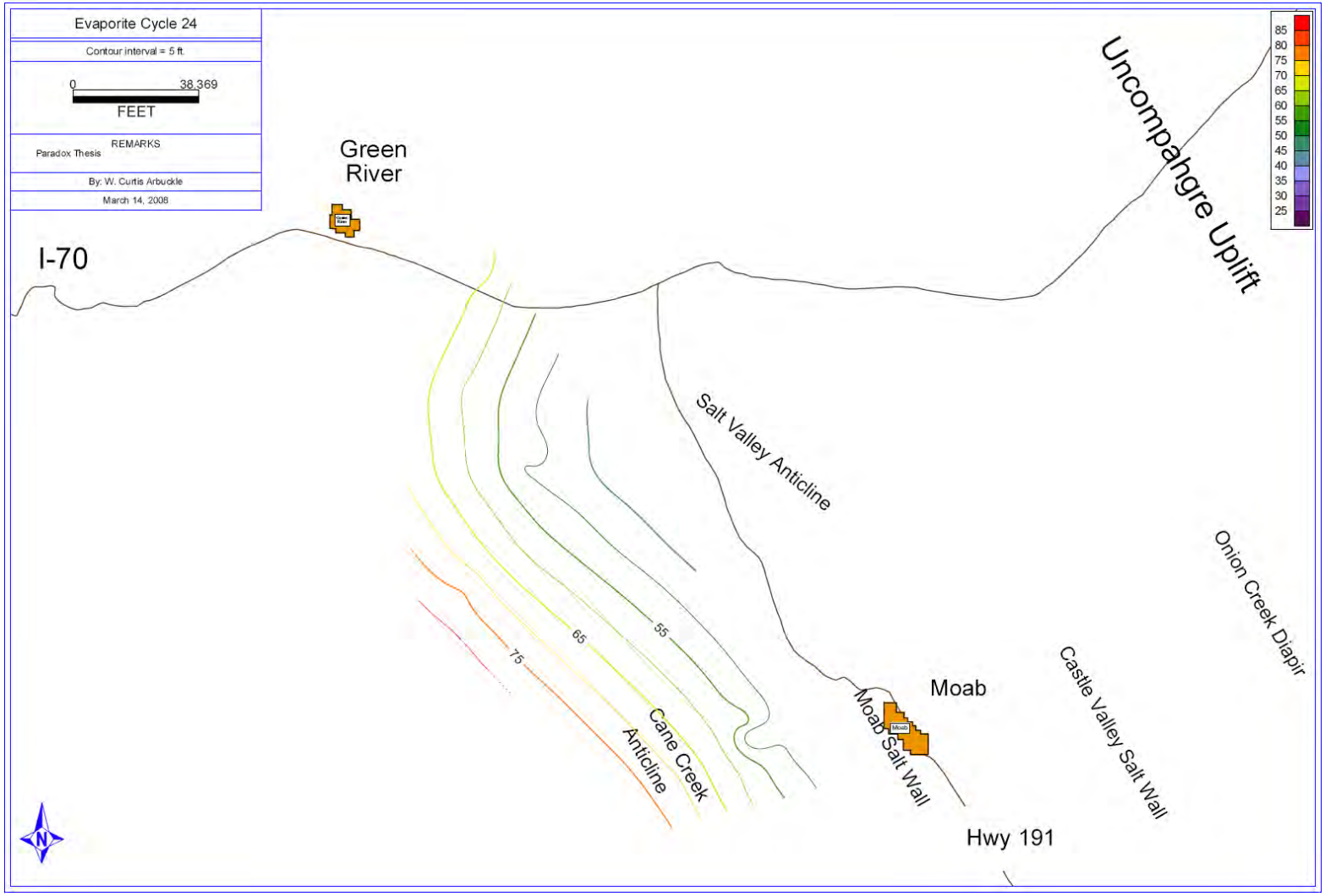

Figure B-6: ***Isopach map of evaporite cycle 24 within the Paradox Formation. See text for analysis. Contour interval = 5 feet (1.52 m).***

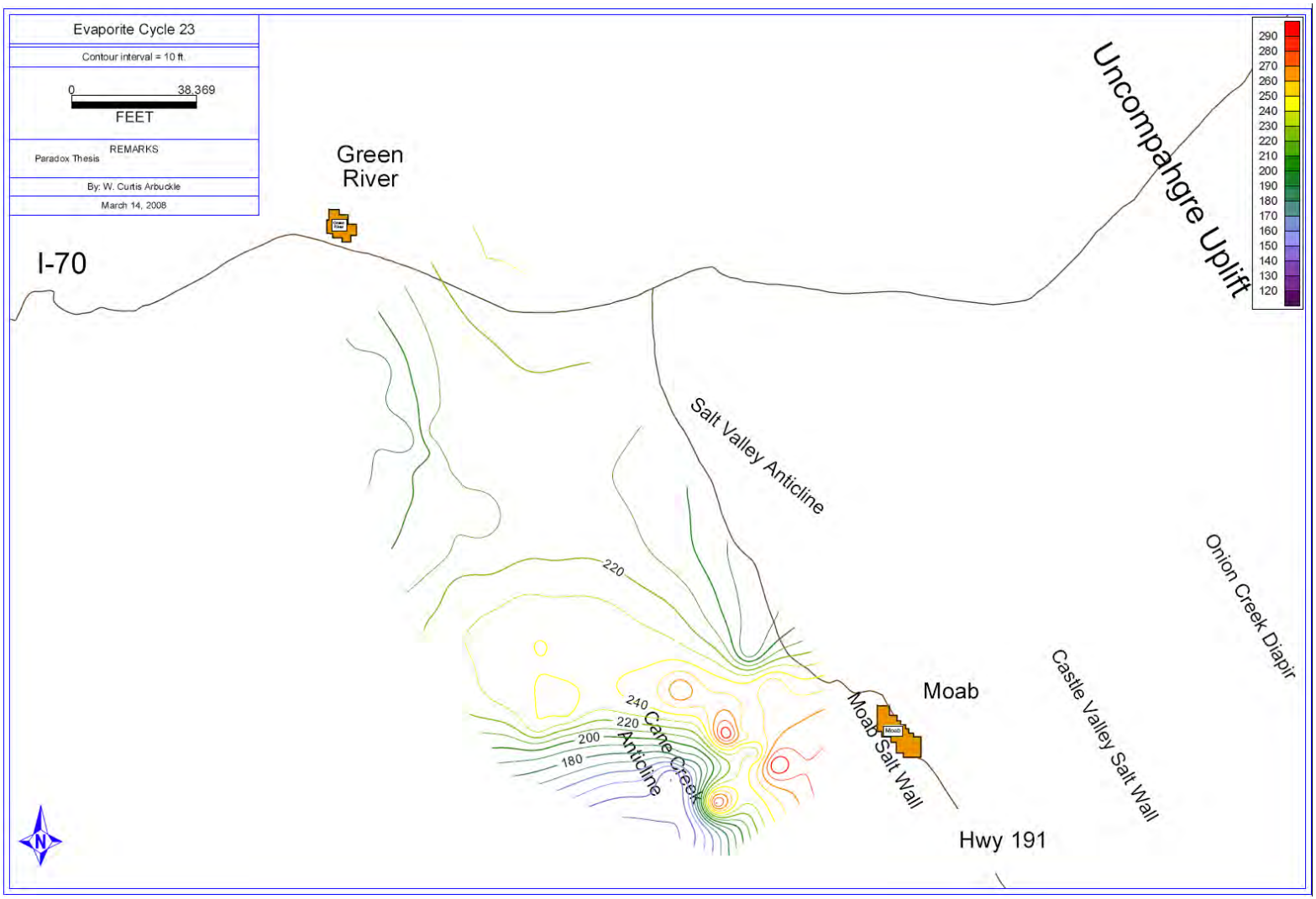

Figure B-7: ***Isopach map of evaporite cycle 23 within the Paradox Formation. See text for analysis. Contour interval = 10 feet (3.05 m).***

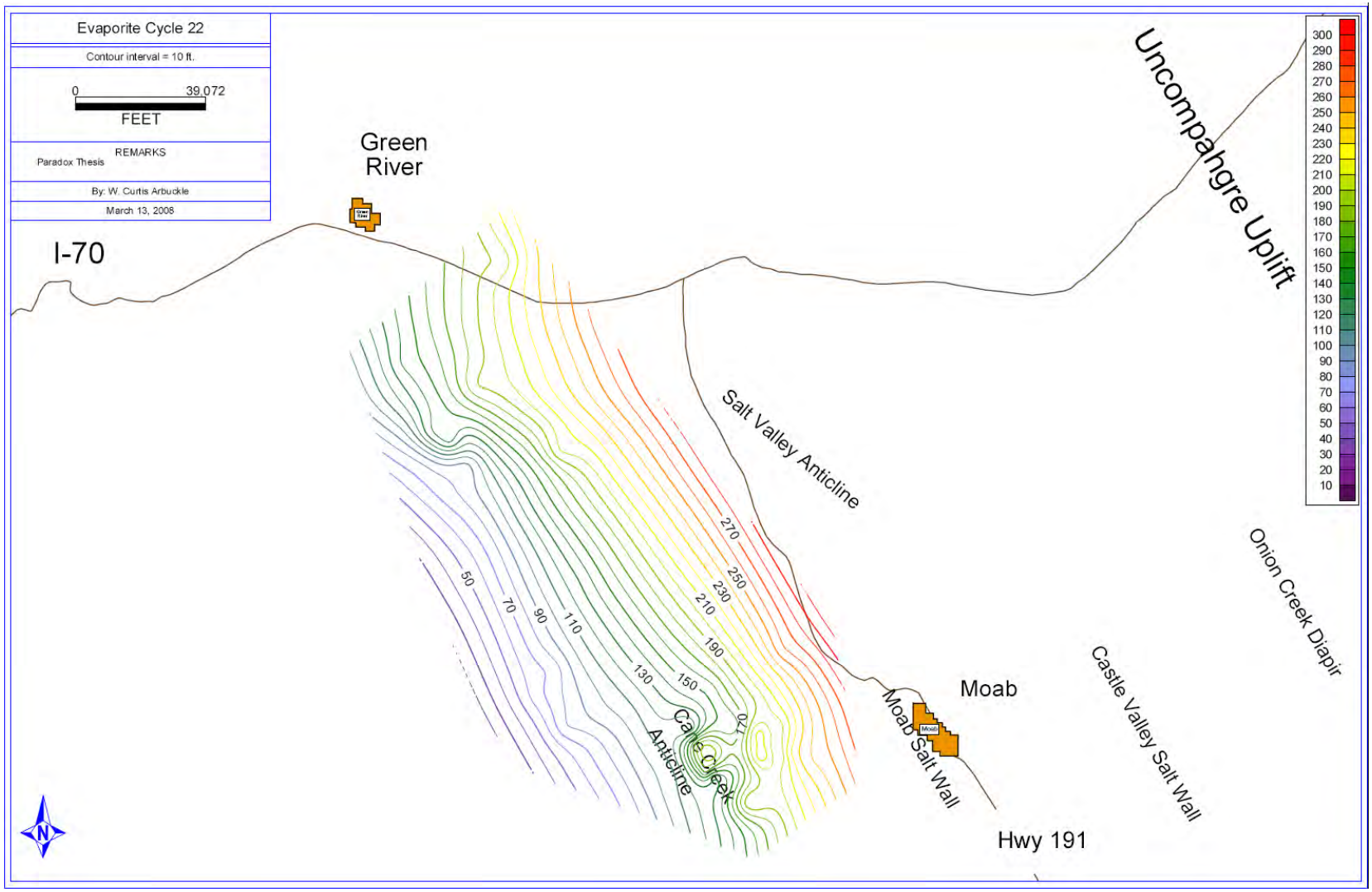

Figure B-8: ***Isopach map of evaporite cycle 22 within the Paradox Formation. See text for analysis. Contour interval = 10 feet (3.05 m).***

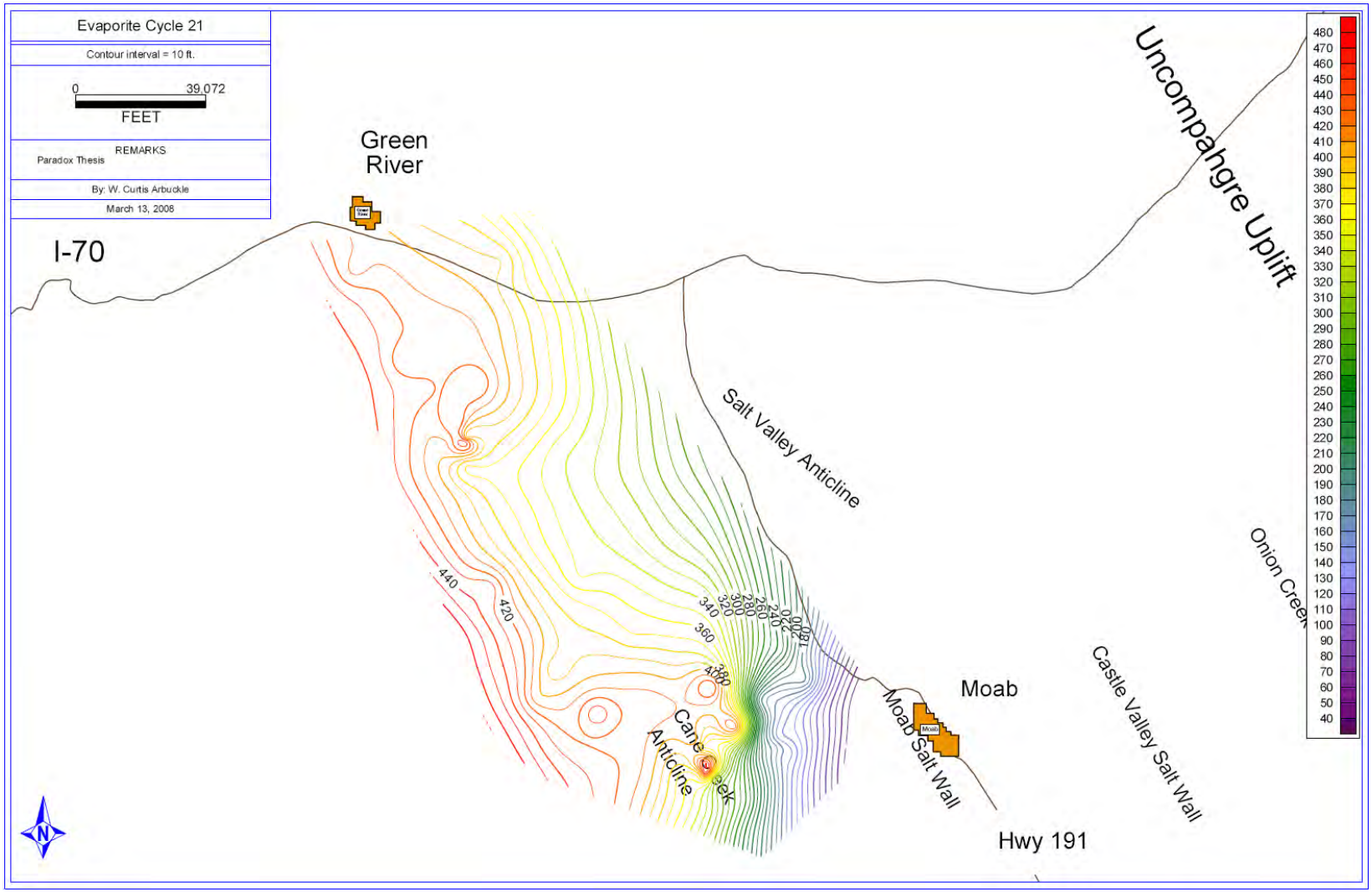

Figure B-9: ***Isopach map of evaporite cycle 21 within the Paradox Formation. See text for analysis. Contour interval = 10 feet (3.05 m).***

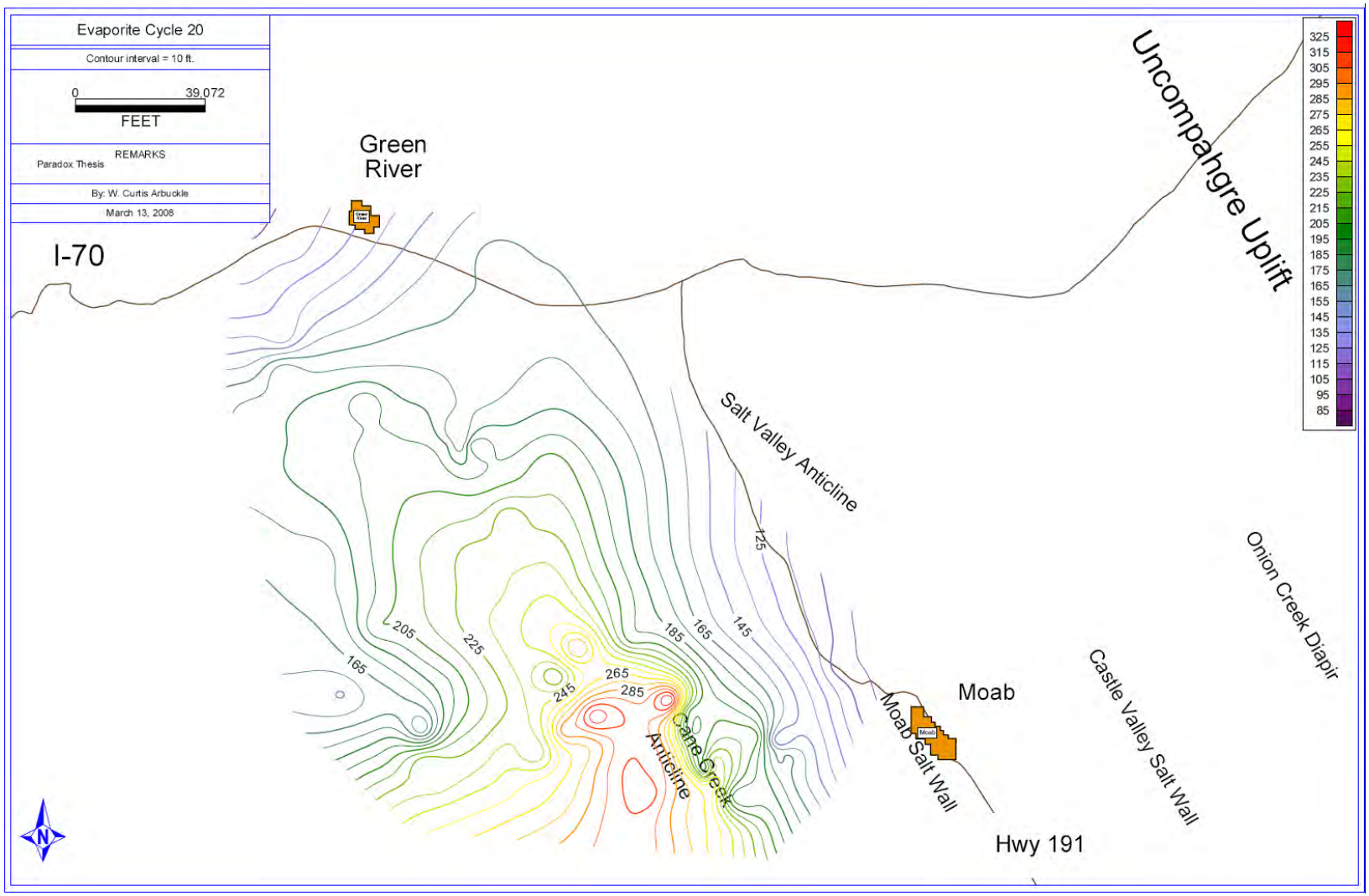

Figure B-10: ***Isopach map of evaporite cycle 20 within the Paradox Formation. See text for analysis. Contour interval = 10 feet (3.05 m).***

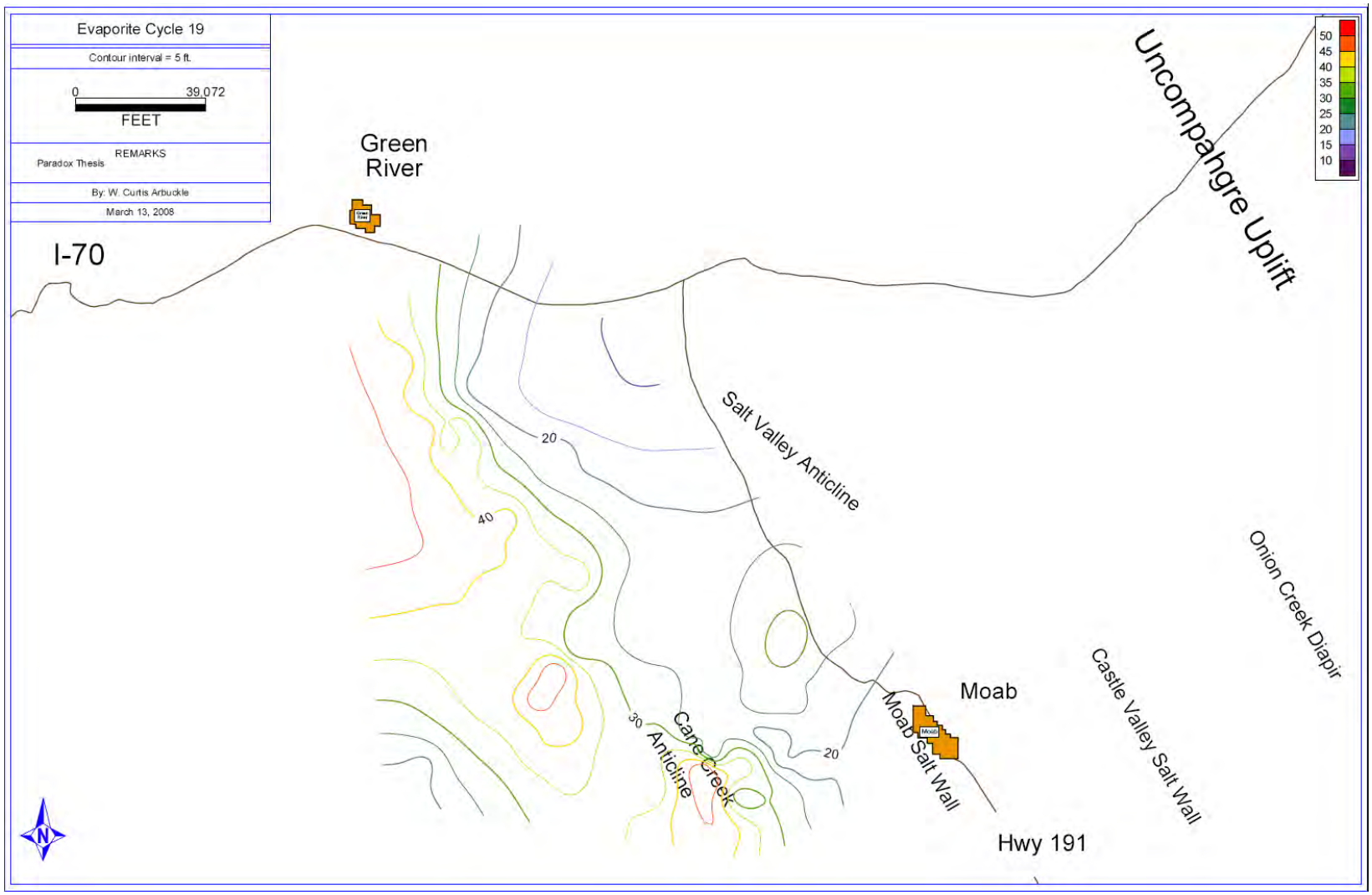

***Figure** B-11: Isopach map of evaporite cycle 19 within the Paradox Formation. See text for analysis. Contour interval = 5 feet (1.52 m).*

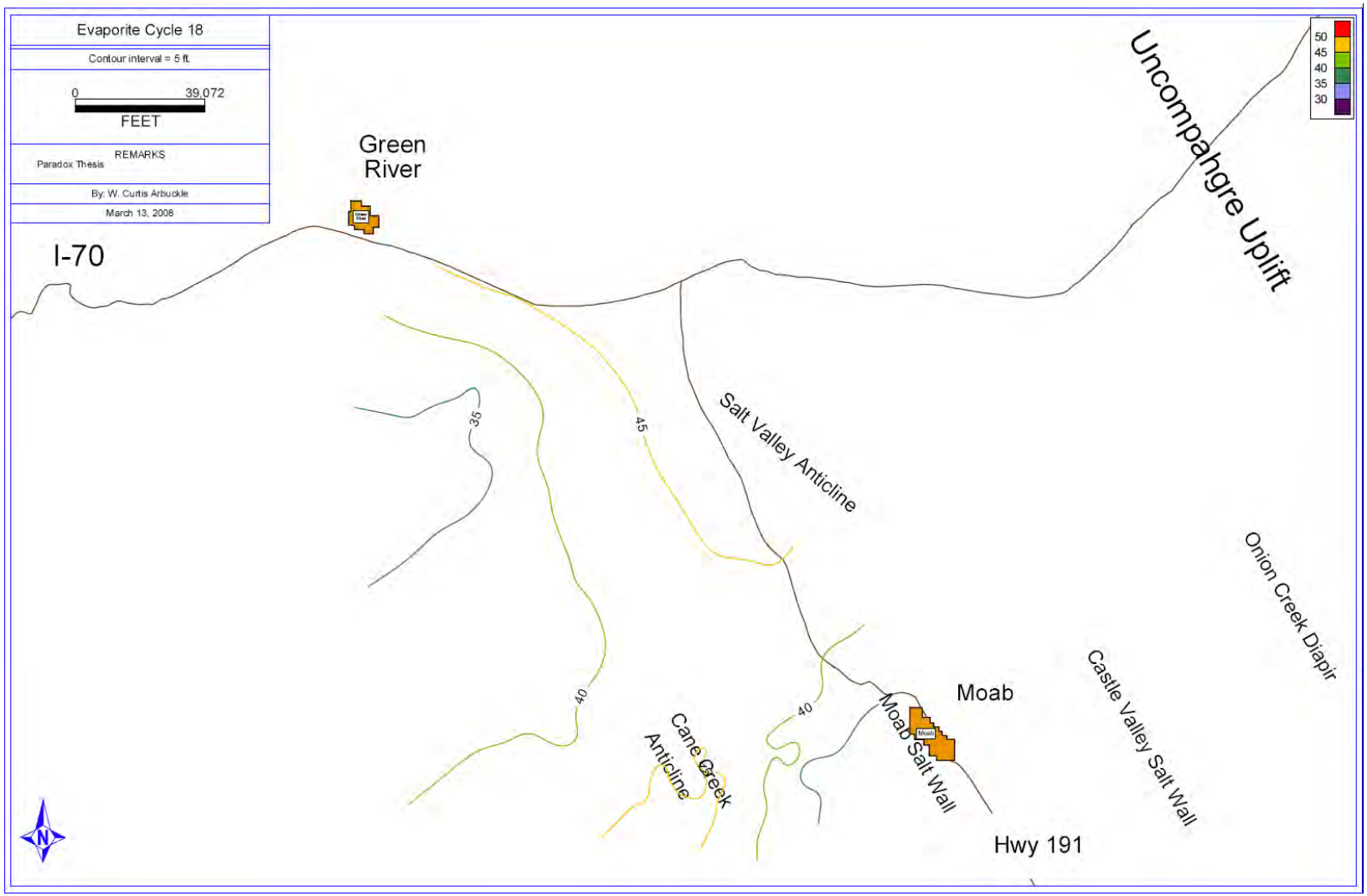

***Figure** B-12: Isopach map of evaporite cycle 18 within the Paradox Formation. See text for analysis. Contour interval = 5 feet (1.52 m).*

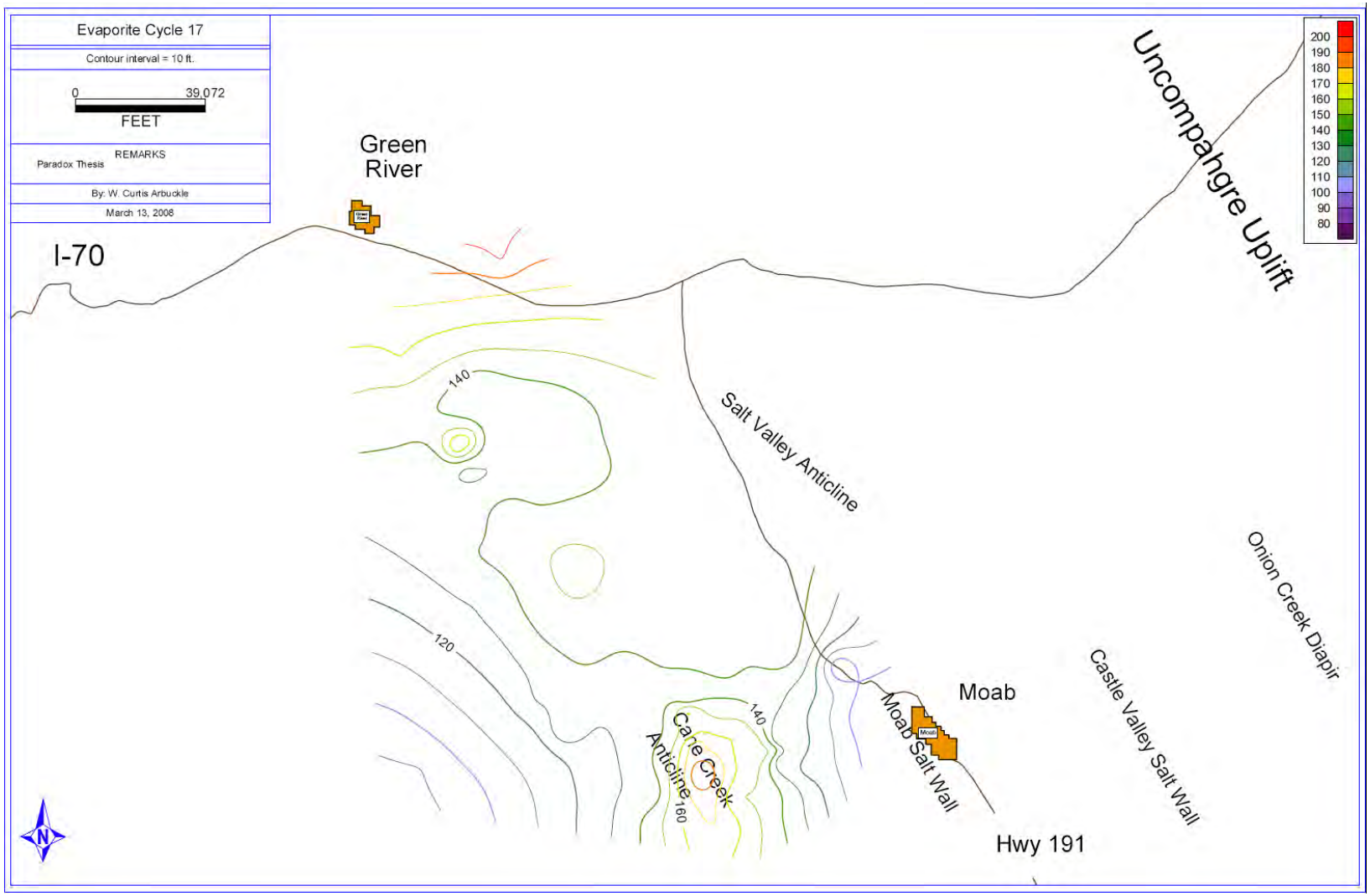

Figure B-13: Isopach map of evaporite cycle 17 within the Paradox Formation. See text for analysis. Contour interval = 10 feet (3.05 m).

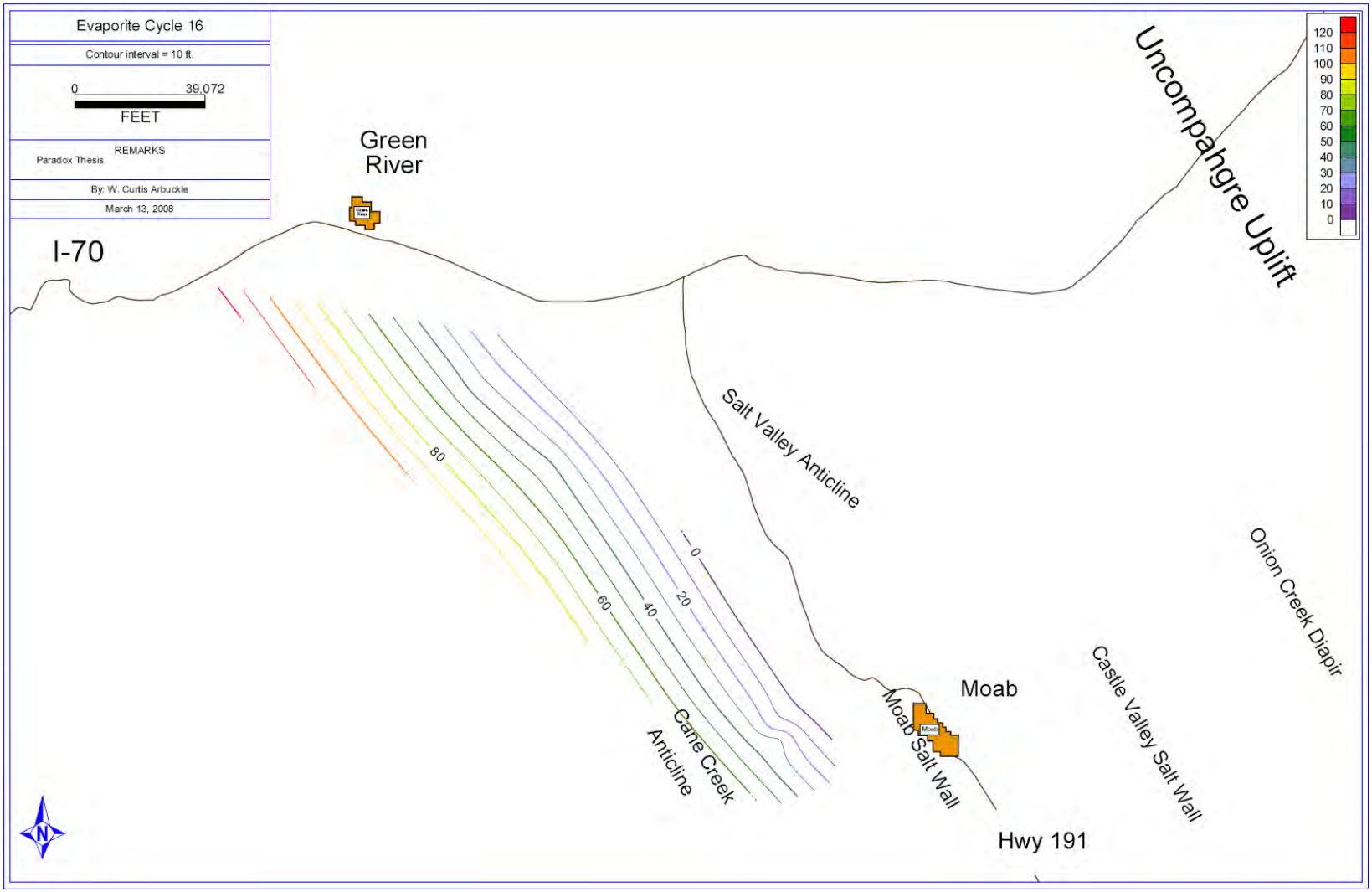

***Figure** B-14: Isopach map of evaporite cycle 16 within the Paradox Formation. See text for analysis. Contour interval = 10 feet (3.05 m).*

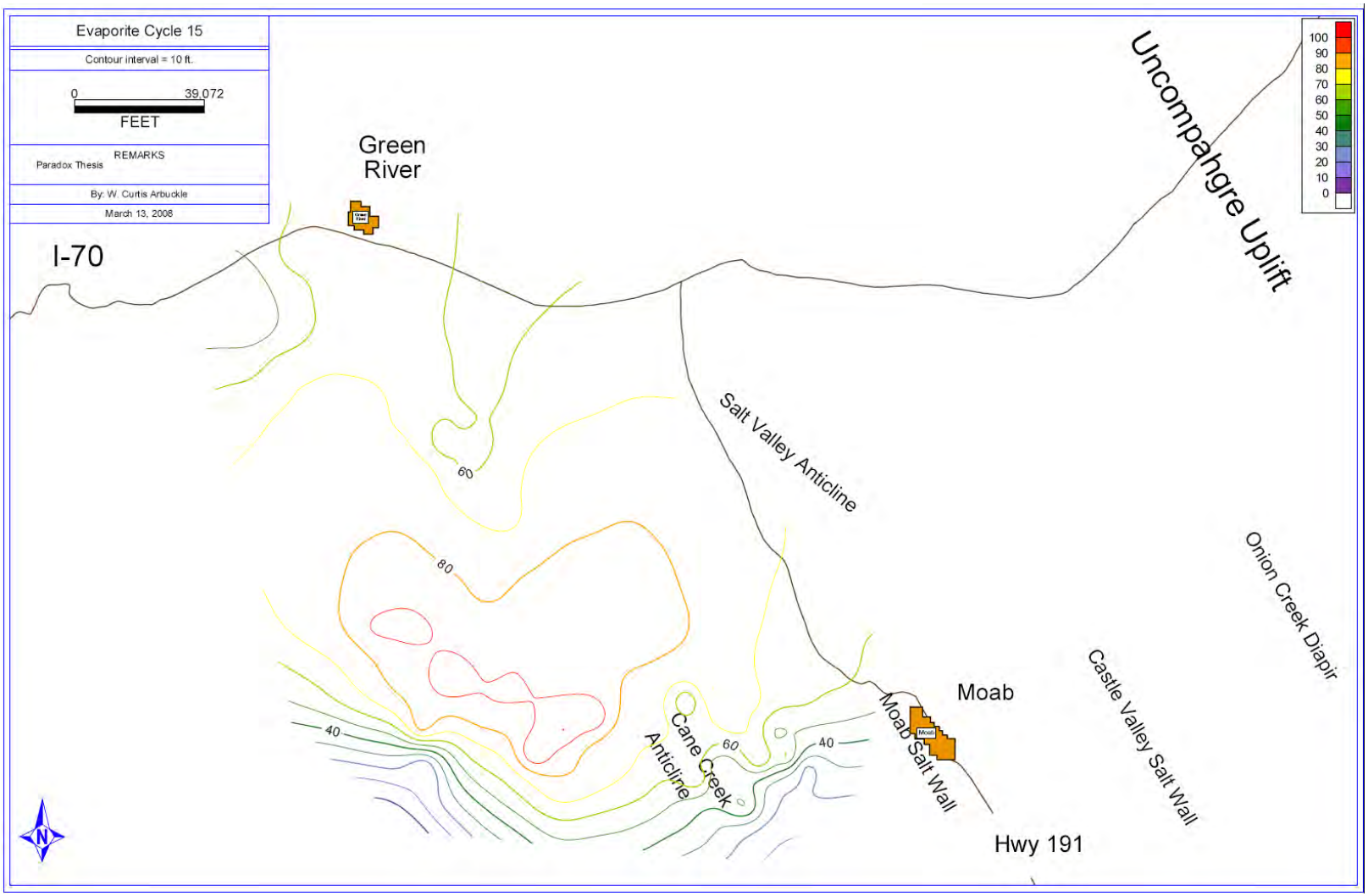

Figure B-15: Isopach map of evaporite cycle 15 within the Paradox Formation. See text for analysis. Contour interval = 10 feet (3.05 m).

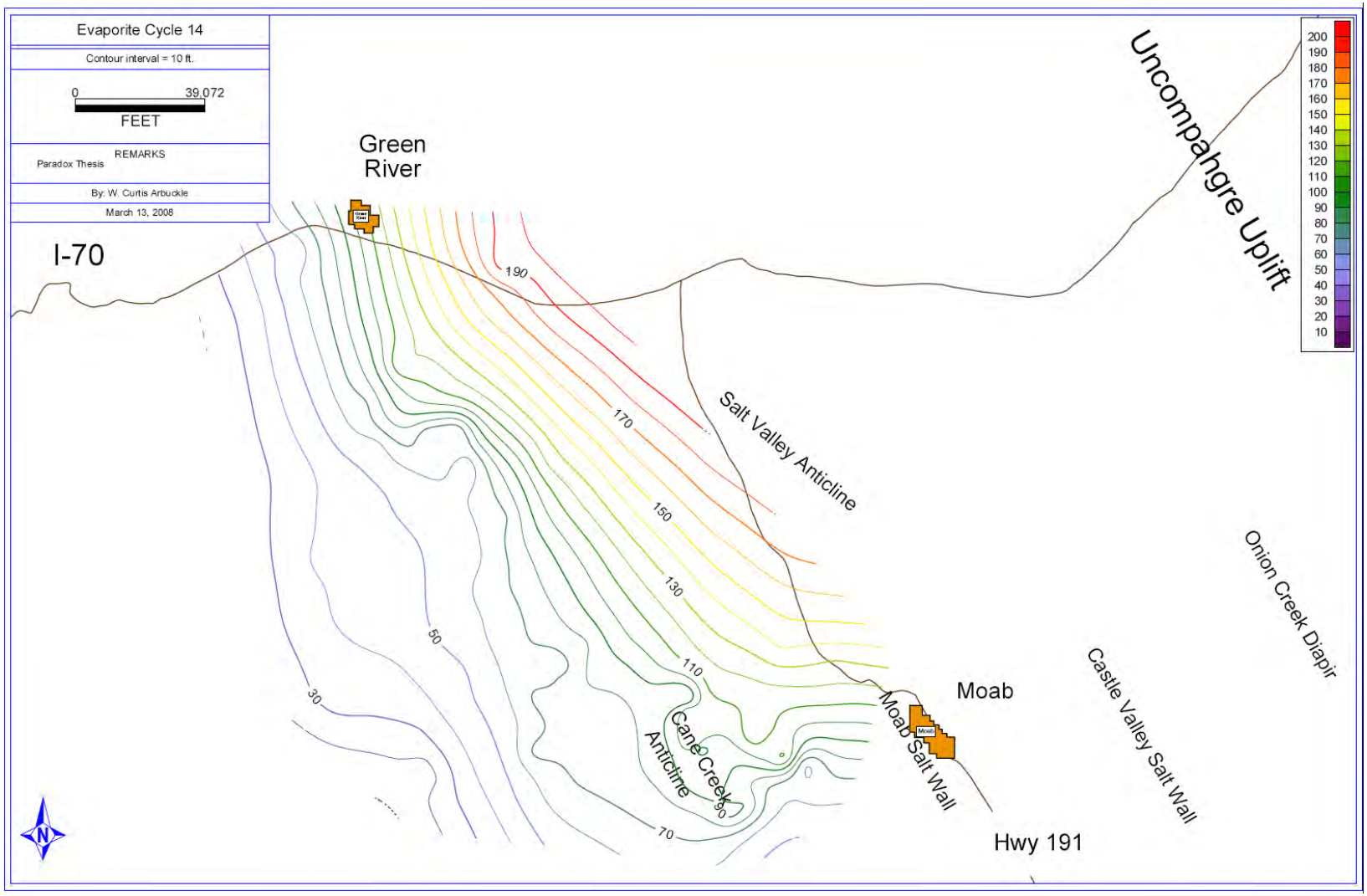

Figure B-16: ***Isopach map of evaporite cycle 14 within the Paradox Formation. See text for analysis. Contour interval = 10 feet (3.05 m).***

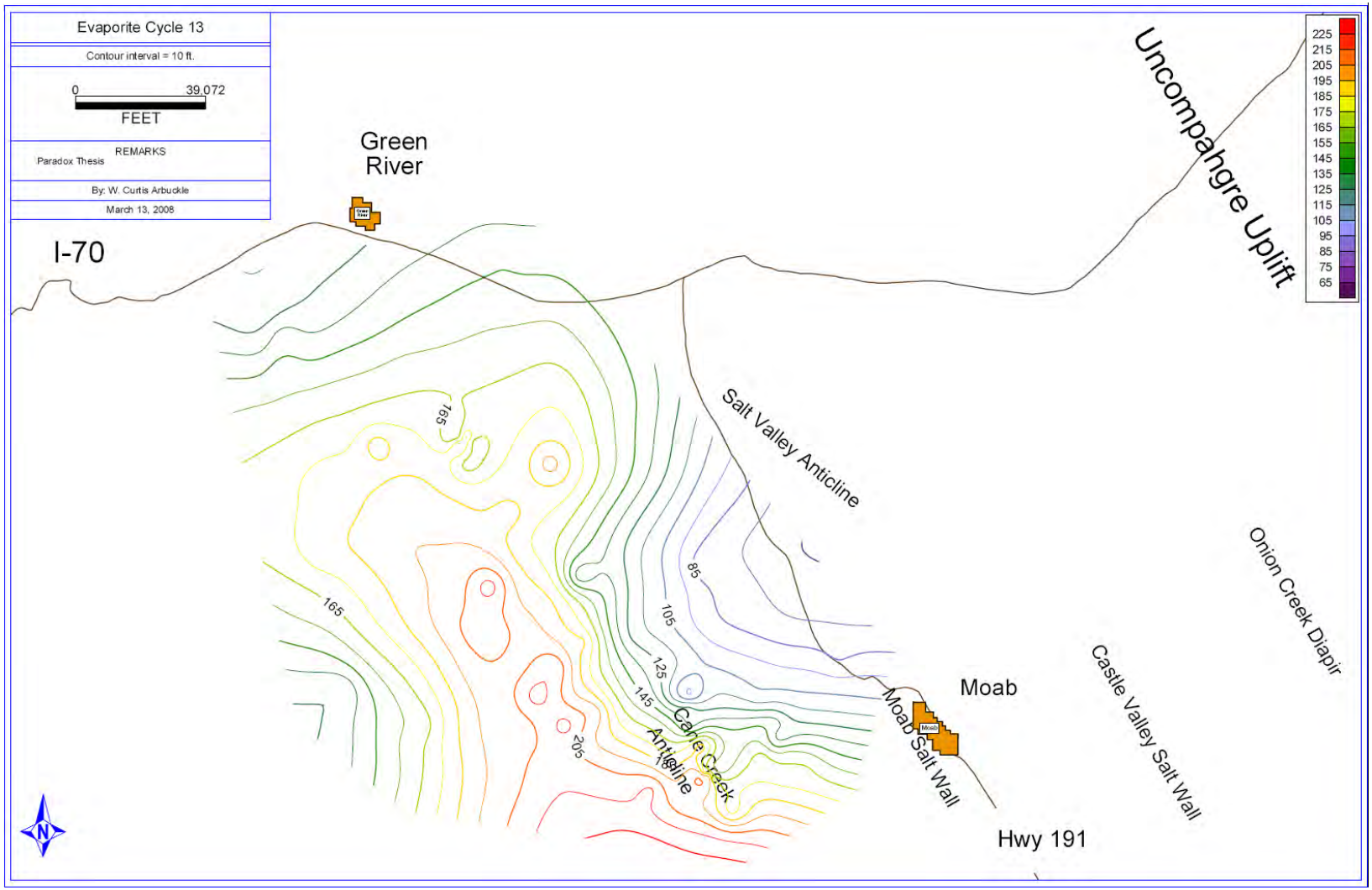

Figure B-17: Isopach map of evaporite cycle 13 within the Paradox Formation. See text for analysis. Contour interval = 10 feet (3.05 m).

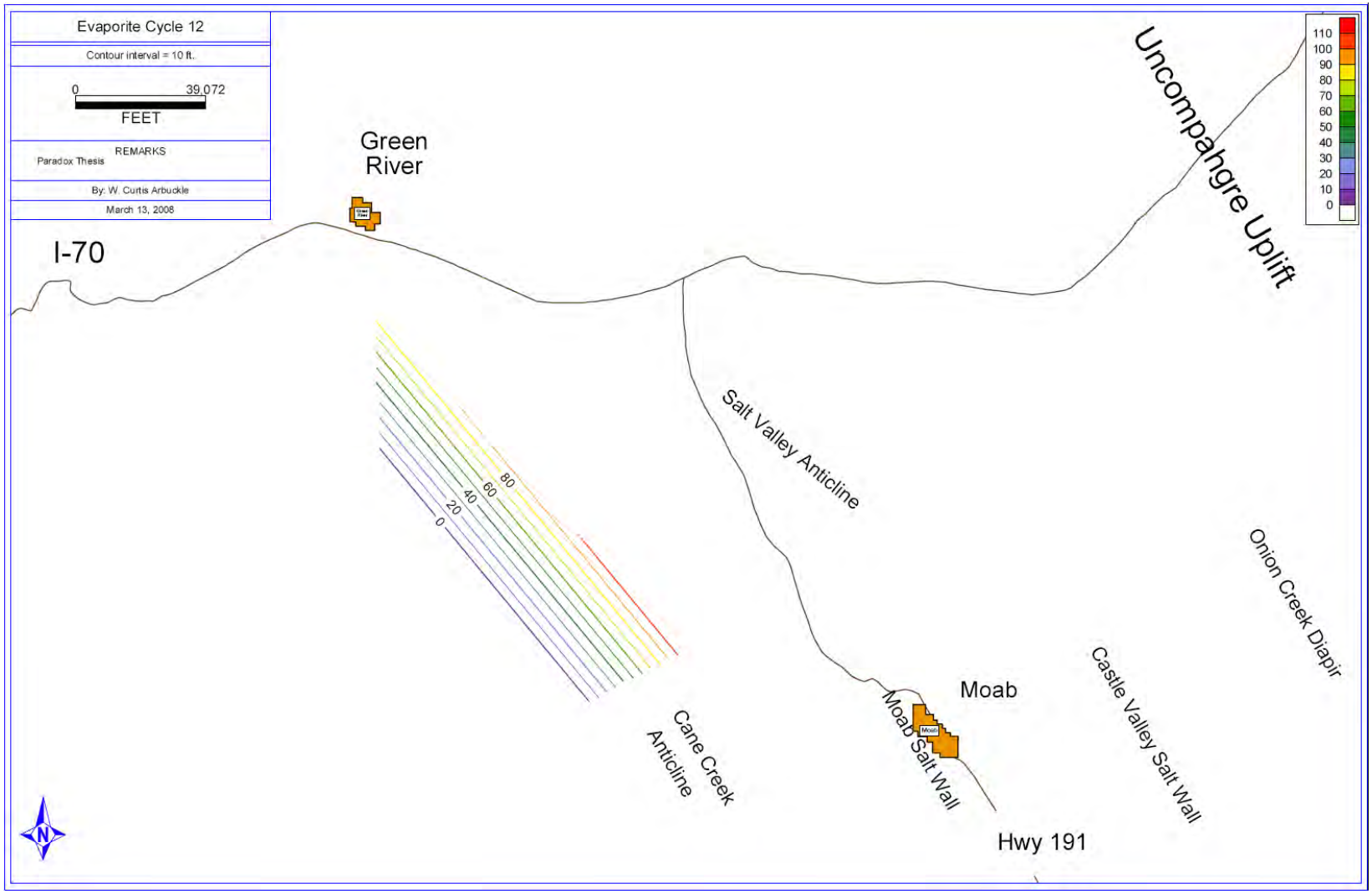

***Figure** B-18: Isopach map of evaporite cycle 12 within the Paradox Formation. See text for analysis. Contour interval = 10 feet (3.05 m).*

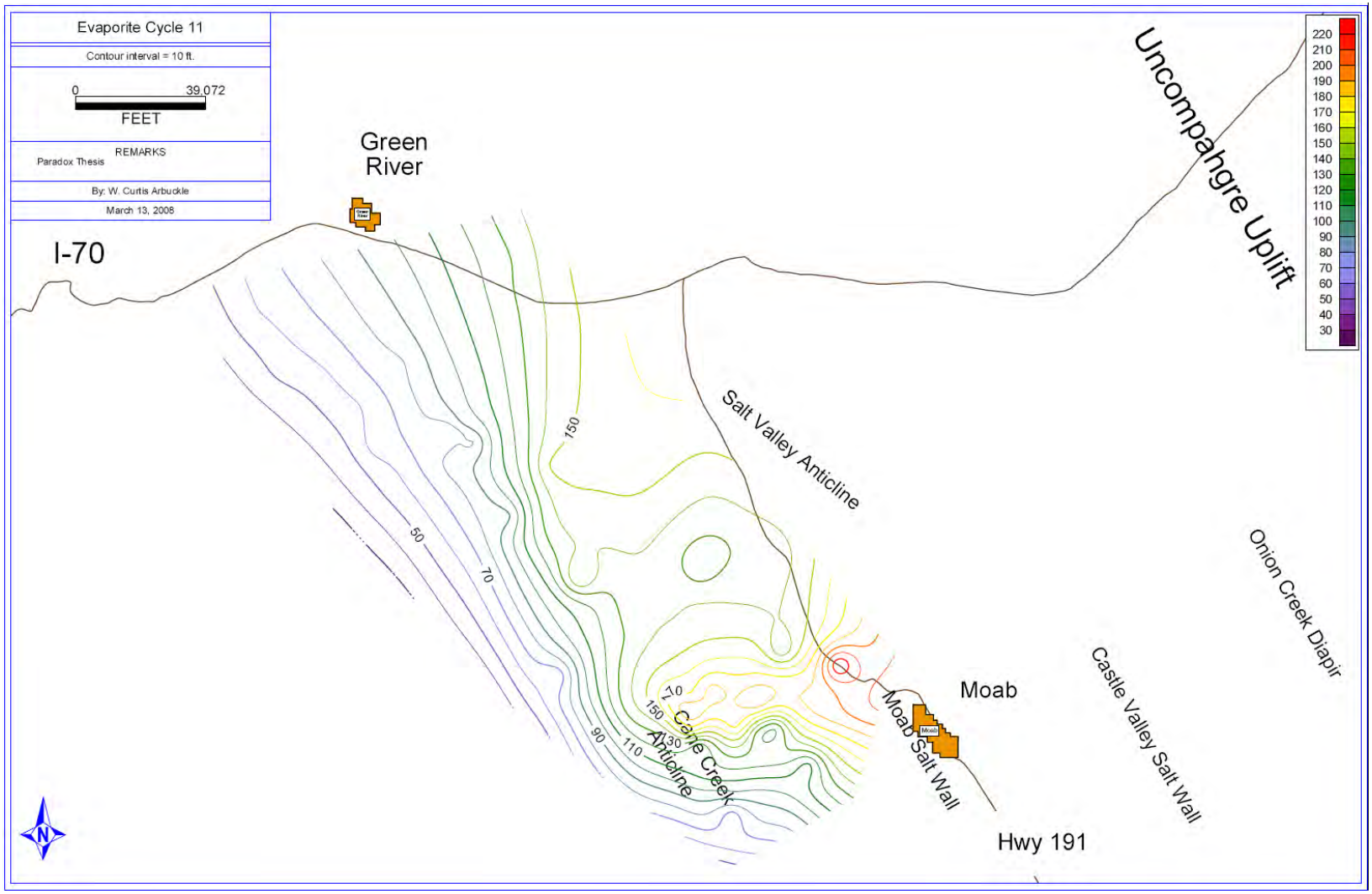

Figure B-19: Isopach map of evaporite cycle 11 within the Paradox Formation. See text for analysis. Contour interval = 10 feet (3.05 m).

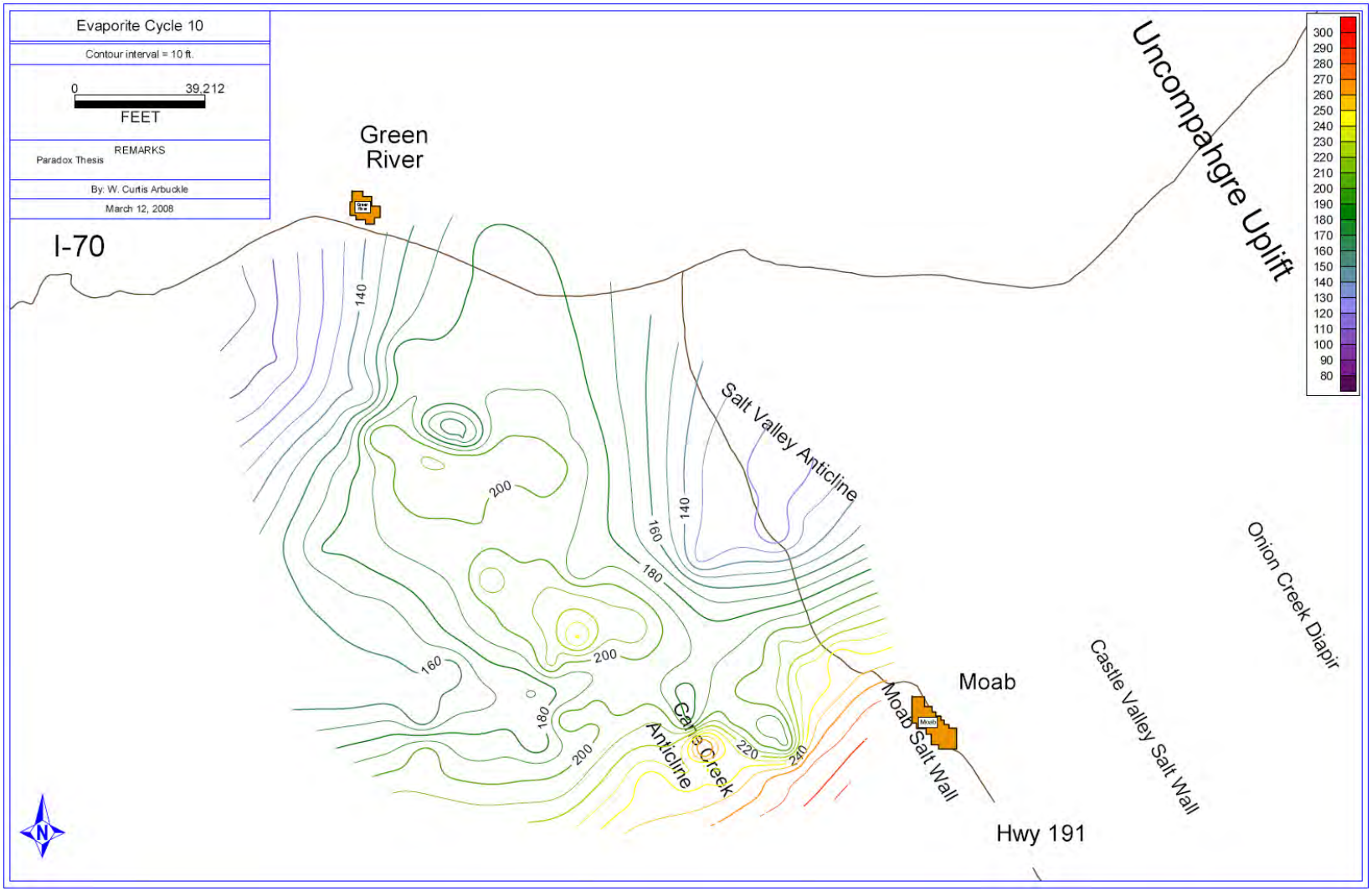

***Figure** B-20: Isopach map of evaporite cycle 10 within the Paradox Formation. See text for analysis. Contour interval = 10 feet (3.05 m).*

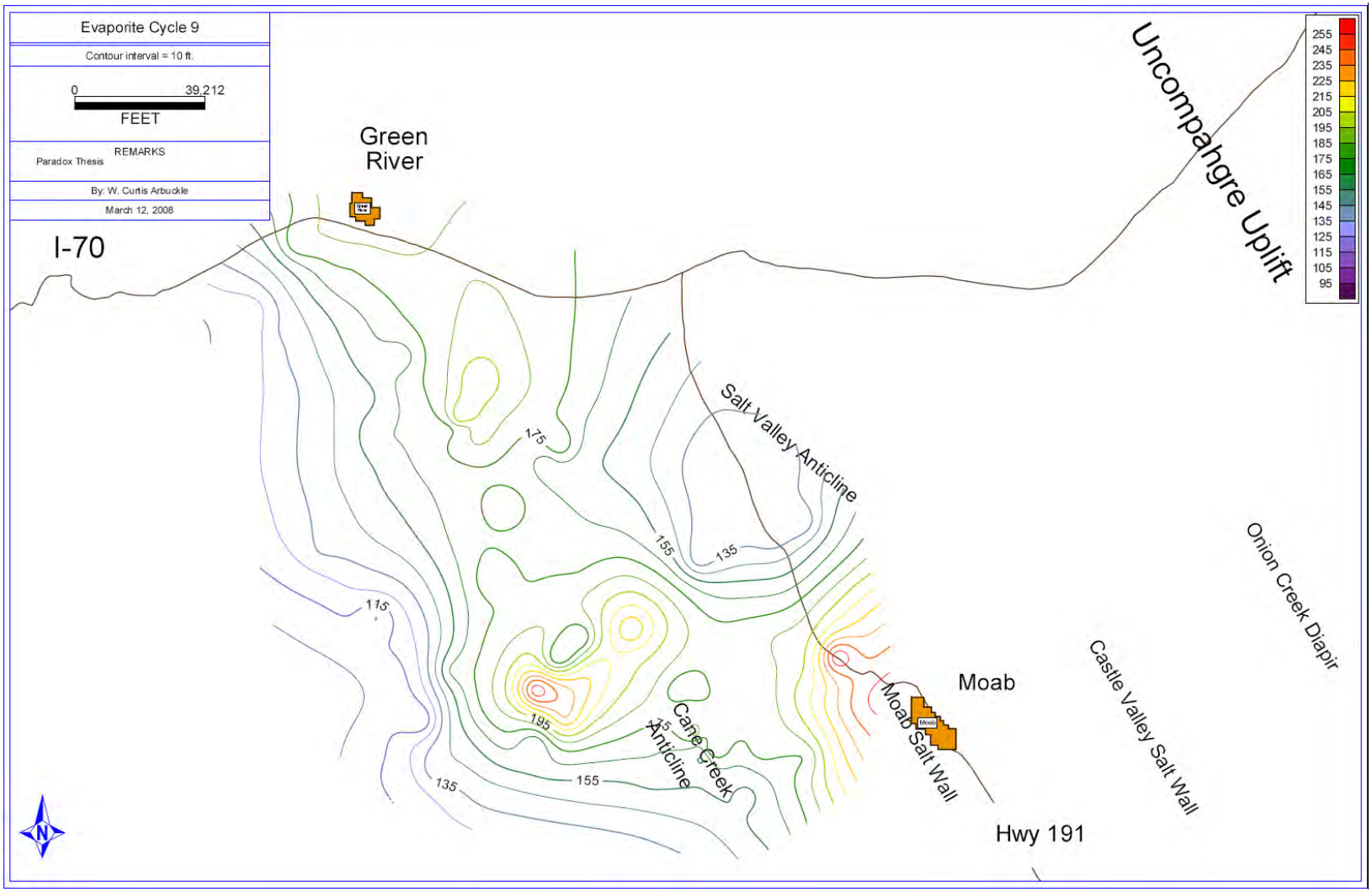

***Figure** B-21: Isopach map of evaporite cycle 9 within the Paradox Formation. See text for analysis. Contour interval = 10 feet (3.05 m).*

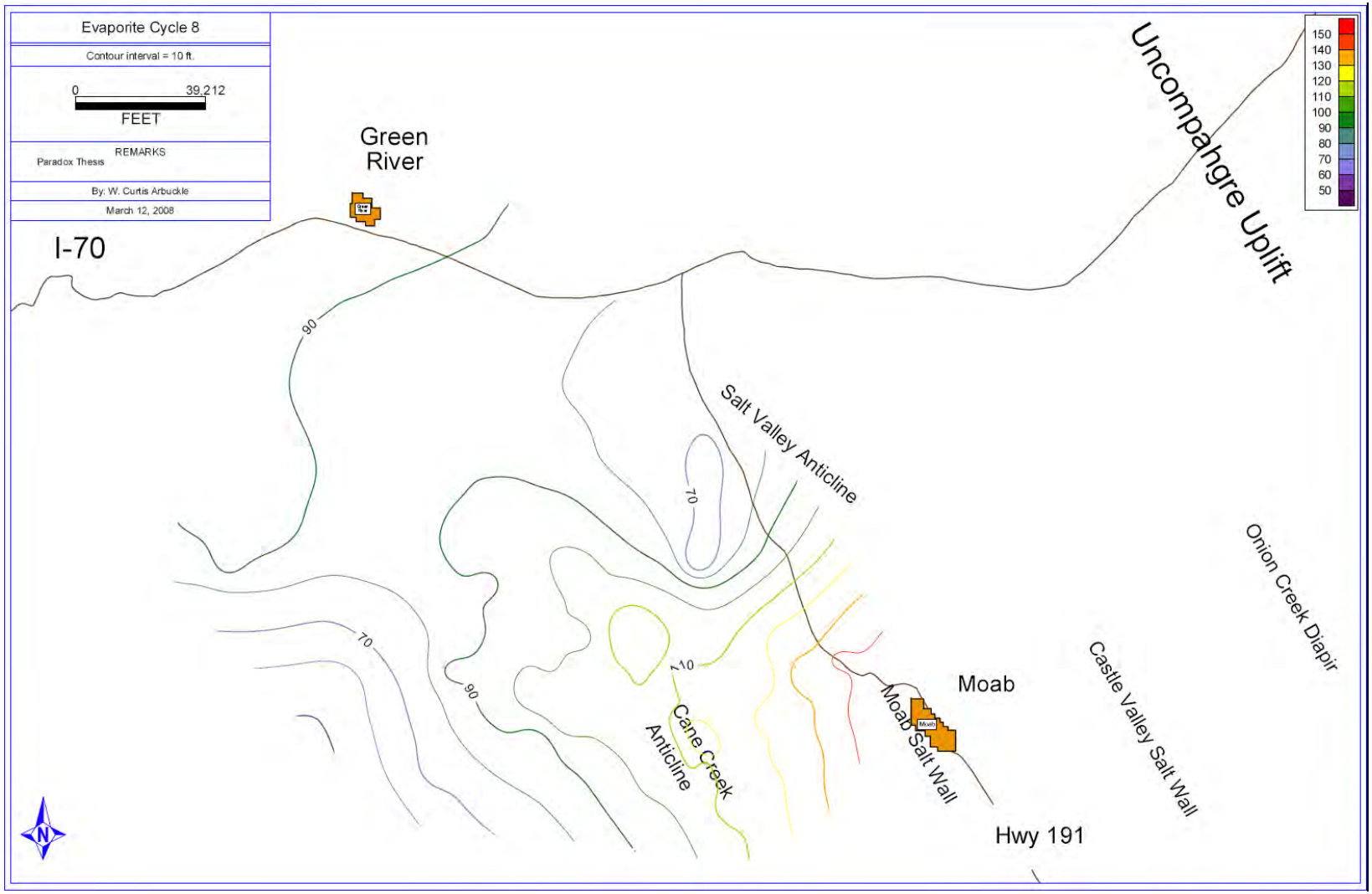

***Figure** B-22: Isopach map of evaporite cycle 8 within the Paradox Formation. See text for analysis. Contour interval = 10 feet (3.05 m).*

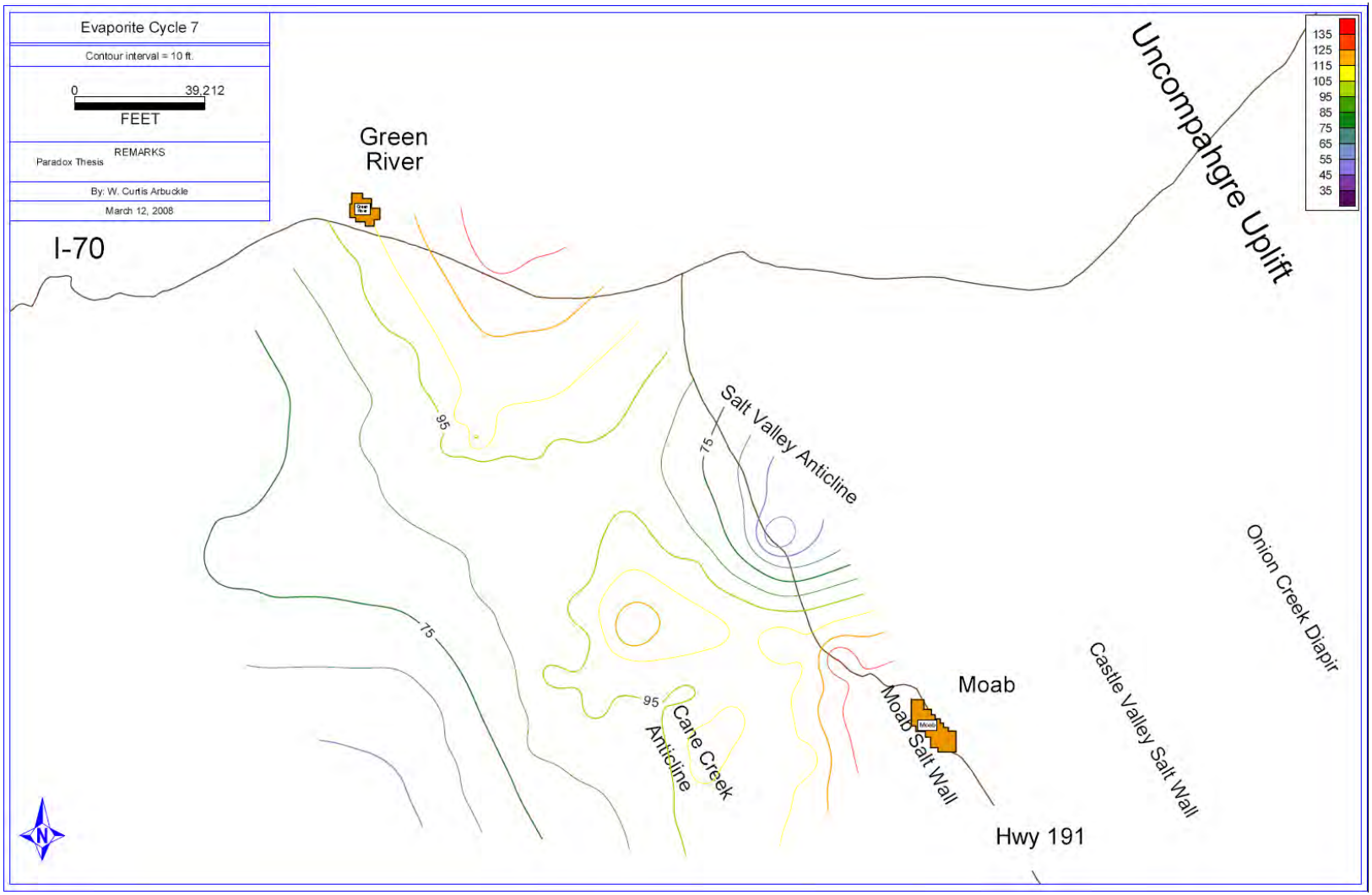

***Figure** B-23: Isopach map of evaporite cycle 7 within the Paradox Formation. See text for analysis. Contour interval = 10 feet (3.05 m).*

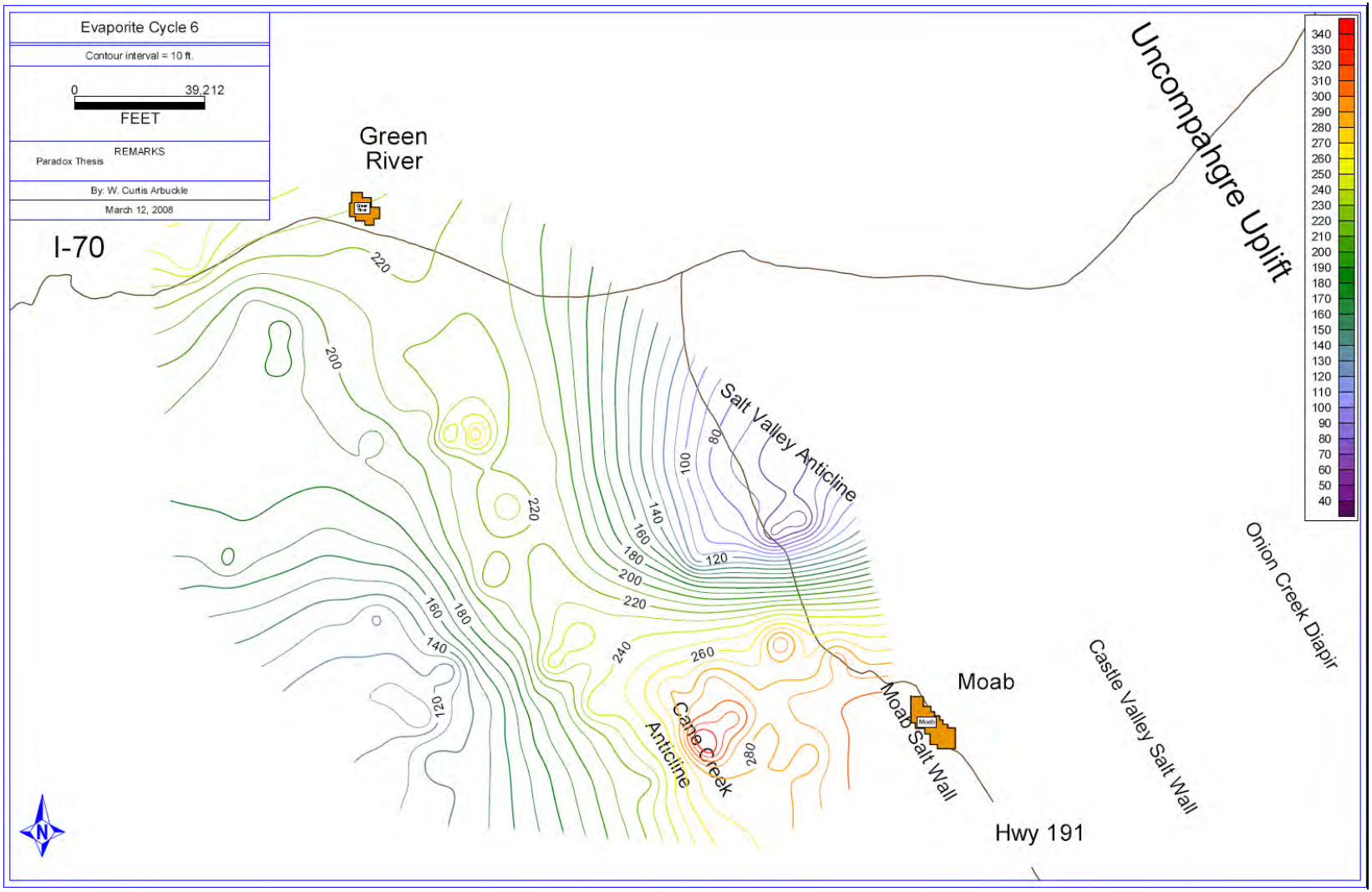

***Figure** B-24: Isopach map of evaporite cycle 6 within the Paradox Formation. See text for analysis. Contour interval = 10 feet (3.05 m).*

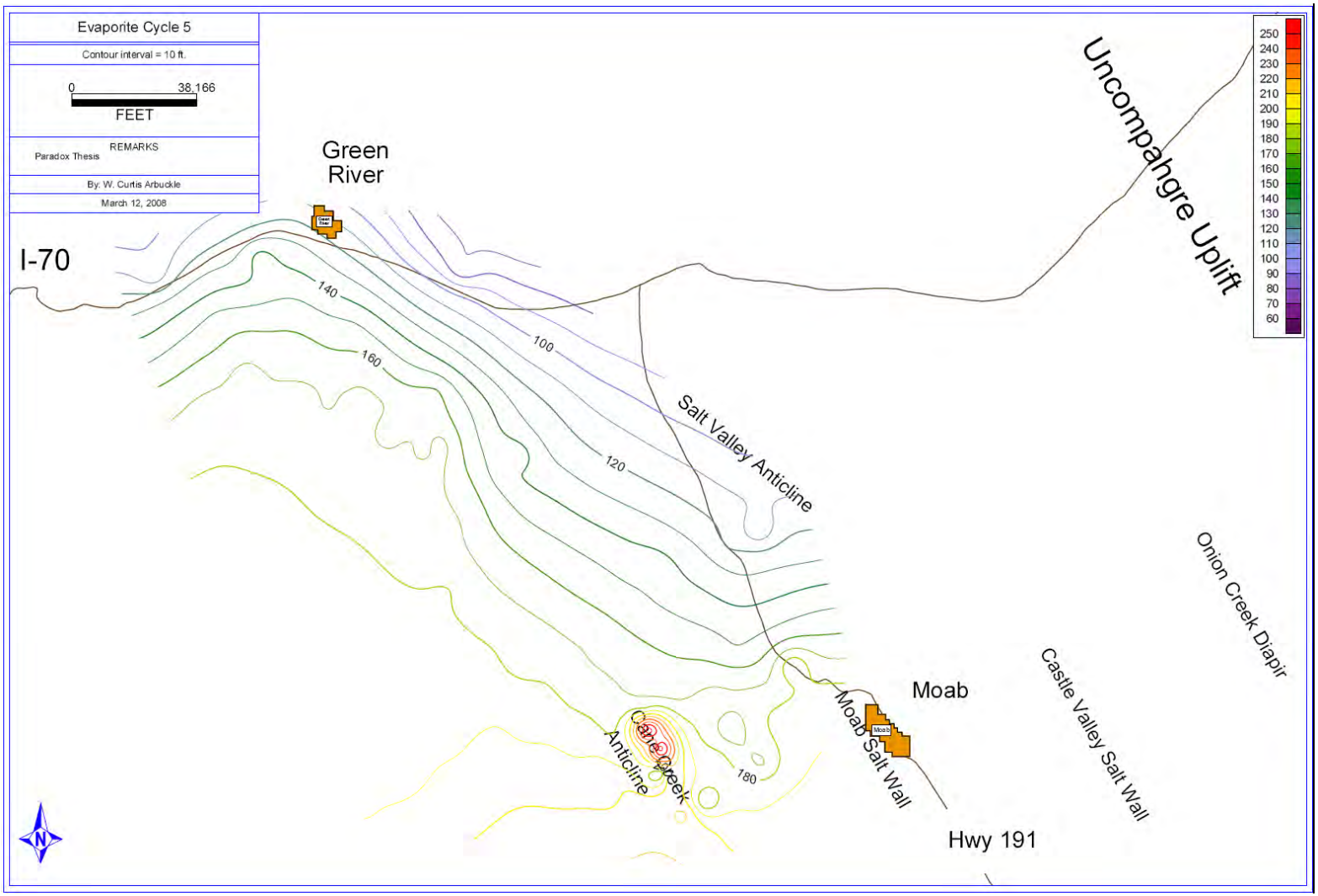

***Figure** B-25: Isopach map of evaporite cycle 5 within the Paradox Formation. See text for analysis. Contour interval = 10 feet (3.05 m).*

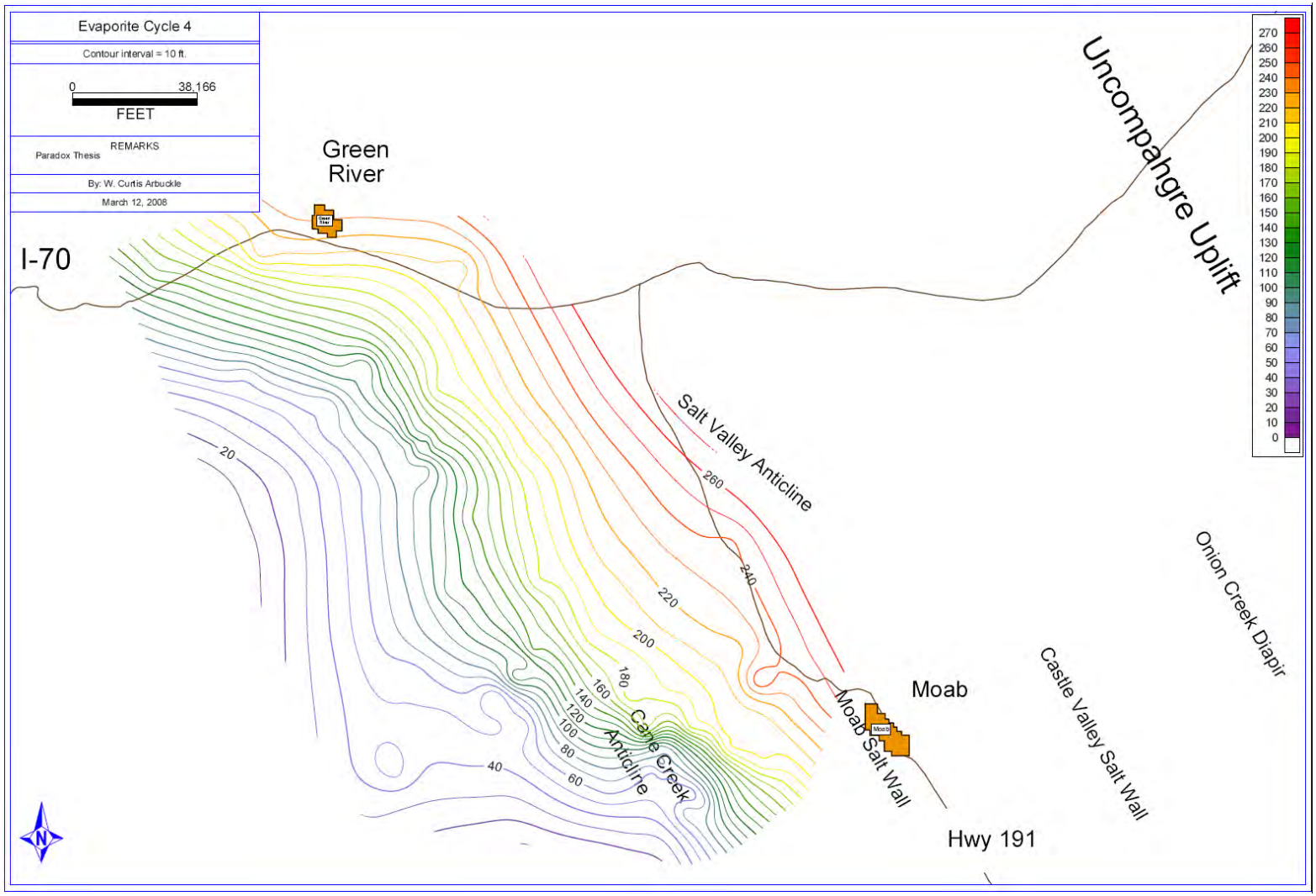

***Figure** B-26: Isopach map of evaporite cycle 4 within the Paradox Formation. See text for analysis. Contour interval = 10 feet (3.05 m).*

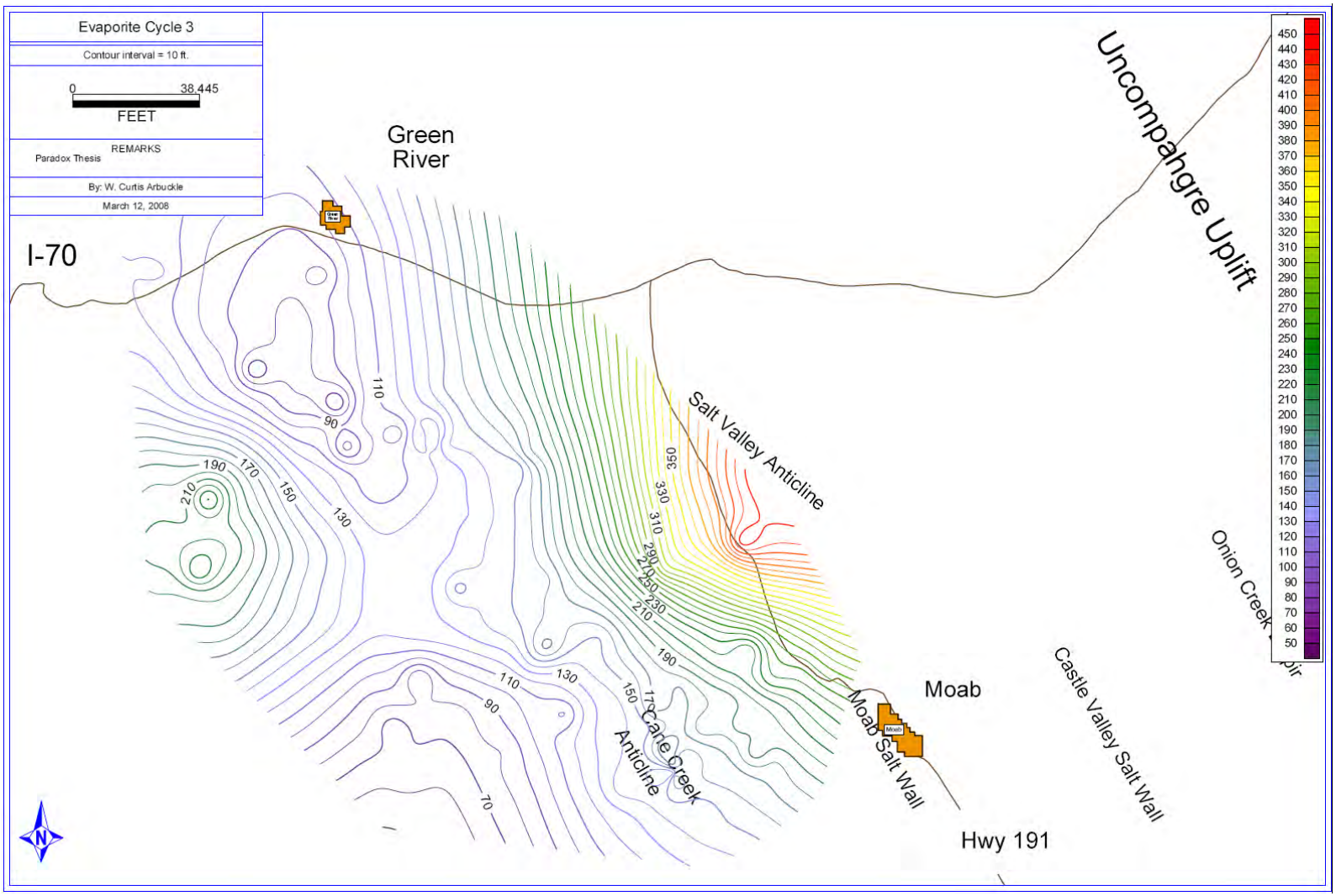

***Figure** B-27: Isopach map of evaporite cycle 3 within the Paradox Formation. See text for analysis. Contour interval = 10 feet (3.05 m).*

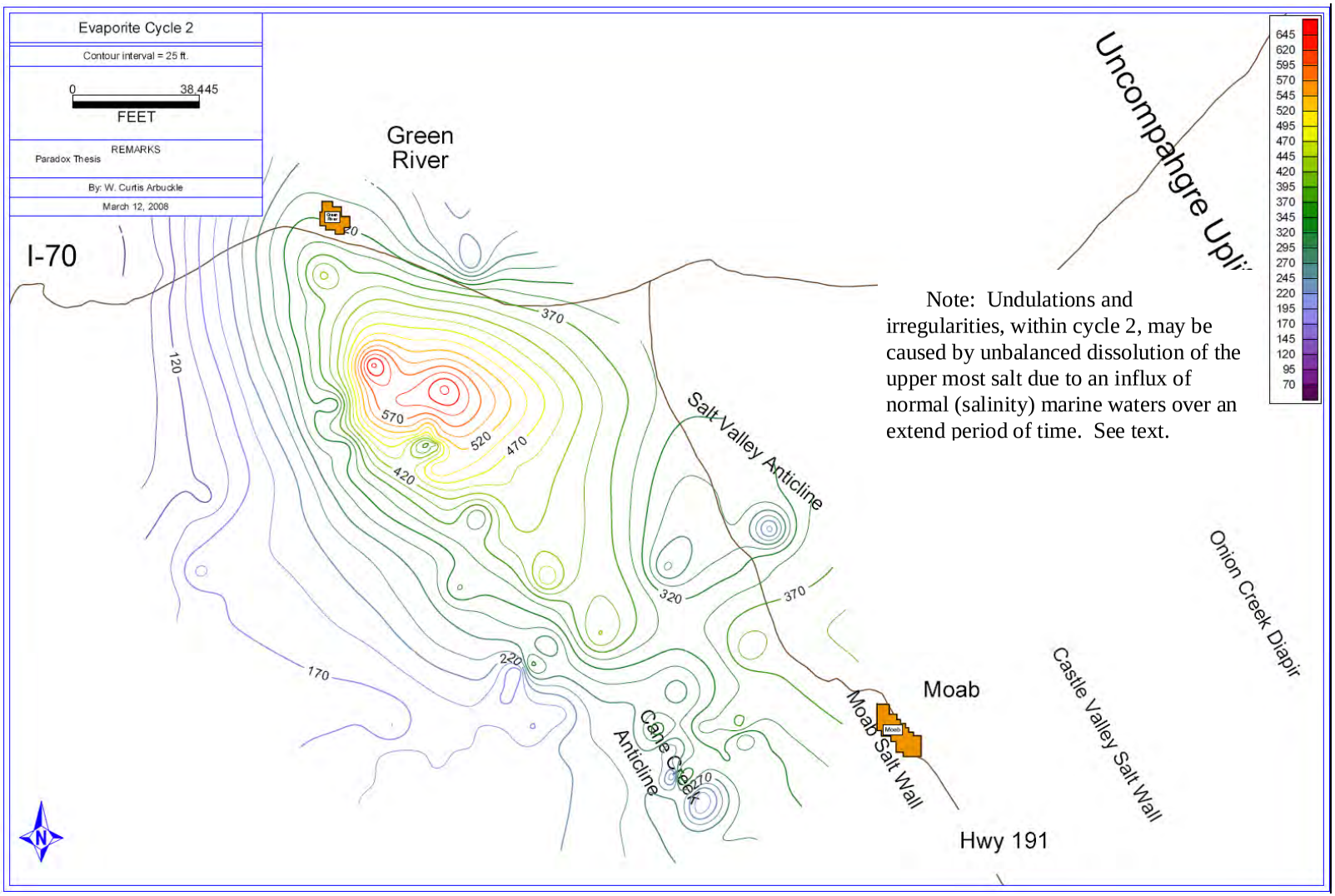

Figure B-28: ***Isopach map of evaporite cycle 2 within the Paradox Formation. See text for analysis. Contour interval = 25 feet (7.62 m).***

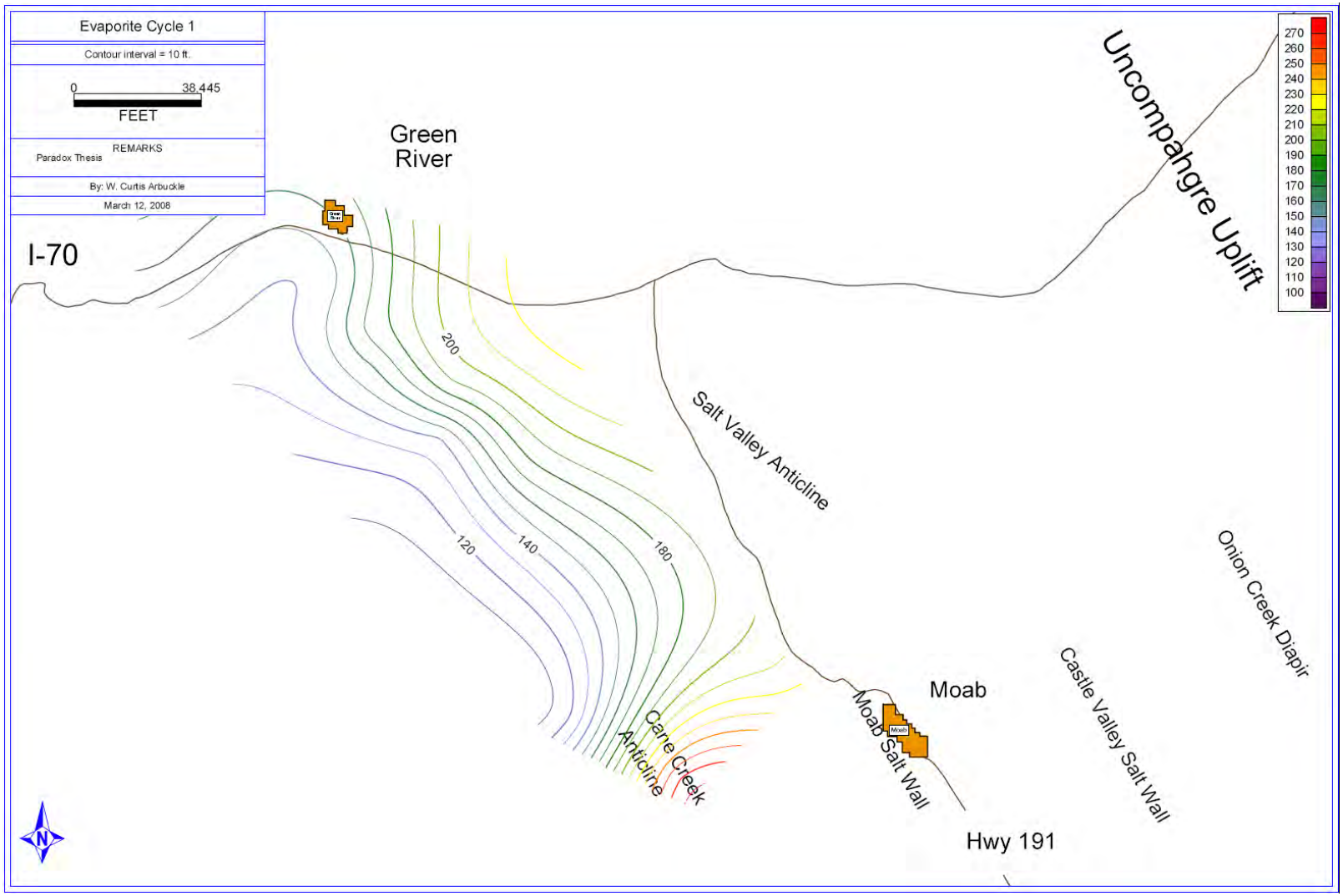

***Figure** B-29: Isopach map of evaporite cycle 1 within the Paradox Formation. See text for analysis. Contour interval = 10 feet (3.05 m).*

APPENDIX C

Table C-1: A table showing the thicknesses (in feet) anhydrite, silty dolomite (T = transgressive), black shale, silty dolomite (R = regressive) and halite for 10 wells used in age estimation for the Paradox Formation.

No.	API #	Well Name	Lithology Thicknesses (feet)					
			Anhydrite (total)	Silt/Dolo (T)	Black Shale	Silt/Dolo (R)	Halite	Total
1	4301511182	GRAND FAULT UNIT 14	249	387.1	136	428.9	1,196	2,397
2	4301530079	GEYSER DOME 1-14	251	210.35	87	220.65	1,211	1,980
3	4301930124	MT FUEL-SKYLINE GEYS	275	324.78	184	251.22	2,693	3,728
4	4301930282	SALT WASH NORTH 1	238	311.8	140	255.2	2,381	3,326
5	4301930688	FEDERAL 1-26	281	283.8	155	246.2	2,354	3,320
6	4301930050	BIG ROCK FED 1	273	392.4	176	208.6	2,910	3,960
7	4301930910	MOAB FED 16-9	334	198.45	214	192.55	2,691	3,630
8	4301530145	POOL UNIT 1	264	147.3	68	145.7	1,210	1,835
9	4301931190	COORS USA 1-10LC	426	267.85	162	227.15	3,876	4,959
10	4301910767	LITTLE VALLEY-FED 1	360	189.15	259	136.85	2,286	3,231

Table C-2: A table displaying evaporite cycle 2 age estimations for 10 wells within the northern Paradox Basin. Ages were calculated using sedimentation rates listed in Table 5 and thicknesses tallied from well logs.

Cycle 2

No.	API #	Operator	Well Name	Age (years)	
				(max.)	(min.)
1	4301511182	SUPERIOR OIL COMPANY	GRAND FAULT UNIT 14	96,894	85,524
2	4301530079	MEGADON ENTERPRISES	GEYSER DOME 1-14	109,340	99,017
3	4301930124	MOUNTAIN FUEL SUPPLY	MT FUEL-SKYLINE GEYS	112,254	104,076
4	4301930282	RESERVE OIL & GAS	SALT WASH NORTH 1	99,798	91,769
5	4301930688	MEGADON ENTERPRISES	FEDERAL 1-26	124,620	119,334
6	4301930050	GENERAL CRUDE OIL CO	BIG ROCK FED 1	92,974	85,344
7	4301930910	CHANDLER & ASSOCIATE	MOAB FED 16-9	102,303	93,177
8	4301530145	DAVIS OIL COMPANY	POOL UNIT 1	98,551	96,706
9	4301931190	COORS ENERGY	COORS USA 1-10LC	102,303	93,177
10	4301910767	MURPHY CONSTRUCTION	LITTLE VALLEY-FED 1	91,980	79,712

Table C-3: A table displaying evaporite cycle 3 age estimations for 10 wells within the northern Paradox Basin. Ages were calculated using sedimentation rates listed in Table 5 and thicknesses tallied from well logs. N/A = insufficient data needed for calculation.

Cycle 3

No.	API #	Operator	Well Name	Age (years)	
				(max.)	(min.)
1	4301511182	SUPERIOR OIL COMPANY	GRAND FAULT UNIT 14	N/A	N/A
2	4301530079	MEGADON ENTERPRISES	GEYSER DOME 1-14	N/A	N/A
3	4301930124	MOUNTAIN FUEL SUPPLY	MT FUEL-SKYLINE GEYS	85,426	76,200
4	4301930282	RESERVE OIL & GAS	SALT WASH NORTH 1	84,714	78,929
5	4301930688	MEGADON ENTERPRISES	FEDERAL 1-26	88,372	79,495
6	4301930050	GENERAL CRUDE OIL CO	BIG ROCK FED 1	75,527	64,058
7	4301930910	CHANDLER & ASSOCIATE	MOAB FED 16-9	83,483	70,367
8	4301530145	DAVIS OIL COMPANY	POOL UNIT 1	53,979	50,837
9	4301931190	COORS ENERGY	COORS USA 1-10LC	83,483	70,367
10	4301910767	MURPHY CONSTRUCTION	LITTLE VALLEY-FED 1	79,588	66,373

Table C-4: A table displaying evaporite cycle 5 age estimations for 10 wells within the northern Paradox Basin. Ages were calculated using sedimentation rates listed in table 5 and thicknesses tallied from well logs.

Cycle 5

No.	API #	Operator	Well Name	Age (years)	
				(max.)	(min.)
1	4301511182	SUPERIOR OIL COMPANY	GRAND FAULT UNIT 14	99,516	94,629
2	4301530079	MEGADON ENTERPRISES	GEYSER DOME 1-14	88,314	81,282
3	4301930124	MOUNTAIN FUEL SUPPLY	MT FUEL-SKYLINE GEYS	86,751	78,174
4	4301930282	RESERVE OIL & GAS	SALT WASH NORTH 1	102,677	99,386
5	4301930688	MEGADON ENTERPRISES	FEDERAL 1-26	79,250	72,368
6	4301930050	GENERAL CRUDE OIL CO	BIG ROCK FED 1	73,751	63,478
7	4301930910	CHANDLER & ASSOCIATE	MOAB FED 16-9	64,359	55,382
8	4301530145	DAVIS OIL COMPANY	POOL UNIT 1	61,500	53,570
9	4301931190	COORS ENERGY	COORS USA 1-10LC	65,227	56,500
10	4301910767	MURPHY CONSTRUCTION	LITTLE VALLEY-FED 1	53,442	42,621

Table C-5: A table displaying evaporite cycle 9 age estimations for 10 wells within the northern Paradox Basin. Ages were calculated using sedimentation rates listed in table 5 and thicknesses tallied from well logs.

Cycle 9

No.	API #	Operator	Well Name	Age (years)	
				(max.)	(min.)
1	4301511182	SUPERIOR OIL COMPANY	GRAND FAULT UNIT 14	83,994	81,002
2	4301530079	MEGADON ENTERPRISES	GEYSER DOME 1-14	54,820	52,177
3	4301930124	MOUNTAIN FUEL SUPPLY	MT FUEL-SKYLINE GEYS	56,781	53,989
4	4301930282	RESERVE OIL & GAS	SALT WASH NORTH 1	72,305	68,615
5	4301930688	MEGADON ENTERPRISES	FEDERAL 1-26	65,101	61,660
6	4301930050	GENERAL CRUDE OIL CO	BIG ROCK FED 1	44,912	42,667
7	4301930910	CHANDLER & ASSOCIATE	MOAB FED 16-9	34,028	28,991
8	4301530145	DAVIS OIL COMPANY	POOL UNIT 1	58,200	55,408
9	4301931190	COORS ENERGY	COORS USA 1-10LC	38,800	33,115
10	4301910767	MURPHY CONSTRUCTION	LITTLE VALLEY-FED 1	32,395	29,752

Table C-6: A table displaying evaporite cycle 10 age estimations for 10 wells within the northern Paradox Basin. Ages were calculated using sedimentation rates listed in table 5 and thicknesses tallied from well logs. N/A = insufficient data needed for calculation.

Cycle 10

No.	API #	Operator	Well Name	Age (years)	
				(max.)	(min.)
1	4301511182	SUPERIOR OIL COMPANY	GRAND FAULT UNIT 14	N/A	N/A
2	4301530079	MEGADON ENTERPRISES	GEYSER DOME 1-14	N/A	N/A
3	4301930124	MOUNTAIN FUEL SUPPLY	MT FUEL-SKYLINE GEYS	54,284	50,594
4	4301930282	RESERVE OIL & GAS	SALT WASH NORTH 1	49,865	45,925
5	4301930688	MEGADON ENTERPRISES	FEDERAL 1-26	N/A	N/A
6	4301930050	GENERAL CRUDE OIL CO	BIG ROCK FED 1	43,141	40,648
7	4301930910	CHANDLER & ASSOCIATE	MOAB FED 16-9	32,762	29,471
8	4301530145	DAVIS OIL COMPANY	POOL UNIT 1	N/A	N/A
9	4301931190	COORS ENERGY	COORS USA 1-10LC	39,789	36,198
10	4301910767	MURPHY CONSTRUCTION	LITTLE VALLEY-FED 1	44,029	41,635